

**INVESTIGATING THE INBRED STRAIN-SPECIFIC RESPONSE TO
BIGLYCAN-DEFICIENCY AND EXERCISE: A STUDY IN
GENETICALLY-MEDIATED SKELETAL ADAPTATION**

by

Joseph Michael Wallace III

A dissertation submitted in partial fulfillment
of the requirements for the degree of
Doctor of Philosophy
(Biomedical Engineering)
in The University of Michigan
2007

Doctoral Committee:

Professor David H. Kohn, Chair
Professor Steven A. Goldstein
Assistant Professor Kurt D. Hankenson, University of Pennsylvania
Marian F. Young, National Institute of Dental and Craniofacial Research,
National Institutes of Health

© Joseph Michael Wallace III

All rights reserved

2007

To Sarah, who was an anchor when I was blown astray and
kept me sane when the world was spinning.
I could not have done this without you

ACKNOWLEDGEMENTS

I have to start by thanking Dave Kohn. I started in the Biomedical Engineering program here at Michigan fresh out of an undergraduate program in Aerospace Engineering. I had no lab experience and very little biological background, but you had faith in my abilities (sometime when I did not), and you gave me a chance. While always facilitating my work in any way you could, you challenged me both technically and intellectually. Sometime I was frustrated and I floundered, but if it were not for the type of training I received in your lab, I wouldn't be the Bioengineer I am today.

To Steve Goldstein, Marian Young and Kurt Hankenson - I want to thank the rest of my thesis committee for their contributions to my education and to this dissertation. Thanks for never standing in my way, even when I proposed an experiment that may have been a bit over my head. Through your guidance and resources, I was able to weave an important story out of an (sometimes) overwhelming amount of data. A special thanks to Marian, who supplied me with the bgn-deficient mice that were so integral to this work.

This study could not have happened without the funding I received over the past 5 years through DoD/US Army DAMD17-03-1-0556, NIH T32-DE07057, NIH IPA Agreement and The University of Michigan Regenerative Sciences Training Grant R90-DK071506.

Thanks to Rupak Rajachar. Aside from being the 2nd author on each of my first two manuscripts, you were the first friend and lab mate I had here at Michigan. Starting graduate school, especially in a new program at a new school, is a little overwhelming. You showed me how to make it in classes and in lab, and taught me to always have a life away from work to keep myself balanced. Although you left Ann Arbor less than a year after I got here, you are a friend for life.

Thanks to Jaclynn Kreider and Jeff Meganck from the Orthopaedic Research Laboratories here at The University of Michigan for your help with μ CT. You each had

to deal with some of my 180 samples, but I never heard a single complaint (even during a pregnancy/birth). This work could not have been completed without the data derived from the μ CT.

Thanks to Mike Morris and Kurt Golcuk from the Department of Chemistry here at The University of Michigan. My original experimental designs did not include a spectroscopic outlook, but your help measuring and understanding the compositional differences that occurred in these studies added insight that would not have been possible otherwise.

Thanks to those who have been co-authors on each of my manuscripts. In chronological order, those authors are: Rupak M. Rajachar, Xiao-Dong Chen, Songtao Shi, Matthew R. Allen, Susan A. Bloomfield, Clifford M. Les, Pamela G. Robey, Marian F. Young, David H. Kohn, Michael S. Ron, Kurtulus Golcuk and Michael D. Morris.

To Sharon Segvich and Nadder Sahar: Over the past 5 years, the three of us have gone from classmates, to labmates, to the best of friends. Your friendship means the world to me. I can't imagine what grad school would have been without the 2 of you around. You have both been able to tolerate everything I dish out (which is a lot), but somehow you always still stick with me. I love that we can talk about everything from football to the mechanisms governing the initial nucleation of hydroxyapatite in the organic matrix of bone. Don't forget the pact we made to vacation someplace exotic once a year....I am holding you both to it.

Thanks to the members of the Kohn Research Lab that I have had the pleasure to work with, both current and past: Erin Gatenby, Sun Ig Hong, Shan Lee, Elena Leonova, Linh Luong, Steve Obreiter, Rupak Rajachar, Mike Ron, Ricardo Rossello, Nadder Sahar, Sharon Segvich, Kyungsup Shin, Hayes Smith, Lisa Winkel.

A special thanks to my family for putting up with the 24 years of my education: Mom, Dad, Jason, Jeremy, Leslie, Ryan and Brady. Someday, I will stop being a student, but I will never stop learning.

And finally, thanks to Sarah. We have only known each other for 4 years, but I feel like you have been there every step of the way. Our house is just the beginning of our journey together. I look forward to moving through life knowing I have a companion and partner like you standing by my side.

TABLE OF CONTENTS

DEDICATION.....	ii
ACKNOWLEDGEMENTS.....	iii
LIST OF FIGURES.....	ix
LIST OF TABLES.....	xii
ABSTRACT.....	xiii
CHAPTER 1: INTRODUCTION.....	1
The Hierarchical Structure of Bone.....	2
Bone at the Structural Level	
Bone at the Macrostructural (Tissue) Level	
Bone Ultrastructure	
Models of Bone Disease (Biglycan Deficiency)	5
Skeletal-Related Effects of Exercise and Mechanical Loading	6
Inbred Mouse Strains and Their Importance to Skeletal Research.....	7
Hypotheses and Specific Aims	8
References.....	16
CHAPTER 2: THE MECHANICAL PHENOTYPE OF BIGLYCAN DEFICIENT MICE IS BONE AND GENDER SPECIFIC.....	22
Introduction.....	22
Materials and Methods.....	24
Animals	
Mechanical Testing	
Peripheral Quantitative Computed Tomography (pQCT)	
Histomorphometry	
Statistical Analysis	
Results	27
Phenotypic Changes in Biglycan-Deficient Male Tibiae	
Phenotypic Changes in Biglycan-Deficient Male Femora	
Phenotypic Changes in Biglycan-Deficient Female Femora and Tibiae	
Discussion.....	29
Acknowledgements	35
Funding sources for this study	
References.....	44
CHAPTER 3: EXERCISE-INDUCED CHANGES IN THE CORTICAL BONE OF GROWING MICE ARE BONE AND GENDER SPECIFIC	50

Introduction.....	50
Materials and Methods.....	52
Animals and Treatment	
Mechanical Testing	
Peripheral Quantitative Computed Tomography (pQCT)	
Statistical Analysis	
Results	55
Discussion.....	56
Acknowledgements	60
Funding sources for this study	
References.....	69

CHAPTER 4: INBRED STRAIN-SPECIFIC RESPONSE TO BIGLYCAN DEFICIENCY IN THE CORTICAL BONE OF C57BL6/129 AND C3H/HE MICE

.....	75
Introduction.....	75
Materials and Methods.....	77
Animals	
Micro Computed Tomography (μ CT) Evaluation	
Mechanical Testing	
Histomorphometry	
Raman Microspectroscopy	
Real-Time Quantitative RT-PCR	
Statistical Analysis	
Results	84
Bgn-deficient phenotype in B6;129 mice at 8 weeks of age	
Bgn-deficient phenotype in C3H mice at 8 weeks of age	
Inbred strain-specific response to bgn-deficiency at 8 weeks of age	
B6;129 Bgn-deficient phenotype at 11 weeks of age and effects of growth	
C3H Bgn-deficient phenotype at 11 weeks of age and effects of growth	
Inbred strain-specific response to bgn-deficiency at 11 weeks of age	
Discussion.....	90
Acknowledgements	94
Funding sources for this study	
References.....	103

CHAPTER 5: EXERCISE MODULATES THE PHENOTYPE OF BIGLYCAN-DEFICIENT MICE IN AN INBRED STRAIN-SPECIFIC MANNER BY ALTERING BONE TISSUE COMPOSITION AND MECHANICAL INTEGRITY

.....	108
Introduction.....	108
Materials and Methods.....	110

Animals	
Micro Computed Tomography (μ CT) Evaluation	
Mechanical Testing	
Raman Microspectroscopy	
Statistical Analysis	
Results	115
Effects of exercise in B6;129 WT mice	
Effects of exercise in B6;129 KO mice	
Bgn-deficient phenotype in B6;129 mice and the ability of exercise to alter this phenotype	
Effects of exercise in C3H WT mice and inbred strain specificity of the response to exercise	
Effects of exercise in C3H KO mice and inbred strain specificity of the response to exercise	
Bgn-deficient phenotype in C3H mice and the ability of exercise to alter this phenotype	
Discussion	120
Acknowledgements	125
Funding sources for this study	
References	136
CHAPTER 6: CONCLUSIONS	142
<i>In Vivo</i> Influences of BGN on Collagen and Mineral (Chapter 4)	143
Mechanical Effects on the Bone Ultrastructure (Chapter 5)	146
Broader Implications of This Dissertation	148
Future Studies	149
References.....	154
APPENDIX A: DEVELOPING THE STATISTICAL ANALYSIS TO DETECT INBRED STRAIN-SPECIFICITY	156
APPENDIX B: INCREASED POST-YIELD PROPERTIES INDUCED WHEN EXERCISE IS SUPERIMPOSED ON GROWTH ARE MAINTAINED AFTER 2 WEEKS WITH ADDED STRENGTH	160
Introduction	160
Materials and Methods	161
Animals and Treatment	
Mechanical Testing	
Histomorphometry	
Statistical Analysis	
Results	165

Growth-related effects between 8 and 13 weeks of age	
The effects of exercise superimposed upon growth between 8 and 11 weeks of age	
The effects of a 2 week tissue maturation period on exercised bones	
Body weight changes due to exercise and tissue maturation	
Discussion	168
Acknowledgements	171
Funding sources for this study	
References	177

APPENDIX C: PROTOCOLS DEVELOPED FOR THE COMPLETION OF

THIS DISSERTATION	179
Introduction	179
Protocol for processing mouse bones for undecalcified histology	179
Protocol For Harvesting and Preparing Whole Mouse Bone for qRT-PCR	186
Protocol For Total RNA Isolation From Whole Bones	191
Protocol For Cleaning RNA Samples With DNase	197
Protocol For Cleaning RNA Samples With DNase	202
Protocol For qRT-PCR	205

LIST OF FIGURES

Chapter 1

Figure 1.1: The Hierarchical Structure of Bone.....	13
Figure 1.2: Anatomical Structure of a Long Bone.....	14
Figure 1.3: Collagen fibril structure.....	15

Chapter 2

Figure 2.1: Geometric Properties of the Male and Female Tibial Diaphyses of Biglycan-Deficient vs. Wild Type Mice.....	36
Figure 2.2: Mechanical Properties of the Male and Female Tibial Diaphyses of Biglycan-Deficient vs. Wild Type Mice.....	37
Figure 2.3: Histomorphometry of the Male and Female Tibial Diaphyses of Biglycan-Deficient vs. Wild Type Mice.....	38
Figure 2.4: Bone Mineral Quantification in the Male Tibial Diaphysis of Biglycan-Deficient vs. Wild Type Mice.....	39
Figure 2.5: Correlations of Structural and Tissue-Level Mechanical Properties to Geometric Properties of the Biglycan-Deficient Male Tibial Diaphyses.....	40

Chapter 3

Figure 3.1: Body Weights of Male and Female C57BL6/129 Mice Prior To and Following Exercise.....	61
Figure 3.2: Geometric Properties of the Male and Female Tibial Diaphyses Following Exercise.....	62
Figure 3.3: Periosteal and Endocortical Perimeters of the Male Tibial Diaphyses Following Exercise.....	63
Figure 3.4: Structural Level Mechanical Properties of the Male and Female Tibial Diaphyses Following Exercise.....	64

Figure 3.5: Tissue Level Mechanical Properties of the Male and Female Tibial Diaphyses Following Exercise.....	65
---	----

Chapter 4

Figure 4.1: Body mass (A,B) and tibial length (C,D) of wild type (WT) and bgn-deficient (knockout, KO) mice.	95
Figure 4.2: Volumetric bone mineral density (vBMD) and tissue compositional measures from the tibial mid-diaphysis of wild type (WT) and bgn-deficient (knockout, KO) mice.	96
Figure 4.3: Estimated tissue-level mechanical properties from the tibial mid-diaphysis of wild type (WT) and bgn-deficient (knockout, KO) mice.....	97
Figure 4.4: Cross-sectional geometric properties from the tibial mid-diaphysis of wild type (WT) and bgn-deficient (knockout, KO) mice.....	98
Figure 4.5: Structural-level mechanical properties from the tibial mid-diaphysis of wild type (WT) and bgn-deficient (knockout, KO) mice.....	99
Figure 4.6: mRNA expression from the right tibiae of wild type (WT) and bgn-deficient (knockout, KO) mice at 11 weeks of age.....	100
Figure 4.7: Histomorphometry from the tibial mid-diaphysis of wild type (WT) and bgn-deficient (knockout, KO) mice at 11 weeks of age.	101
Figure 4.8: Linear regressions between failure deformation and failure strain (A) and a size/shape factor (B) for all 120 mice.....	102

Chapter 5

Figure 5.1: Body Mass (A,B) and tibial length (C,D) of wild type (WT) and bgn-deficient (KO) mice from the B6;129 inbred strain.	126
Figure 5.2: Tissue composition and volumetric bone mineral density (vBMD) in the tibial diaphysis of wild type (WT) and bgn-deficient (KO) B6;129 mice.....	127
Figure 5.3: Estimated tissue-level mechanical properties from wild type (WT) and bgn-deficient (KO) B6;129 tibiae	128

Figure 5.4: Standard site geometric properties of the tibial diaphysis in wild type (WT) and bgn-deficient (KO) B6;129 mice.....	129
Figure 5.5: Structural-level mechanical properties from wild type (WT) and bgn-deficient (KO) B6;129 tibiae.....	130
Figure 5.6: Body Mass (A,B) and tibial length (C,D) of wild type (WT) and bgn-deficient (KO) mice from the C3H inbred strain.....	131
Figure 5.7: Tissue composition and volumetric bone mineral density (vBMD) in the tibial diaphysis of wild type (WT) and bgn-deficient (KO) C3H mice.	132
Figure 5.8: Estimated tissue-level mechanical properties from wild type (WT) and bgn-deficient (KO) C3H tibiae	133
Figure 5.9: Standard site geometric properties of the tibial diaphysis in wild type (WT) and bgn-deficient (KO) C3H mice.....	134
Figure 5.10: Structural-level mechanical properties from wild type (WT) and bgn-deficient (KO) C3H tibiae	135

Appendix B

Figure B.1: Body Weights Measurements at Days -11, 0, 18 and 35.....	172
Figure B.2: Histomorphometry from Days-10, -3, 0, 9, 19 and 30.....	173

LIST OF TABLES

Chapter 2

Table 2.1: Geometric Properties of the Male and Female Femoral Diaphyses of Biglycan-Deficient Vs. Wild Type Mice.....	41
Table 2.2: Structural Mechanical Properties of the Male and Female Femoral Diaphyses of Biglycan-Deficient Vs, Wild Type Mice.....	42
Table 2.3: Tissue-Level Mechanical Properties of the Male and Female Femoral Diaphyses of Biglycan Deficient Vs. Wild Type Mice.....	43

Chapter 3

Table 3.1: Geometric Properties of the Male and Female Femoral Diaphyses of Control and Exercise Mice	66
Table 3.2: Structural Mechanical Properties of the Male and Female Femoral Diaphyses of Control and Exercise Bones.....	67
Table 3.3: Tissue-Level Mechanical Properties of the Male and Female Femoral Diaphyses of Control and Exercise Bones	68

Appendix B

Table B.1: Geometric Properties of the Tibial Diaphyses.....	174
Table B.2: Tissue-Level Mechanical Properties of the Tibial Diaphyses.....	175
Table B.3: Structural-Level Mechanical Properties of the Tibial Diaphyses.....	176

ABSTRACT

INVESTIGATING THE INBRED STRAIN-SPECIFIC RESPONSE TO BIGLYCAN-DEFICIENCY AND EXERCISE: A STUDY IN GENETICALLY-MEDIATED SKELETAL ADAPTATION

by

Joseph Michael Wallace III

CHAIR: David H. Kohn

Bone is an exquisitely evolved connective tissue that serves structural and metabolic roles in the body. Bone fragility leading to fracture is a significant medical and economic burden facing our society. Each year, 1.5 million Americans suffer an age-related fracture, resulting in direct-care expenditures of 18 billion dollars a year and often leading to decreased quality of life or even death.

Animals with targeted mutations in a bone matrix protein (KO) are utilized to study the protein's roles in regulating extracellular matrix (ECM) deposition and architecture and understanding how these functions relate to bone disease and fracture etiology.

The importance of skeletal loading for the maintenance/increase of bone mass was suggested as early as 1892. In addition to increased size, mechanical loading influences bone ECM quality. Since many diseases influence the mechanical integrity of

bone through altered tissue quality, mechanical stimulation may be a practical way to prevent/treat ECM deficiencies.

Mouse inbred strain-specific responses in bone have been demonstrated following mechanical stimulation and bone regeneration. No study has demonstrated that the response to a genetic deletion can exhibit inbred-strain-specific characteristics, or that phenotypic changes can be modulated with mechanical stimulation. It was hypothesized that the response to a genetic deletion (the bone matrix protein biglycan, *bgn*), mechanical stimulation (running) and a combination of these two variables would display inbred-strain-specific characteristics in the tibiae of C57BL6/129 (B6;129) and C3H/He (C3H) male mice.

This dissertation establishes for the first time that an inbred strain-specific response to genetic deletion exists, further develops the roles that biglycan plays in regulating collagen and mineral *in vivo* and links these *in vivo* roles with mechanical integrity. Without addition of new bone, exercise altered the pre-existing ECM which influenced tissue quality and mechanical integrity. In B6;129 KO, exercise-induced changes in tissue composition compensated for tissue-level mechanical deficiencies, suggesting that mechanical stimulation may be effective as a therapeutic intervention for diseases associated with deficiencies in bone quality. These studies provide new insights into inbred strain research which has important implications to the proper interpretation of investigations into the effects of genetic deficiencies and loading on the skeleton.

CHAPTER 1

INTRODUCTION

Bone is an exquisitely evolved connective tissue that serves three integral and interconnected functions in the body. First, bone provides protection for the body's vital organs. The skull encloses the brain, protecting it from external trauma. Most other major organs, including the heart and lungs, are enclosed by the ribcage while the spinal cord is enclosed in vertebrae. While not an organ in classic terms, the bone marrow is housed in a protected environment inside the bones of the extremities and hips. The second major function of bone is to support the weight of soft tissue and provide a structural framework for mobility. In combination with other tissues in the musculoskeletal system (e.g. muscles, tendons and ligaments), bones act as an elaborate lever system upon which contractile muscle forces act to coordinate movement. Bone needs to maintain a certain level of stiffness and strength to perform these locomotive functions effectively. Bone's third and final role involves mineral ion homeostasis. Maintenance of ion concentrations in the blood (e.g. calcium, phosphorous, magnesium) is essential for a multitude of functions, and the skeleton acts as reservoir for the storage and controlled release of these minerals. Mineral ions are freed from the skeleton by the coordinated sequence of cellular events which demineralize bone tissue at specific locations in the skeleton. In normal physiological conditions, bone changes in response to the needs of the body, maintaining a balance between these three major functions. However, any number of pathological conditions can disrupt this balance.

Bone fragility leading to fracture is a significant medical and economic burden facing our society. Each year, an estimated 1.5 million Americans suffer an age-related fracture, resulting in direct-care expenditures of 18 billion dollars a year and often leading to a downward spiral in quality of life or even death. Today, about 10 million Americans over the age of 50 have osteoporosis [1], a skeletal disorder characterized by compromised strength in both cortical and trabecular bone due to a combination of low

bone mass and poor tissue quality [2]. Since it is generally accepted that fracture risk and biomechanical competence of bone are affected by both bone mass and tissue quality [3], understanding the composition, structure and function of bone is essential if we are to uncover how and why pathological conditions occur and ultimately develop better diagnostics and therapies for these conditions.

The Hierarchical Structure of Bone

Bone is a hierarchical material, meaning that it is composed of structural elements which themselves have structure on a smaller size scale. When properties are measured at any size scale, those properties are assumed to represent a continuum of homogenous material that is influenced by the architectural organization at that level. However, it is also understood that those properties are the product of all hierarchical levels below the level of interest. By systematically investigating the structure of bone at multiple levels of its hierarchy, it is possible to begin closing the gap between the biology of bone and biomechanical outcomes. Many views of the hierarchical structure of bone exist. For the purposes of this dissertation, 3 levels of hierarchy will be investigated (Figure 1.1): the whole bone structural-level (on the order of 10^2 mm), the tissue level (on the order of 10^{-5} to 10^{-4} m) and the ultrastructural-level (on the order of 1 nm).

Bone at the Structural Level

The whole bone or structural level is clinically important as this is the size scale where all lower levels of hierarchy culminate and impact the function of the skeletal system. At this level, each bone represents one of the 206 bones that make up the adult skeleton. While varying in size, shape and function, all bones are composed of the same set of tissues and structures. A typical long bone (Figure 1.2) has 3 main regions (epiphysis, metaphysis and diaphysis) composed of 2 types of tissue (trabecular or cancellous bone and cortical or compact bone). The ends of long bones are covered in articular cartilage (for smooth joint articulation) and tend to flare out for increased surface area at the points of force transmission. The rest of the outer (periosteal) surface is covered in a fibrous membrane called the periosteum which contains a vascular supply and cells associated with bone formation.

Bone at the Macrostructural (Tissue) Level

At the macrostructural or tissue-level, bone is distinguished into the intermediate structures of cortical and trabecular bone. Cortical bone is present for mechanical support and stability and to provide anchor points for the attachment of muscles (via tendons). With an average porosity of between 5-10%, it is well suited for these structural roles. Approximately 80% of the total mass of the skeleton is composed of cortical bone, which forms the hollow tube-like diaphysis of long bones and a shell surrounding regions of trabecular bone (e.g. the ends of long bones, the pelvis and the vertebrae) creating a sandwich structure which protects the enclosed marrow.

Trabecular bone forms a structure of interconnected rods and plates. Because of its high surface area (due to a porosity ranging from 40-90%) and its intimate contact with a highly cellular and vascularized marrow, the primary role of trabecular bone may be metabolic. Given the right cellular cues, this porous trabecular structure is ideal for the rapid liberation of bone mineral ions into the general circulation.

Bone Ultrastructure

At its simplest level, bone is a two-phase composite material composed of a ductile organic phase impregnated with and surrounded by a stiff reinforcing mineral phase. These constituents represent the output of the bone forming osteoblast cells. The intimate interaction between these two phases results in the unique combination of stiffness, strength and toughness associated with bone tissue.

Bone's Mineral Phase

About 2/3 of the weight of bone is occupied by the mineral phase. The mineral in bone is often generically described as a form of the naturally occurring mineral hydroxyapatite, with a chemical formula of $\text{Ca}_{10}(\text{PO}_4)_6(\text{OH})_2$ [4]. However, the most thermodynamically stable mineral in bone is a non-stoichiometric, calcium-deficient apatite similar to dahllite [5, 6]. The ions in bone mineral form a hexagonal crystal lattice, but the mature crystals are plate shaped, with an average size of 50 nm x 25 nm and an average thickness of about 2-3 nm [6]. In mature bone mineral, calcium is the most predominant ion, but other ions can easily substitute into each space in the crystalline lattice including carbonate, magnesium, sodium, strontium and fluoride [4]. As ions of

different size and charge substitute into the lattice, distortions and vacancies occur which cause strain in the lattice and change the crystal size and perfection (or crystallinity). Ultimately, these properties along with crystal orientation have significant impacts on the mechanical characteristics of bone at higher levels of organization.

Bone's Organic Phase and Water

The remaining 1/3 of the weight of bone is composed primarily of Type I collagen (~90%). The basic building block of the collagenous framework is a triple-helical collagen molecule composed of two $\alpha 1$ chains and one $\alpha 2$ chain (Figure 1.3). In osteoblasts, these chains are linked together by inter- and intra-chain disulfide and hydrogen bonds. After secretion from the cell, enzymes cleave non-helical regions from the ends of each molecule (propeptides) leaving a cylindrically-shaped tropocollagen molecule with average diameter and length of 1.5 nm and 300 nm respectively. These molecules then self-assemble into fibrils that are generally 80-100 nm in diameter. Within a fibril, the tropocollagen molecules are parallel. However, adjacent molecules are staggered in their long axis creating a 67 nm repeating pattern of hole zones (40 nm) and overlap zones (27 nm). Cross-linking between tropocollagen molecules occurs through the action of lysyl oxidase, a copper-dependent enzyme which catalyzes the oxidative deamination of lysine and hydroxylysine residues in the telopeptide region of collagen molecules creating aldehydes. These newly created telopeptide aldehydes form reducible, immature divalent cross links with lysine or hydroxylysine residues within the helical region of adjacent tropocollagen molecules. Divalent cross-links can then mature into trivalent, non-reducible forms (pyridinoline and pyrrole) which are both intra- and interfibrillar. Cross-link quantity and maturity are important to the overall mechanical stability of the tissue, including tissue strength, stiffness and ductility [7, 8].

In addition to Type I collagen, other NCPs, growth factors and lipids make up the remaining 10% of the organic phase of bone and are present in varying amounts depending on the age of the bone tissue. Although their functions are not completely understood, multiple *in vitro* studies suggest that NCPs generally play a role in the organization, mineralization and maturation of bone. Over the past 20 years, particular attention has been paid to a group of molecules in the extracellular matrix (ECM) of bone

called small leucine-rich proteoglycans (SLRPs). During the development and repair of bone, SLRPs regulate ECM organization and mineralization by interacting with other matrix molecules [9-11] and growth factors [12-16] and directing their function. An example of this is biglycan (bgn), a SLRP that is enriched in the ECM of bone and other connective tissues [17-19]. In bone, bgn may direct the growth and differentiation of osteoblast precursor cells through its effects on TGF- β and BMP signaling [13, 20, 21]. Bgn is also implicated in regulating collagen fibril diameter and spacing [9, 22]. Finally, bgn plays a role in the mineralization of bone by regulating crystal size and the degree of mineralization [23, 24].

Models of Bone Disease (Biglycan Deficiency)

An estimated 1.5 million Americans suffer a bone-disease related fracture each year [1]. While osteoporosis is the most prevalent bone disease in the United States, many other diseases have been linked to skeletal fragility, including osteomalacia (mineralization disorder), osteopetrosis (impaired osteoclast activity), osteogenesis imperfecta (Type I collagen defect), Paget's Disease (overactive osteoclastic activity followed by increased formation leading to increased bone size with disorganized tissue) and hyperparathyroidism (excessive bone resorption). Though the etiology of these and other skeletal diseases differ from one another, they all are associated with problems arising in one or more of the cell types responsible for maintaining bone homeostasis. Bone diseases demonstrate how even small perturbations (e.g. the mutation of a single base pair in a gene encoding a type I collagen molecule) can disturb the delicate relationship between cellular metabolism and the mechanical integrity of the skeleton by influencing the various levels of bone hierarchy.

Animals with targeted mutations in a specific bone matrix protein have been utilized to study the protein's roles in regulating matrix deposition and architecture and understanding how these functions may relate to bone disease and fracture etiology [25-28]. This type of protein disruption allows for an analysis of changes in structure and function at multiple levels of the bone hierarchy, leading to a better understanding of the roles the protein plays *in vivo*.

One such model of disrupted protein production is the biglycan (bgn)-deficient mouse [9, 22, 29]. Bgn-deficient mice exhibit a defect in the growth and differentiation of osteoblast precursor cells resulting in reduced bone tissue production and mechanical deficiencies [13, 20, 21]. Bgn-deficient mice have decreased tissue-level yield strength compared with control mice along with structural-level deficiencies in yield deformation and yield work [23]. Altered tissue yield strength, which is independent of the amount of tissue present, suggests that deficiencies in bone tissue quality are responsible. ECM alterations have been shown in bgn-deficient mice from the B6;129 background strain [9, 22, 23, 30]. For example, the diameter of collagen fibrils in bgn-deficient bone is larger and more variable and often exhibits notches, protuberances and irregular spacing [9, 22]. Bgn-deficient bones also have greater volumetric bone mineral density (vBMD) [23] and larger mineral crystal size [30] compared to wild type mice, possibly due to the altered collagen template upon which mineralization occurs. The bones of bgn-deficient mice also become progressively weaker and less ductile with age. Since altered tissue quality and low peak bone mass in trabecular and cortical locations are hallmarks of human osteoporosis, the bgn-deficient mouse constitutes a good model for studying the development and treatment of this condition [29, 31]. The bgn-deficient phenotype also shares characteristics with other human diseases including Turner Syndrome [31] and Ehlers-Danlos Syndrome [9].

Skeletal-Related Effects of Exercise and Mechanical Loading

The importance of skeletal loading for the maintenance and increase of bone mass was suggested by Wolff as early as 1892 [32]. Although the idea that mechanical loading of bone is important is universally accepted today, many questions remain including the mechanisms by which bone responds to loading and what type of loading is best (exercise, control loading, etc.). One further question involves the age at the initiation of loading such as exercise, as the growing skeleton has a greater capacity to accrue bone than does the adult skeleton [33-35]. Since adult peak bone mass has often been considered the most important factor influencing fracture risk later in life, exercise during growth has been touted as the best preventive step one can take to avoid osteoporosis [1]. However, mechanical loading also has effects on bone that influence the quality of the

bone matrix [36, 37] in addition to any increase in bone mass or change in bone formation activity. This influence on tissue quality may be as important as increased bone mass, as small changes in quality and architecture could have large impacts on mechanical properties at higher levels in the bone hierarchy. Since many diseases influence the mechanical integrity of bone through alterations in tissue quality, mechanical stimulation may be practical way to prevent and treat ECM deficiencies [38-40].

Inbred Mouse Strains and Their Importance to Skeletal Research

The majority of mice used in skeletal research are referred to as “inbred.” Because of their importance in genetic and immunologic studies, a strict set of guidelines exist for generating inbred mouse strains [41]. First published in 1952, the guidelines state:

“A strain shall be regarded as inbred when it has been mated brother X sister for 20 or more consecutive generations (F20), and can be traced to a single ancestral breeding pair in the 20th or subsequent generation. Parent X offspring matings may be substituted for brother X sister matings provided that, in the case of consecutive parent X offspring matings, the mating in each case is to the younger of the two parents. Exceptionally, other breeding systems may be used, provided that the inbreeding coefficient achieved is at least equal to that at F20 (0.99).”

At 20 generations, mice are homozygous in at least 98.6% of their genetic loci. However, many inbred strains are bred to more than 150 generations, at which time the mice are considered 100% homozygous or isogenic (genetically identical). Having a pool of genetically identical animals with which to work has two important implications for research. By working with one inbred strain and holding all other environmental conditions constant, the isolated effects of a particular variable (e.g. drug treatment, mechanical stimulation, psychological stress) can be studied. Similarly, a study of variability between inbred strains can give a measure of genetic differences. Thus, differences in bone properties can be linked directly to genetics. The controlled crossing of two phenotypically different mouse strains has made it possible to begin dissecting out

quantitative trait loci (QTL), segments of DNA that are closely linked to genes that underlie the specific skeletal trait in question [42].

Today, almost 100 years after the generation of the first inbred mouse strain by Clarence C. Little (the DBA strain in 1909), there are over 450 genetically distinct inbred mouse strains [43]. Because inbred strains display large variations in bone-related traits of interest, utilization of these strains has increased our knowledge of the influences of genetics on skeletal structure, function and adaptation. While the bone phenotypes of many inbred strains have been investigated [44, 45], the last 10 years have shown a spike in research surrounding 2 particular strains whose skeletal phenotypes stand in contrast to one another [44, 46-49]. The C57BL6 (B6) and C3H/He (C3H) inbred strains initially stood out because of differences in bone density [44], and since then have been utilized as models of high (C3H) and low (B6) bone density in a variety of bone-related studies. The B6 and C3H inbred strains display differences not only in mineralization levels [44, 50], but also in bone cross-sectional geometric properties (greater cross-sectional area in B6, greater cortical area and cortical thickness in C3H) [47, 50], whole bone and tissue level mechanical properties (greater strength and stiffness at both levels in C3H) [45, 47, 50, 51] and indices of bone formation in all bones and ages (increased mineral apposition rate as a measure of increased osteoblast activity and metabolism in C3H mice) [46, 52-54]. Inbred strain-specific responses to external stimuli including mechanical loading, unloading [55-58] and bone regeneration [59-61] also exist and demonstrate that the bones from C3H mice consistently fail to respond to changes in the mechanical environment. However, the effects of background strain in other cases such as gene disruption are unknown.

Hypotheses and Specific Aims

Mouse inbred-strain-specific responses in bone have been demonstrated following mechanical stimulation, fracture healing and bone regeneration. It is clear that the genetic makeup of inbred strains govern these responses. However, no study has demonstrated that the response to a genetic deletion can exhibit inbred-strain-specific characteristics, or that these phenotypic changes can be modulated with mechanical

stimulation. Therefore, the studies contained in this dissertation were designed with a global hypothesis in mind:

The response to a genetic deletion, mechanical stimulation and a combination of these two variables will display inbred-strain-specific characteristics in the tibial cortical bone of male mice.

To test this global hypothesis, mice from 2 inbred strains [C57BL6/129 (B6;129) and C3H] were used to address three specific aims that were developed to test three sub-hypotheses. The hybrid B6;129 strain was used because mice from this strain have been utilized as the wild type background strain for many genetic knockouts, including the bgn-deficient mouse [23, 29, 62, 63]. The B6;129 mice have a low bone mass phenotype that is generally similar to that of C57BL6 mice [45].

***Hypothesis 1:** The bone response to the targeted disruption of biglycan will exhibit inbred-strain-specific characteristics. Compared with the response in B6;129 mice, C3H mice will be more resistant to changes in tissue composition and bone size. Therefore, the negative mechanical effects of bgn-deficiency, particularly decreased strength and ductility, will be reduced in C3H mice relative to B6;129 mice.*

Specific Aim 1: Changes in tissue composition (Raman Microspectroscopy), bone formation (dynamic histomorphometry), cross-sectional geometry and mineralization (microCT), mechanical properties (four-point bending) and mRNA expression (qRT-PCR) will be investigated in the tibiae of 8 and 11 week old male bgn-deficient mice bred on B6;129 and C3H backgrounds to uncover an inbred strain-specific response to bgn-deficiency at the ultrastructural level, the tissue-level and the structural (whole bone) level.

***Hypothesis 2:** The bones from wild type B6;129 mice will be more responsive to exercise versus control mice than the bones from C3H mice. Compared with the lack of response in C3H mice, increased bone formation and altered tissue composition will result in increased mechanical strength of the bone at the whole bone and tissue levels in B6;129 mice versus B6;129 control mice .*

Specific Aim 2: At 11 weeks of age, following 21 consecutive days of training, the response to running will be investigated in wild type mice bred on B6;129 and C3H backgrounds. Changes in tissue composition (Raman Microspectroscopy), bone formation (dynamic histomorphometry), cross-sectional geometry and mineralization (microCT) and mechanical properties (four-point bending) will be investigated to assess the effects of growth and exercise to uncover an inbred strain-specific response to exercise at the ultrastructural level, the tissue-level and the structural (whole bone) level.

Hypothesis 3: *The bones from bgn-deficient B6;129 mice will be more responsive to exercise than the bones from C3H mice compared with control mice from the same inbred strain. Compared with the response in C3H mice, increased bone formation and altered tissue composition will result in increased mechanical strength of the bone at the whole bone and tissue level in B6;129 mice versus control mice. Exercise-induced changes will compensate for phenotypic deficiencies in tissue strength and bone size, and ultimately structural strength in B6;129 mice while the bgn-deficient phenotype in C3H mice will remain unchanged.*

Specific Aim 3: At 11 weeks of age, following 21 consecutive days of training, the response to running will be investigated in bgn-deficient mice bred on B6;129 and C3H backgrounds. Changes in tissue composition (Raman Microspectroscopy), bone formation (dynamic histomorphometry), cross-sectional geometry and mineralization (microCT) and mechanical properties (four-point bending) will be investigated to assess the effects of growth and exercise as a function of inbred strain to uncover an inbred strain-specific response to exercise at the ultrastructural level, the tissue-level and the structural (whole bone) level. Bgn-deficient exercise and control mice will also be compared with wild type control mice from the same inbred strain to assess the ability of exercise to compensate for phenotypic deficiencies in bone size and strength.

Chapter 2 of this dissertation describes studies demonstrating the bone and gender specific nature of bgn-deficiency in C57BL6/129 mice. At 11 weeks of age, the phenotype was most prominent in the tibiae of male mice, resulting in larger, more highly mineralized bones with target deficiencies in pre-yield mechanical properties. Chapter 3

discusses the effects of running on male and female C57BL6/129 mice between 8 and 11 weeks of age. The exercise model preferentially impacted the male tibiae, where greater size and mineralization compared with control mice resulted in increased post-yield mechanical behavior at the expense of pre-yield mechanical properties. Chapter 4 addresses hypothesis 1, and results indicate that the bgn-deficient phenotype is inbred-strain specific at both 8 and 11 weeks, impacting chemical, geometric and mechanical properties in the C57BL6/129 mice with limited effects in the C3H mice. Chapter 5 addresses hypothesis 2 and the response of wild type mice within each inbred strain to exercise. While neither inbred strain had increased bone formation in response to exercise, C57BL6/129 mice had the hypothesized increase in post-yield mechanical properties in response to exercise compared with control mice while the C3H mice were unresponsive. The remainder of chapter 5 addresses hypothesis 3 by discussing the effects of exercise in bgn-deficient mice bred on the B6;129 and C3H inbred strains. Exercise had relatively little effect in the bgn-deficient mice from either inbred strain. The main effects of exercise were seen when comparing bgn-deficient exercise mice with wild type control mice. In C57BL6/129 mice, exercise compensated for tissue-level mechanical deficiencies caused by bgn deficiency through alterations in the chemical makeup of the tissue. However, exercise failed to compensate for phenotypic deficiencies in cross-sectional size and, therefore, structural-level mechanical deficiencies were not impacted. In the C3H mice, the combination of bgn-deficiency and exercise failed to change the bgn-deficient phenotype and failed to impact the mechano-responsiveness of the C3H bones. Finally, Chapter 6 discusses the implications this research has to the engineering, biological and clinical communities and proposes future studies to further elucidate changes that occur in response to bgn-deficiency and exercise.

Taken as a whole, this dissertation establishes for the first time that an inbred strain-specific response to a genetic deletion exists, further develops the roles that biglycan plays in the chemical and physical makeup of bone *in vivo* and links these roles with bone mechanical integrity. Additionally, it is demonstrated that mechanical loading can impact the mechanical integrity of bone via changes in tissue composition and quality independent of change in bone size. These studies provide new insights into inbred strain research which has important implications to the design and interpretation of

experimental investigations into the effects of genetic deficiencies on skeletal structure and function.

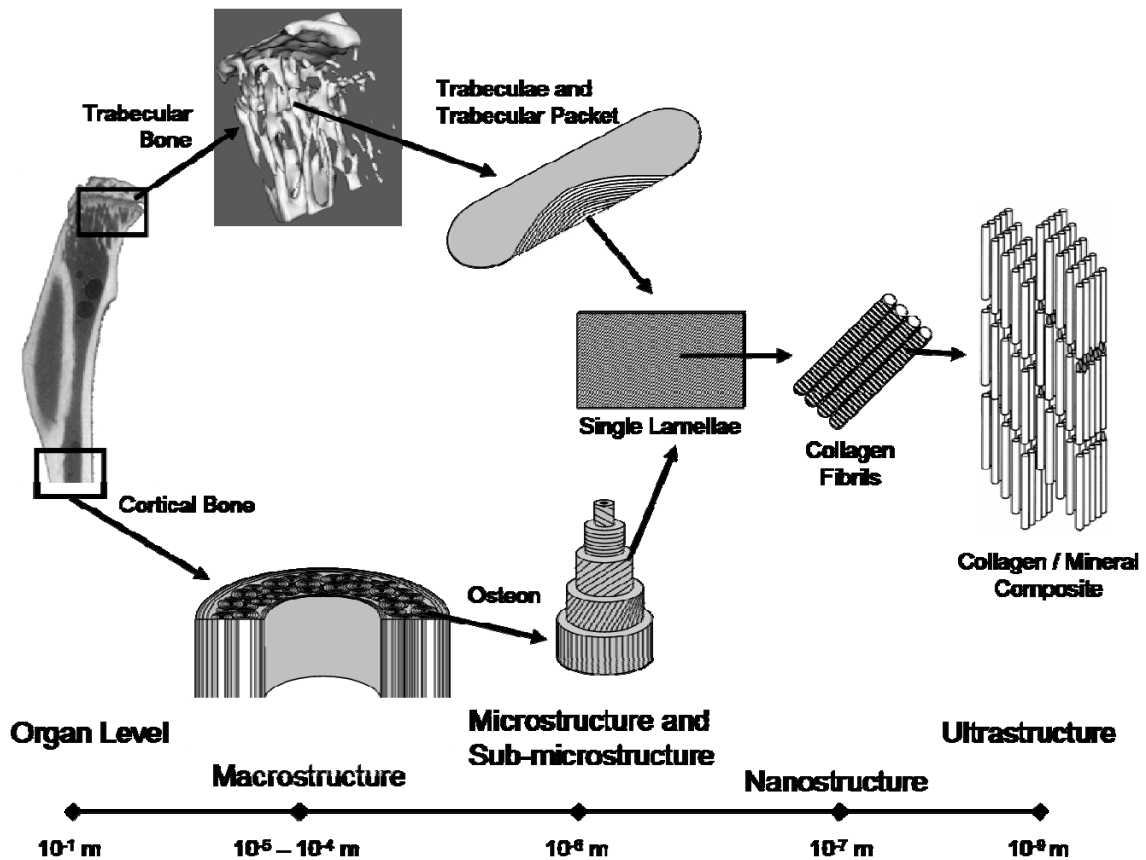


Figure 1.1: The Hierarchical Structure of Bone. At the organ (structural) level, each bone represents one of the 206 bones that make up the adult skeleton. At the macrostructural level, bone is distinguished into the intermediate structures of cortical (compact) and trabecular (cancellous or spongy) bone. The underlying microstructure of cortical bone is composed of osteons, while that of cancellous bone is made up of trabeculae. Trabeculae and osteons are each composed of sheet-like lamellae, which represent the arrangement of parallel-aligned collagen fibrils. At the ultrastructural level, these fibrils are a two phase composite material composed of a ductile organic phase that is impregnated with a stiff, reinforcing mineral phase. This image was adapted from [64].

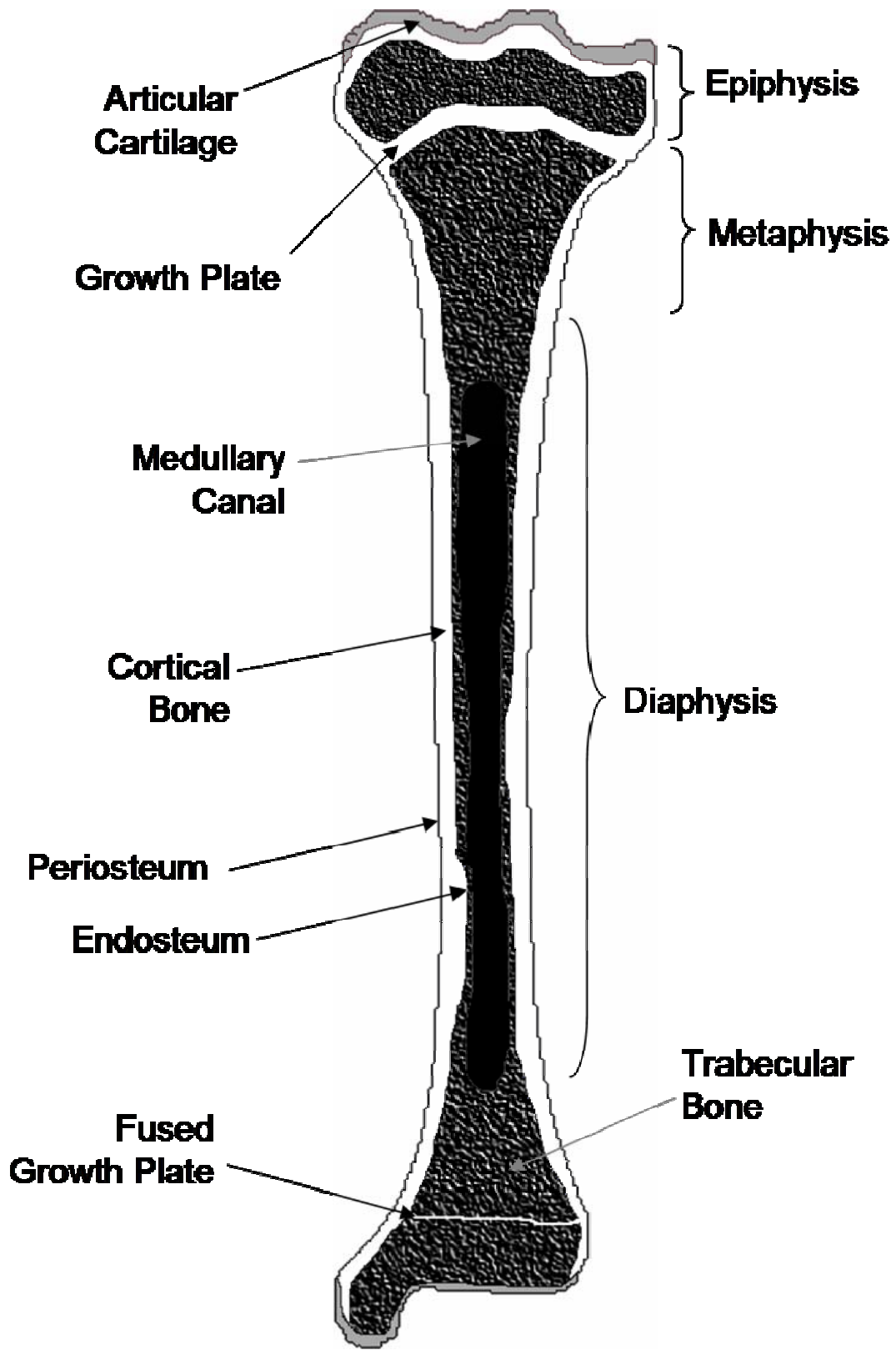


Figure 1.2: Anatomical Structure of a Long Bone

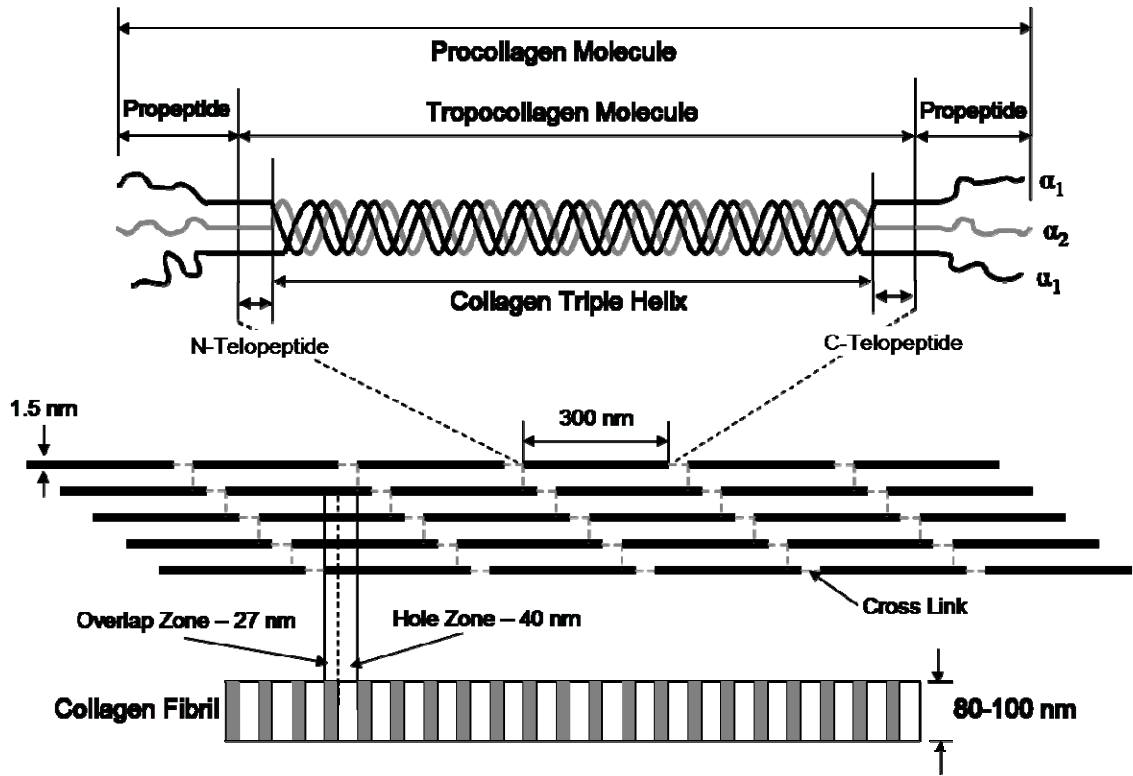


Figure 1.3: Collagen fibril structure. Fibrils are composed of individual collagen molecules that are assembled into a staggered array creating a structure that is 80-100 μm in width. This image is not to scale. This image was adapted from [65]

References

- (1) U.S. Department of Health and Human Services, Office of the Surgeon General (2004) Bone Health and Osteoporosis: A Report of the Surgeon General.
- (2) NIH Consensus Development Panel on Osteoporosis Prevention, Diagnosis, and Therapy (2001) Osteoporosis prevention, diagnosis, and therapy. *JAMA* 285:785-795
- (3) Burr DB, Forwood MR, Fyhrie DP, Martin RB, Schaffler MB, Turner CH (1997) Bone microdamage and skeletal fragility in osteoporotic and stress fractures. *J.Bone Miner.Res.* 12:6-15
- (4) POSNER AS, DUYCKAERTS G (1954) Infrared study of the carbonate in bone, teeth and francolite. *Experientia* 10:424-425
- (5) Roseberry HH, Hastings AB, Morse JK (1931) X-Ray Analysis of Bone and Teeth. *J.Biol.Chem.* 90:395-409
- (6) Weiner S, Traub W (1992) Bone structure: from angstroms to microns. *FASEB J.* 6:879-885
- (7) Knott L, Bailey AJ (1998) Collagen cross-links in mineralizing tissues: a review of their chemistry, function, and clinical relevance. *Bone* 22:181-187
- (8) Oxlund H, Barckman M, Ortoft G, Andreassen TT (1995) Reduced concentrations of collagen cross-links are associated with reduced strength of bone. *Bone* 17:365S-371S
- (9) Corsi A, Xu T, Chen XD, Boyde A, Liang J, Mankani M, Sommer B, Iozzo RV, Eichstetter I, Robey PG, Bianco P, Young MF (2002) Phenotypic effects of biglycan deficiency are linked to collagen fibril abnormalities, are synergized by decorin deficiency, and mimic Ehlers-Danlos-like changes in bone and other connective tissues. *J.Bone Miner.Res.* 17:1180-1189
- (10) Wiberg C, Hedbom E, Khairullina A, Lamande SR, Oldberg A, Timpl R, Morgelin M, Heinegard D (2001) Biglycan and decorin bind close to the n-terminal region of the collagen VI triple helix. *J.Biol.Chem.* 276:18947-18952
- (11) Schonherr E, Witsch-Prehm P, Harrach B, Robenek H, Rauterberg J, Kresse H (1995) Interaction of biglycan with type I collagen. *J.Biol.Chem.* 270:2776-2783
- (12) Hocking AM, Shinomura T, McQuillan DJ (1998) Leucine-rich repeat glycoproteins of the extracellular matrix. *Matrix Biol.* 17:1-19

- (13) Chen XD, Fisher LW, Robey PG, Young MF (2004) The small leucine-rich proteoglycan biglycan modulates BMP-4-induced osteoblast differentiation. *FASEB J.* 18:948-958
- (14) Ruoslahti E (1989) Proteoglycans in cell regulation. *J.Biol.Chem.* 264:13369-13372
- (15) Takagi M, Yamada T, Kamiya N, Kumagai T, Yamaguchi A (1999) Effects of bone morphogenetic protein-2 and transforming growth factor-beta1 on gene expression of decorin and biglycan by cultured osteoblastic cells. *Histochem.J.* 31:403-409
- (16) Yamada T, Kamiya N, Harada D, Takagi M (1999) Effects of transforming growth factor-beta1 on the gene expression of decorin, biglycan, and alkaline phosphatase in osteoblast precursor cells and more differentiated osteoblast cells. *Histochem.J.* 31:687-694
- (17) Fisher LW, Termine JD, Dejter SW, Jr, Whitson SW, Yanagishita M, Kimura JH, Hascall VC, Kleinman HK, Hassell JR, Nilsson B (1983) Proteoglycans of developing bone. *J.Biol.Chem.* 258:6588-6594
- (18) Bianco P, Fisher LW, Young MF, Termine JD, Robey PG (1990) Expression and localization of the two small proteoglycans biglycan and decorin in developing human skeletal and non-skeletal tissues. *J.Histochem.Cytochem.* 38:1549-1563
- (19) Matsuura T, Duarte WR, Cheng H, Uzawa K, Yamauchi M (2001) Differential expression of decorin and biglycan genes during mouse tooth development. *Matrix Biol.* 20:367-373
- (20) Chen XD, Shi S, Xu T, Robey PG, Young MF (2002) Age-related osteoporosis in biglycan-deficient mice is related to defects in bone marrow stromal cells. *J.Bone Miner.Res.* 17:331-340
- (21) Chen XD, Allen MR, Bloomfield S, Xu T, Young M (2003) Biglycan-deficient mice have delayed osteogenesis after marrow ablation. *Calcif.Tissue Int.* 72:577-582
- (22) Ameye L, Aria D, Jepsen K, Oldberg A, Xu T, Young MF (2002) Abnormal collagen fibrils in tendons of biglycan/fibromodulin-deficient mice leads to gait impairment, ectopic ossification, and osteoarthritis. *The FASEB Journal* 16:673-680
- (23) Wallace JM, Rajachar RM, Chen XD, Shi S, Allen MR, Bloomfield SA, Les CM, Robey PG, Young MF, Kohn DH (2006) The mechanical phenotype of biglycan-deficient mice is bone- and gender-specific. *Bone* 39:106-116

- (24) Boskey AL, Moore DJ, Amling M, Canalis E, Delany AM (2003) Infrared analysis of the mineral and matrix in bones of osteonectin-null mice and their wildtype controls. *J.Bone Miner.Res.* 18:1005-1011
- (25) Camacho NP, Hou L, Toledano TR, Ilg WA, Brayton CF, Raggio CL, Root L, Boskey AL (1999) The material basis for reduced mechanical properties in oim mice bones. *J.Bone Miner.Res.* 14:264-272
- (26) Akhter MP, Wells DJ, Short SJ, Cullen DM, Johnson ML, Haynatzki GR, Babij P, Allen KM, Yaworsky PJ, Bex F, Recker RR (2004) Bone biomechanical properties in LRP5 mutant mice. *Bone* 35:162-169
- (27) Kozloff KM, Carden A, Bergwitz C, Forlino A, Uveges TE, Morris MD, Marini JC, Goldstein SA (2004) Brittle IV mouse model for osteogenesis imperfecta IV demonstrates postpubertal adaptations to improve whole bone strength. *J.Bone Miner.Res.* 19:614-622
- (28) Dabovic B, Levasseur R, Zambuto L, Chen Y, Karsenty G, Rifkin DB (2005) Osteopetrosis-like phenotype in latent TGF-beta binding protein 3 deficient mice. *Bone* 37:25-31
- (29) Xu T, Bianco P, Fisher LW, Longenecker G, Smith E, Goldstein S, Bonadio J, Boskey A, Heegaard AM, Sommer B, Satomura K, Dominguez P, Zhao C, Kulkarni AB, Robey PG, Young MF (1998) Targeted disruption of the biglycan gene leads to an osteoporosis-like phenotype in mice. *Nat.Genet.* 20:78-82
- (30) Boskey AL, Young MF, Kilts T, Verdelis K (2005) Variation in mineral properties in normal and mutant bones and teeth. *Cells Tissues Organs* 181:144-153
- (31) Ameye L, Young MF (2002) Mice deficient in small leucine-rich proteoglycans: novel in vivo models for osteoporosis, osteoarthritis, Ehlers-Danlos syndrome, muscular dystrophy, and corneal diseases. *Glycobiology* 12:107R-16R
- (32) Wolff J (1892) *Das gesetz der transformation der knochen*. August Hirschwald, Berlin
- (33) Khan K, McKay HA, Haapasalo H, Bennell KL, Forwood MR, Kannus P, Wark JD (2000) Does childhood and adolescence provide a unique opportunity for exercise to strengthen the skeleton? *J.Sci.Med.Sport* 3:150-164
- (34) Heinonen A, Sievanen H, Kannus P, Oja P, Pasanen M, Vuori I (2000) High-impact exercise and bones of growing girls: a 9-month controlled trial. *Osteoporos.Int.* 11:1010-1017

- (35) Mackelvie KJ, McKay HA, Khan KM, Crocker PR (2001) A school-based exercise intervention augments bone mineral accrual in early pubertal girls. *J.Pediatr.* 139:501-508
- (36) Sahar ND, Kohn DH, Golcuk K, Morris MD Effects of Exercise on Bone Quality As Shown By Raman Microspectroscopy, paper No. 1619. 2006 Annual Meeting of the Orthopaedic Society
- (37) Wallace JM, Rajachar RM, Allen MR, Bloomfield SA, Robey PG, Young MF, Kohn DH (2007) Exercise-Induced Changes in the Cortical Bone of Growing Mice are Bone- and Gender-Specific. *Bone* 40:1120-1127
- (38) Rubin C, Turner AS, Bain S, Mallinckrodt C, McLeod K (2001) Anabolism. Low mechanical signals strengthen long bones. *Nature* 412:603-604
- (39) Rubin C, Recker R, Cullen D, Ryaby J, McCabe J, McLeod K (2004) Prevention of postmenopausal bone loss by a low-magnitude, high-frequency mechanical stimuli: a clinical trial assessing compliance, efficacy, and safety. *J.Bone Miner.Res.* 19:343-351
- (40) Ward K, Alsop C, Caulton J, Rubin C, Adams J, Mughal Z (2004) Low magnitude mechanical loading is osteogenic in children with disabling conditions. *J.Bone Miner.Res.* 19:360-369
- (41) Davisson MT (1996) Genetic variants and strains of the laboratory mouse. In: M. F. Lyon, S. Rastan and S. D. M. Brown, (eds) Oxford University Press, Oxford ; New York : p 1532
- (42) Klein RF, Mitchell SR, Phillips TJ, Belknap JK, Orwoll ES (1998) Quantitative trait loci affecting peak bone mineral density in mice. *J.Bone Miner.Res.* 13:1648-1656
- (43) Beck JA, Lloyd S, Hafezparast M, Lennon-Pierce M, Eppig JT, Festing MF, Fisher EM (2000) Genealogies of mouse inbred strains. *Nat.Genet.* 24:23-25
- (44) Beamer WG, Donahue LR, Rosen CJ, Baylink DJ (1996) Genetic variability in adult bone density among inbred strains of mice. *Bone* 18:397-403
- (45) Wergedal JE, Sheng MH, Ackert-Bicknell CL, Beamer WG, Baylink DJ (2005) Genetic variation in femur extrinsic strength in 29 different inbred strains of mice is dependent on variations in femur cross-sectional geometry and bone density. *Bone* 36:111-122
- (46) Sheng MH, Baylink DJ, Beamer WG, Donahue LR, Rosen CJ, Lau KH, Wergedal JE (1999) Histomorphometric studies show that bone formation and

bone mineral apposition rates are greater in C3H/HeJ (high-density) than C57BL/6J (low-density) mice during growth. *Bone* 25:421-429

- (47) Turner CH, Hsieh YF, Muller R, Bouxsein ML, Baylink DJ, Rosen CJ, Grynpas MD, Donahue LR, Beamer WG (2000) Genetic regulation of cortical and trabecular bone strength and microstructure in inbred strains of mice. *J.Bone Miner.Res.* 15:1126-1131
- (48) Koller DL, Schriefer J, Sun Q, Shultz KL, Donahue LR, Rosen CJ, Foroud T, Beamer WG, Turner CH (2003) Genetic effects for femoral biomechanics, structure, and density in C57BL/6J and C3H/HeJ inbred mouse strains. *J.Bone Miner.Res.* 18:1758-1765
- (49) Schriefer JL, Robling AG, Warden SJ, Fournier AJ, Mason JJ, Turner CH (2005) A comparison of mechanical properties derived from multiple skeletal sites in mice. *J.Biomech.* 38:467-475
- (50) Akhter MP, Iwaniec UT, Covey MA, Cullen DM, Kimmel DB, Recker RR (2000) Genetic variations in bone density, histomorphometry, and strength in mice. *Calcif.Tissue Int.* 67:337-344
- (51) Akhter MP, Fan Z, Rho JY (2004) Bone intrinsic material properties in three inbred mouse strains. *Calcif.Tissue Int.* 75:416-420
- (52) Sheng MH, Baylink DJ, Beamer WG, Donahue LR, Lau KH, Wergedal JE (2002) Regulation of bone volume is different in the metaphyses of the femur and vertebra of C3H/HeJ and C57BL/6J mice. *Bone* 30:486-491
- (53) Sheng MH, Lau KH, Beamer WG, Baylink DJ, Wergedal JE (2004) In vivo and in vitro evidence that the high osteoblastic activity in C3H/HeJ mice compared to C57BL/6J mice is intrinsic to bone cells. *Bone* 35:711-719
- (54) Sheng MH, Lau KH, Mohan S, Baylink DJ, Wergedal JE (2006) High osteoblastic activity in C3H/HeJ mice compared to C57BL/6J mice is associated with low apoptosis in C3H/HeJ osteoblasts. *Calcif.Tissue Int.* 78:293-301
- (55) Akhter MP, Cullen DM, Pedersen EA, Kimmel DB, Recker RR (1998) Bone response to in vivo mechanical loading in two breeds of mice. *Calcif.Tissue Int.* 63:442-449
- (56) Kodama Y, Dimai HP, Wergedal J, Sheng M, Malpe R, Kutilek S, Beamer W, Donahue LR, Rosen C, Baylink DJ, Farley J (1999) Cortical tibial bone volume in two strains of mice: effects of sciatic neurectomy and genetic regulation of bone response to mechanical loading. *Bone* 25:183-190

- (57) Kodama Y, Umemura Y, Nagasawa S, Beamer WG, Donahue LR, Rosen CR, Baylink DJ, Farley JR (2000) Exercise and mechanical loading increase periosteal bone formation and whole bone strength in C57BL/6J mice but not in C3H/HeJ mice. *Calcif.Tissue Int.* 66:298-306
- (58) Amblard D, Lafage-Proust MH, Laib A, Thomas T, Ruegsegger P, Alexandre C, Vico L (2003) Tail suspension induces bone loss in skeletally mature mice in the C57BL/6J strain but not in the C3H/HeJ strain. *J.Bone Miner.Res.* 18:561-569
- (59) Marusic A, Katavic V, Grcevic D, Lukic IK (1999) Genetic variability of new bone induction in mice. *Bone* 25:25-32
- (60) Li X, Gu W, Masinde G, Hamilton-Ulland M, Rundle CH, Mohan S, Baylink DJ (2001) Genetic variation in bone-regenerative capacity among inbred strains of mice. *Bone* 29:134-140
- (61) Hadi N, Price C, Nasser P, Morgan E, Einhorn TA, Gerstenfeld LC, Jepsen KJ Genetic Variation In The Regain of Bone Strength During Fracture Healing, Paper No. 0225. 2007 Annual Meeting of the Orthopaedic Society
- (62) Alam I, Warden SJ, Robling AG, Turner CH (2005) Mechanotransduction in bone does not require a functional cyclooxygenase-2 (COX-2) gene. *J.Bone Miner.Res.* 20:438-446
- (63) Li CY, Jepsen KJ, Majeska RJ, Zhang J, Ni R, Gelb BD, Schaffler MB (2006) Mice lacking cathepsin K maintain bone remodeling but develop bone fragility despite high bone mass. *J.Bone Miner.Res.* 21:865-875
- (64) Rho JY, Kuhn-Spearing L, Zioupos P (1998) Mechanical properties and the hierarchical structure of bone. *Med.Eng.Phys.* 20:92-102
- (65) Nyman JS, Reyes M, Wang X (2005) Effect of ultrastructural changes on the toughness of bone. *Micron* 36:566-582

CHAPTER 2

THE MECHANICAL PHENOTYPE OF BIGLYCAN DEFICIENT MICE IS BONE AND GENDER SPECIFIC

Introduction

The bone extracellular matrix (ECM) is approximately one-third organic material by weight. This organic portion of bone is composed of type I collagen (roughly 90%) and a multitude of non-collagenous proteins [1]. Since one of bone's primary functions is to provide a mechanical support system for muscular activity, skeletal structure and function are heavily influenced by mechanical principles [2]. The strength and toughness of bone are derived from the organized mineralization of the ECM [3-7], which is dependent on many factors including age [8, 9], gender [10-13], genetic makeup [14-17], anatomic location [18-20] and mechanical milieu [21-23]. Over the past 20 years, particular attention has been paid to a group of molecules in the ECM called small leucine-rich proteoglycans (SLRPs) which, during the development and repair of bone, regulate ECM organization and mineralization by interacting with other matrix molecules [24-26] and growth factors [27-31] and directing their function. Specifically, in *in vitro* studies, SLRPs interact with the surface of collagen fibrils, regulating fibril formation, size and morphology [26, 32], while also being implicated in mineralization [24, 33].

Biglycan (bgn) is a SLRP that is enriched in the ECM of bone and other specialized connective tissues including cartilage, muscle and the keratinocyte layer of the skin [27, 34-36]. Bgn is an X-linked gene that plays a role in the postnatal spatial patterning of bone [37] and appears to be directly involved in the growth and differentiation of osteoblast precursor cells [30]. While extensive work has been performed trying to uncover the structure of bgn and its role in bone formation and mineralization at the molecular level [32, 34, 35, 38], the role of bgn in regulating higher levels of organization, such as geometric and mechanical properties of bone, is not well

understood. Bgn-deficient mice displayed reduced skeletal growth, characterized by reduced trabecular bone volume in the femora by 3 months of age and reduced cortical thickness in the femora at 9 months [39]. Consistent with reduced bone volume at 3 months of age, bgn-deficient males show trends toward decreased failure load and yield energy in the femora compared with wild type males, and these trends become statistically significant at 6 months [39]. Beyond these limited studies, the mechanical and geometric effects of bgn-deficiency on bone are unknown.

In vitro, bone marrow stromal cells from bgn-deficient male mice show increased apoptosis and decreased proliferation compared to cells from wild type mice, as well as lower colony forming efficiency in response to exogenous TGF- β [38]. In the femoral metaphyses of 3 month old bgn-deficient males, osteoblast number is decreased, while osteoclast number is unchanged compared to wild type littermates [39]. Consistent with these cellular responses, trabecular mineral apposition rate and bone formation rate are decreased. The collective tissue and cellular-level data suggest that the bone phenotype may be due to a deficiency in matrix formation and/or mineralization. Contrary to the response in males, trabecular bone volume was unaffected while mineral apposition rate was increased in bgn-deficient female tibiae compared to wild type females, suggesting a gender specific response to bgn deficiency [40].

From studies of inbred [14-17] and congenic [20, 41] mouse strains and identification of quantitative trait loci (QTLs) responsible for bone geometric and mechanical properties [11, 13, 42, 43], it is known that the genetic control of bone is both local (bone and regional specific) and gender specific. Further, there is evidence of gender specific effects associated with genetic deficiencies [40, 44, 45]. It is therefore hypothesized that a genetic disruption, in this case an engineered deletion of the gene encoding biglycan, will result in a cortical bone mechanical phenotype, defined here by geometric, material, and mechanical properties, that is bone and gender specific. Because of biglycan's role in regulating bone matrix structural organization, the bgn-deficient mechanical phenotype will be manifested by decreased tissue-level strength which will detrimentally impact structural mechanical integrity. This study characterizes the bgn-deficient mechanical phenotype in mice at 11 weeks of age in the cortical bone at the mid-diaphysis of the femora and tibiae of both genders. Phenotypic changes relative to

wild type controls are assayed by four-point bending tests to determine mechanical properties at the whole bone (structural) and tissue levels, as well as analyses of bone geometry and bone formation using histomorphometry.

Materials and Methods

Animals

All animal procedures were performed at the National Institute of Dental and Craniofacial Research (NIDCR) with NIDCR Institutional Animal Care and Use Committee approval (NIDCR animal approval protocol #NIDCR 001-151). Inbred lines of bgn-deficient and wild type mice were bred on a C57BL6/129 background. Bgn-deficient mice were originally generated by homologous recombination in embryonic stem cells [39]. Genotyping of the F1 generation of mice was performed via standard polymerase chain reaction (PCR) using DNA extracted from the tail of each mouse. PCR products were determined using agarose gel electrophoresis yielding bands of 212 (wild type allele) and 310 (disrupted allele) base pairs.

To determine proper sample sizes for detecting effects of genotype across bones and gender, power calculations were performed based on measured differences and standard deviations in mechanical and geometric properties due to Bgn deficiency [39] using a value of $\alpha=0.05$ and a power ($1-\beta$) of 0.80 [46]. Twenty mice from each gender (2 genotypes, 10 mice per group) were housed in standard cages and given access to food, water and cage activity ad libitum. In order to assess bone formation during the last 3 weeks of the experiment (8-11 weeks of age), all mice were given a single intraperitoneal (IP) injection of tetracycline (20 mg per kg body weight) at day -20 before sacrifice and a single IP injection of calcein (15 mg per kg body weight) at day -6 before sacrifice. All mice were sacrificed at 11 weeks of age, at which time body weight was measured and both femora and tibiae were harvested, stripped of soft tissue and stored in either 70% ethanol at 4°C (for peripheral quantitative computed tomography (pQCT) and histology) or in a Ca^{2+} -buffered saline solution at -65°C (for mechanical testing) [47].

Mechanical Testing

Left femora and tibiae were tested to failure in 4 point bending in displacement control using a custom-designed, solenoid driven loading apparatus with a support span (L) of 6 mm and a loading span of 4 mm at a rate of 0.01 mm/sec [48]. Before testing, the length of each femur was measured from the greater trochanter to the most distal portion of the femoral chondyles and the length of each tibia was measured from the most proximal portion of the tibial chondyles to the most distal portion of the medial malleolus using digital calipers accurate to 0.01 mm (Mitutoyo, Aurora, IL). Femora were tested in the anterior-posterior (AP) direction (posterior surface in compression) with the middle of the bone positioned halfway between the two supports. Tibiae were tested in the medial-lateral (ML) direction (lateral surface in compression). The tibiae were positioned such that the most distal portion of the junction of the tibia and fibula (TFJ) was aligned with the left-most support point. During each test, load and deflection were recorded, from which structural strength (force at yield and ultimate force), energy or work (measured as the area under the force vs. displacement curve to yield and to failure), stiffness (the slope of the linear portion of the force vs. displacement curve) and deformation (displacement to yield, total displacement and post-yield displacement) were derived at the whole bone level.

During each test, the bone was closely monitored and the point of fracture initiation was noted. Because fractures often propagated at an angle across the bone (i.e. oblique fractures), the half of the fractured bone containing both the fracture initiation site and a full planar section of bone at that site was processed for histology, embedded, and sectioned as described below (see histomorphometry section). The jagged edge of the bone was trimmed off, and a 200 μm thick planar section was used to determine geometric parameters (average cortical thickness from four quadrants, cortical area and AP and ML diameters) using a light microscope and digital analysis software (Nikon Eclipse TE 300, Image Pro-Plus v4.5, Matlab v5.3). The moment of inertia about the axis of bending was measured from each section using a Matlab script [49]. Together with the load and deflection data, the distance from the centroid to the surface of the bone in tension, c , and moment of inertia were used to derive estimated tissue-level mechanical properties from standard beam-bending equations for 4 point bending:

$$\text{Stress} = \sigma = \frac{Fac}{2 * I} \quad (\text{MPa})$$

$$\text{Strain} = \varepsilon = \frac{6cd}{a(3L - 4a)} * 10^6 \quad (\mu\varepsilon)$$

In these equations, F is the force, d is the displacement, a is the distance from the support to the inner loading point (1 mm), L is the span between the outer supports (6 mm) and I is moment of inertia. The modulus of elasticity was calculated as the slope of the linear portion of the stress vs. strain curve.

Peripheral Quantitative Computed Tomography (pQCT)

Ex vivo scans of right femora and tibiae from the male mice were performed using an XCT Research-M device (Stratec Corp., Norland, Fort Atkinson, WI) [37]. Machine calibration was performed using a hydroxyapatite cone phantom. Scans were performed at a CT speed of 2.5 mm/sec with a voxel resolution of 0.07 x 0.07 x 0.50 mm and a scanning beam thickness of 0.50 mm. Two slices were scanned at the mid-diaphysis of each bone (50% of the total bone length \pm 0.50 mm). A standardized analysis of diaphyseal bone (threshold of 700 mg/cm³) was applied to each section. Values of total bone mineral content (BMC, coefficient of variation = \pm 1.18 %) and total volumetric bone mineral density (vBMD, coefficient of variation = \pm 0.63 %) obtained for each of the sites were averaged to get mean values.

Histomorphometry

Right tibiae from all animals (male bones were used following pQCT) were dehydrated in graded ethanol (70%, 95%, 100%) at 4°C, defatted in acetone and infiltrated in a liquid methyl methacrylate monomer (Koldmount™ Cold Mounting Liquid, Mager Scientific). The bones were then embedded in methyl methacrylate (Koldmount™ Cold Mounting Kit, Mager Scientific) and sectioned using a low-speed sectioning saw (South Bay Technology, Model 650, San Clemente, CA) with a diamond wafering blade (Mager Scientific, Dexter, MI). Sections 200 μ m thick were made at the mid-diaphysis, 1 to 2 mm proximal to the TFJ, and were hand ground and polished to a

final thickness of between 50 and 75 μm using wet silicon carbide abrasive discs. Sections were imaged using the Nikon DAPI-FITC-TRITC triple band filter combination (DAPI excitation at 385-400 nm and emission at 450-465 nm; FITC excitation at 475-490 nm and emission at 505-535 nm; TRITC excitation at 545-565 nm and emission at 580-620 nm) at a magnification of 200X and analyzed using digital analysis software (Nikon Eclipse TE 300, Image Pro-Plus v4.1). All histomorphometric analyses were performed using standard ASBMR methods and nomenclature [50]. Single and double labeled surfaces (sLs; dLs) were measured on both the endocortical and periosteal surfaces, from which endocortical and periosteal mineralizing surfaces (Es.MS; Ps.MS) were determined and normalized to the total corresponding surface length. The center-to-center interlabel distance was measured on each surface to determine mineral apposition rate (MAR). MS and MAR were further used to calculate bone formation rate (BFR = $\text{MAR} \times \text{MS}$) at each surface.

Statistical Analysis

All data are presented as mean \pm standard error of the mean (SEM). Statistical analyses were performed on body mass and all geometric, mechanical, histomorphometric and bone mineral parameters in each gender and/or bone using an ANOVA checking for effects of genotype, followed by post-hoc Student-Newman-Keuls tests (Sigma Stat 2.0, Jandel Scientific). A value of $p < 0.05$ was considered significant while a p -value between 0.05 and 0.10 was also noted as a trend. In order to assess any predictive relationships between geometric and structural-level mechanical properties, tissue-level mechanical properties and structural-level mechanical properties or bone mineral density and structural or tissue-level mechanical properties, Pearson's Product-Moment Correlations were performed within each subgroup (e.g. bgn-deficient male tibiae).

Results

The geometric and mechanical phenotypes associated with bgn deficiency are bone and gender specific in 11 week old mice. Bgn-deficient males exhibited geometric

and mechanical changes almost exclusively in the tibiae (Figure 2.1 and Figure 2.4), with little effect seen in the femora (Table 2.1-Table 2.3). In contrast, bgn-deficient females demonstrated changes to a much lesser degree than the males, and in the femora (Table 2.1 and Table 2.2) rather than the tibiae (Figure 2.2A). Both bgn-deficient males and females had significantly lower body mass at 11 weeks of age compared to wild types [(wild type male= 26.55 ± 0.61 g, bgn-deficient male= 23.73 ± 0.76 g; $p < 0.02$); (wild type female= 20.84 ± 0.60 g, bgn-deficient females= 17.56 ± 0.88 g; $p < 0.01$)].

Phenotypic Changes in Biglycan-Deficient Male Tibiae

The most significant geometric and mechanical effects of bgn-deficiency were displayed in the male tibiae (Figure 2.1 and Figure 2.2). Bgn-deficient male tibiae were significantly shorter than those of their wild type counterparts (Figure 2.1A, $p < 0.012$). This decrease in longitudinal growth was in contrast to increased radial growth, characterized by increased ML width (Figure 2.1B, $p < 0.007$) and moment of inertia (Figure 2.1C, $p < 0.031$). Also, the AP/ML ratio was significantly closer to a value of 1 in bgn-deficient males (Figure 2.1B, $p < 0.05$). Improved geometric properties were not accompanied by changes in MS (Figure 2.3A), MAR (Figure 2.3B) or BFR (Figure 2.3C), though endocortical surface trends suggest increased matrix formation activity in the bgn-deficient males (29%, 14% and 27% increases in Es.MS, Es.MAR and Es.BFR respectively). The bgn-deficient male tibial diaphyses also had significantly greater vBMD (Figure 2.4A, $p < 0.001$) than wild type males, though there was no change in BMC (Figure 2.4B). Together with larger cross-sectional dimensions and increased mineral density, bgn-deficient male tibiae exhibited significant decreases in tissue-level yield strength (Figure 2.2A, $p < 0.048$), structural elastic deformation (Figure 2.2B, $p < 0.038$) and structural work-to-yield (Figure 2.2C, $p < 0.044$), all of which are measures of pre-yield behavior. No statistically significant changes occurred in post-yield properties. There were significant negative correlations between geometric properties (ML width and moment of inertia, independent variables) and tissue-level yield strength, structural elastic deformation and structural work-to-yield in the bgn-deficient mice (Figure 2.5), but similar relationships did not exist in the wild type mice (Data not

shown). Further, there was no correlation between vBMD and any geometric or mechanical properties in either genotype (Data not shown).

Phenotypic Changes in Biglycan-Deficient Male Femora

There were few differences in the geometric and mechanical properties of bgn-deficient male femora versus wild type males (Table 2.1Table 2.3). There was a significant reduction in structural work-to-yield (Table 2.2, $p < 0.033$) and tissue-level yield strength (Table 2.3, $p < 0.026$) of the bgn-deficient male femoral diaphyses, and a marginal increase in BMC (Wild Type: 1.06 ± 0.05 mg/mm, bgn-deficient: 1.29 ± 0.06 mg/mm; $p < 0.058$). Femoral length was not different between the two groups (Table 2.1), and no other geometric or material parameters were affected.

Phenotypic Changes in Biglycan-Deficient Female Femora and Tibiae

Bgn-deficient females expressed an altered mechanical phenotype to a lesser degree than the male mice, and in the femur rather than the tibia (Figure 2.1Figure 2.3,Table 2.1Table 2.3). There were significant decreases in femoral structural strength (Table 2.2, $p < 0.023$) and work-to-failure (Table 2.2, $p < 0.017$), and marginal decreases in femoral length (Table 2.1, $p < 0.075$), AP/ML ratio (Table 2.1, $p < 0.079$), total structural deformation (Table 2.2, $p < 0.067$) and tissue-level strain to failure ($p < 0.08$) in the bgn-deficient females. No other properties were affected in the femora. The bgn-deficient female tibiae displayed no differences in cross-sectional geometry relative to the wild types (Figure 2.1). Tissue-level yield stress (Figure 2.2A, $p < 0.025$) was significantly greater in bgn-deficient females. No other mechanical properties were different in the tibiae (Figure 2.2), though periosteal mineralizing surface was marginally increased in bgn-deficient females compared to wild type animals (Figure 2.3A, $p < 0.075$).

Discussion

The mechanical phenotype in bgn-deficient mice, characterized by geometric, material, and mechanical properties, displayed bone and gender specificity in 11 week

old mice. In the two long bones examined in this study, *bgn*-deficient male mice exhibited geometric and mechanical changes almost exclusively in the tibial diaphysis with little effect in the femora. While several studies have shown bone specific responses to stimuli like exercise [18, 51] and hormonal treatment [19], most investigations evaluate multiple cancellous sites (femoral or tibial metaphyses or lumbar vertebrae) and/or a single cortical site. When characterizing the cortical bone phenotype of animals with an engineered genetic deficiency, the femoral diaphysis is the usual site chosen [11, 17, 20, 39, 45]. Data from this study demonstrate that in some genetically compromised mice, the tibia exhibits a more pronounced phenotype, and evaluation of just the femora may be insufficient to characterize the phenotype.

The *bgn*-deficient male tibial diaphyses exhibited enhanced cross sectional geometric properties compared with wild type males, including ML width and moment of inertia (Figure 2.1). The contribution of material quantity to strength increases as the square of the distance from the centroid, and therefore a high moment of inertia is favorable for structural stiffness and strength. The AP/ML ratio, a measure of the structural anisotropy of the bone, was reduced to a value closer to 1 in the *bgn*-deficient males, indicating tissue which is more isotropically distributed around the bone's centroidal axis. An AP/ML ratio closer to 1 reiterates the increase in ML width and suggests a bone that is more resistant to bending in the ML direction, the direction of mechanical testing in this study. Looking at the geometric data alone, one would therefore predict that the bones of the *bgn*-deficient male mice would be structurally stronger. In the tibiae of the *bgn*-deficient male mice, this is not the case (Figure 2.2D), indicating that geometric factors do not predict structural mechanical integrity.

Mineral is known to confer tissue-level stiffness and strength to bone. However, even though the volumetric bone mineral density (*vBMD*) was significantly increased in the cortical bone of the *bgn*-deficient male tibiae, there was a significant decrease in tissue-level yield strength. In this case, the result of a greater quantity of more highly mineralized tissue is a bone with lower structural pre-yield deformation and energy dissipation (Figure 2.2). No correlations were noted between *vBMD* and any geometric or mechanical properties (Data not shown). Energy dissipation negatively correlated with ML width (Figure 2.5C, $r=-0.892$, $p<0.001$) and moment of inertia (Figure 2.5F, $r=-$

0.851, $p < 0.001$). Similar correlations were found between ML width and moment of inertia and tissue-level strength and elastic deformation (Figure 2.5). These pre-yield mechanical deficits reinforce the notion that mechanical properties are dependent on both tissue quantity and quality, and increased quantity of material with an increased percentage of mineral may still be insufficient to increase structural mechanical properties if the quality of the tissue is poor.

The most likely interpretation for altered pre-yield properties is that the *bgn* gene deletion causes important alterations in mineral and/or the matrix/mineral ultrastructure. *Bgn* is most often implicated in the regulation of collagen fibril formation, size and morphology [26, 32]. The organic matrix of bone, which is predominantly Type I collagen, dictates post-yield behavior in bone [3, 9, 52-56], so it is reasonable to hypothesize that if collagen were being affected in *bgn*-deficient mice, post-yield mechanical changes would be present. However, pre-yield properties were exclusively altered in this case, and this is likely the result of changes in the mineral compartment of bone versus matrix changes [3, 57-59], suggesting a new understanding of the functional role of *bgn* in regulating bone mineralization in vivo. While SLRPs have not been directly implicated in the mineralization of bone in vivo, *bgn* has a strong affinity for apatite and calcium and facilitates initiation of apatite formation in vitro [33]. The ability for *bgn* to influence the mineral in bone in vivo is supported by the increase in volumetric bone mineral density in the *bgn*-deficient male tibial diaphysis (Figure 2.4), and locally altered mineral content and mineral to matrix ratios [24]. As bone in *bgn*-deficient mice is developing, the altered quality of the tissue may activate a compensatory increase in matrix formation and/or mineralization in an attempt to redistribute the tissue to a more structurally isotropic configuration with greater moment of inertia. It is also possible that the lack of *bgn* is influencing the integrity of the collagen network, and because the organic matrix forms the scaffold for mineral formation, changes in collagen could induce detrimental alterations in mineral organization leading to the decrease in strength noted [9, 52, 60].

It might seem contradictory that there were no differences in histomorphometric measures in the *bgn*-deficient male tibial diaphyses versus wild type animals, though large differences were noted in geometric properties. What we can conclude is that during

the window of time observed with fluorochrome labels, BFR was not greater in the bgn-deficient males. However, injections were given at Day -20 and -6 and therefore only measured BFR during weeks 8 and 10 of life. Therefore, the bone formation that led to greater geometric properties in the bgn-deficient mice likely occurred before this age and had slowed down by the time it was measured. This is consistent with the idea that osteopenia and decreased osteoblast activity caused by biglycan-deficiency are age-dependent, and become progressively worse as the animal ages [39].

The significant difference in body weight between bgn-deficient and wild type males is likely not responsible for the differences in tibial properties between genotypes. If body weight were having an effect, the lower body weight in the bgn-deficient males would impart lesser loads on the tibia, producing lower strains and a lesser bone formation response. Male tibial properties were normalized by body weight (data not shown) and while significance was marginalized in some cases (yield stress, work-to-yield) or disappeared (elastic deformation, length), other properties showed increased significance (ML width, moment of inertia) or newly acquired significance (increased cortical area, increased AP width, increased cortical thickness), and all trends were still in the same direction. Further, similar differences in body weight exist in bgn-deficient females versus wild type females, with no corresponding alteration in tibial properties. This suggests that while the body weight difference may play a role, it is alone not responsible for the altered properties of the bgn-deficient male tibiae.

There are some factors which may help explain the bone specificity seen in the male mice in response to bgn deficiency. Studies between inbred mouse strains have demonstrated that bone mechanical properties [14-17] as well as the mechanical response of bones to the local environment [21, 22, 61, 62] are under genetic control. It is possible that the specific genetic deficiency in this study impacts osteoblast progenitors, and therefore bone properties, in certain bones and not in others, leading to the bone specificity demonstrated. The mapping of quantitative trait loci (QTLs) [11, 13, 42, 43] for individual bone traits is a powerful tool and is rapidly uncovering discrete chromosomal locations that affect geometric parameters in individual bones. A second, but less likely factor is related to the observation that collagen fibrils in tendons from bgn-deficient mice are structurally and mechanically altered, resulting in joint laxity, gait

impairment and early-onset osteoarthritis [32]. If differences were present in the joints of bgn-deficient mice, this may cause the femora and tibiae to be exposed to different loading states during normal activity than the same bones from wild type animals, possibly influencing the dimorphism in phenotype noted between these two bones. However, bgn-deficient mice demonstrated no gait impairment up to 11 weeks of age and were able to run on a treadmill with no noticeable problems and no differences in gait compared with wild type animals [63], suggesting that the problem of joint laxity was not present in this study.

The mechanical phenotype in females was more subtle than in males, and was almost completely femoral-specific. Bgn-deficiency has minimal effects on basal bone metabolism in the proximal tibiae of 6 month old female mice [40], but the femora were not examined and no geometric or mechanical indices were measured in this study. The mechanisms behind the gender specificity seen in the current study are unknown. Estrogen receptor β deficient [44] and aromatase deficient [45] mice both showed gender differences in bone properties, but these two molecules are responsible for interactions with estrogen so sexual dimorphism can be expected. It is possible that the gender specific response in bgn-deficient mice is connected to estrogen, and this is supported by work showing that bgn-deficient females are protected from the trabecular bone loss normally associated with ovariectomy [40].

While hormones likely contribute to the sexual dimorphism observed in this study, other possible explanations exist. Congenic mouse studies and QTL analyses reveal sex-specific regulation of certain skeletal characteristics [11-13]. Further, because the gene encoding bgn lies on the X chromosome, the genetic insult in this study may have affected the genes responsible for regulating some bone properties in males while bypassing the genes in females. Whatever the cause, female mice are spared most of the deleterious effects in cortical bone caused by this genetic insult.

Some of the data presented here differ from previously published work on bgn-deficient mice. The enhancement in geometric properties in 11 week old bgn-deficient males versus wild type males (Figure 2.1) is in contrast to a decrease in average cortical thickness noted in the femoral diaphysis [39], though these data were from 9 month old mice. This previous study showed no femoral changes, consistent with our data at 11

weeks. At 11 weeks, mice are still in a state of growth while at 9 months, the mice have finished growth. Trends toward increased tibial endocortical histomorphometric indices seen in the current study contrast with decreases in the same indices in the femoral metaphyses of 3 month old mice [39], reinforcing the site-specific effects of genetic alterations.

There are several methodological considerations worthy of discussion. pQCT was performed only on male bones for two reasons. First, the geometric and mechanical phenotypes were displayed in males, indicating that the females may be protected from the deleterious effects of the gene deletion in cortical bone. Second, bone mineral density in the proximal tibiae of bgn-deficient females was unchanged from wild type female levels at 6 months, while bgn-deficient male tibiae showed a significant decrease in vBMD compared to wild type males [40]. Since the bgn-deficient phenotype is known to be age-dependent [39], and no bone mineral phenotype was seen in the females at 6 months, it is unlikely that there would be a mineral related phenotype in female bones at 11 weeks.

It is important to point out that limitations do exist when making area and density measurements of mouse bones using pQCT [64, 65]. These values depend on specimen thickness, as one would expect when trying to clearly define the edges of a bone that has a cortical thickness of ~200 μm using a resolution of 70 μm . A key point is that much of this error occurs when trying to make comparisons among groups differing in cortical thickness. Since the mean cortical thickness of each group in this study was not statistically different, any partial volume effects pertinent to vBMD and BMC measures should be consistent among groups.

In summary, the mechanical phenotype associated with targeted disruption of biglycan is both bone and gender specific in mice at 11 weeks of age. The bgn-deficient male tibiae exhibited improved cross-sectional geometric properties and greater bone mineral density compared to their wild type counterparts, while having lower tissue-level yield strength and structural pre-yield deformation and energy dissipation. Because pre-yield properties alone were impacted, this implies that the gene deletion causes important alterations in mineral and/or the matrix/mineral ultrastructure, suggesting a new understanding of the functional role of bgn in regulating bone mineralization in vivo.

Acknowledgements

I would like to acknowledge my coauthors on this manuscript:

Dr. Rupak M. Rajachar, Dr. Xiao-Dong Chen, Dr. Songtao Shi, Dr. Matthew R. Allen, Dr. Susan A. Bloomfield, Dr. Clifford M. Les, Dr. Pamela G. Robey, Dr. Marian F. Young and Dr. David H. Kohn.

I would further like to thank Tina Kilts for help genotyping the mice in this study.

Funding sources for this study:

DoD/US Army DAMD17-03-1-0556; NIH T32-DE07057; NIH IPA Agreement; Regenerative Sciences Training Grant T90-DK071506

This chapter was published as: Wallace et.al, Bone 2006; 39 (1): 106-116

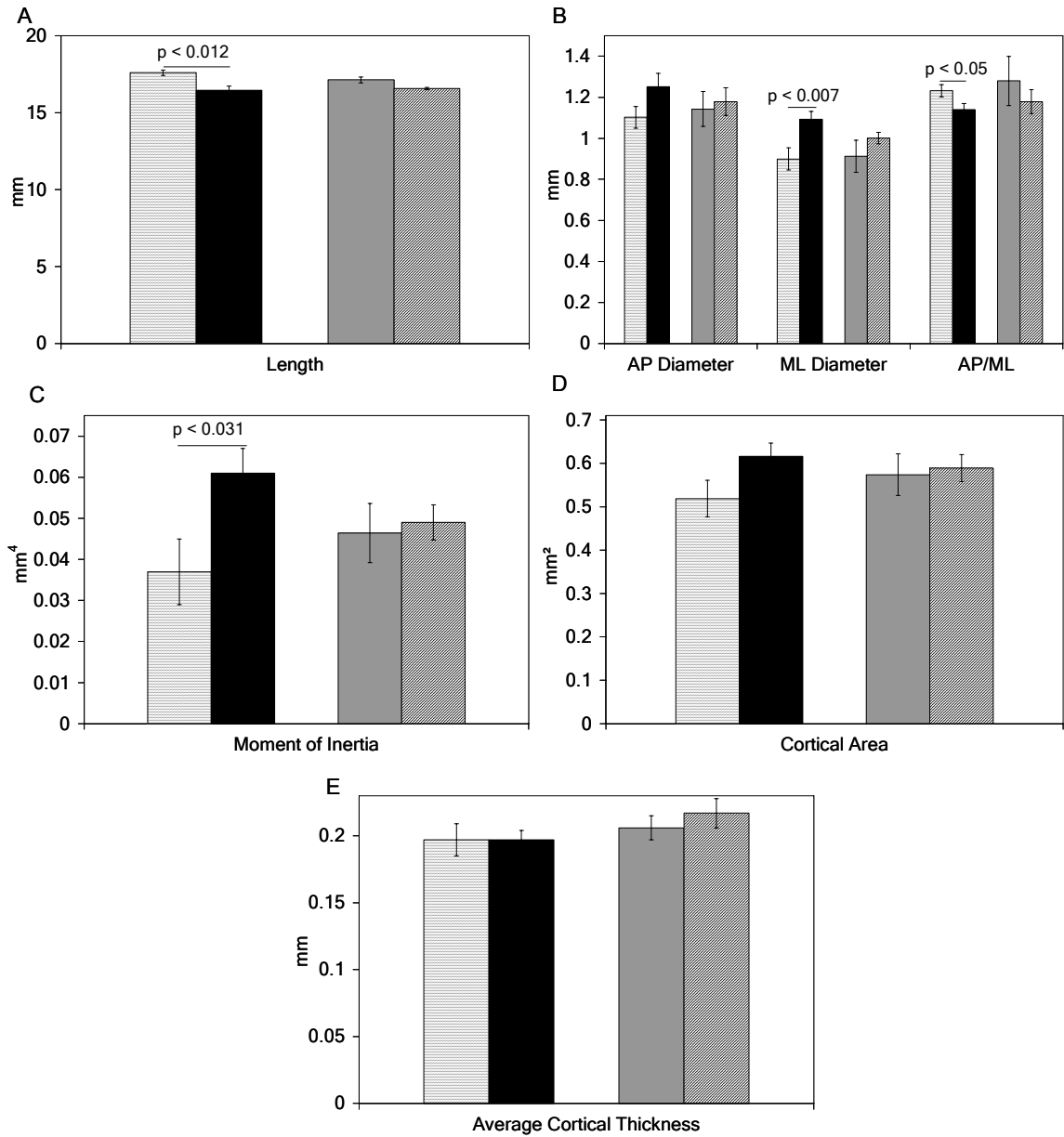


Figure 2.1: Geometric Properties of the Male and Female Tibial Diaphyses of Biglycan-Deficient vs. Wild Type Mice. 11 week old *bgn*-deficient males had decreased tibial length (A) with increased ML diameter (B) and moment of inertia (C) and an AP/ML closer to 1 versus wild type males. Cortical area (D) and cortical thickness (E) were unchanged compared with wild type males. No changes were noted in any properties in females. Data are presented as mean \pm SEM. = wild type male, = biglycan-deficient male, = wild type female, = biglycan-deficient female.

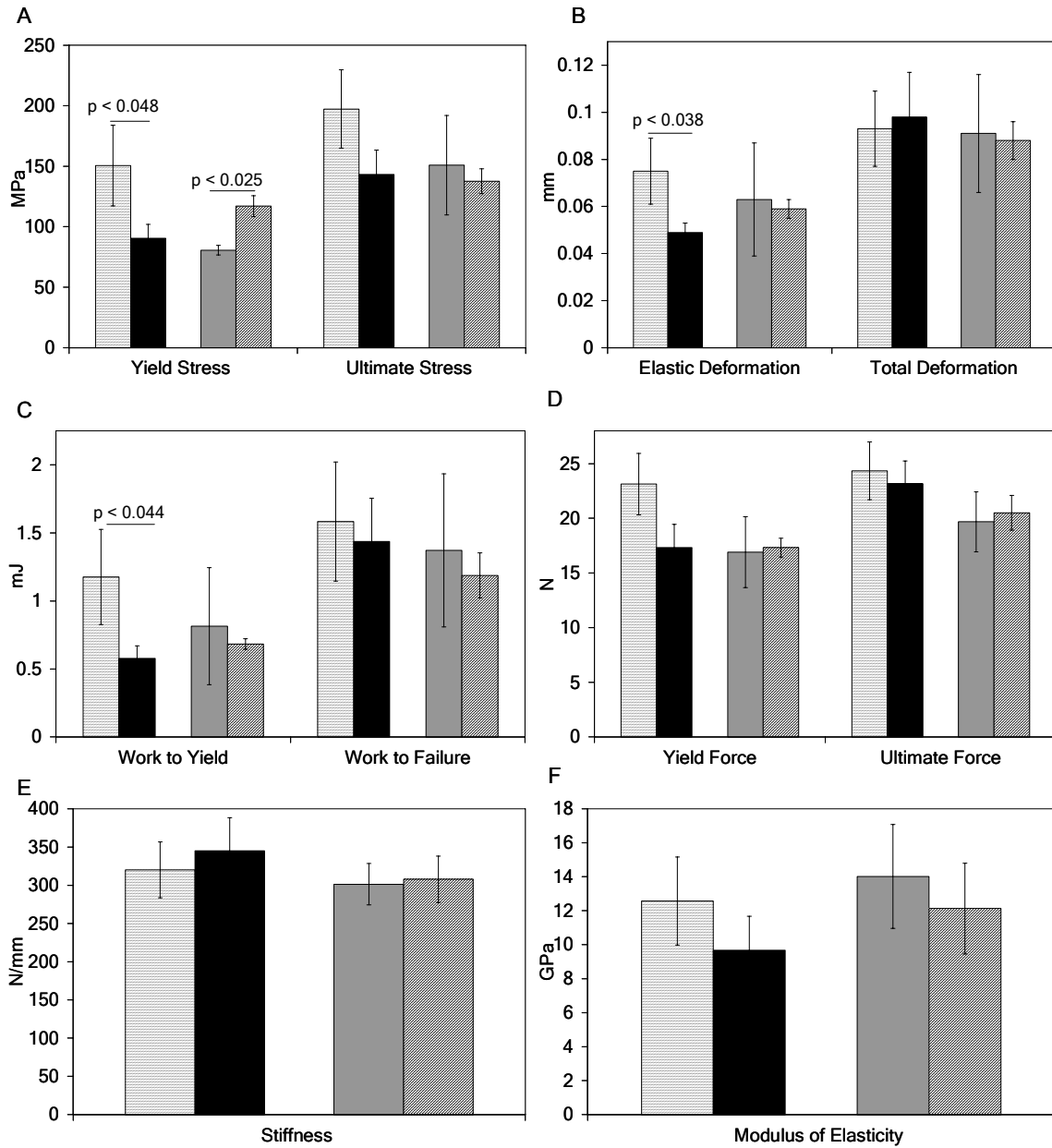


Figure 2.2: Mechanical Properties of the Male and Female Tibial Diaphyses of Biglycan-Deficient vs. Wild Type Mice. 11 week old *bgn*-deficient males displayed decreased tibial yield stress (A) and elastic deformation (B) as well as decreased work-to-yield (C) versus wild type males. Yield and ultimate forces (D), structural stiffness (E) and tissue modulus (F) were unchanged. In females, the only difference noted was an increase in yield stress (A) versus wild type females. Data are presented as mean \pm SEM. = wild type male, = biglycan-deficient male, = wild type female, = biglycan-deficient female.

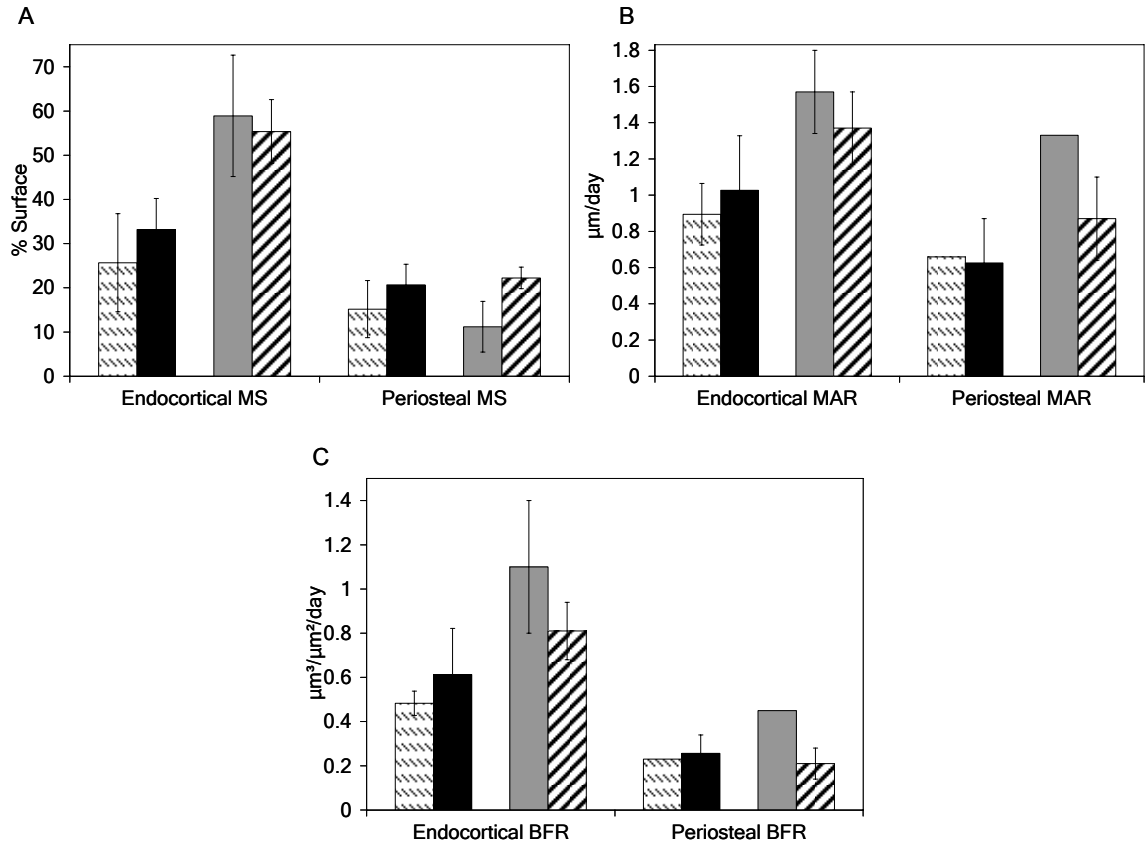
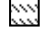
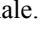




Figure 2.3: Histomorphometry of the Male and Female Tibial Diaphyses of Biglycan-Deficient vs. Wild Type Mice. Between 8 and 10 weeks of age, there were no significant differences in mineralizing surface (A), mineral apposition rate (B) or bone formation rate (C) in the male tibial diaphysis, though endocortical trends suggest increased activity in the *bgn*-deficient animals. Similarly, no differences were noted between wild type and biglycan-deficient females. Data are presented as mean \pm SEM.  = wild type male,  = biglycan-deficient male,  = wild type female,  = biglycan-deficient female.

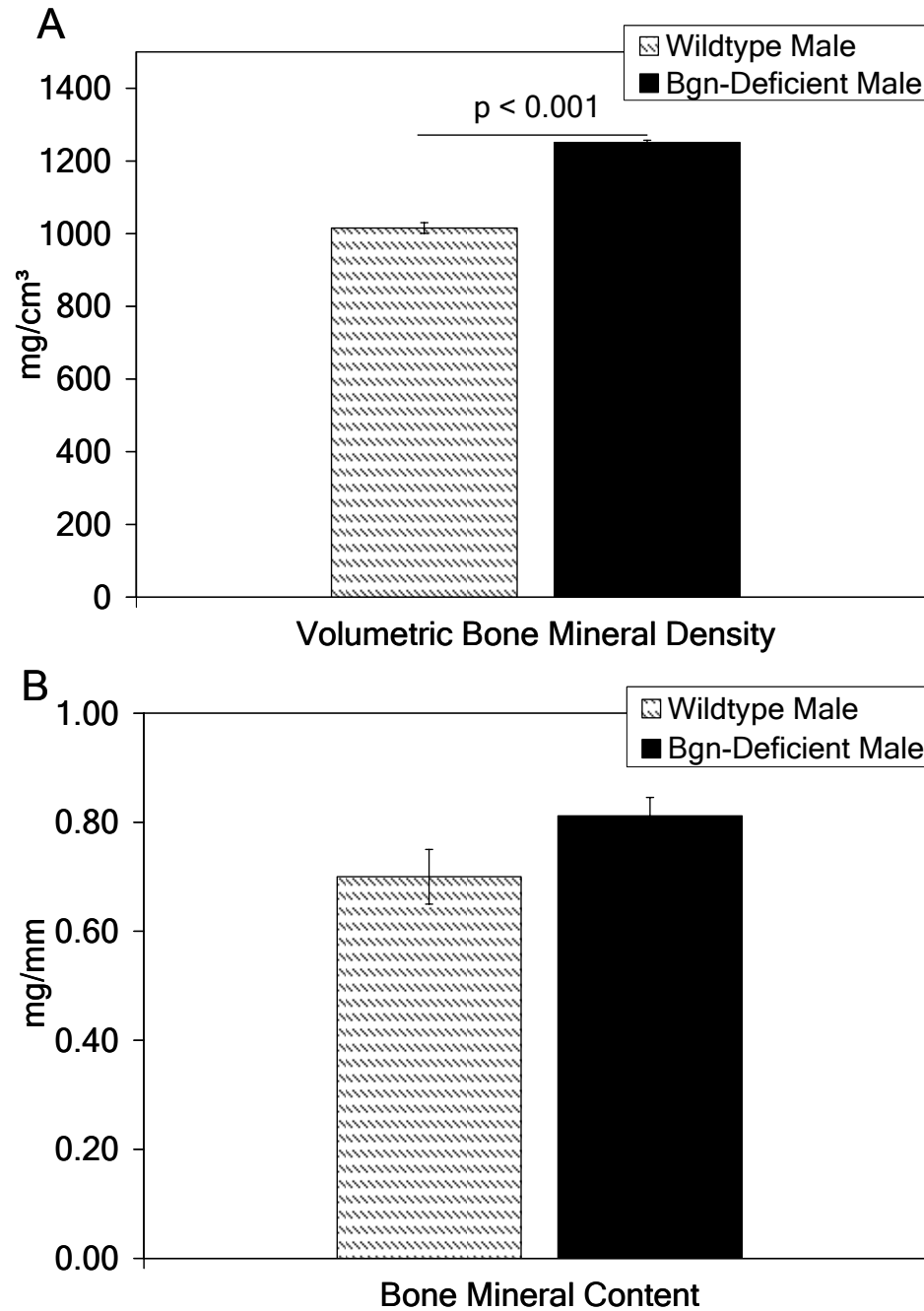


Figure 2.4: Bone Mineral Quantification in the Male Tibial Diaphysis of Biglycan-Deficient vs. Wild Type Mice. 11 week old bgn-deficient males had increased volumetric bone mineral density (A) in the tibial diaphyses compared with wild type males. Data are presented as mean \pm SEM.

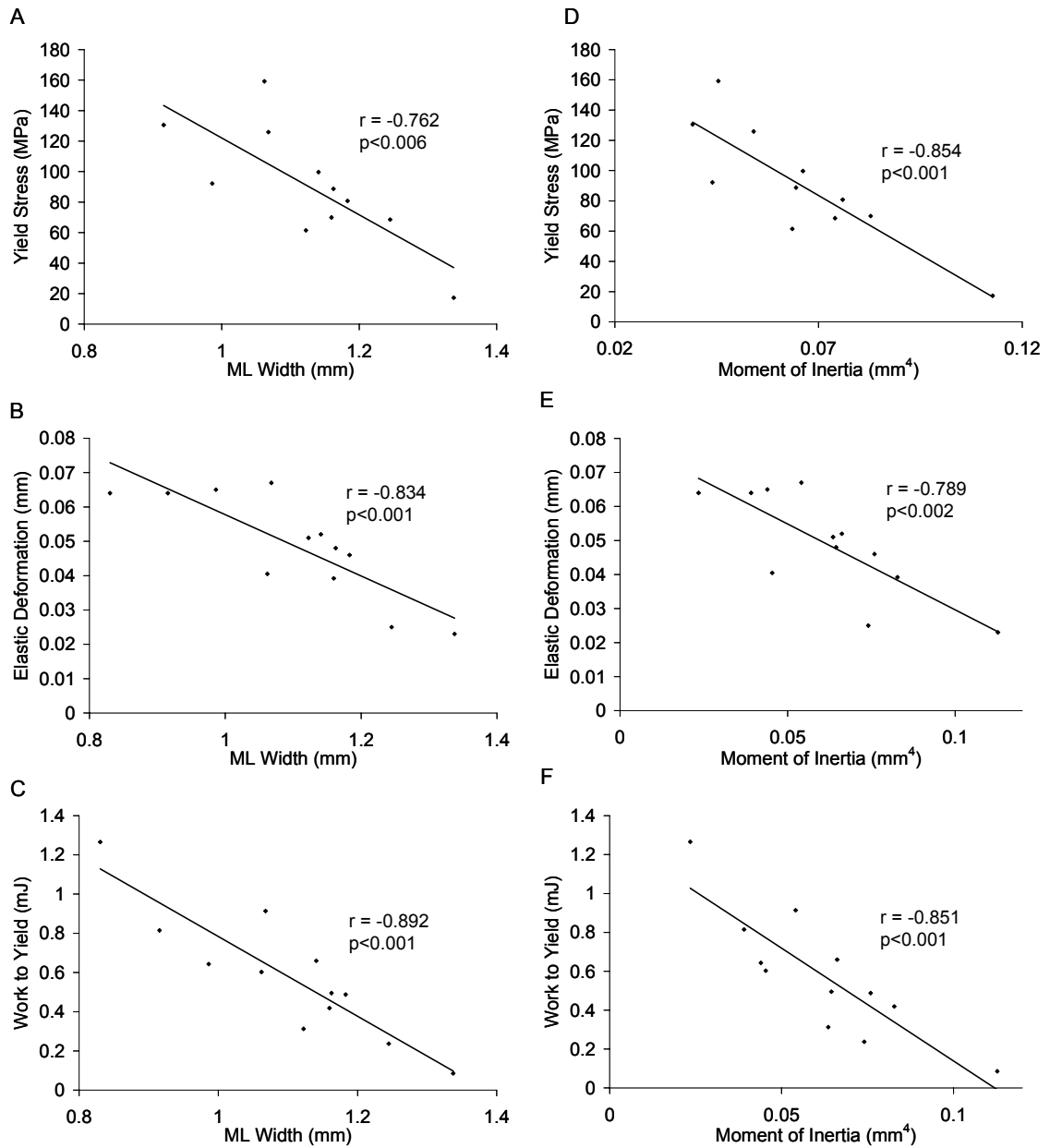


Figure 2.5: Correlations of Structural and Tissue-Level Mechanical Properties to Geometric Properties of the Biglycan-Deficient Male Tibial Diaphyses. ML width and moment of inertia in the *bgn*-deficient males are negatively correlated with tissue-level yield strength (A and D), structural elastic deformation (B and E) and structural work-to-yield (C and F).

Table 2.1: Geometric Properties of the Male and Female Femoral Diaphyses of Biglycan-Deficient Vs. Wild Type Mice

Group	Length (mm)	AP Diameter (mm)	ML Diameter (mm)	AP/ML	Moment of Inertia (mm ⁴)	Average Thickness (mm)
Male Femora (Wild Type)	13.94 ± 0.82	1.16 ± 0.02	1.78 ± 0.12	0.67 ± 0.05	0.103 ± 0.003	0.224 ± 0.013
Male Femora (Bgn-deficient)	14.27 ± 0.25	1.18 ± 0.02	1.81 ± 0.03	0.65 ± 0.01	0.121 ± 0.007	0.237 ± 0.013
Female Femora (Wild Type)	14.42 ± 0.07	1.23 ± 0.02	1.63 ± 0.04	0.76 ± 0.03	0.110 ± 0.007	0.224 ± 0.018
Female Femora (Bgn-Deficient)	13.67 ± 0.36^b	1.14 ± 0.05	1.76 ± 0.08	0.65 ± 0.04^b	0.109 ± 0.013	0.247 ± 0.025

Data are presented as mean ± SEM. b indicates 0.05 < p < 0.10 vs. wild type for the same gender.

Table 2.2: Structural Mechanical Properties of the Male and Female Femoral Diaphyses of Biglycan-Deficient Vs, Wild Type Mice

Group	Yield Force (N)	Ultimate Force (N)	Elastic Deformation (mm)	Post-Yield Deformation (mm)	Total Deformation (mm)	Stiffness (N/mm)	Work to Yield (mJ)	Work to Failure (mJ)
Male Femora (Wild Type)	21.38 ± 2.68	29.06 ± 2.89	0.080 ± 0.15	0.061 ± 0.017	0.141 ± 0.024	274.3 ± 41.8	1.06 ± 0.21	2.63 ± 0.54
Male Femora (Bgn-deficient)	19.74 ± 2.19	30.21 ± 1.93	0.058 ± 0.01	0.060 ± 0.009	0.119 ± 0.010	314.3 ± 15.9	0.62 ± 0.08^a	2.29 ± 0.27
Female Femora (Wild Type)	26.01 ± 1.66	35.91 ± 1.59	0.066 ± 0.012	0.054 ± 0.008	0.120 ± 0.014	495.6 ± 38.0	1.02 ± 0.14	2.75 ± 0.32
Female Femora (Bgn-Deficient)	24.86 ± 2.04	30.94 ± 0.79^a	0.56 ± 0.008	0.032 ± 0.009	0.088 ± 0.006^b	475.5 ± 66.9	0.90 ± 0.18	1.83 ± 0.15^a

Data are presented as mean ± SEM. a indicates $p < 0.05$ vs. wild type for the same gender, b indicates $0.05 < p < 0.10$ vs. wild type for the same gender.

Table 2.3: Tissue-Level Mechanical Properties of the Male and Female Femoral Diaphyses of Biglycan Deficient Vs. Wild Type Mice

Group	Yield Stress (MPa)	Ultimate Stress (MPa)	Strain to Failure ($\mu\epsilon$)	Modulus of Elasticity (GPa)
Male Femora (Wild Type)	62.75 \pm 10.10	85.05 \pm 11.64	36000 \pm 5446	3.13 \pm 0.50
Male Femora (Bgn-deficient)	43.69 \pm 2.52^a	74.69 \pm 5.24	31625 \pm 2097	3.20 \pm 0.21
Female Femora (Wild Type)	73.47 \pm 4.03	101.49 \pm 3.00	31804 \pm 4617	5.26 \pm 0.19
Female Femora (Bgn-Deficient)	68.02 \pm 8.06	85.35 \pm 10.28	21625 \pm 2135	5.96 \pm 1.99

Data are presented as mean \pm SEM. a indicates $p < 0.05$ vs. wild type for the same gender.

References

- (1) Baron R (2004) General Principles of Bone Biology. In: Anonymous (eds) Primer on the Metabolic Bone Diseases and Disorders of Mineral Metabolism. The American Society for Bone and Mineral Research, p 1-8
- (2) Burr DB, Turner CH (2004) Biomechanics of Bone. In: Anonymous (eds) Primer on the Metabolic Bone Diseases and Disorders of Mineral Metabolism. The American Society for Bone and Mineral Research, p 58-64
- (3) Burstein AH, Zika JM, Heiple KG, Klein L (1975) Contribution of collagen and mineral to the elastic-plastic properties of bone. *J.Bone Joint Surg.Am.* 57:956-961
- (4) Currey JD (1988) The effect of porosity and mineral content on the Young's modulus of elasticity of compact bone. *J.Biomech.* 21:131-139
- (5) Martin RB, Ishida J (1989) The relative effects of collagen fiber orientation, porosity, density, and mineralization on bone strength. *J.Biomech.* 22:419-426
- (6) Martin RB, Boardman DL (1993) The effects of collagen fiber orientation, porosity, density, and mineralization on bovine cortical bone bending properties. *J.Biomech.* 26:1047-1054
- (7) Landis WJ (1995) The strength of a calcified tissue depends in part on the molecular structure and organization of its constituent mineral crystals in their organic matrix. *Bone* 16:533-544
- (8) Ferguson VL, Ayers RA, Bateman TA, Simske SJ (2003) Bone development and age-related bone loss in male C57BL/6J mice. *Bone* 33:387-398
- (9) Wang X, Shen X, Li X, Agrawal CM (2002) Age-related changes in the collagen network and toughness of bone. *Bone* 31:1-7
- (10) Duan Y, Beck TJ, Wang XF, Seeman E (2003) Structural and biomechanical basis of sexual dimorphism in femoral neck fragility has its origins in growth and aging. *J.Bone Miner.Res.* 18:1766-1774
- (11) Turner CH, Sun Q, Schriefer J, Pitner N, Price R, Bouxsein ML, Rosen CJ, Donahue LR, Shultz KL, Beamer WG (2003) Congenic mice reveal sex-specific genetic regulation of femoral structure and strength. *Calcif.Tissue Int.* 73:297-303
- (12) Klein RF, Turner RJ, Skinner LD, Vartanian KA, Serang M, Carlos AS, Shea M, Belknap JK, Orwoll ES (2002) Mapping quantitative trait loci that influence femoral cross-sectional area in mice. *J.Bone Miner.Res.* 17:1752-1760

- (13) Orwoll ES, Belknap JK, Klein RF (2001) Gender specificity in the genetic determinants of peak bone mass. *J.Bone Miner.Res.* 16:1962-1971
- (14) Akhter MP, Iwaniec UT, Covey MA, Cullen DM, Kimmel DB, Recker RR (2000) Genetic variations in bone density, histomorphometry, and strength in mice. *Calcif.Tissue Int.* 67:337-344
- (15) Jepsen KJ, Pennington DE, Lee YL, Warman M, Nadeau J (2001) Bone brittleness varies with genetic background in A/J and C57BL/6J inbred mice. *J.Bone Miner.Res.* 16:1854-1862
- (16) Sheng MH, Baylink DJ, Beamer WG, Donahue LR, Lau KH, Wergedal JE (2002) Regulation of bone volume is different in the metaphyses of the femur and vertebra of C3H/HeJ and C57BL/6J mice. *Bone* 30:486-491
- (17) Turner CH, Hsieh YF, Muller R, Bouxsein ML, Baylink DJ, Rosen CJ, Grynpas MD, Donahue LR, Beamer WG (2000) Genetic regulation of cortical and trabecular bone strength and microstructure in inbred strains of mice. *J.Bone Miner.Res.* 15:1126-1131
- (18) Iwamoto J, Yeh JK, Aloia JF (1999) Differential effect of treadmill exercise on three cancellous bone sites in the young growing rat. *Bone* 24:163-169
- (19) Mosekilde L, Thomsen JS, Orhii PB, McCarter RJ, Mejia W, Kalu DN (1999) Additive effect of voluntary exercise and growth hormone treatment on bone strength assessed at four different skeletal sites in an aged rat model. *Bone* 24:71-80
- (20) Turner CH, Hsieh YF, Muller R, Bouxsein ML, Rosen CJ, McCrann ME, Donahue LR, Beamer WG (2001) Variation in bone biomechanical properties, microstructure, and density in BXH recombinant inbred mice. *J.Bone Miner.Res.* 16:206-213
- (21) Robling AG, Turner CH (2002) Mechanotransduction in bone: genetic effects on mechanosensitivity in mice. *Bone* 31:562-569
- (22) Kodama Y, Umemura Y, Nagasawa S, Beamer WG, Donahue LR, Rosen CR, Baylink DJ, Farley JR (2000) Exercise and mechanical loading increase periosteal bone formation and whole bone strength in C57BL/6J mice but not in C3H/HeJ mice. *Calcif.Tissue Int.* 66:298-306
- (23) Carter DR, Van Der Meulen MC, Beaupre GS (1996) Mechanical factors in bone growth and development. *Bone* 18:5S-10S

- (24) Corsi A, Xu T, Chen XD, Boyde A, Liang J, Mankani M, Sommer B, Iozzo RV, Eichstetter I, Robey PG, Bianco P, Young MF (2002) Phenotypic effects of biglycan deficiency are linked to collagen fibril abnormalities, are synergized by decorin deficiency, and mimic Ehlers-Danlos-like changes in bone and other connective tissues. *J.Bone Miner.Res.* 17:1180-1189
- (25) Wiberg C, Hedbom E, Khairullina A, Lamande SR, Oldberg A, Timpl R, Morgelin M, Heinegard D (2001) Biglycan and decorin bind close to the n-terminal region of the collagen VI triple helix. *J.Biol.Chem.* 276:18947-18952
- (26) Schonherr E, Witsch-Prehm P, Harrach B, Robenek H, Rauterberg J, Kresse H (1995) Interaction of biglycan with type I collagen. *J.Biol.Chem.* 270:2776-2783
- (27) Hocking AM, Shinomura T, McQuillan DJ (1998) Leucine-rich repeat glycoproteins of the extracellular matrix. *Matrix Biol.* 17:1-19
- (28) Chen XD, Fisher LW, Robey PG, Young MF (2004) The small leucine-rich proteoglycan biglycan modulates BMP-4-induced osteoblast differentiation. *FASEB J.* 18:948-958
- (29) Ruoslahti E (1989) Proteoglycans in cell regulation. *J.Biol.Chem.* 264:13369-13372
- (30) Takagi M, Yamada T, Kamiya N, Kumagai T, Yamaguchi A (1999) Effects of bone morphogenetic protein-2 and transforming growth factor-beta1 on gene expression of decorin and biglycan by cultured osteoblastic cells. *Histochem.J.* 31:403-409
- (31) Yamada T, Kamiya N, Harada D, Takagi M (1999) Effects of transforming growth factor-beta1 on the gene expression of decorin, biglycan, and alkaline phosphatase in osteoblast precursor cells and more differentiated osteoblast cells. *Histochem.J.* 31:687-694
- (32) Ameye L, Young MF (2002) Mice deficient in small leucine-rich proteoglycans: novel in vivo models for osteoporosis, osteoarthritis, Ehlers-Danlos syndrome, muscular dystrophy, and corneal diseases. *Glycobiology* 12:107R-16R
- (33) Boskey AL, Spevak L, Doty SB, Rosenberg L (1997) Effects of bone CS-proteoglycans, DS-decorin, and DS-biglycan on hydroxyapatite formation in a gelatin gel. *Calcif.Tissue Int.* 61:298-305
- (34) Bianco P, Fisher LW, Young MF, Termine JD, Robey PG (1990) Expression and localization of the two small proteoglycans biglycan and decorin in developing human skeletal and non-skeletal tissues. *J.Histochem.Cytochem.* 38:1549-1563

- (35) Fisher LW, Termine JD, Dejter SW, Jr, Whitson SW, Yanagishita M, Kimura JH, Hascall VC, Kleinman HK, Hassell JR, Nilsson B (1983) Proteoglycans of developing bone. *J.Biol.Chem.* 258:6588-6594
- (36) Fisher LW, Termine JD, Young MF (1989) Deduced protein sequence of bone small proteoglycan I (biglycan) shows homology with proteoglycan II (decorin) and several nonconnective tissue proteins in a variety of species. *J.Biol.Chem.* 264:4571-4576
- (37) Chen XD, Allen MR, Bloomfield S, Xu T, Young M (2003) Biglycan-deficient mice have delayed osteogenesis after marrow ablation. *Calcif.Tissue Int.* 72:577-582
- (38) Chen XD, Shi S, Xu T, Robey PG, Young MF (2002) Age-related osteoporosis in biglycan-deficient mice is related to defects in bone marrow stromal cells. *J.Bone Miner.Res.* 17:331-340
- (39) Xu T, Bianco P, Fisher LW, Longenecker G, Smith E, Goldstein S, Bonadio J, Boskey A, Heegaard AM, Sommer B, Satomura K, Dominguez P, Zhao C, Kulkarni AB, Robey PG, Young MF (1998) Targeted disruption of the biglycan gene leads to an osteoporosis-like phenotype in mice. *Nat.Genet.* 20:78-82
- (40) Nielsen KL, Allen MR, Bloomfield SA, Andersen TL, Chen XD, Poulsen HS, Young MF, Heegaard AM (2003) Biglycan deficiency interferes with ovariectomy-induced bone loss. *J.Bone Miner.Res.* 18:2152-2158
- (41) Yershov Y, Baldini TH, Villagomez S, Young T, Martin ML, Bockman RS, Peterson MG, Blank RD (2001) Bone strength and related traits in HcB/Dem recombinant congenic mice. *J.Bone Miner.Res.* 16:992-1003
- (42) Shultz KL, Donahue LR, Bouxsein ML, Baylink DJ, Rosen CJ, Beamer WG (2003) Congenic strains of mice for verification and genetic decomposition of quantitative trait loci for femoral bone mineral density. *J.Bone Miner.Res.* 18:175-185
- (43) Volkman SK, Galecki AT, Burke DT, Paczas MR, Moalli MR, Miller RA, Goldstein SA (2003) Quantitative trait loci for femoral size and shape in a genetically heterogeneous mouse population. *J.Bone Miner.Res.* 18:1497-1505
- (44) Sims NA, Dupont S, Krust A, Clement-Lacroix P, Minet D, Resche-Rigon M, Gaillard-Kelly M, Baron R (2002) Deletion of estrogen receptors reveals a regulatory role for estrogen receptors-beta in bone remodeling in females but not in males. *Bone* 30:18-25

- (45) Oz OK, Zerwekh JE, Fisher C, Graves K, Nanu L, Millsaps R, Simpson ER (2000) Bone has a sexually dimorphic response to aromatase deficiency. *J.Bone Miner.Res.* 15:507-514
- (46) Moore DS, McCabe GP (2003) *Introduction to the Practice of Statistics*. 4W.H. Freeman & Company, New York, NY
- (47) Gustafson MB, Martin RB, Gibson V, Storms DH, Stover SM, Gibeling J, Griffin L (1996) Calcium buffering is required to maintain bone stiffness in saline solution. *J.Biomech.* 29:1191-1194
- (48) Rajachar RM (2003) *Effects of Age-Related Ultra-Structural Changes in Bone on Microdamage Mechanisms*. PhD Dissertation.
- (49) Sommer HJ (2002) Polygeom Matlab Function Available at: <http://www.me.psu.edu/sommer/me562/polygeom.m>
- (50) Parfitt AM, Drezner MK, Glorieux FH, Kanis JA, Malluche H, Meunier PJ, Ott SM, Recker RR (1987) Bone histomorphometry: standardization of nomenclature, symbols, and units. Report of the ASBMR Histomorphometry Nomenclature Committee. *J.Bone Miner.Res.* 2:595-610
- (51) Sakakura Y, Shide N, Tsuruga E, Irie K, Yajima T (2001) Effects of running exercise on the mandible and tibia of ovariectomized rats. *J.Bone Miner.Metab.* 19:159-167
- (52) Boskey AL, Wright TM, Blank RD (1999) Collagen and bone strength. *J.Bone Miner.Res.* 14:330-335
- (53) Burr DB (2002) The contribution of the organic matrix to bone's material properties. *Bone* 31:8-11
- (54) Currey JD, Foreman J, Laketic I, Mitchell J, Pegg DE, Reilly GC (1997) Effects of ionizing radiation on the mechanical properties of human bone. *J.Orthop.Res.* 15:111-117
- (55) Wang X, Bank RA, TeKoppele JM, Agrawal CM (2001) The role of collagen in determining bone mechanical properties. *J.Orthop.Res.* 19:1021-1026
- (56) Wang X, Li X, Bank RA, Agrawal CM (2002) Effects of collagen unwinding and cleavage on the mechanical integrity of the collagen network in bone. *Calcif.Tissue Int.* 71:186-192
- (57) Alho A, Husby T, Hoiseth A (1988) Bone mineral content and mechanical strength. An ex vivo study on human femora at autopsy. *Clin.Orthop.Relat.Res.* 227:292-297

- (58) Follet H, Boivin G, Rumelhart C, Meunier PJ (2004) The degree of mineralization is a determinant of bone strength: a study on human calcanei. *Bone* 34:783-789
- (59) Wachter NJ, Krischak GD, Mentzel M, Sarkar MR, Ebinger T, Kinzl L, Claes L, Augat P (2002) Correlation of bone mineral density with strength and microstructural parameters of cortical bone in vitro. *Bone* 31:90-95
- (60) Oxlund H, Barckman M, Ortoft G, Andreassen TT (1995) Reduced concentrations of collagen cross-links are associated with reduced strength of bone. *Bone* 17:365S-371S
- (61) Akhter MP, Cullen DM, Pedersen EA, Kimmel DB, Recker RR (1998) Bone response to in vivo mechanical loading in two breeds of mice. *Calcif.Tissue Int.* 63:442-449
- (62) Kodama Y, Dimai HP, Wergedal J, Sheng M, Malpe R, Kutilek S, Beamer W, Donahue LR, Rosen C, Baylink DJ, Farley J (1999) Cortical tibial bone volume in two strains of mice: effects of sciatic neurectomy and genetic regulation of bone response to mechanical loading. *Bone* 25:183-190
- (63) Wallace JM, Rajachar RM, Chen X, Shi S, Allen MR, Bloomfield SA, Les CM, Robey PG, Young MF, Kohn DH The Phenotype of Biglycan-Deficient Mice Can Be Modified By Mechanical Loading, paper No. 197. 2004 Annual Meeting of the Orthopaedic Society
- (64) Brodt MD, Pelz GB, Taniguchi J, Silva MJ (2003) Accuracy of peripheral quantitative computed tomography (pQCT) for assessing area and density of mouse cortical bone. *Calcif.Tissue Int.* 73:411-418
- (65) Schmidt C, Priemel M, Kohler T, Weusten A, Muller R, Amling M, Eckstein F (2003) Precision and accuracy of peripheral quantitative computed tomography (pQCT) in the mouse skeleton compared with histology and microcomputed tomography (microCT). *J.Bone Miner.Res.* 18:1486-1496

CHAPTER 3

EXERCISE-INDUCED CHANGES IN THE CORTICAL BONE OF GROWING MICE ARE BONE AND GENDER SPECIFIC

Introduction

Skeletal fragility leading to fracture is a significant medical and economic burden facing society. Each year, an estimated 1.5 million Americans suffer an age-related fracture, resulting in direct care expenditures of 18 billion dollars a year, measured in 2002 dollars [1]. Though skeletal fragility is often considered an age-related condition, stress and/or trauma-related fractures are a clinically significant problem in younger people as well [2, 3]. The weight bearing bones of the lower extremities, particularly the cortical bone of the tibial and metatarsal diaphyses, are most often affected [4, 5]. However, fracture risk is not equivalent between genders, with female long-distance runners and military recruits demonstrating a higher propensity for stress-fractures than males [6-8].

It is generally accepted that fracture risk and mechanical integrity of bone are not only affected by bone mass, but are also functions of tissue quality [9]. While influenced by many environmental factors (e.g. nutrition, hormones, pharmacological factors), the quantity and quality of bone are also significantly dependent on biomechanical influences. The importance of skeletal loading for the maintenance and increase of bone mass was suggested by Wolff as early as 1892 [10], and is universally accepted today.

Many animal models exist to study the effects of mechanical stimulation on bone structure and tissue quality, and ultimately skeletal function. Multiple exercise-based rat models have shown a link between the loading of bone and increased bone formation, resulting in increased bone mass and maintenance or improvement of mechanical properties [11-14]. Exercise also increases bone formation in mice, resulting in increased bone cross-sectional geometric properties and mass [15-19]. The primary deficiency in

most murine exercise studies is that few investigate mechanical properties. The consensus from those murine studies that do look at mechanical properties is that moderate exercise improves or maintains whole-bone strength, though only a limited number of properties are reported in these studies (e.g. structural strength, ultimate stress, modulus, total deformation). Since the mechanical competence of bone is a clinically important metric, information regarding the alteration of a range mechanical properties following an exercise regimen, including changes in energy dissipation and deformation, is essential to assess the efficacy of the exercise and its ability to increase fracture resistance.

The bones of male mice show greater sensitivity to swimming than females [17, 18]. However, weight-bearing exercise may be more efficient than non-weight-bearing exercise at eliciting structural changes in bone due to the direct loading of the whole bone rather than loading applied mainly at points of muscle insertion [20, 21]. Further, the age at the initiation of such loading is important, since the growing skeleton has a greater capacity to accrue bone than does the adult skeleton [22-24]. Therefore, the aim of this study was to test the hypothesis that short-term weight-bearing exercise during growth would have a greater positive impact on cross sectional geometry and mechanical competence in the femora and tibiae of male C57BL6/129 mice versus the response in females. Further, based on the orientation of the legs during running and the proximity of the tibia to the point of impact, the response to this type of exercise was hypothesized to be greater in the tibia versus the femur. At 11 weeks of age and after 21 consecutive days of training, exercise-related changes relative to non-exercise controls were assessed in the cortical bone of the femora and tibiae of both genders. Four-point bending tests were performed to determine mechanical properties at the whole bone (structural) and tissue levels. Additionally, volumetric bone mineral density (from peripheral quantitative computed tomography) and cross-sectional geometry were assessed.

Materials and Methods

Animals and Treatment

All animal procedures were performed at the National Institute of Dental and Craniofacial Research (NIDCR) with NIDCR Institutional Animal Care and Use Committee approval (NIDCR animal approval protocol #NIDCR 001-151). To determine proper sample sizes for detecting effects of exercise across bones and gender, power calculations were performed based on published values for differences and standard deviations in mechanical and geometric properties due to mechanical loading in C57BL6 mice [19] using a value of $\alpha=0.05$ and a power $(1-\beta)$ of 0.80.

Mice were bred on a C57BL6/129 (B6;129) background [25]. Twenty mice from each gender (2 exercise groups, 10 mice per group) were housed in standard cages and given access to food, water and cage activity ad libitum. At 8 weeks of age, mice from each gender were randomly assigned to 1 of 2 weight matched groups (control, exercise). Exercise consisted of running on a treadmill (12 meters/minute at a 5° incline) for 30 minutes/day, 7 days/week for 21 consecutive days (Columbus Instruments, Model 1055M, Columbus, OH). Each lane of the treadmill was equipped with an adjustable-amperage (0-1.5 mA) shock grid at the rear of the belt to stimulate each mouse to run independently of all others. By the end of the second day of the experiment, all mice were running without the need of shock stimulation. Three days after the end of exercise, animals were sacrificed, at which time body weights were measured again and both femora and tibiae were harvested, stripped of soft tissue and stored in either 70% ethanol at 4° C (for peripheral quantitative computed tomography (pQCT)) or wrapped in gauze soaked in a Ca²⁺-buffered saline solution at -80°C (for mechanical testing). The bones used for mechanical testing were brought to room temperature before testing.

Mechanical Testing

Left femora and tibiae were tested to failure in 4 point bending in displacement control using a custom-designed, solenoid driven loading apparatus with a support span (L) of 6 mm and a loading span of 4 mm at a rate of 0.01 mm/sec [25, 26]. Before testing, the length of each femur was measured from the greater trochanter to the most

distal portion of the femoral condyles and the length of each tibia was measured from the most proximal portion of the tibial plateau to the most distal portion of the medial malleolus using digital calipers accurate to 0.01 mm (Mitutoyo; Aurora, IL). Femora were tested in the anterior-posterior (AP) direction (anterior surface in tension) with the middle of the bone positioned halfway between the two supports. Tibiae were tested in the medial-lateral (ML) direction (medial surface in tension). The tibiae were positioned such that the most distal portion of the junction of the tibia and fibula (TFJ) was aligned with the left-most support point. During each test, load and deflection were recorded, from which structural strength (yield force and ultimate force), energy or work (measured as the area under the force vs. displacement curve to yield and to failure), stiffness (the slope of the linear portion of the force vs. displacement curve) and deformation (yield deformation, total deformation and post-yield deformation) were derived at the whole bone level [25]. Load was measured using a linear force transducer with an operating range of 0-25 lb (Sensotec, Precision Linear Load Cell Model 34; Columbus, OH) while deflection was measured using an eddy current sensor with 0.27 μm resolution and operating range of 0-3.81 mm (Kaman Measuring Systems, Model 2440 5CM; Middletown, CT).

During each test, the bone was visually monitored and the point of fracture initiation was noted. Because fractures often propagated at an angle across the bone (i.e. oblique fractures), the half of the fractured bone containing both the fracture initiation site and a full planar section of bone transverse to that site was dehydrated in graded ethanol (70%, 95%, 100%) at 4°C, defatted in acetone and infiltrated in a liquid methyl methacrylate monomer (Koldmount™ Cold Mounting Liquid; Mager Scientific) [25]. The bones were then embedded in methyl methacrylate (Koldmount™ Cold Mounting Kit; Mager Scientific). Using a low-speed sectioning saw (South Bay Technology, Model 650; San Clemente, CA) with a diamond wafering blade (Mager Scientific; Dexter, MI), the jagged edge of the bone adjacent to the fracture site was removed. A 200 μm thick planar section (hand ground to a final thickness of between 50 and 75 μm using wet silicon carbide abrasive discs) was then used to determine geometric parameters (average cortical thickness from four quadrants, cortical area, and AP and ML diameters) using a light microscope and digital analysis software (Nikon Eclipse TE 300,

Image Pro-Plus v4.5, Matlab v5.3) [25]. The moment of inertia (I) about the axis of bending (I_{ML} for the femur and I_{AP} for the tibia) was measured from a binary image of each section using a Matlab script that integrates the distribution of material points about the calculated neutral axes [27]. Together with the load and deflection data, the distance from the centroid to the surface of the bone in tension (c) and I were used to map force and displacement (structural level) into stress and strain (tissue level) from standard beam-bending equations for 4 point bending:

$$Stress = \sigma = \frac{Fac}{2I} \quad (MPa)$$

$$Strain = \varepsilon = \frac{6cd}{a(3L - 4a)} \times 10^6 \quad (\mu\varepsilon)$$

In these equations, F is the force, d is the displacement, a is the distance from the support to the inner loading point (1 mm) and L is the span between the outer supports (6 mm). The yield point was calculated using the 0.2% offset method based on the stress-strain curve [28]. The modulus of elasticity was calculated as the slope of the linear portion of the stress-strain curve.

Peripheral Quantitative Computed Tomography (pQCT)

Ex vivo scans of right femora and tibiae from the male mice were performed at Texas A&M University using an XCT Research-M device (Stratec Corp., Norland, Fort Atkinson, WI) [29]. Machine calibration was performed using a hydroxyapatite cone phantom. Scans were performed at a scan speed of 2.5 mm/sec with a voxel resolution of $70 \mu\text{m}^2$ and a scanning beam thickness of 0.50 mm. Two slices were scanned at the mid-diaphysis of each bone (50% of the total bone length \pm 0.50 mm). A standardized analysis of diaphyseal bone (threshold of 700 mg/cm^3) was applied to each section. Values of total volumetric bone mineral density (vBMD, coefficient of variation = \pm 0.63 %) obtained for the two slices were averaged to get mean values for each bone. Because of the small size of bones from these mice (cortical thickness on the order of $200 \mu\text{m}$) and the scanning resolution of $70 \mu\text{m}^2$, there is an increased probability of error in clearly defining the edges of the bones [30, 31]. Therefore, geometric properties were not determined from pQCT scans, but rather from histological sections as described above.

Statistical Analysis

All data are presented as mean \pm standard error of the mean (SEM). Statistical analyses were performed on body mass, vBMD and all geometric and mechanical properties using Student's t-tests, checking for the effects of exercise in each bone and gender (Sigma Stat 2.0, Jandel Scientific). In groups which failed to exhibit normal distributions or equal variance, Mann-Whitney rank sum tests were performed. A value of $p < 0.05$ was considered significant while a p-value between 0.05 and 0.10 was also noted as a trend.

Results

At the beginning of the exercise regimen (Day 0), control and exercise groups in each gender were body weight matched. Body weights were again measured at the end of the study (Day 23), with no significant difference noted between exercise and control groups in either gender (Figure 3.1). Though not significant, both control and exercise male mice gained weight during the study (5.9% in control, 7.4% in exercise). A similar non-significant trend was noted in female control mice (5.6%), but female exercise mice lost weight during the study (-1.2%).

A relatively brief 21 day period of running initiated at 8 weeks of age induced changes in geometric and mechanical properties that most strongly impacted the male tibiae (Figure 3.2-Figure 3.5). Tibial length was not impacted by exercise in male mice (Male Control: 17.59 ± 0.18 mm, Male Exercise: 17.47 ± 0.12 mm). Exercise significantly increased cortical area (Figure 3.2A) and medial-lateral (ML) width (Figure 3.2B) in the tibial mid-diaphysis of males, resulting in a significant increase in bending moment of inertia about the AP axis (Figure 3.2C). These changes in geometric properties were primarily the result of an exercise-induced increase in periosteal perimeter (indicating greater periosteal formation with exercise, Figure 3.3), though endocortical perimeter was also greater (indicating endocortical resorption with exercise, Figure 3.3). Volumetric bone mineral density (vBMD) was also significantly increased with exercise (Male Control: 1015 ± 15 mg/cm³, Male Exercise: 1219 ± 9 mg/cm³; $p < 0.001$).

At the structural level, there was a significant increase in post-yield deformation in the male tibiae (Figure 3.4A); however, this occurred at the expense of reduced yield deformation (Figure 3.4A) and yield force (Figure 3.4B). Further, there was a marginal decrease in work-to-yield (Figure 3.4C, $p < 0.066$). Similar trends were noted at the tissue level, where strain-to-failure was significantly greater with exercise (Figure 3.5A), but at the expense of decreased yield and ultimate stress (Figure 3.5B). Further, tissue-level stiffness was marginally decreased (Figure 3.5C, $p < 0.061$). No exercise-induced effects were noted in any properties in the male femora versus controls (Table 3.1-Table 3.3), with the exception of a decrease in vBMD (Male Control: $1240 \pm 5 \text{ mg/cm}^3$, Male Exercise: $1205 \pm 6 \text{ mg/cm}^3$; $p < 0.009$). In males, the percent change with exercise in every property except total deformation and work-to-failure was greater in the tibiae than in the femur, indicating a bone specific response to exercise in males.

The bones of female mice exhibited little geometric or mechanical response to the exercise regime (Figure 3.3-Figure 3.5, Table 3.1-Table 3.3). No geometric (Table 3.1) or structural mechanical properties (Table 3.2) were impacted in the femora, though structural stiffness was marginally decreased with exercise ($p < 0.072$). At the tissue-level, modulus of elasticity was significantly decreased (Table 3.3), while ultimate stress was marginally decreased ($p < 0.082$). Tibial length was not impacted by exercise in female mice (Female Control: $17.13 \pm 0.19 \text{ mm}$, Female Exercise: $17.16 \pm 0.19 \text{ mm}$), nor was any other tibial property (Figure 3.2-Figure 3.4-Figure 3.5). In contrast to males, where a majority of properties in the tibia had a greater response to exercise than in the femur, the female femora and tibia both showed similar lack of response to exercise.

Discussion

This study demonstrates that in growing B6;129 mice, the skeletal response to three weeks of running on a treadmill at a low incline and moderate intensity is bone and gender specific. This short term exercise regime most significantly affected the male tibial diaphysis, which responded to exercise via increased cross-sectional dimensions (Figure 3.2). Measures of periosteal and endocortical perimeters (Figure 3.3) reveal that changes in cross-sectional geometry occurred primarily due to periosteal expansion,

though endocortical resorption also occurred. While the tibiae from exercise mice had superior structural post-yield deformation and tissue strain-to-failure compared to non-exercise controls, these benefits came at the expense of reduced yield deformation, structural and tissue-level yield strength, and tissue-level ultimate strength (Figure 3.4Figure 3.5). Growth is actively occurring in 8 week old mice [32, 33]. This study demonstrates that exercise accelerated this growth in the tibiae of male mice by increasing cross-sectional dimensions compared with non-exercise control mice (Figure 3.2 and Figure 3.3). Because a baseline group was not included, it is unclear how much bone was forming in the control mice. However, it is clear that due to growth effects, the exercise bones contain more tissue that formed under exposure to mechanical stimulation than the simple difference in size between exercise and control mice. This mechanical stimulation had a profound effect on the forming bone resulting in the observed improvements in post-yield properties.

Because the contribution of bone material to structural strength increases as the square of the distance from the centroid, a large moment of inertia is favorable and normally results in greater structural strength. In this study, however, the loaded tibial diaphyses had more material and a greater moment of inertia, but decreased structural yield strength and yield deformation. Decreases in structural mechanical properties in response to exercise have also been observed in growing rats. For example, ten weeks of strenuous running in 8 week old rats detrimentally affected structural properties of the growing tibiae (decreased yield force and ultimate force, decreased work-to-failure) [34]. Similarly, ten weeks of high intensity running in 4 month old rats decreased twist angle and energy absorption in the femur [21], while three weeks of moderate intensity running in 3 month old rats decreased stiffness but increased twist angle of the tibia [35]. However, to the best of our knowledge, detrimental functional effects in response to moderate exercise or loading have not been demonstrated in mice.

Increased quantity of tissue resulting in decreased structural yield strength implies that changes in tissue quality are driving the decreases in structural properties. While not measured in the current study, it seems likely that exercise-induced changes within the newly forming and pre-existing bone matrix are occurring [36]. The organic matrix, predominantly Type I collagen, dictates post-yield behavior in bone [37-40]. Therefore,

it is reasonable to hypothesize that the post-yield changes noted here are a toughening-mechanism in the bone due to alterations in collagen, possibly in the orientation of newly-forming fibers or in the number, quality or maturity of cross-linking as has been shown in other exercise studies using Raman Spectroscopy [41]. However, the integrity of the collagen network and bone strength are not mutually exclusive, since collagen forms the scaffold for mineralization. Differences in collagen that improve post-yield properties could induce alterations in mineral crystal size and/or orientation, resulting in greater vBMD in the exercise bones, but leading to the decrease in tissue-level strength [37, 40, 42]. It is also possible that given more time between the termination of exercise and sacrifice, newly formed bone may mature and alterations that occurred in the pre-existing bone may further change leading to increased strength [43].

In males, the contrast between a strong response to exercise in the tibia with little response noted in the femora supports the hypothesis of a bone-specific response to running. Others have demonstrated surface or site-specific responses to exercise in a single location in one bone (increased periosteal bone formation with no effect on endocortical formation of the femoral diaphysis; [13, 16, 44]), two locations in the same bone (greater increase in cancellous bone mass of the distal tibia than in the proximal tibia; [45]) and among different bones [13, 20, 21, 35]. One problem with many studies investigating the response of bone to exercise is that one bone (e.g. the femur) is used to determine some properties while another bone (e.g. the tibia) is used to determine other properties, making it difficult to detect a differential response in the long bones of the leg. Because the femoral diaphysis is the standard site for investigations in murine cortical bone, the tibial diaphysis is frequently not evaluated. However, especially in murine running models, the tibia is also an important location to investigate due to the proximity of this bone to the point of impact and the orientation of the bones during running. One possible explanation for the bone specific response to exercise relates to the biomechanics of mice running on a treadmill. We observed that mice tend to run with both hind legs flared out laterally. This qualitatively appears to subject the tibia to a more complex loading state (axial loads, bending and torsion) versus the mostly bending loads on the femora. Perhaps this loading state causes the bone formation threshold to be exceeded in the tibia more easily than in the femora.

Gender specificity in response to exercise in rodents is not unknown [17, 18, 46, 47], but the mechanisms remain elusive and are most often attributed to hormonal differences between the genders. The tibiae of young female mice can respond to loading [48-52] and exercise [19]. The fact that this tibial response to loading and exercise is regulated by genetic factors [19, 48, 51] may explain why mice from the hybrid strain used in this study were unable to respond. The hybrid strain was used because mice from this strain have been utilized as the wild type background strain for many genetic knockouts [25, 53, 54]. All mice in the current study were wild type animals which have a low bone mass phenotype that is generally similar to that of C57BL6 mice [55].

At baseline, the mean body weight of female mice was less than males (Figure 3.1), whereas cortical bone area and bending moment of inertia were slightly larger than in males (NS, Figure 3.2). Even with running, a critical strain threshold for stimulating increases in bone formation activity [56, 57] may never have been surpassed in females suggesting that a longer duration or greater intensity of running might be necessary in female mice [17, 19, 58]. The actual strains experienced by each bone during running could be determined directly using strain gauges, or indirectly using a finite element model. However, these experiments are beyond the scope of the current study, and strain-gauging mice during running is non-trivial.

Differences in growth rates between male and female mice may be contributing to the disparity in response to mechanical loading [47]. One of the limitations of the current study is that formation activity using fluorochrome labeling was not performed. A further limitation is that a baseline group of mice was not included. Therefore, it is not possible to determine how the effects of growth and growth rate during exercise are influencing the properties that are measured.

Unlike mice in voluntary running studies, the mice in the current study were forced to run on a treadmill. This speed and daily duration were considered moderate and were sufficient to elicit a bone formation response in male (5 weeks old) and female (7 weeks old) mice [16, 59]. However, the 3 week duration of the exercise regimen used in the current study is 1 week shorter than in these previous studies and at a lesser incline in an attempt to elicit a response in the shortest time possible. With this type of forced exercise, it is possible that the exercise mice were subjected to an increased stress

response which has implications to bone health. Though not measured in the current study, the stress effects associate with running on a treadmill have been investigated (data not shown). Hormone levels (testosterone, corticosterone) were measured at various time points in the blood, and body weight was tracked every day. At the end of the study, geometric and mechanical properties were measured. No discernible effects on hormone levels were found with exercise or stress. Geometric and mechanical properties in the stress group were the same as in the control group, suggesting that the effects of exercise on these properties were truly the results of mechanical loading and not stress.

In summary, this study demonstrates that in growing B6;129 mice, the response to three weeks of running on a treadmill is bone and gender-specific. As opposed to the minimal effect noted in females and in the male femora, this short-term exercise regime impacted the male tibial diaphysis, which responded to exercise via an increase in periosteal perimeter, endocortical perimeter, tissue area and distribution compared with growth alone. The exercise mice had greater structural post-yield deformation and tissue-level strain, but these benefits of exercise came at the expense of tissue-level strength, and structural yield strength and deformation. These results suggest that exercise superimposed upon growth accelerated growth-related increases in tibial cross-sectional dimensions. Exercise also influenced the quality of this forming bone, significantly impacting structural and tissue-level mechanical properties.

Acknowledgements

I would like to acknowledge my coauthors on this manuscript:

Dr. Rupak M. Rajachar, Dr. Matthew R. Allen, Dr. Susan A. Bloomfield, Dr. Pamela G. Robey, Dr. Marian F. Young and Dr. David H. Kohn.

Funding sources for this study:

DoD/US Army DAMD17-03-1-0556; NIH T32-DE07057; NIH IPA Agreement; Regenerative Sciences Training Grant T90-DK071506

This chapter was published as: Wallace et.al, Bone 2007; 40 (4): 1120-1127

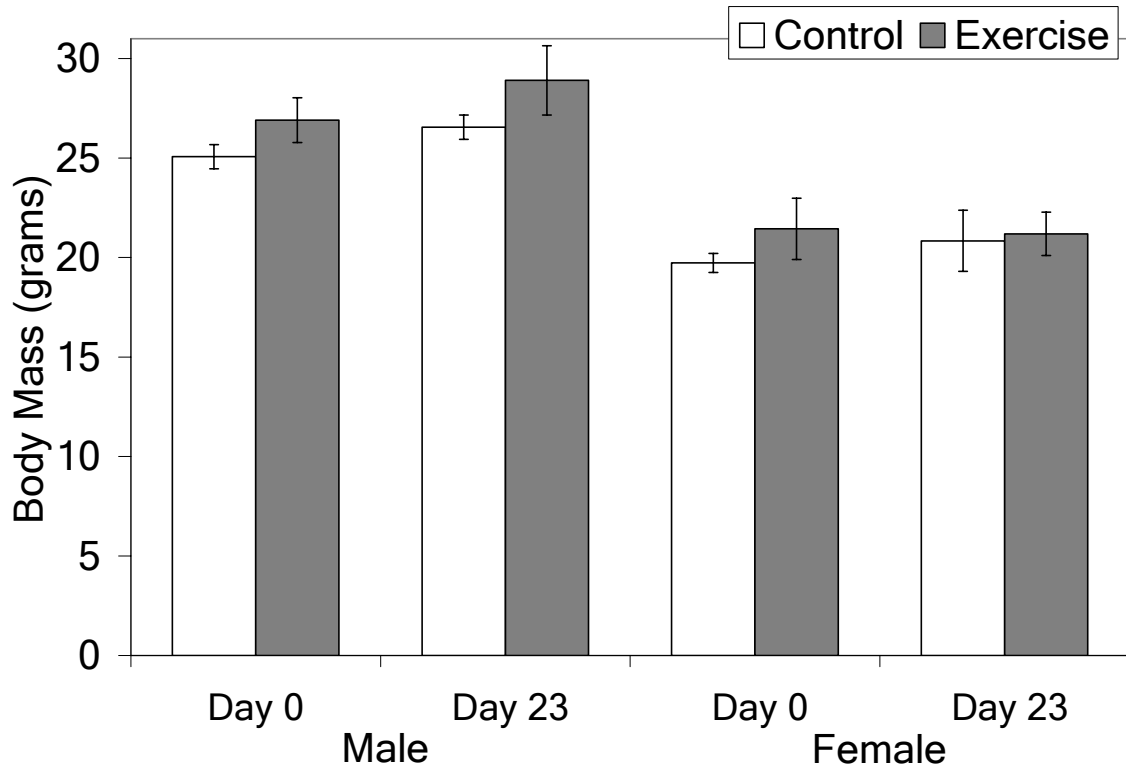


Figure 3.1: Body Weights of Male and Female C57BL/129 Mice Prior To and Following Exercise. At the beginning of the study at 8 weeks of age (Day 0), control and exercise groups in each gender were body weight matched. Body weights were again measured following sacrifice (Day 23), with no difference noted between exercise and control groups in either gender. Data are presented as mean \pm SEM.

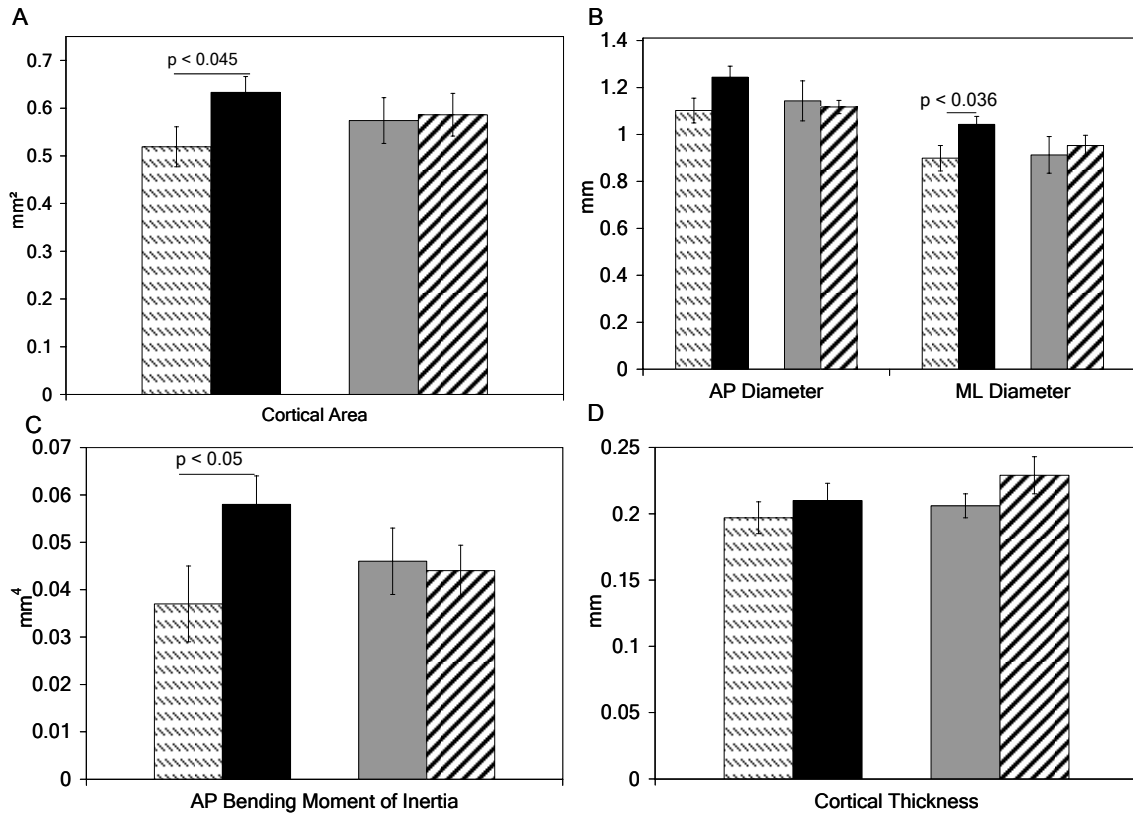


Figure 3.2: Geometric Properties of the Male and Female Tibial Diaphyses Following Exercise. In C57BL/6/129 males, 3 weeks of exercise beginning at 8 weeks of age resulted in a statistically significant increase in cortical area (A) and medial-lateral (ML) width (B) at the tibial mid-diaphysis, resulting in an increase in Anterior-Posterior (AP) bending moment of inertia (C). No changes were noted in any properties in females. Data are presented as mean \pm SEM. = control male, = exercise male, = control female, = exercise female.

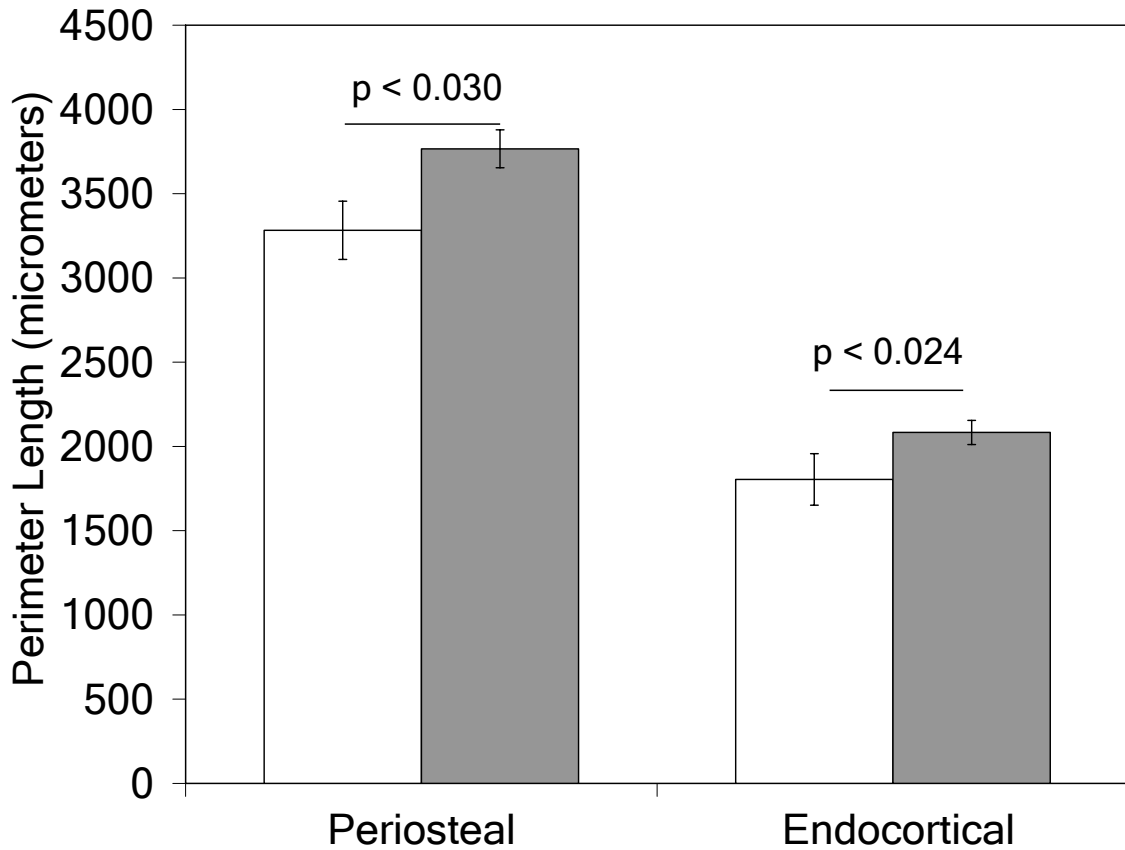




Figure 3.3: Periosteal and Endocortical Perimeters of the Male Tibial Diaphyses Following Exercise. In C57BL6/129 males, 3 weeks of exercise beginning at 8 weeks of age resulted in a statistically significant increase in periosteal and endocortical perimeter, indicating greater periosteal formation and endocortical resorption in the exercise mice. Data are presented as mean \pm SEM.  = control male,  = exercise male.

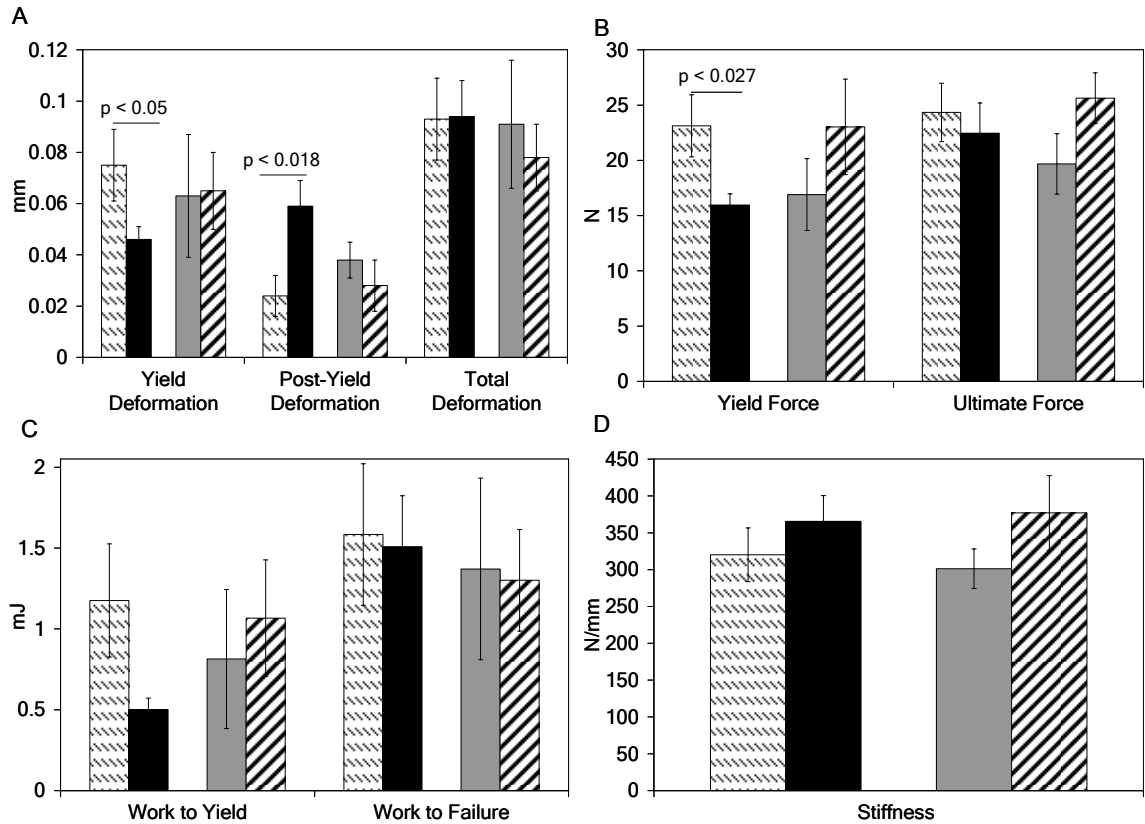


Figure 3.4: Structural Level Mechanical Properties of the Male and Female Tibial Diaphyses Following Exercise. In C57BL/129 males, 3 weeks of exercise beginning at 8 weeks of age increased tibial post-yield deformation (A), but at the expense of yield deformation (A) and yield force (B). No changes were noted in any properties in females. Data are presented as mean \pm SEM. = control male, = exercise male, = control female, = exercise female.

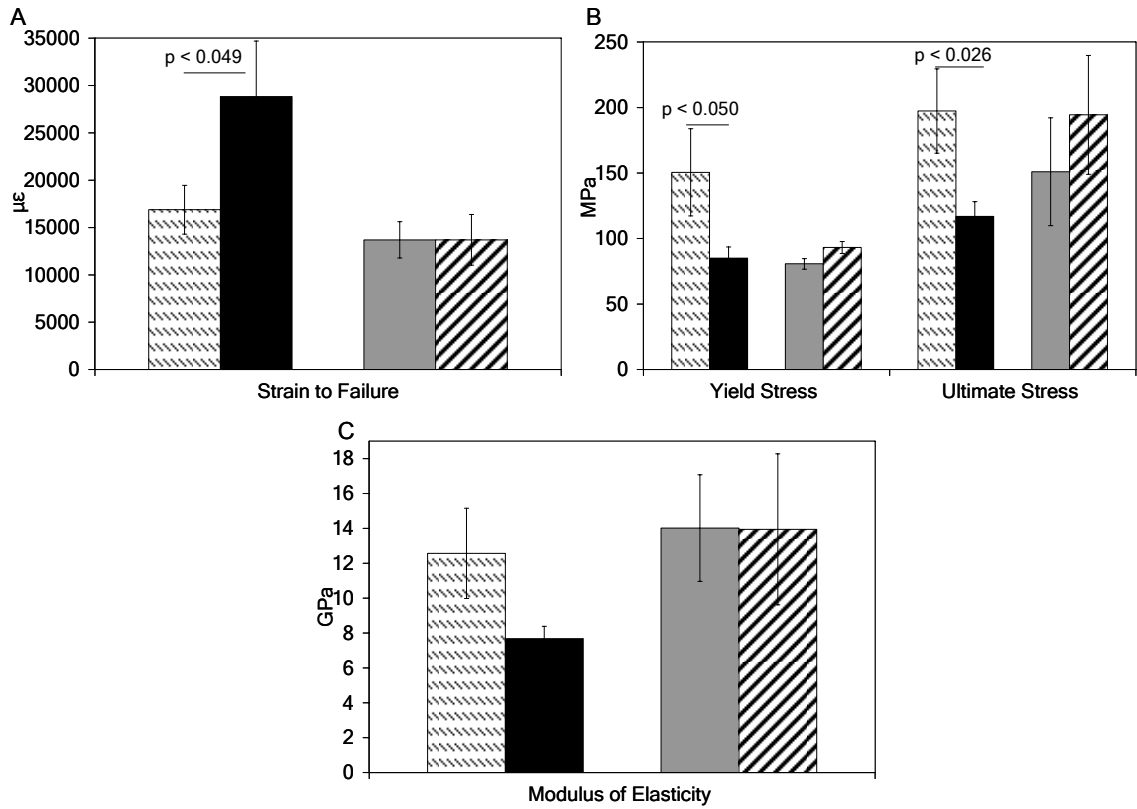


Figure 3.5: Tissue Level Mechanical Properties of the Male and Female Tibial Diaphyses Following Exercise. In C57BL/6/129 males, 3 weeks of exercise beginning at 8 weeks of age increased tibial strain to failure (A), but at the expense of yield and ultimate tissue strength (B). No changes were noted in any properties in females. Data are presented as mean \pm SEM. = control male, = exercise male, = control female, = exercise female.

Table 3.1: Geometric Properties of the Male and Female Femoral Diaphyses of Control and Exercise Mice

Group	Length (mm)	Cortical Area (mm ²)	AP Diameter (mm)	ML Diameter (mm)	Moment of Inertia (mm ⁴)	Average Thickness (mm)
Male Femora (Control)	13.94 ± 0.82	0.88 ± 0.05	1.16 ± 0.02	1.78 ± 0.12	0.103 ± 0.003	0.224 ± 0.013
Male Femora (Exercise)	14.71 ± 0.04	0.85 ± 0.07	1.18 ± 0.04	1.69 ± 0.06	0.113 ± 0.013	0.223 ± 0.019
Female Femora (Control)	14.42 ± 0.07	0.80 ± 0.03	1.23 ± 0.02	1.63 ± 0.04	0.110 ± 0.007	0.224 ± 0.018
Female Femora (Exercise)	14.22 ± 0.28	0.76 ± 0.02	1.19 ± 0.03	1.64 ± 0.09	0.115 ± 0.013	0.241 ± 0.021

Geometric properties were determined from histology at the fracture site. Data are presented as mean ± SEM.

Table 3.2: Structural Mechanical Properties of the Male and Female Femoral Diaphyses of Control and Exercise Bones

Group	Yield Force (N)	Ultimate Force (N)	Yield Deformation (mm)	Post-Yield Deformation (mm)	Total Deformation (mm)	Stiffness (N/mm)	Work to Yield (mJ)	Work to Failure (mJ)
Male Femora (Control)	21.38 ± 2.68	29.06 ± 2.89	0.080 ± 0.015	0.061 ± 0.017	0.141 ± 0.024	274.3 ± 41.8	1.06 ± 0.21	2.63 ± 0.54
Male Femora (Exercise)	21.33 ± 2.56	29.34 ± 1.59	0.080 ± 0.008	0.074 ± 0.026	0.153 ± 0.020	265.5 ± 24.1	1.04 ± 0.19	2.86 ± 0.45
Female Femora (Control)	26.01 ± 1.66	35.91 ± 1.59	0.066 ± 0.012	0.054 ± 0.008	0.120 ± 0.014	495.6 ± 38.0	1.02 ± 0.14	2.75 ± 0.32
Female Femora (Exercise)	26.76 ± 3.35	33.49 ± 2.85	0.084 ± 0.019	0.037 ± 0.01	0.115 ± 0.01	364.2 ± 49.3^b	1.42 ± 0.35	2.50 ± 0.43

Data are presented as mean ± SEM. b indicates 0.05 < p < 0.10 vs. control for the same gender.

Table 3.3: Tissue-Level Mechanical Properties of the Male and Female Femoral Diaphyses of Control and Exercise Bones

Group	Yield Stress (MPa)	Ultimate Stress (MPa)	Strain to Failure ($\mu\epsilon$)	Modulus of Elasticity (GPa)
Male Femora (Control)	62.75 \pm 10.10	85.05 \pm 11.64	36000 \pm 5446	3.13 \pm 0.50
Male Femora (Exercise)	56.67 \pm 7.05	78.17 \pm 5.33	38637 \pm 5021	2.78 \pm 0.23
Female Femora (Control)	73.47 \pm 4.03	101.49 \pm 3.00	31804 \pm 4617	5.26 \pm 0.19
Female Femora (Exercise)	74.67 \pm 11.44	90.23 \pm 6.83^b	29878 \pm 3236	3.73 \pm 0.40^a

Data are presented as mean \pm SEM. a indicates $p < 0.05$ vs. control for the same gender. b indicates $0.05 < p < 0.10$ vs. control for the same gender.

References

- (1) U.S. Department of Health and Human Services, Office of the Surgeon General (2004) Bone Health and Osteoporosis: A Report of the Surgeon General.
- (2) Burr DB (2001) Musculoskeletal Fatigue and Stress Fractures. CRC Press, Boca Raton, FL
- (3) Bennell KL, Malcolm SA, Thomas SA, Reid SJ, Brukner PD, Ebeling PR, Wark JD (1996) Risk factors for stress fractures in track and field athletes. A twelve-month prospective study. *Am.J.Sports Med.* 24:810-818
- (4) Bennell KL, Brukner PD (1997) Epidemiology and site specificity of stress fractures. *Clin.Sports Med.* 16:179-196
- (5) Maitra RS, Johnson DL (1997) Stress fractures. Clinical history and physical examination. *Clin.Sports Med.* 16:259-274
- (6) Jones BH, Harris JM, Vinh TN, Rubin C (1989) Exercise-induced stress fractures and stress reactions of bone: epidemiology, etiology, and classification. *Exerc.Sport Sci.Rev.* 17:379-422
- (7) Jones BH, Bovee MW, Harris JM,3rd, Cowan DN (1993) Intrinsic risk factors for exercise-related injuries among male and female army trainees. *Am.J.Sports Med.* 21:705-710
- (8) Reinker KA, Ozburne S (1979) A comparison of male and female orthopaedic pathology in basic training. *Mil.Med.* 144:532-536
- (9) Burr DB, Forwood MR, Fyhrie DP, Martin RB, Schaffler MB, Turner CH (1997) Bone microdamage and skeletal fragility in osteoporotic and stress fractures. *J.Bone Miner.Res.* 12:6-15
- (10) Wolff J (1892) *Das gesetz der transformation der knochen.* August Hirschwald, Berlin
- (11) Umemura Y, Ishiko T, Yamauchi T, Kurono M, Mashiko S (1997) Five jumps per day increase bone mass and breaking force in rats. *J.Bone Miner.Res.* 12:1480-1485
- (12) Iwamoto J, Yeh JK, Aloia JF (2000) Effect of deconditioning on cortical and cancellous bone growth in the exercise trained young rats. *J.Bone Miner.Res.* 15:1842-1849

- (13) Notomi T, Okimoto N, Okazaki Y, Tanaka Y, Nakamura T, Suzuki M (2001) Effects of tower climbing exercise on bone mass, strength, and turnover in growing rats. *J.Bone Miner.Res.* 16:166-174
- (14) Huang TH, Lin SC, Chang FL, Hsieh SS, Liu SH, Yang RS (2003) Effects of different exercise modes on mineralization, structure, and biomechanical properties of growing bone. *J.Appl.Physiol.* 95:300-307
- (15) Mori T, Okimoto N, Sakai A, Okazaki Y, Nakura N, Notomi T, Nakamura T (2003) Climbing exercise increases bone mass and trabecular bone turnover through transient regulation of marrow osteogenic and osteoclastogenic potentials in mice. *J.Bone Miner.Res.* 18:2002-2009
- (16) Wu J, Wang XX, Higuchi M, Yamada K, Ishimi Y (2004) High bone mass gained by exercise in growing male mice is increased by subsequent reduced exercise. *J.Appl.Physiol.* 97:806-810
- (17) Hoshi A, Watanabe H, Chiba M, Inaba Y (1998) Bone density and mechanical properties in femoral bone of swim loaded aged mice. *Biomed.Enviro.Sci.* 11:243-250
- (18) Gordon KR, Levy C, Perl M, Weeks OI (1994) Experimental perturbation of the development of sexual size dimorphism in the mouse skeleton. *Growth Dev.Aging* 58:95-104
- (19) Kodama Y, Umemura Y, Nagasawa S, Beamer WG, Donahue LR, Rosen CR, Baylink DJ, Farley JR (2000) Exercise and mechanical loading increase periosteal bone formation and whole bone strength in C57BL/6J mice but not in C3H/HeJ mice. *Calcif.Tissue Int.* 66:298-306
- (20) van der Wiel HE, Lips P, Graafmans WC, Danielsen CC, Nauta J, van Lingen A, Mosekilde L (1995) Additional weight-bearing during exercise is more important than duration of exercise for anabolic stimulus of bone: a study of running exercise in female rats. *Bone* 16:73-80
- (21) Wheeler DL, Graves JE, Miller GJ, Vander Griend RE, Wronski TJ, Powers SK, Park HM (1995) Effects of running on the torsional strength, morphometry, and bone mass of the rat skeleton. *Med.Sci.Sports Exerc.* 27:520-529
- (22) Khan K, McKay HA, Haapasalo H, Bennell KL, Forwood MR, Kannus P, Wark JD (2000) Does childhood and adolescence provide a unique opportunity for exercise to strengthen the skeleton? *J.Sci.Med.Sport* 3:150-164
- (23) Heinonen A, Sievanen H, Kannus P, Oja P, Pasanen M, Vuori I (2000) High-impact exercise and bones of growing girls: a 9-month controlled trial. *Osteoporos.Int.* 11:1010-1017

- (24) Mackelvie KJ, McKay HA, Khan KM, Crocker PR (2001) A school-based exercise intervention augments bone mineral accrual in early pubertal girls. *J.Pediatr.* 139:501-508
- (25) Wallace JM, Rajachar RM, Chen XD, Shi S, Allen MR, Bloomfield SA, Les CM, Robey PG, Young MF, Kohn DH (2006) The mechanical phenotype of biglycan-deficient mice is bone- and gender-specific. *Bone* 39:106-116
- (26) Rajachar RM (2003) Effects of Age-Related Ultra-Structural Changes in Bone on Microdamage Mechanisms. PhD Dissertation.
- (27) Sommer HJ (2002) Polygeom Matlab Function Available at: <http://www.me.psu.edu/sommer/me562/polygeom.m>
- (28) Turner CH, Burr DB (1993) Basic Biomechanical Measurements of Bone: A Tutorial. *Bone* 14:595-607
- (29) Chen XD, Allen MR, Bloomfield S, Xu T, Young M (2003) Biglycan-deficient mice have delayed osteogenesis after marrow ablation. *Calcif.Tissue Int.* 72:577-582
- (30) Brodt MD, Pelz GB, Taniguchi J, Silva MJ (2003) Accuracy of peripheral quantitative computed tomography (pQCT) for assessing area and density of mouse cortical bone. *Calcif.Tissue Int.* 73:411-418
- (31) Schmidt C, Priemel M, Kohler T, Weusten A, Muller R, Amling M, Eckstein F (2003) Precision and accuracy of peripheral quantitative computed tomography (pQCT) in the mouse skeleton compared with histology and microcomputed tomography (microCT). *J.Bone Miner.Res.* 18:1486-1496
- (32) Ferguson VL, Ayers RA, Bateman TA, Simske SJ (2003) Bone development and age-related bone loss in male C57BL/6J mice. *Bone* 33:387-398
- (33) Somerville JM, Aspden RM, Armour KE, Armour KJ, Reid DM (2004) Growth of C57BL/6 mice and the material and mechanical properties of cortical bone from the tibia. *Calcif.Tissue Int.* 74:469-475
- (34) Li KC, Zernicke RF, Barnard RJ, Li AF (1991) Differential response of rat limb bones to strenuous exercise. *J.Appl.Physiol.* 70:554-560
- (35) Forwood MR, Parker AW (1991) Repetitive loading, in vivo, of the tibiae and femora of rats: effects of repeated bouts of treadmill-running. *Bone Miner.* 13:35-46

- (36) Sahar ND, Kohn DH, Golcuk K, Morris MD Effects of Exercise on Bone Quality As Shown By Raman Microspectroscopy, paper No. 1619. 2006 Annual Meeting of the Orthopaedic Society
- (37) Boskey AL, Wright TM, Blank RD (1999) Collagen and bone strength. *J.Bone Miner.Res.* 14:330-335
- (38) Burr DB (2002) The contribution of the organic matrix to bone's material properties. *Bone* 31:8-11
- (39) Burstein AH, Zika JM, Heiple KG, Klein L (1975) Contribution of collagen and mineral to the elastic-plastic properties of bone. *J.Bone Joint Surg.Am.* 57:956-961
- (40) Wang X, Shen X, Li X, Agrawal CM (2002) Age-related changes in the collagen network and toughness of bone. *Bone* 31:1-7
- (41) Kohn DH, Sahar ND, Hong S, Golcuk K, Morris MD (2005) Local Mineral and Matrix Changes Associated with Bone Adaptation and Microdamage, Paper No. 0898-L09-03. *Mater. Res. Soc. Symp. Proc.* 898E
- (42) Oxlund H, Barckman M, Ortoft G, Andreassen TT (1995) Reduced concentrations of collagen cross-links are associated with reduced strength of bone. *Bone* 17:365S-371S
- (43) Wallace JM, Ron MS, Kohn DH Increased Post-Yield Properties Induced When Exercise is Superimposed on Growth Are Maintained After 2 Weeks With The Addition of Strength, abstract 080261. *Proceedings of the 2005 Summer Bioengineering Conference*
- (44) Notomi T, Lee SJ, Okimoto N, Okazaki Y, Takamoto T, Nakamura T, Suzuki M (2000) Effects of resistance exercise training on mass, strength, and turnover of bone in growing rats. *Eur.J.Appl.Physiol.* 82:268-274
- (45) Iwamoto J, Yeh JK, Aloia JF (1999) Differential effect of treadmill exercise on three cancellous bone sites in the young growing rat. *Bone* 24:163-169
- (46) Yingling VR, Davies S, Silva MJ (2001) The effects of repetitive physiologic loading on bone turnover and mechanical properties in adult female and male rats. *Calcif.Tissue Int.* 68:235-239
- (47) Mosley JR, Lanyon LE (2002) Growth rate rather than gender determines the size of the adaptive response of the growing skeleton to mechanical strain. *Bone* 30:314-319

- (48) Akhter MP, Cullen DM, Pedersen EA, Kimmel DB, Recker RR (1998) Bone response to in vivo mechanical loading in two breeds of mice. *Calcif.Tissue Int.* 63:442-449
- (49) Gross TS, Srinivasan S, Liu CC, Clemens TL, Bain SD (2002) Noninvasive loading of the murine tibia: an in vivo model for the study of mechanotransduction. *J.Bone Miner.Res.* 17:493-501
- (50) LaMothe JM, Zernicke RF (2004) Rest insertion combined with high-frequency loading enhances osteogenesis. *J.Appl.Physiol.* 96:1788-1793
- (51) Kesavan C, Mohan S, Oberholtzer S, Wergedal JE, Baylink DJ (2005) Mechanical loading-induced gene expression and BMD changes are different in two inbred mouse strains. *J.Appl.Physiol.* 99:1951-1957
- (52) De Souza RL, Matsuura M, Eckstein F, Rawlinson SC, Lanyon LE, Pitsillides AA (2005) Non-invasive axial loading of mouse tibiae increases cortical bone formation and modifies trabecular organization: A new model to study cortical and cancellous compartments in a single loaded element. *Bone* 37:810-818
- (53) Alam I, Warden SJ, Robling AG, Turner CH (2005) Mechanotransduction in bone does not require a functional cyclooxygenase-2 (COX-2) gene. *J.Bone Miner.Res.* 20:438-446
- (54) Li CY, Jepsen KJ, Majeska RJ, Zhang J, Ni R, Gelb BD, Schaffler MB (2006) Mice lacking cathepsin K maintain bone remodeling but develop bone fragility despite high bone mass. *J.Bone Miner.Res.* 21:865-875
- (55) Wergedal JE, Sheng MH, Ackert-Bicknell CL, Beamer WG, Baylink DJ (2005) Genetic variation in femur extrinsic strength in 29 different inbred strains of mice is dependent on variations in femur cross-sectional geometry and bone density. *Bone* 36:111-122
- (56) Hsieh YF, Robling AG, Ambrosius WT, Burr DB, Turner CH (2001) Mechanical loading of diaphyseal bone in vivo: the strain threshold for an osteogenic response varies with location. *J.Bone Miner.Res.* 16:2291-2297
- (57) Turner CH, Forwood MR, Rho JY, Yoshikawa T (1994) Mechanical loading thresholds for lamellar and woven bone formation. *J.Bone Miner.Res.* 9:87-97
- (58) Hoshi A, Watanabe H, Chiba M, Inaba Y (1998) Effects of exercise at different ages on bone density and mechanical properties of femoral bone of aged mice. *Tohoku J.Exp.Med.* 185:15-24

- (59) Wu J, Wang XX, Takasaki M, Ohta A, Higuchi M, Ishimi Y (2001) Cooperative effects of exercise training and genistein administration on bone mass in ovariectomized mice. *J. Bone Miner. Res.* 16:1829-1836

CHAPTER 4

INBRED STRAIN-SPECIFIC RESPONSE TO BIGLYCAN DEFICIENCY IN THE CORTICAL BONE OF C57BL6/129 AND C3H/HE MICE

Introduction

The ability to selectively disrupt protein production in mice has provided invaluable insight into the roles that different proteins play and how these roles relate to human disease. Mice with targeted mutations in specific bone matrix proteins have been utilized to study the proteins' roles in regulating bone matrix deposition, composition, architecture and mechanical integrity and understanding how these functions relate to bone disease and fracture etiology [1-3].

One such model of disrupted protein production is the biglycan (bgn)-deficient mouse [4-6]. Bgn is a small leucine-rich proteoglycan (SLRP) that is enriched in the extracellular matrix (ECM) of bone and other connective tissues [7-9]. Bgn-deficient mice exhibit a defect in the growth and differentiation of osteoblast precursor cells resulting in altered bone production and function [10-12]. For example, 11 week old bgn-deficient male mice bred on the C57BL6/129 (B6;129) inbred background strain have decreased tissue-level yield strength along with structural-level deficiencies in yield deformation and work to yield [13]. Reduced tissue yield strength, which is independent of the amount of tissue present, suggests that deficiencies in bone ECM quality are responsible, and this notion is supported by data showing that the diameter of collagen fibrils in bgn-deficient bone is larger and more variable and often exhibits notches, protuberances and irregular spacing [5, 6]. Bgn-deficient bones also have greater volumetric bone mineral density (vBMD) [13] and larger mineral crystal size [14] compared to wild type mice, possibly due to the altered collagen template upon which mineralization occurs.

The C57BL6 (B6) and C3H/He (C3H) inbred strains have been utilized as models of high (C3H) and low (B6) bone density in a variety of bone-related studies [15]. Inbred strain-specific differences exist in bone cross-sectional geometric properties (greater cross-sectional area in B6, greater cortical area and cortical thickness in C3H [16, 17]), whole bone and tissue level mechanical properties (greater strength and stiffness at both levels in C3H [16-19]) and indices of bone formation in all bones and ages (increased mineral apposition rate as a measure of increased osteoblast activity and metabolism in C3H mice on periosteal and endocortical surfaces of the femora and tibiae, in trabecular bone of the metaphyses of the femora and the lumbar vertebrae and in membranous parietal bones of the calvaria at ages range from newborns through to at least 26 weeks of age [20-23]). Inbred strain-specific responses to external stimuli including mechanical loading, unloading [24-27] and bone regeneration [28-30] also exist and demonstrate that the bones from C3H mice consistently fail to respond to changes in the mechanical environment. However, the effects of background strain in other experimental situations such as gene disruption are unknown.

Because of the described inherent differences in inbred mouse strains, particularly increased bone formation [20-23] and mineralization [15] in C3H mice, it was hypothesized that an inbred strain-specific response would exist in response to a gene deletion. *Bgn*-deficiency impacts the bone matrix through negative regulation of osteoblast number and function, which results in ECM alterations. Because C3H osteoblasts are highly active and robust versus osteoblasts from B6 mice, and the bones of C3H mice are unresponsive to other insults, it was hypothesized that compared with the response in B6;129 mice, C3H mice would be relatively more resistant to changes in ECM production and mineralization associated with *bgn*-deficiency. Therefore, the negative mechanical effects of *bgn*-deficiency would be minimized in C3H mice relative to the effects in B6;129 mice. The hybrid B6;129 strain was used in this study because mice from this inbred strain have been utilized as the wild type background strain for many genetic knockouts, including the *bgn*-deficient mouse [4, 13, 31, 32]. The B6;129 inbred strain has a low bone mass phenotype that is generally similar to that of B6 mice [19], and is therefore an appropriate inbred mouse strain to use in comparison to the high bone mass C3H mice. Because the *bgn*-deficient phenotype is strongest in the male tibia

[13], changes in tissue composition (Raman Microspectroscopy), bone formation (dynamic histomorphometry), cross-sectional geometry and vBMD (microCT) mechanical properties (four-point bending) and mRNA expression (qRT-PCR) were investigated in the tibiae of 8 and 11 week old male bgn-deficient mice bred on B6;129 and C3H backgrounds to uncover an inbred strain-specific response to bgn-deficiency at the ultrastructural level, the tissue-level and the structural (whole bone) level.

Materials and Methods

Animals

All animal procedures were performed at the University of Michigan with University Committee on Use and Care of Animals (UCUCA) approval (UCUCA animal approval protocol #8518). Biglycan-deficient (KO) and wild type (WT) breeder mice were the generous gift of Dr. Marian F. Young from the National Institute of Dental and Craniofacial Research (NIDCR). Mice from the B6;129 background strain were originally generated by homologous recombination in embryonic stem cells [4]. Mice from this background strain were then backcrossed to the C3H/HeNHsd (C3H) strain to a purity of greater than 95%. Upon arrival at the University of Michigan, the genotype of all breeder pairs was verified via standard polymerase chain reaction (PCR) using DNA extracted from a tail biopsy of each mouse as previously described [33]. This process was repeated for the F1 generation of mice from each breeder pair as verification.

To determine proper sample sizes for detecting effects of genotype and background strain, power calculations were performed based on published values for differences and standard deviations in mechanical and geometric properties between inbred mouse strains [17, 19] and due to bgn deficiency in B6;129 male mice [13] using a value of $\alpha=0.05$ and a power $(1-\beta)$ of 0.80. To statistically detect inbred strain-specificity in response to the gene deletion, further power calculations were carried out based on expected ratios of values (KO/WT) between the two inbred strains [34]. To be able to statistically detect inbred-strain specific responses in primary outcome measures of interest based on expected differences (tibial length, vBMD, cross-sectional size, strength

at whole bone and tissue-levels, total deformation and failure strain), a sample size of $n=15$ was used for each group.

At 3 weeks of age, mice were weaned and maintained in standard cages with access to food, water and cage activity *ad libitum*. At 8 weeks of age (Day 0), mice from each background strain/genotype were randomly assigned to 1 of 2 weight-matched groups (2 inbred strains x 2 age groups x 2 genotypes x $n=15$ per group = a total of 120 mice). The first group was sacrificed at 8 weeks of age and the second group was sacrificed at 11 weeks of age. Mice in the 11 week groups were given intraperitoneal (IP) injections of calcein (15 mg/kg body mass on Day 4) and xylene orange (80 mg/kg body mass on Day 9) to assess bone formation. Mice were sacrificed by CO₂ inhalation, at which time final body mass was measured and left tibiae were harvested, stripped of soft tissue, wrapped in gauze soaked in a calcium-buffered saline solution and stored at -20°C.

Micro Computed Tomography (μ CT) Evaluation

Left tibiae were analyzed by micro computed tomography (μ CT) to assess length, cross-sectional geometric properties and volumetric bone mineral density (vBMD). Bones were scanned at 18 μ m/voxel resolution (GE/EVS MS-8 specimen scanner, GE Healthcare, London, Ontario, Canada) and three-dimensional images were reconstructed. Each three-dimensional data set was arranged as a series of 18 μ m-thick slices oriented along the long axis of the tibia. Tibial length was measured directly on each reconstructed image from the most proximal portion of the chondyles to the most distal portion of the medial malleolus (MicroView version 2.1.2, GE Healthcare).

Cross-sectional geometry from the fracture site (to normalize whole bone mechanical properties, see methods section on mechanical testing) and both geometry and vBMD from a standard site in the diaphysis of each bone were determined. The standard site was located at a position 792 μ m proximal to the location where the tibia and fibula first become fused (TFJ), and was chosen to lie just distal to the mechanical loading region (which began 800 μ m proximal to the TFJ). Averaged over all bones, this corresponded to a standard location that was $4.83 \pm 0.14\%$ of the total bone length

proximal to the TFJ. Properties were determined from 6 μ CT slices centered at this location.

After investigating histograms of voxel values from all standard sections, vBMD was determined at each section using a standard threshold level of 2000 (MicroView version 2.1.2, GE Healthcare). For the measurement of geometric properties, each section was thresholded into bone and non-bone voxels using a previously defined method [35]. Geometric properties for each standard region of interest were then determined using a custom analysis program. Properties of interest included total cross-sectional area, cortical area, marrow area (data not shown in Figure 4.4, but is equal to the difference between cross-sectional area and cortical area), anterior-posterior (AP) width, medial-lateral (ML) width, bending moment of inertia about the AP and ML axes (I_{AP} , I_{ML}) and average cortical thickness.

Mechanical Testing

Left tibiae were brought to room temperature before testing and were kept hydrated in calcium-buffered saline until the test was complete. Each bone was tested in the ML direction (medial surface in tension) in four-point bending (Admet eXpert 450 Universal Testing Machine; Norwood, MA). The bone was positioned such that the TFJ was lined up with the outside edge of one loading roller. The bones were preloaded to 0.5 N, preconditioned for 15 seconds (2 Hz, mean load of $2 \text{ N} \pm 2 \text{ N}$) and then monotonically tested to failure in displacement control at a rate of 0.025 mm/sec. During each test, load and deflection were recorded, from which structural strength (yield force and ultimate force), stiffness (the slope of the linear portion of the force vs. displacement curve), deformation (yield deformation, total deformation and post-yield deformation) and energy or work (measured as the area under the force vs. displacement curve), were derived at the whole bone level [13, 36]. After testing, the distal end of each bone was placed in 70% ethanol.

During testing, the bone was visually monitored and the point of fracture initiation was noted and measured relative to the proximal end. In order to normalize structural-level mechanical properties and estimate tissue-level mechanical properties, a

subset of geometric properties at the fracture site was obtained from μ CT data (I_{AP} and the distance from the centroid to the tensile surface of the bone, c). Together with the load and deflection data, I_{AP} and c were used to map force and displacement (structural level properties dependent on bone structural organization) into stress and strain (predicted tissue level properties) from standard beam-bending equations for four-point bending:

$$Stress = \sigma = \frac{Fac}{2I_{AP}} \quad (MPa)$$

$$Strain = \varepsilon = \frac{6cd}{a(3L - 4a)} \times 10^6 \quad (\mu\varepsilon)$$

In these equations, F is the force, d is the displacement, a is the distance from the support to the inner loading point (3 mm) and L is the span between the outer supports (9 mm). The yield point was calculated using the 0.2% offset method based on the stress-strain curve [37]. The modulus of elasticity was calculated as the slope of the linear portion of the stress-strain curve.

Histomorphometry

Following fracture testing, the distal half of all 11 week old bones was dehydrated in graded ethanol (70%, 80%, 95%, 100%), defatted in Clear-Rite 3 (Richard-Allen Scientific; Kalamazoo, MI) and infiltrated in a liquid methyl methacrylate monomer (Koldmount™ Cold Mounting Liquid, Mager Scientific). The bones were then embedded in poly methyl methacrylate (Koldmount™ Cold Mounting Kit, Mager Scientific). Using a low-speed sectioning saw (South Bay Technology, Model 650; San Clemente, CA) with a diamond wafering blade (Mager Scientific), sections approximately 100-150 μ m thick were made. These sections were then hand ground and polished to a final thickness of between 50 and 75 μ m using wet silicon carbide abrasive discs. These histomorphometric sections were intended to be located at a standard site in the tibial diaphysis proximal to the TFJ. However, because the bones were used following fracture, and because fracture did not occur in the same place in every bone, variation in this location occurred (sections were located an average distance of $570 \pm$

397 μm proximal to the TFJ). Sections were imaged using the Nikon DAPI-FITC-TRITC triple band filter combination (DAPI excitation at 385-400 nm and emission at 450-465 nm; FITC excitation at 475-490 nm and emission at 505-535 nm; TRITC excitation at 545-565 nm and emission at 580-620 nm) at a magnification of 200X (Nikon Eclipse TE 300) and analyzed using digital analysis software (ImageJ, version 1.36b). All histomorphometric analyses were performed using standard ASBMR methods and nomenclature [38]. For dynamic measures, bone surface lengths (BS), labeled surfaces (single label - sLs; double label - dLs) and center-to-center interlabel distances (Ir.L.Th) were measured on both the endocortical and periosteal surfaces (Es., Ps.). The amount of time between each injection (Ir.L.t) was 5 days. Mineralizing surface (MS, % total surface), mineral apposition rate (MAR, $\mu\text{m}/\text{day}$) and bone formation rate (BFR, $\mu\text{m}^3/\mu\text{m}^2/\text{day}$) were determined at each surface using the following calculation:

$$MS = \left(\frac{\frac{1}{2}sLs + dLs}{BS} \right) \times 100 \quad \quad \quad MAR = \frac{Ir.L.Th}{Ir.L.t} \quad \quad \quad BFR = MAR \times MS$$

Raman Microspectroscopy

Of the 15 bones in each group, 6 were chosen at random for analysis of composition by Raman Spectroscopy. Bones from the 8 week groups were processed and embedded as described above (11 week bones were used after sectioning for histomorphometry was complete). Using the sectioning method described above, thick sections (≥ 3 mm) were made and hand polished using wet silicon carbide abrasive discs. These sections were intended to be located at a standard site distal to the TFJ. Because they were hand cut and ground, variation in this location occurred (the average distance of this section was 510 ± 262 μm distal to the TFJ).

The Raman imaging system used in this study has been previously described [39-41]. Briefly, Raman scatter was excited using a 785 nm laser with a rectangular beam profile (Kaiser Optical Systems). The beam was passed through a 20X objective onto the sample which focuses the line-shaped beam (~ 100 μm in length). Raman scattered light from every point on the line was simultaneously passed back through the objective and through a dichroic mirror to a charge coupled device (CCD) detector.

Once Raman spectra were collected, band areas were determined for select Raman peaks representing specific components of the mineral and organic matrix. Three bands were investigated: a phosphate band (PO_4^{3-} ν_1 symmetric stretch at 957 cm^{-1}), a carbonate band (CO_3^{2-} ν_1 symmetric stretch at 1070 cm^{-1}) and the Amide I collagen band (C=O stretch at $1595\text{-}1720\text{ cm}^{-1}$). The Amide I band at 1660 cm^{-1} was decomposed into 2 smaller underlying bands at 1660 cm^{-1} and 1690 cm^{-1} . From these bands, 3 band area ratios were determined to characterize the chemical composition of the sample. The degree of mineralization in the tissue was determined from the mineral/matrix ratio by dividing the phosphate band by the Amide I band. The carbonate/phosphate ratio, which is indicative of the level of Type B carbonate substitution in the mineral (carbonate substituting in the crystal lattice for phosphate ions), was determined by dividing the carbonate band by the phosphate band. Finally, the collagen cross-linking ratio was determined by dividing the 1660 cm^{-1} band by the 1690 cm^{-1} band [42]. The area ratio between these two bands is indicative of changes in the amount of non-reducible/reducible cross-linking in Type I collagen. Therefore, this ratio increases with increasing number of stable cross-links. Mineral crystallinity, which takes into account the size, shape and perfection of mineral crystals, was obtained from the inverse of the full bandwidth at half peak intensity of the phosphate band at 957 cm^{-1} .

A total of 12 spectral lines were collected from each sample. In each anatomic quadrant (anterior, posterior, lateral, medial), three total spectra were taken in regions corresponding to periosteal, intracortical and endocortical locations. Before statistical analysis, all 12 lines were averaged to obtain an overall measurement for each specimen.

Real-Time Quantitative RT-PCR

Right tibiae from 11 week mice that were reserved in RNA-STAT60 following sacrifice were thawed on ice for RNA isolation. Samples were vortexed and centrifuged ($12,000g$ at 4°C for 10 minutes), and the liquid in each was transferred to a new tube. Equal volumes of the 15 samples from each group were randomly pooled into 3 samples (5 bones in each). RNA was isolated from each pooled sample following manufacturer's instructions (RNA-STAT 60, IsoTex Diagnostics Inc.), and then each sample was cleaned

of contaminating DNA (Qiagen RNase-Free DNase Set). From 1 μ g of each pooled and cleaned RNA sample, cDNA was synthesized using both Oligo dT and random hexamers (Invitrogen SuperScript II kit, Invitrogen Corporation). Following cDNA synthesis, samples were diluted by 10X to a total volume of 200 μ l, then aliquoted into smaller volumes to reduce freeze/thaw cycles. One sample from each group was randomly chosen as the main sample, with the other 2 samples from each group serving as biological replicates to confirm reproducibility.

Real time qRT-PCR was performed on an ABI 7500 PCR System (Applied Biosystems). For each PCR run, universal mouse RNA (XpressRef Universal Reference Total RNA, SuperArray Bioscience Corporation) with 4 serial dilutions was run in triplicate to establish a standard curve following manufacturer's instructions (TaqMan One-Step RT-PCR Master Mix Reagents Kit, Applied Biosystems). Each sample was run in quadruplicate following manufacturer's instructions (TaqMan Universal Master Mix, Applied Biosystems). Analysis was performed by first setting an appropriate standard threshold level in the linear part of the reaction for each primer. Then, the crossing value of this threshold was determined (C_t) for each sample. Following manufacturer's protocols (ABI Prism 7700 Sequence Detection System, User Bulletin #2), mRNA expression levels for each sample/primer were normalized to rRNA 18S levels and expressed as a fold change relative to the background-strain WT level.

All primers/probe mixtures used in this study were TaqMan Gene Expression Assays (Applied Biosystems). As such, primer/probe sequences are proprietary and are not provided. In lieu of this, ABI Assay ID numbers are given for each primer used in the current study. These primer/probes sets were: decorin (dcn; Mm00514535_m1), fibromodulin (fm; Mm00491215_m1), Type I procollagen α 1 chain (Col1a1; Mm00801666_g1), Type I procollagen α 2 chain (Col1a2; Mm00483888_m1) and transforming growth factor β 1 (TGF- β 1; Mm00441724_m1). As an endogenous control, rRNA 18S was used (ABI assay 4352930E). The exception to this was the biglycan primer which was custom designed to span the restriction site of Exon 2 originally used to create the bgn-deficient mouse. This primer was used as a final verification of mouse genotype. The sequences for biglycan are: 5'GCTTCAGGTTTCAGACACCACTT3' (forward); 5'ACATGGCACTGAAGGTAGGT3' (reverse).

Statistical Analysis

All statistical analyses were performed using Sigma Stat (Version 3.1, Systat Software Inc.) or SPSS (Version 11.0, SPSS Inc.). The primary goal of this study was to determine if inbred strain-specific differences in the *bgn*-deficient phenotype existed at each age. For each property of interest, ratios of the KO/mean WT value for each KO sample within each age and inbred strain were calculated. The difference in ratios between inbred strains at each age was then analyzed utilizing Student t-tests in an analog to 2-way ANOVA looking for the effects of background strain and genotype at each age. To understand phenotypic effects (KO vs. WT) within each background strain/age and growth effects (11 week vs. 8 week) within each background strain/genotype, Student t-tests were employed. In groups which failed to exhibit normal distributions or equal variance, Mann-Whitney rank sum tests were performed. Round-robin linear regressions were performed to assess predictive relationships between geometric properties, tissue-level mechanical properties and structural-level mechanical properties. For all investigations, a value of $p < 0.05$ was considered significant while a p-value between 0.05 and 0.10 was also noted.

Results

Bgn-deficient phenotype in B6;129 mice at 8 weeks of age (left panel of each sub-figure)

At 8 weeks of age, B6;129 KO mice had increased mineralization and increased tissue-level modulus and strength versus WT mice, but deficiencies in structural-level mechanical properties and cross-sectional geometry. The B6;129 KO mice had significantly decreased body mass ($p=0.048$, Figure 4.1A) and tibial length ($p < 0.001$, Figure 4.1C) versus WT mice. Tibiae from the KO mice had significantly increased vBMD ($p=0.004$, Figure 4.2A) and mineral/matrix ratio ($p=0.028$, Figure 4.2B), while the collagen cross-linking ratio was significantly decreased ($p < 0.001$, Figure 4.2C) versus WT mice. Estimated tissue-level yield stress ($p=0.049$, Figure 4.3A) and modulus ($p=0.012$, Figure 4.3B) were significantly greater in the KO versus WT mice, while no

other tissue-level mechanical properties differed. KO mice had significantly decreased marrow area ($p < 0.001$, data not shown), cortical area ($p = 0.018$, Figure 4.4A), total area ($p < 0.001$, Figure 4.4A), AP width ($p < 0.001$, Figure 4.4B), ML width ($p < 0.001$, Figure 4.4B), I_{AP} ($p < 0.001$, Figure 4.4C) and I_{ML} ($p < 0.001$, Figure 4.4C). At the structural-level, ultimate force ($p = 0.006$, Figure 4.5A) and stiffness ($p = 0.003$, Figure 4.5B) were significantly decreased in the KO mice versus WT mice, while yield deformation was significantly greater ($p = 0.003$; Figure 4.5C).

Bgn-deficient phenotype in C3H mice at 8 weeks of age (right panel of each sub-figure)

At 8 weeks of age, C3H KO mice had increased mineralization and increased tissue-level strength versus WT mice with decreased cross-sectional geometry. The body mass of C3H KO mice was significantly greater than WT mice ($p = 0.014$, Figure 4.1B), while there was no difference in tibial length (Figure 4.1D). vBMD was significantly greater in the KO mice versus WT mice ($p < 0.001$, Figure 4.2A), and this was accompanied by a significant decrease in the collagen cross-linking ratio ($p = 0.031$, Figure 4.2C). At the tissue-level, there was a significant increase in predicted modulus in KO mice versus WT mice ($p = 0.050$, Figure 4.3B), but no other properties differed. Total cross-sectional area ($p = 0.015$, Figure 4.4A), marrow area ($p < 0.001$, data not shown), I_{AP} ($p = 0.034$, Figure 4.4C) and I_{ML} ($p = 0.044$, Figure 4.4C) were all significantly less in the KO mice versus WT values. No structural-level mechanical properties differed between KO and WT mice (Figure 4.5).

Inbred strain-specific response to bgn-deficiency at 8 weeks of age

To investigate inbred strain specificity in response to bgn-deficiency for each property of interest, the relative effects of the gene deletion in B6;129 mice (KO/mean WT values for each KO sample) were statistically compared with the effects in C3H mice (KO/mean WT value) at each age. At 8 weeks of age, B6;129 KO mice weighed less than their WT counterparts while the opposite was true in C3H mice, resulting in a significant inbred strain-specific body mass phenotype ($p < 0.001$, as indicated by # in Figure 4.1A,B). Inbred strain-specificity also existed in the tibial length phenotype

(decreased ratio in B6;129 mice; $p < 0.001$, # in Figure 4.1C,D). Compositional properties were altered in the same manner in KO mice versus WT mice from both inbred strains, so no inbred strain-specificity existed in these properties (Figure 4.2). Similarly, no inbred strain-specific phenotypic differences were present in tissue-level mechanical properties (Figure 4.3). Most cross-sectional geometric properties were decreased in the KO mice from both inbred strains compared with WT levels, but the phenotypic differences were significantly greater in B6;129 KO mice in marrow area ($p = 0.007$, data not shown), cortical area ($p = 0.029$, # in Figure 4.4A), total area ($p = 0.002$, # in Figure 4.4A), AP width ($p = 0.003$, # in Figure 4.4B), ML width ($p = 0.002$, # in Figure 4.4B), I_{AP} ($p = 0.005$, # in Figure 4.4C) and I_{ML} ($p = 0.003$, # in Figure 4.4C) versus the response in C3H KO mice. At the structural level, inbred strain-specific differences existed in ultimate force (decreased ratio in B6;129; $p = 0.013$, # in Figure 4.5A), stiffness (decreased ratio in B6;129; $p = 0.024$, # in Figure 4.5B) and yield deformation (decreased ratio in B6;129; $p = 0.019$, # in Figure 4.5C).

B6;129 Bgn-deficient phenotype at 11 weeks of age and effects of growth (left panel of each sub-figure)

By 11 weeks of age, *bgn*-deficiency in B6;129 mice caused decreased mechanical integrity through altered tissue composition and decreased cross-sectional size. Body mass was no longer different in B6;129 KO mice compared with WT mice (Figure 4.1A), but tibial length was still significantly decreased ($p < 0.001$, Figure 4.1C). mRNA expression levels for all genes of interest were significantly increased in the KO mice relative to WT levels (Figure 4.6). $vBMD$ ($p = 0.011$, Figure 4.2A), the mineral/matrix ratio ($p = 0.004$, Figure 4.2B) and crystallinity ($p < 0.001$, Figure 4.2D) were significantly greater in KO mice versus WT mice while the collagen cross-linking ratio was significantly decreased ($p < 0.001$, Figure 4.2C). No tissue-level mechanical properties were significantly different in KO mice versus WT mice, but ultimate stress ($p = 0.056$, Figure 4.3A), yield strain ($p = 0.098$, Figure 4.3C) and resilience ($p = 0.071$, Figure 4.3D) were marginally decreased, while failure strain ($p = 0.089$, Figure 4.3C) was marginally increased. Although periosteal mineralizing surface was significantly elevated in the KO

mice compared with WT mice ($p=0.006$, Figure 4.7A), KO mice had significantly smaller marrow area ($p<0.001$, data not shown), total area ($p=0.004$, Figure 4.4A), AP width ($p<0.001$, Figure 4.4B), AP/ML ratio ($p<0.001$, data not shown), I_{AP} ($p=0.038$, Figure 4.4C) and I_{ML} ($p=0.005$, Figure 4.4C). At the structural-level, stiffness was significantly decreased ($p=0.034$, Figure 4.5C) and yield force ($p=0.062$, Figure 4.5A) and ultimate force ($p=0.053$, Figure 4.5A) were marginally decreased in KO mice versus WT mice, while post-yield deformation ($p=0.016$, data not shown but equal to the difference between failure deformation and yield deformation) and failure deformation ($p=0.014$, Figure 4.5C) were significantly increased.

Body mass (Figure 4.1A) and tibial length (Figure 4.1C) were unchanged with growth in the B6;129 WT mice. In WT mice, the mineral/matrix ratio ($p<0.001$, Figure 4.2B), the collagen cross-linking ratio ($p<0.001$, Figure 4.2C) and the carbonate/phosphate ratio ($p=0.002$, Figure 4.2E) significantly increased with growth. At the tissue-level in the WT mice, yield stress ($p=0.015$, Figure 4.3A) and resilience ($p=0.016$, Figure 4.3D) significantly increased with growth. No geometric properties changed with growth in the WT mice (Figure 4.4). At the structural-level, there were significant increases in yield deformation ($p=0.034$, Figure 4.5C) and work to yield ($p=0.041$, Figure 4.5D) with growth, while post-yield deformation significantly decreased ($p=0.018$, data not shown).

Body mass increased in the KO mice with growth ($p=0.041$, Figure 4.1A), while tibial length was unchanged (Figure 4.1C). The mineral/matrix ratio ($p<0.001$, Figure 4.2B), the collagen cross-linking ratio ($p<0.001$, Figure 4.2C), crystallinity ($p<0.001$, Figure 4.2D) and the carbonate/phosphate ratio ($p=0.002$, Figure 4.2E) all increased in the KO mice with growth. No tissue-level mechanical properties changed with growth in the KO mice (Figure 4.3). ML width ($p=0.020$, Figure 4.4B) increased with growth in the KO mice, resulting in a significant decrease in the AP/ML ratio ($p=0.034$, data not shown). No structural-level mechanical properties changed with growth in the B6;129 KO mice (Figure 4.5).

C3H Bgn-deficient phenotype at 11 weeks of age and effects of growth (right panel of each sub-figure)

At 11 weeks of age, C3H KO mice had altered tissue composition and greater cortical thickness, but no mechanical properties differed versus WT mice. Body mass was still greater in C3H KO mice versus WT mice ($p=0.049$, Figure 4.1B), while tibial length still did not differ (Figure 4.1D). mRNA expression levels for DCN ($p=0.005$, Figure 4.6) and Col1a2 ($p=0.029$, Figure 4.6) were significantly upregulated in KO mice, but expression was less than 2 fold greater than WT mice. vBMD ($p<0.001$, Figure 4.2A), the mineral/matrix ratio ($p=0.003$, Figure 4.2B) and the carbonate/phosphate ratio ($p=0.028$, Figure 4.2E) were significantly greater in the KO mice versus WT mice, but the collagen cross-linking ratio was significantly decreased ($p<0.001$, Figure 4.2C). No tissue-level mechanical properties differed in the KO mice versus WT mice at 11 weeks of age (Figure 4.3). Endocortical mineralizing surface ($p=0.050$, Figure 4.7A) and periosteal mineral apposition rate ($p=0.019$, Figure 4.7B) were significantly decreased in the KO mice versus WT mice. However, cortical thickness was now significantly greater in the KO mice versus WT mice ($p=0.001$, Figure 4.4D). No structural-level mechanical properties differed between KO and WT mice at 11 weeks of age (Figure 4.5).

Body mass increased with growth in C3H WT mice ($p=0.009$, Figure 4.1B), but tibial length was unchanged (Figure 4.1D). vBMD increased with growth in the WT mice ($p<0.001$, Figure 4.2A), but no other measures of tissue composition changed. In the WT mice, no tissue-level mechanical properties changed with growth (Figure 4.3). WT mice had significantly increased cortical area ($p=0.040$, Figure 4.4A), ML width ($p=0.002$, Figure 4.4B), I_{AP} ($p=0.037$, Figure 4.4C) and cortical thickness ($p=0.033$, Figure 4.4D) with growth, and significantly decreased AP/ML ratio ($p=0.016$, data not shown). No structural-level mechanical properties changed with growth in WT mice (Figure 4.5).

Body mass increased with growth in C3H KO mice ($p=0.026$, Figure 4.1B), but tibial length was unchanged (Figure 4.1D). In the KO mice, vBMD ($p<0.001$, Figure 4.2A), the mineral/matrix ratio ($p<0.001$, Figure 4.2B) and the carbonate/phosphate ratio ($p<0.001$, Figure 4.2E) significantly increased with growth, while the collagen cross-linking ratio significantly decreased ($p=0.001$, Figure 4.2C). There was a significant

decrease in ultimate stress with growth in the KO mice ($p=0.009$, Figure 4.3A). KO mice had significantly increased total area ($p=0.006$, Figure 4.4A), cortical area ($p=0.004$, Figure 4.4A), AP width ($p=0.038$, Figure 4.4B), ML width ($p=0.005$, Figure 4.4B), I_{AP} ($p=0.004$, Figure 4.4C), I_{ML} ($p=0.028$, Figure 4.4C) and cortical thickness ($p=0.007$, Figure 4.4D) with growth. No structural-level mechanical properties changed with growth in C3H KO mice (Figure 4.5).

Inbred strain-specific response to bgn-deficiency at 11 weeks of age (indicated by # in each sub-figure)

At 11 weeks of age, inbred strain-specificity in response to bgn-deficiency spanned all levels of the bone hierarchy that were investigated. Significant inbred strain-specific phenotypic differences existed in both body mass (increased ratio in C3H mice; $p<0.001$, # in Figure 4.1A,B) and tibial length (increased ratio in B6;129 mice; $p<0.001$, # in Figure 4.1C,D). Phenotypic differences in mRNA expression of DCN ($p<0.001$, # in Figure 4.6), FM ($p=0.029$, # in Figure 4.6), *Coll1a1* ($p<0.001$, # in Figure 4.6) and TGF β ($p<0.001$, # in Figure 4.6) were inbred strain specific (ratio increased in B6;129 for all genes). Inbred strain-specificity was noted in the collagen cross-linking ratio (greater decrease in C3H KO mice; $p=0.027$, # in Figure 4.2C), crystallinity (increased ratio in B6;129 mice; $p=0.002$, # in Figure 4.2D) and the carbonate/phosphate ratio (increased ratio in C3H mice; $p=0.027$, # in Figure 4.2E). At the tissue level, inbred strain-specific differences existed in yield stress (decreased ratio in B6;129 mice; $p=0.018$, # in Figure 4.3A) and ultimate stress (decreased ratio in B6;129 mice; $p=0.050$, # in Figure 4.3A). Periosteal mineralizing surface displayed an inbred strain-specific increase in B6;129 KO ($p<0.001$, # in Figure 4.7A). Differences in marrow area ($p<0.001$, data not shown), total area ($p<0.001$, # in Figure 4.4A), AP width ($p<0.001$, # in Figure 4.4B), AP/ML ratio ($p<0.001$, data not shown), I_{AP} ($p=0.018$, Figure 4.4C) and I_{ML} ($p<0.001$, Figure 4.4C) were all inbred strain-specific due to significant decreases in B6;129 KO mice versus WT mice. At the structural-level, inbred strain-specific phenotypic differences were seen in yield force (decreased ratio in B6;129 mice; $p=0.002$, # in Figure 4.5A), ultimate force (decreased ratio in B6;129 mice; $p=0.005$, # in Figure 4.5A), stiffness (decreased ratio in

B6;129 mice; $p=0.007$, # in Figure 4.5B), post-yield deformation (increased ratio in B6;129 mice; $p=0.023$, data not shown) and failure deformation (increased ratio in B6;129 mice; $p=0.011$, # in Figure 4.5C).

Discussion

At 8 weeks of age, the *bgn*-deficient phenotype (KO versus WT) was more significant in B6;129 mice versus C3H mice resulting in an inbred strain-specific response (KO/WT in B6;129 versus KO/WT in C3H) to this genetic change in body mass (ratio decreased in B6;129 and increased in C3H), tibial length (ratio decreased in B6;129), multiple cross-sectional geometric properties (ratio decreased in both inbred strains, but deficiencies all significantly worse in B6;129), yield and ultimate force (ratio decreased in B6;129), stiffness (ratio decreased in B6;129) and yield deformation (ratio increased in B6;129). The relationship between inbred strain and *bgn*-deficient phenotype became more compelling by 11 weeks of age, impacting the B6;129 mice more than the C3H mice at all levels of the bone hierarchy that were investigated. Inbred strain-specific differences existed in body mass (ratio increased in C3H), tibial length (ratio increased in B6;129), mRNA expression (ratio increased in all genes investigated in B6;129), tissue composition (changes in KO mice from both inbred strains), tissue strength (ratio decreased in both yield and ultimate stress in B6;129), cross-sectional geometric properties (deficiencies in multiple properties in B6;129 KO), structural strength (ratio for yield and ultimate force decreased in B6;129), stiffness (ratio decreased in B6;129) and ductility (ratio for post-yield and failure deformation increased in B6;129).

Inbred strain-specificity is not unknown in skeletal research, but to the best of our knowledge, this study marks the first time an inbred strain-specific response in bone has been demonstrated following a genetic deletion. Due to genetic differences that are present between inbred mouse strains, bone phenotypes between inbred strains vary in terms of mineral density [15], geometric properties [16, 17], mechanical properties [16-19] and cellular behavior [20-23]. These same mouse strains exhibit inbred strain-specific responses to external stimuli including mechanical loading [24-27] and bone regeneration [28-30]. Because of the weight that is placed on conclusions drawn from

gene deletion studies, results from the current investigation highlight the importance of properly interpreting and explaining results drawn from such studies to take into account variability that can arise from one inbred mouse strain to another.

Using Raman Microspectroscopy (and vBMD from μ CT) to infer how *bgn*-deficiency influenced bone composition was an invaluable tool in the current study. In bones from B6;129 KO mice, there are differences in the size, shape and spacing of collagen fibrils versus WT mice [5, 6], but no studies have investigated differences in collagen between C3H KO and WT mice. In the current study, KO mice from both inbred strains had a decrease in the collagen cross-linking ratio versus WT mice (Figure 4.2C), implying a change in the secondary structure of collagen most often associated with a decrease in the number of mature cross-links relative to immature cross-link levels [42]. *Bgn* also regulates mineralization *in vivo* [13]. In the current study, KO mice from both inbred strains had significantly greater vBMD (Figure 4.2A) and mineral/matrix ratio (Figure 4.2B) versus WT mice, further supporting *bgn*'s role in regulating mineralization in bone. However, B6;129 KO mice had significantly increased crystallinity (Figure 4.2D) while C3H KO mice had significantly increased carbonate/phosphate ratio (Figure 4.2E) versus WT mice, indicating that genetic differences between the two inbred strains are governing the response to this gene deletion.

Altered collagen and mineral in KO bones suggest two scenarios. In the first, *bgn*-deficiency causes direct changes in the collagen matrix, as supported by a decreased collagen cross-linking ratio in KO mice versus WT mice (Figure 4.2C), as well as changes in the expression of procollagen mRNAs (Figure 4.6). Since the collagen matrix is a template for mineralization, the mineral that forms on an altered matrix can be changed in both chemical composition and density [43], as supported by increased crystallinity in B6;129 KO mice versus WT mice (Figure 4.2D) and increased carbonate/phosphate ratio in C3H KO mice versus WT mice (Figure 4.2E). Mineral is thought to nucleate in the gap zones of collagen, and SLRPs are known to localize within these zones [9]. It is therefore possible that mineral nucleation sites that are normally blocked by *bgn* are now exposed and more mineral can form, as supported by increased vBMD (Figure 4.2A) and mineral/matrix ratio (Figure 4.2B). A second scenario has the

lack of bgn directly impacting mineralization. While bgn might facilitate the initial nucleation of mineral, further crystal growth in preferential directions may be blocked by the presence of bgn near a specific crystal face [44-46], meaning that in the absence of bgn, crystals can grow to larger than normal dimensions. Unrestricted crystal growth along specific planes could explain both the increase in vBMD (Figure 4.2A) as well as increased crystallinity (Figure 4.2D). As mineral beyond normal levels fills the spaces within collagen fibrils and the fibrils are distorted [47, 48], the dissociation/rupture of some cross-links may occur. The reason for inbred strain-specific differences in tissue composition may be due to a different combination of these two mechanisms due to genetic differences between the two inbred strains.

Inbred strain-specific differences in estimated tissue-level mechanical properties (Figure 4.3) are independent of the amount of tissue in the bone and, therefore, arise from differences in the composition of the tissue (Figure 4.2). A few consistent observations were made in regard to the link between tissue composition and mechanical behavior at the tissue-level. When increased amount of mineral (either vBMD or mineral/matrix ratio) was present in the absence of differences in the nature of the mineral (e.g. composition or crystallinity), increased tissue level strength and/or stiffness were noted (e.g. the 8 week phenotype in both inbred strains). Increased mineralization has been linked with increased tissue strength and modulus [49-51]. When mineral composition differed (either with growth or due to bgn-deficiency), pre-yield tissue-level mechanical properties (strength, modulus or resilience) also changed. When an increase in carbonate/phosphate ratio was present, tissue strength and resilience were positively impacted (e.g. B6;129 WT mice with growth). A similar observation was made in Brittle IV mice, where a greater carbonate/phosphate ratio was associated with increased tissue strength and modulus [3]. When increased crystallinity was noted, regardless of other mineral differences, a negative impact on pre-yield tissue-level properties was present (e.g. growth in KO mice from both inbred strains, the 11 week phenotype in B6;129 mice). Increased crystallinity suggests an increase in the size, perfection or the crystalline/amorphous ratio of the mineral crystals and has been correlated with decreased tissue strength and modulus [43, 52, 53]. Because Raman measures in the current study were performed outside of the mechanical testing region to eliminate the

impact that mechanical testing of the bone would have on the collected spectra [39, 54, 55], regressions between properties measured at the different sites were unable to define significant correlations between the two sets of measurements.

At 8 weeks of age, the KO mice from both inbred strains had similar phenotypes in terms of tissue-composition (increased vBMD, decreased collagen cross-linking ratio, Figure 4.2) and tissue-level mechanical properties (increased modulus and strength, Figure 4.3). At the structural-level, the phenotypes were dissimilar, stemming from inbred strain-specific phenotypic differences in cross-sectional geometry (# in Figure 4.4). Structural-level strength (force) is proportional to tissue-level strength (stress) and the size/shape factor of the bone (I_{AP}/c , which takes into account the amount, distribution and size of the bone). In C3H mice, the phenotypic deficiency in the size/shape factor (-6.73% versus WT; DNS) was almost completely balanced by greater tissue-level ultimate stress (+6.94% versus WT, Figure 4.3A), resulting in no difference in structural-level strength compared with WT mice (Figure 4.5A). However, in the B6;129 mice, the larger deficiency in the size/shape factor of the KO mice (-18.20% versus WT, DNS) could not be balanced by the +8.13% greater ultimate stress (Figure 4.3A), and the structural strength was therefore significantly less than in WT mice (Figure 4.5A). Post-yield structural mechanical behavior for all 120 mice (here indicated as failure deformation) was almost completely dependent on tissue level failure strain ($r^2=0.9443$, $p<0.001$; Figure 4.8A), with a weaker negative dependence on bone size/shape ($r^2=0.1156$, $p<0.001$; Figure 4.8B). Therefore, at 8 weeks of age, there were no post-yield structural differences in either inbred strain due to a lack of tissue-level differences in post-yield behavior.

Although cross-sectional geometric growth occurred in KO mice from both inbred strains between 8 and 11 weeks of age (Figure 4.4), phenotypic geometric deficiencies persisted in the B6;129 KO mice versus WT mice while geometric properties in C3H KO mice caught up to WT levels. This pattern of temporally-delayed bone formation in C3H KO mice has been shown in a study of marrow ablation [11]. In the C3H KO mice, a lack of phenotypic differences compared with WT mice in both tissue-level mechanical properties (Figure 4.3) and cross-sectional geometry (Figure 4.4) at 11 weeks of age resulted in a lack of structural-level mechanical differences (Figure 4.5). In contrast,

decreased pre-yield tissue-level mechanical properties (Figure 4.3) and decreased cross-sectional geometry (Figure 4.4) in B6;129 KO mice versus WT mice resulted in inbred strain-specific deficiencies in structural strength and stiffness (# in Figure 4.5A and B). Phenotypically greater post-yield behavior at the tissue-level in B6;129 KO mice versus WT mice (Figure 4.3C) resulted in increased structural-level deformation (Figure 4.5C).

In conclusion, data from two inbred strains suggest that biglycan plays a role in regulating collagen cross-linking and the amount and composition of mineral in bone *in vivo*. The bgn-deficient phenotype was inbred strain-specific at 8 weeks of age, where decreased tibial length, smaller cross-sectional size and decreased structural-level stiffness and strength were present in the B6;129 KO mice. As hypothesized, properties in C3H KO mice (with the exception of measures of tissue composition) were indistinguishable from WT levels by 11 weeks. However, the relationship between inbred strain and bgn-deficient phenotype became more compelling by 11 weeks of age due to differences in the B6;129 KO versus WT mice that spanned all levels of the bone hierarchy that were investigated. To the best of our knowledge, this study marks the first time an inbred strain-specific difference has been demonstrated in response to a genetic deletion in mice, and suggests that in the interpretation of data from bone-related genetic deletion models, careful consideration needs to be taken to address these genetically-regulated responses.

Acknowledgements

I would like to acknowledge my coauthors on this manuscript:

Dr. Kurtulus Golecuk, Dr. Michael D. Morris and Dr. David H. Kohn.

I would also like to thank Dr. Marian F. Young from the National Institute of Dental and Craniofacial Research (NIDCR) for her generous gift of biglycan-deficient and wild type breeder mice from each inbred strain.

Funding sources for this study:

DoD/US Army DAMD17-03-1-0556; NIH T32-DE07057; NIH IPA Agreement; Regenerative Sciences Training Grant R90-DK071506

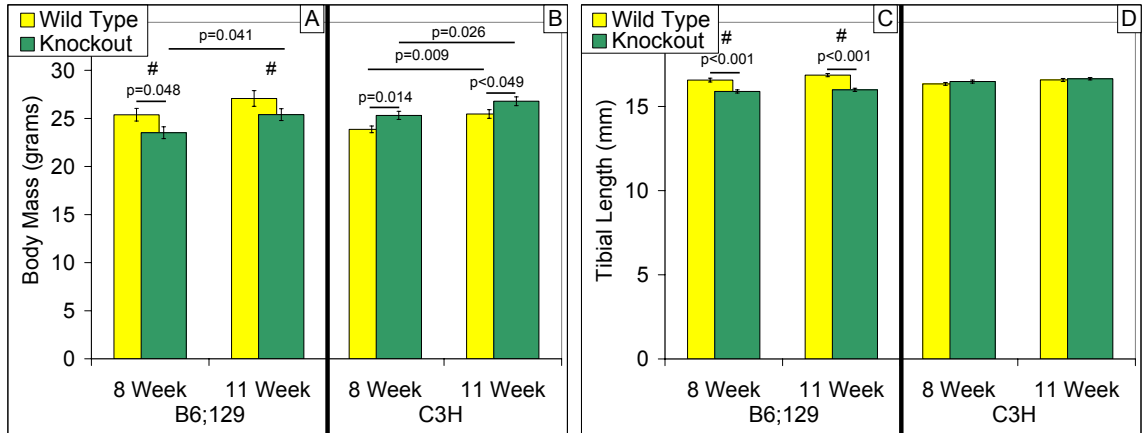


Figure 4.1: Body mass (A,B) and tibial length (C,D) of wild type (WT) and bgn-deficient (knockout, KO) mice. Data are presented as mean \pm SEM. B6;129 KO mice weighed significantly less than WT mice at 8 weeks of age, while C3H KO mice weighed significantly more than WT mice resulting in an inbred strain-specific phenotype. Inbred strain specificity was established by comparing the difference in the ratio of KO/WT between inbred strains at a given age, and is indicated by # over the B6;129 value ($p < 0.050$). By 11 weeks, body mass was no longer different in B6;129 KO versus WT mice since body mass increased in the KO mice with growth, but was unchanged in the WT mice. At 11 weeks of age, body mass was still significantly greater in C3H KO mice versus WT mice since body weight increased with growth in both WT and KO mice. The difference in body mass phenotype was inbred strain-specific at 11 weeks of age. B6;129 KO mice had significantly shorter tibiae than WT mice at 8 weeks of age, and there was no difference in C3H mice resulting in an inbred strain-specific phenotype. At 11 weeks, B6;129 KO mice still had shorter tibiae than WT mice since tibial length was unchanged with growth in either genotype. In C3H KO mice, tibial length was not different between WT and KO mice at 11 weeks of age, since tibial length was unchanged in both genotypes with growth. The difference in tibial length phenotype was inbred strain-specific at 11 weeks of age.

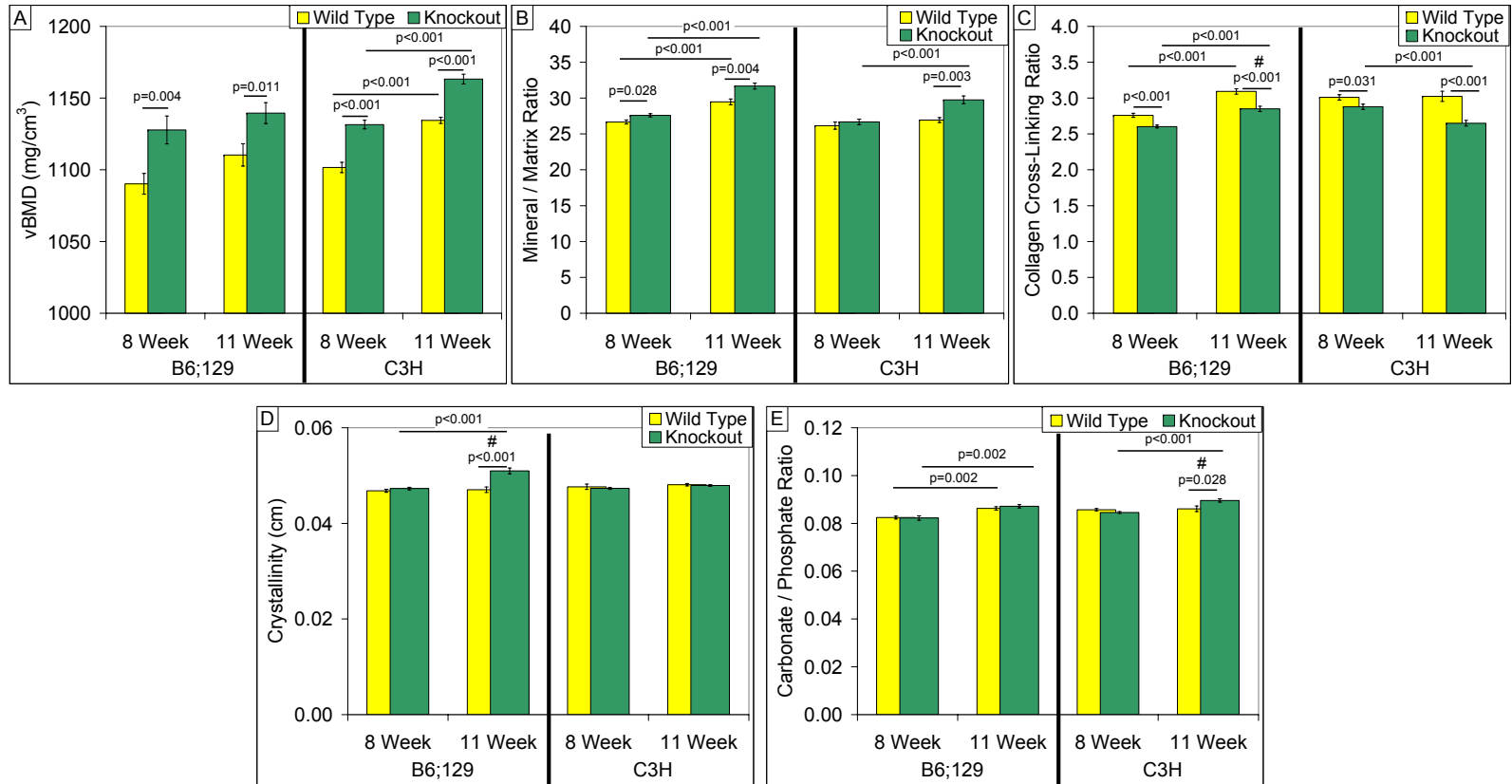


Figure 4.2: Volumetric bone mineral density (vBMD) and tissue compositional measures from the tibial mid-diaphysis of wild type (WT) and *bgn*-deficient (knockout, KO) mice. Data are presented as mean \pm SEM. B6;129 KO mice had significantly increased vBMD (A) and mineral/matrix ratio (B) at 8 weeks of age versus WT mice, while the collagen cross-linking ratio (C) was significantly decreased. In C3H KO mice at 8 weeks of age, vBMD (A) was significantly greater than WT mice and the collagen cross-linking ratio (C) was significantly decreased. No inbred strain specificity existed at 8 weeks of age. Inbred strain specificity in a property was established by comparing the difference in the ratio of KO/WT between inbred strains at a given age, and is indicated by # over the B6;129 value ($p < 0.050$). In B6;129 mice at 11 weeks of age, vBMD (A), the mineral/matrix ratio (B) and crystallinity (D) were significantly greater in KO mice versus WT mice while the collagen cross-linking ratio was significantly decreased (C). In C3H mice at 11 weeks of age, vBMD (A), the mineral/matrix ratio (B) and the carbonate/phosphate ratio (E) were significantly greater in the KO mice versus WT mice, but the collagen cross-linking ratio was significantly decreased (C). Inbred strain-specificity was noted in the collagen cross-linking ratio (C), crystallinity (D) and the carbonate/phosphate ratio (E) at 11 weeks of age.

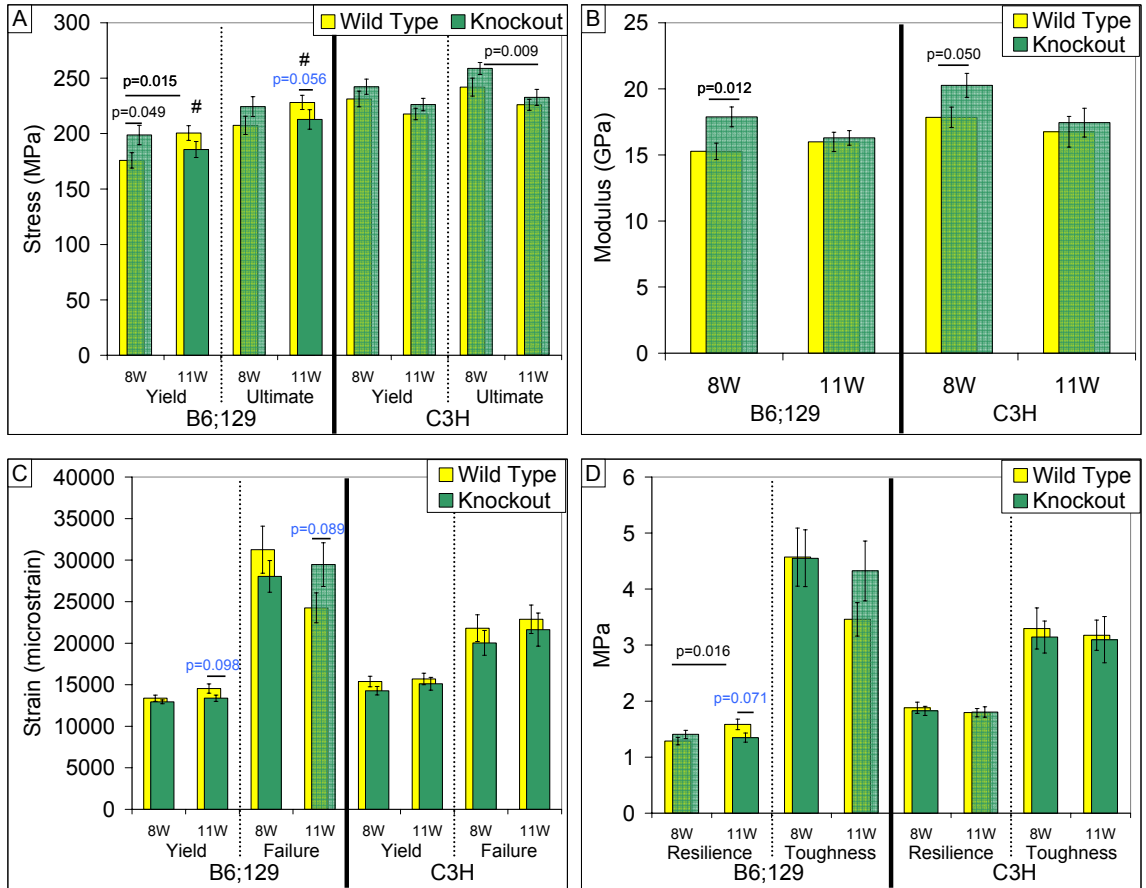


Figure 4.3: Estimated tissue-level mechanical properties from the tibial mid-diaphysis of wild type (WT) and *bgn*-deficient (knockout, KO) mice. Data are presented as mean \pm SEM. 8W and 11W indicate 8 and 11 weeks of age, respectively. In B6;129 KO mice, yield stress (A) and modulus (B) were significantly greater than WT mice at 8 weeks of age while in C3H KO mice versus WT mice, modulus (B) was significantly greater. No inbred strain specificity existed at 8 weeks of age. Inbred strain specificity in a property was established by comparing the difference in the ratio of KO/WT between inbred strains at a given age, and is indicated by # over the B6;129 value ($p < 0.050$). No tissue-level mechanical properties were significantly different in B6;129 KO mice versus WT mice at 11 weeks of age, but ultimate stress (A), yield strain (C) and resilience (D) were marginally decreased, while failure strain (C) was marginally increased. No tissue-level mechanical properties differed in C3H KO mice versus WT mice at 11 weeks of age. At 11 weeks of age, inbred strain-specific differences existed in yield stress and ultimate stress (A).

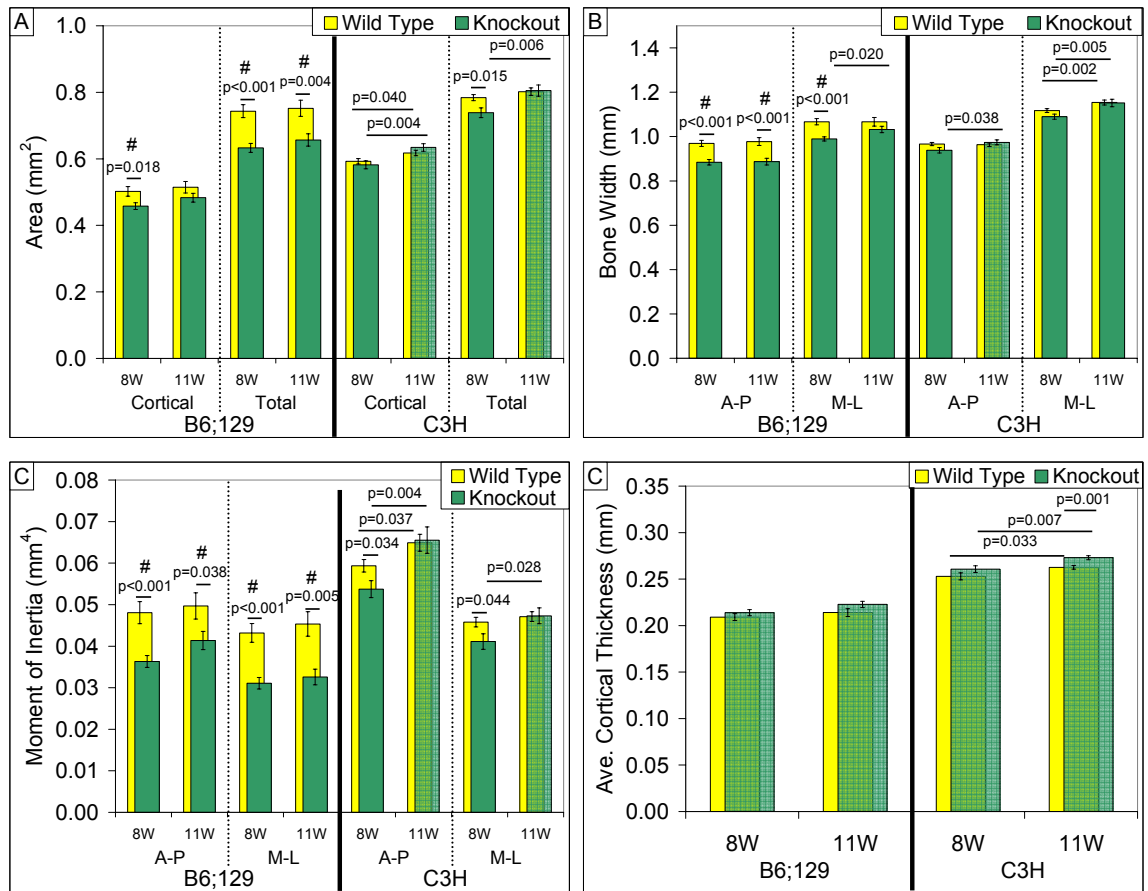


Figure 4.4: Cross-sectional geometric properties from the tibial mid-diaphysis of wild type (WT) and bgn-deficient (knockout, KO) mice. Data are presented as mean \pm SEM. 8W and 11W indicate 8 and 11 weeks of age, respectively. At 8 weeks of age, B6;129 KO mice had significantly decreased marrow area (difference between total area and cortical area, A), cortical area (A), total area (A), AP width (B), ML width (B), AP moment of inertia (MOI, B) (C) and ML MOI (C) versus WT mice. C3H KO mice had significantly decreased marrow area (A), total area (A) AP MOI (C) and ML MOI (C) versus WT mice at 8 weeks of age. Phenotypic differences at 8 weeks of age were significantly greater in B6;129 KO mice in marrow area (A), cortical area (A), total area (A), AP width (B), ML width (B), AP MOI (C) and ML MOI (C) versus the response in C3H KO mice. Inbred strain specificity in a property was established by comparing the difference in the ratio of KO/WT between inbred strains at a given age, and is indicated by # over the B6;129 value ($p < 0.05$). B6;129 KO mice still had significantly smaller marrow area (A), total area (A), AP width (B), AP MOI (C) and ML MOI (C) versus WT mice at 11 weeks of age. In C3H KO mice, cortical thickness was significantly greater than WT mice at 11 weeks of age (D). Differences in marrow area (A), total area (A), AP width (B) AP MOI (C) and ML MOI (C) were inbred strain-specific at 11 weeks of age.

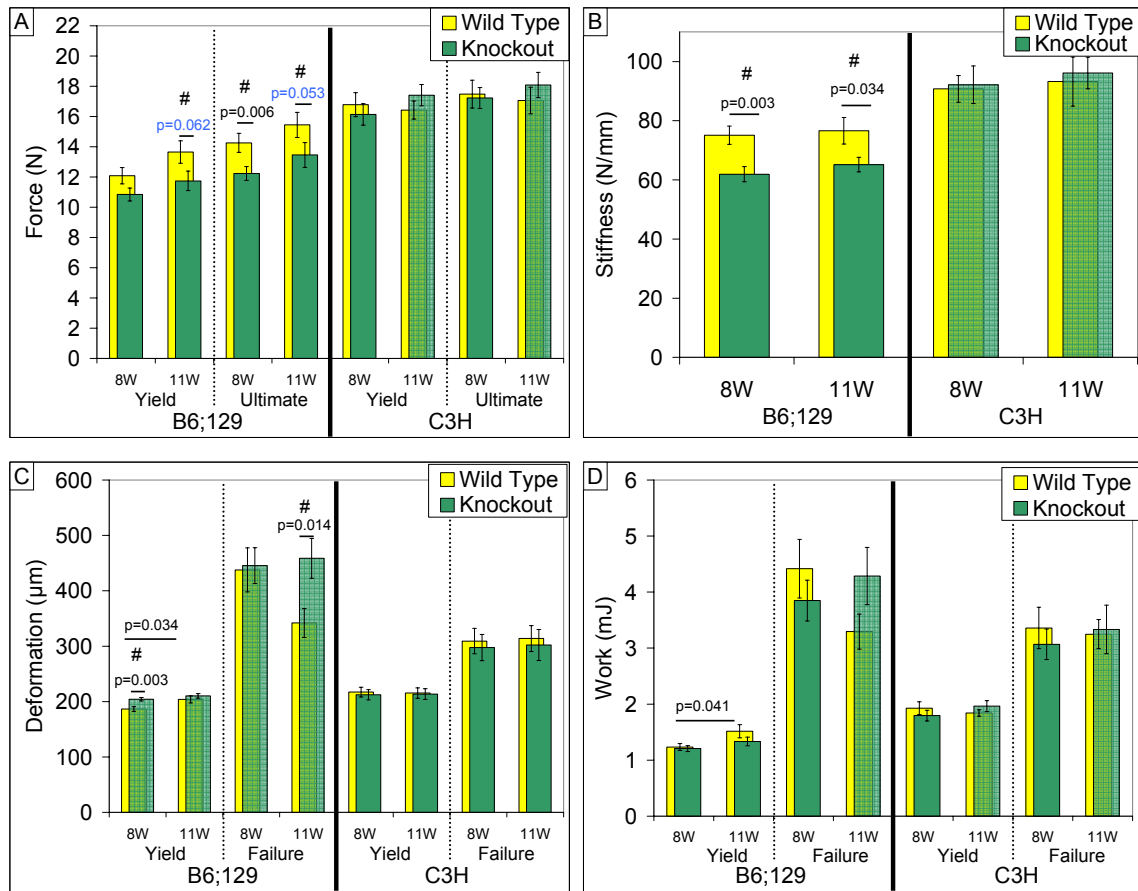


Figure 4.5: Structural-level mechanical properties from the tibial mid-diaphysis of wild type (WT) and *bgn*-deficient (knockout, KO) mice. Data are presented as mean \pm SEM. 8W and 11W indicate 8 and 11 weeks of age, respectively. At 8 weeks of age, ultimate force (A) and stiffness (B) were significantly decreased in the B6;129 KO mice versus WT mice, while yield deformation was significantly greater (C). No properties were significantly different in C3H KO versus WT mice, so inbred strain specificity existed in ultimate force (A), stiffness (B) and yield deformation (C). Inbred strain specificity in a property was established by comparing the difference in the ratio of KO/WT between inbred strains at a given age, and is indicated by # over the B6;129 value ($p < 0.05$). At 11 weeks of age, stiffness was significantly decreased (B) and yield force (A) and ultimate force (A) were marginally decreased in B6;129 KO mice versus WT mice, while post-yield deformation (equal to the difference between failure deformation and yield deformation) and failure deformation (C) were significantly increased. No properties were significantly different in C3H KO versus WT mice at 11 weeks, so inbred strain specificity existed in yield force (A), ultimate force (A), stiffness (B), post-yield deformation (C) and failure deformation (C).

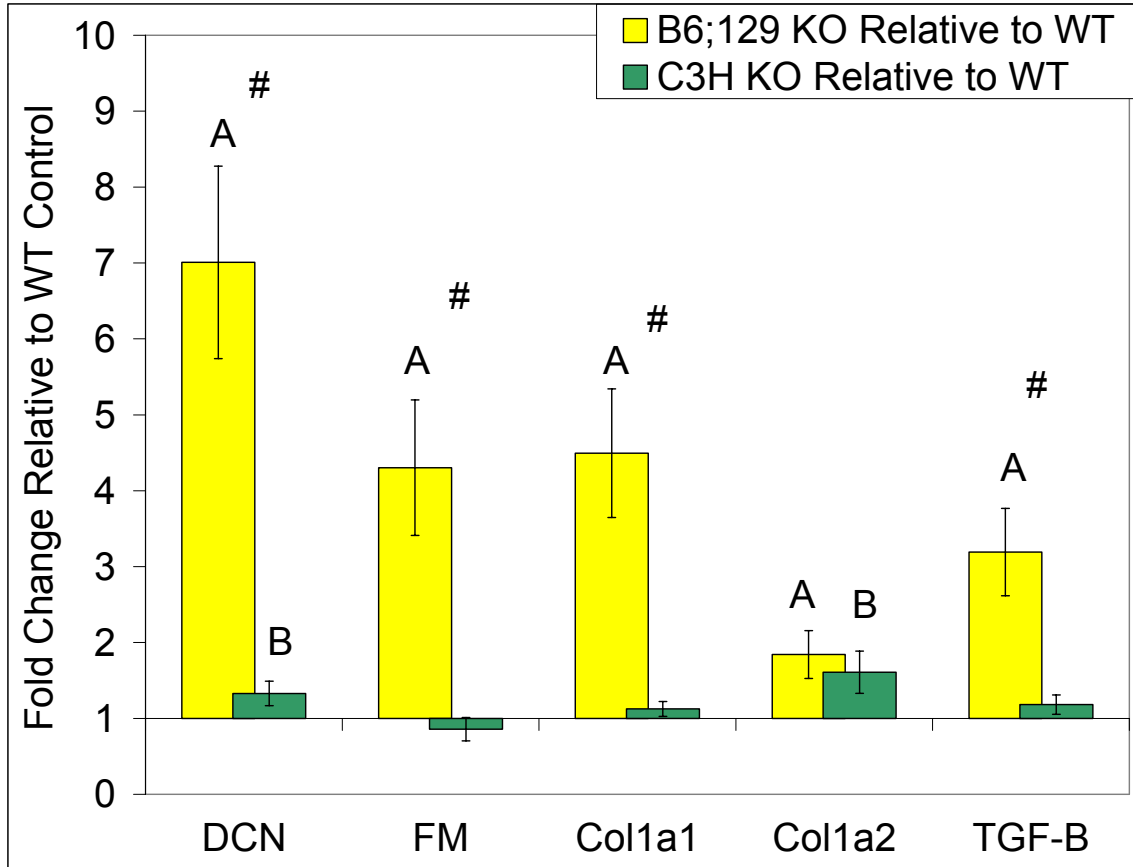


Figure 4.6: mRNA expression from the right tibiae of wild type (WT) and bgn-deficient (knockout, KO) mice at 11 weeks of age. Data are presented as mean \pm standard deviation. mRNA expression levels for decorin (DCN), fibromodulin (FM), procollagen1 α 1 (Col1a1), procollagen1 α 2 (Col1a2) and TGF β were significantly upregulated (indicated by A) in B6;129 KO versus WT mice. C3H KO mice had significantly elevated expression of DCN and Col1a2 (indicated by B) versus WT mice. Changes in mRNA expression of DCN, FM, Col1a1 and TGF β were inbred strain specific. Inbred strain specificity was established by comparing the difference in the ratio of KO/WT between inbred strains at a given age, and is indicated by # ($p < 0.050$).

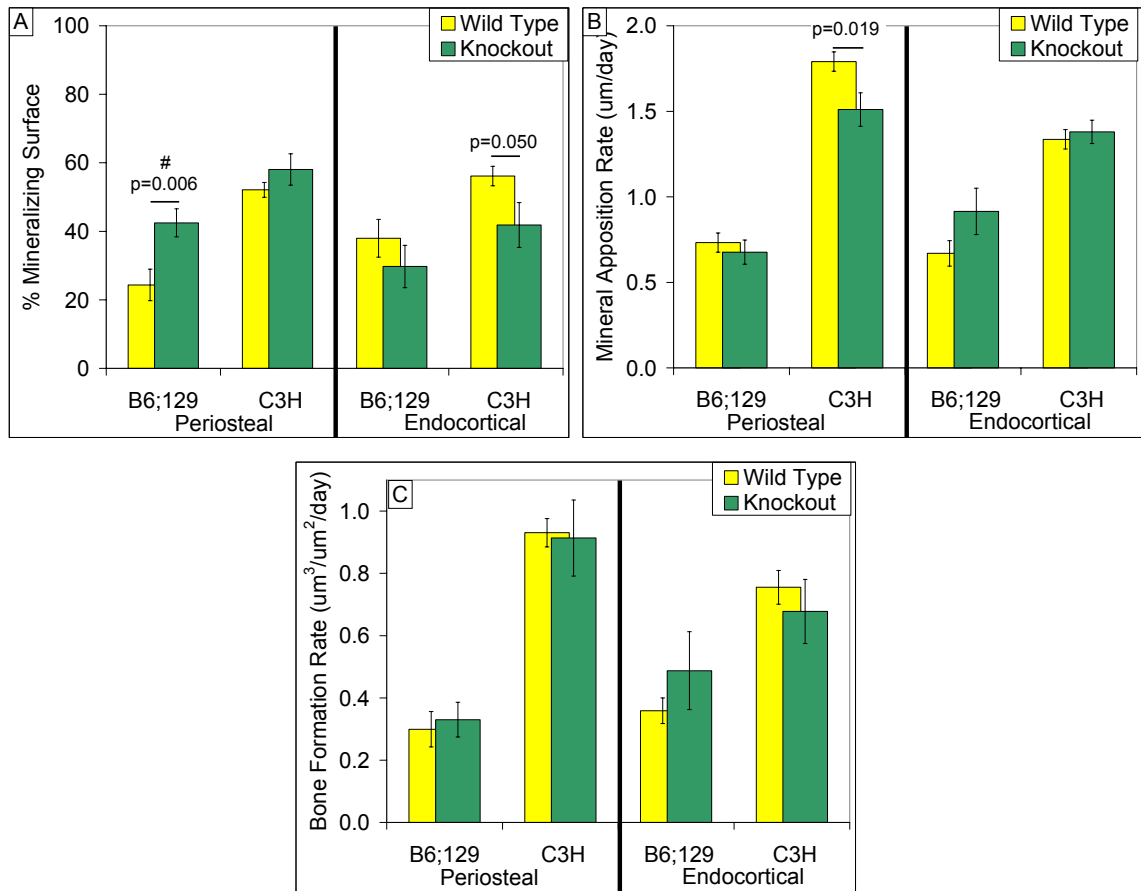


Figure 4.7: Histomorphometry from the tibial mid-diaphysis of wild type (WT) and *bgn*-deficient (knockout, KO) mice at 11 weeks of age. Data are presented as mean \pm SEM. B6;129 KO mice had significantly increased periosteal mineralizing surface (A), but no other properties differed versus WT mice. C3H KO mice had significantly decreased endocortical mineralizing surface (A) and periosteal mineral apposition rate (B). The difference in periosteal mineralizing was inbred strain-specific. Inbred strain specificity in a property was established by comparing the difference in the ratio of KO/WT between inbred strains at a given age, and is indicated by # over the B6;129 value ($p < 0.050$).

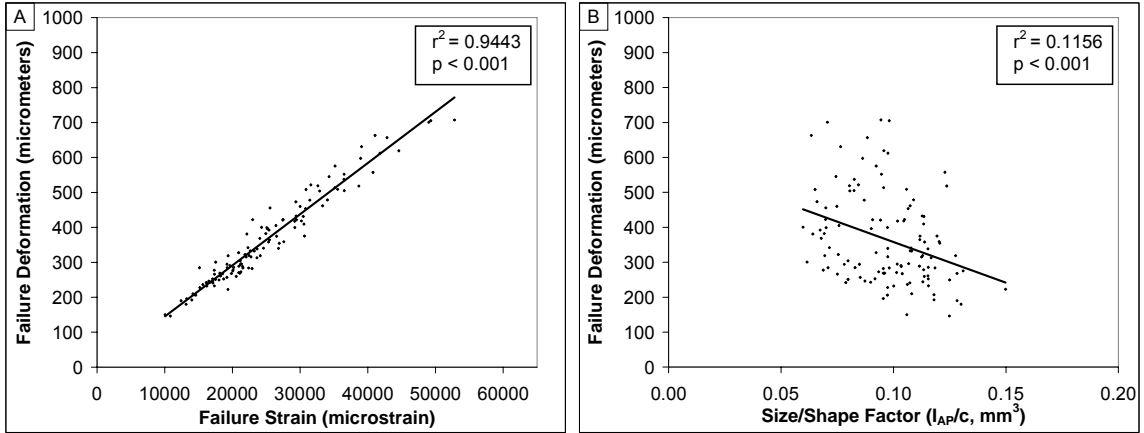


Figure 4.8: Linear regressions between failure deformation and failure strain (A) and a size/shape factor (B) for all 120 mice. Post-yield structural mechanical behavior (here indicated as failure deformation) was almost completely dependent on tissue-level failure strain ($r^2=0.9443$, $p<0.001$), with a weaker negative dependence on bone size/shape ($r^2=0.1156$, $p<0.001$). This size/shape factor takes into account the amount, distribution and external size of the bone. These regressions indicate that as opposed to pre-yield structural behavior, which is heavily dependent on both tissue-level mechanical properties and bone geometry, post-yield structural behavior is derived from tissue-level properties alone.

References

- (1) Camacho NP, Hou L, Toledano TR, Ilg WA, Brayton CF, Raggio CL, Root L, Boskey AL (1999) The material basis for reduced mechanical properties in oim mice bones. *J.Bone Miner.Res.* 14:264-272
- (2) Akhter MP, Wells DJ, Short SJ, Cullen DM, Johnson ML, Haynatzki GR, Babij P, Allen KM, Yaworsky PJ, Bex F, Recker RR (2004) Bone biomechanical properties in LRP5 mutant mice. *Bone* 35:162-169
- (3) Kozloff KM, Carden A, Bergwitz C, Forlino A, Uveges TE, Morris MD, Marini JC, Goldstein SA (2004) Brittle IV mouse model for osteogenesis imperfecta IV demonstrates postpubertal adaptations to improve whole bone strength. *J.Bone Miner.Res.* 19:614-622
- (4) Xu T, Bianco P, Fisher LW, Longenecker G, Smith E, Goldstein S, Bonadio J, Boskey A, Heegaard AM, Sommer B, Satomura K, Dominguez P, Zhao C, Kulkarni AB, Robey PG, Young MF (1998) Targeted disruption of the biglycan gene leads to an osteoporosis-like phenotype in mice. *Nat.Genet.* 20:78-82
- (5) Ameye L, Aria D, Jepsen K, Oldberg A, Xu T, Young MF (2002) Abnormal collagen fibrils in tendons of biglycan/fibromodulin-deficient mice leads to gait impairment, ectopic ossification, and osteoarthritis. *The FASEB Journal* 16:673-680
- (6) Corsi A, Xu T, Chen XD, Boyde A, Liang J, Mankani M, Sommer B, Iozzo RV, Eichstetter I, Robey PG, Bianco P, Young MF (2002) Phenotypic effects of biglycan deficiency are linked to collagen fibril abnormalities, are synergized by decorin deficiency, and mimic Ehlers-Danlos-like changes in bone and other connective tissues. *J.Bone Miner.Res.* 17:1180-1189
- (7) Fisher LW, Termine JD, Dejter SW, Jr, Whitson SW, Yanagishita M, Kimura JH, Hascall VC, Kleinman HK, Hassell JR, Nilsson B (1983) Proteoglycans of developing bone. *J.Biol.Chem.* 258:6588-6594
- (8) Bianco P, Fisher LW, Young MF, Termine JD, Robey PG (1990) Expression and localization of the two small proteoglycans biglycan and decorin in developing human skeletal and non-skeletal tissues. *J.Histochem.Cytochem.* 38:1549-1563
- (9) Matsuura T, Duarte WR, Cheng H, Uzawa K, Yamauchi M (2001) Differential expression of decorin and biglycan genes during mouse tooth development. *Matrix Biol.* 20:367-373
- (10) Chen XD, Shi S, Xu T, Robey PG, Young MF (2002) Age-related osteoporosis in biglycan-deficient mice is related to defects in bone marrow stromal cells. *J.Bone Miner.Res.* 17:331-340

- (11) Chen XD, Allen MR, Bloomfield S, Xu T, Young M (2003) Biglycan-deficient mice have delayed osteogenesis after marrow ablation. *Calcif.Tissue Int.* 72:577-582
- (12) Chen XD, Fisher LW, Robey PG, Young MF (2004) The small leucine-rich proteoglycan biglycan modulates BMP-4-induced osteoblast differentiation. *FASEB J.* 18:948-958
- (13) Wallace JM, Rajachar RM, Chen XD, Shi S, Allen MR, Bloomfield SA, Les CM, Robey PG, Young MF, Kohn DH (2006) The mechanical phenotype of biglycan-deficient mice is bone- and gender-specific. *Bone* 39:106-116
- (14) Boskey AL, Young MF, Kilts T, Verdelis K (2005) Variation in mineral properties in normal and mutant bones and teeth. *Cells Tissues Organs* 181:144-153
- (15) Beamer WG, Donahue LR, Rosen CJ, Baylink DJ (1996) Genetic variability in adult bone density among inbred strains of mice. *Bone* 18:397-403
- (16) Turner CH, Hsieh YF, Muller R, Bouxsein ML, Baylink DJ, Rosen CJ, Grynpas MD, Donahue LR, Beamer WG (2000) Genetic regulation of cortical and trabecular bone strength and microstructure in inbred strains of mice. *J.Bone Miner.Res.* 15:1126-1131
- (17) Akhter MP, Iwaniec UT, Covey MA, Cullen DM, Kimmel DB, Recker RR (2000) Genetic variations in bone density, histomorphometry, and strength in mice. *Calcif.Tissue Int.* 67:337-344
- (18) Akhter MP, Fan Z, Rho JY (2004) Bone intrinsic material properties in three inbred mouse strains. *Calcif.Tissue Int.* 75:416-420
- (19) Wergedal JE, Sheng MH, Ackert-Bicknell CL, Beamer WG, Baylink DJ (2005) Genetic variation in femur extrinsic strength in 29 different inbred strains of mice is dependent on variations in femur cross-sectional geometry and bone density. *Bone* 36:111-122
- (20) Sheng MH, Baylink DJ, Beamer WG, Donahue LR, Rosen CJ, Lau KH, Wergedal JE (1999) Histomorphometric studies show that bone formation and bone mineral apposition rates are greater in C3H/HeJ (high-density) than C57BL/6J (low-density) mice during growth. *Bone* 25:421-429
- (21) Sheng MH, Baylink DJ, Beamer WG, Donahue LR, Lau KH, Wergedal JE (2002) Regulation of bone volume is different in the metaphyses of the femur and vertebra of C3H/HeJ and C57BL/6J mice. *Bone* 30:486-491

- (22) Sheng MH, Lau KH, Beamer WG, Baylink DJ, Wergedal JE (2004) In vivo and in vitro evidence that the high osteoblastic activity in C3H/HeJ mice compared to C57BL/6J mice is intrinsic to bone cells. *Bone* 35:711-719
- (23) Sheng MH, Lau KH, Mohan S, Baylink DJ, Wergedal JE (2006) High osteoblastic activity in C3H/HeJ mice compared to C57BL/6J mice is associated with low apoptosis in C3H/HeJ osteoblasts. *Calcif.Tissue Int.* 78:293-301
- (24) Akhter MP, Cullen DM, Pedersen EA, Kimmel DB, Recker RR (1998) Bone response to in vivo mechanical loading in two breeds of mice. *Calcif.Tissue Int.* 63:442-449
- (25) Kodama Y, Dimai HP, Wergedal J, Sheng M, Malpe R, Kutilek S, Beamer W, Donahue LR, Rosen C, Baylink DJ, Farley J (1999) Cortical tibial bone volume in two strains of mice: effects of sciatic neurectomy and genetic regulation of bone response to mechanical loading. *Bone* 25:183-190
- (26) Kodama Y, Umemura Y, Nagasawa S, Beamer WG, Donahue LR, Rosen CR, Baylink DJ, Farley JR (2000) Exercise and mechanical loading increase periosteal bone formation and whole bone strength in C57BL/6J mice but not in C3H/HeJ mice. *Calcif.Tissue Int.* 66:298-306
- (27) Amblard D, Lafage-Proust MH, Laib A, Thomas T, Ruegsegger P, Alexandre C, Vico L (2003) Tail suspension induces bone loss in skeletally mature mice in the C57BL/6J strain but not in the C3H/HeJ strain. *J.Bone Miner.Res.* 18:561-569
- (28) Marusic A, Katavic V, Grcevic D, Lukic IK (1999) Genetic variability of new bone induction in mice. *Bone* 25:25-32
- (29) Li X, Gu W, Masinde G, Hamilton-Ulland M, Rundle CH, Mohan S, Baylink DJ (2001) Genetic variation in bone-regenerative capacity among inbred strains of mice. *Bone* 29:134-140
- (30) Hadi N, Price C, Nasser P, Morgan E, Einhorn TA, Gerstenfeld LC, Jepsen KJ Genetic Variation In The Regain of Bone Strength During Fracture Healing, Paper No. 0225. 2007 Annual Meeting of the Orthopaedic Society
- (31) Alam I, Warden SJ, Robling AG, Turner CH (2005) Mechanotransduction in bone does not require a functional cyclooxygenase-2 (COX-2) gene. *J.Bone Miner.Res.* 20:438-446
- (32) Li CY, Jepsen KJ, Majeska RJ, Zhang J, Ni R, Gelb BD, Schaffler MB (2006) Mice lacking cathepsin K maintain bone remodeling but develop bone fragility despite high bone mass. *J.Bone Miner.Res.* 21:865-875

- (33) Nielsen KL, Allen MR, Bloomfield SA, Andersen TL, Chen XD, Poulsen HS, Young MF, Heegaard AM (2003) Biglycan deficiency interferes with ovariectomy-induced bone loss. *J.Bone Miner.Res.* 18:2152-2158
- (34) Wallace JM (2007) Investigating the Inbred Strain-Specific Response to Biglycan-Deficiency and Exercise: A Study in Genetically-Medicated Skeletal Adaptation. PhD Dissertation.
- (35) Kuhn JL, Goldstein SA, Feldkamp LA, Goulet RW, Jesion G (1990) Evaluation of a microcomputed tomography system to study trabecular bone structure. *J.Orthop.Res.* 8:833-842
- (36) Wallace JM, Rajachar RM, Allen MR, Bloomfield SA, Robey PG, Young MF, Kohn DH (2007) Exercise-Induced Changes in the Cortical Bone of Growing Mice are Bone- and Gender-Specific. *Bone* 40:1120-1127
- (37) Turner CH, Burr DB (1993) Basic Biomechanical Measurements of Bone: A Tutorial. *Bone* 14:595-607
- (38) Parfitt AM, Drezner MK, Glorieux FH, Kanis JA, Malluche H, Meunier PJ, Ott SM, Recker RR (1987) Bone histomorphometry: standardization of nomenclature, symbols, and units. Report of the ASBMR Histomorphometry Nomenclature Committee. *J.Bone Miner.Res.* 2:595-610
- (39) Carden A, Rajachar RM, Morris MD, Kohn DH (2003) Ultrastructural changes accompanying the mechanical deformation of bone tissue: a Raman imaging study. *Calcif.Tissue Int.* 72:166-175
- (40) Timlin J, Carden A, Morris M (1999) Chemical Microstructure of Cortical Bone Probed by Raman Transects. *Appl.Spectrosc.* 53:1429-1435
- (41) Timlin JA, Carden A, Morris MD, Rajachar RM, Kohn DH (2000) Raman spectroscopic imaging markers for fatigue-related microdamage in bovine bone. *Anal.Chem.* 72:2229-2236
- (42) Paschalis EP, Verdelis K, Doty SB, Boskey AL, Mendelsohn R, Yamauchi M (2001) Spectroscopic characterization of collagen cross-links in bone. *J.Bone Miner.Res.* 16:1821-1828
- (43) Boskey AL (2003) Bone mineral crystal size. *Osteoporos.Int.* 14 Suppl 5:16-21
- (44) Hoang QQ, Sicheri F, Howard AJ, Yang DS (2003) Bone recognition mechanism of porcine osteocalcin from crystal structure. *Nature* 425:977-980

- (45) Romberg RW, Werness PG, Riggs BL, Mann KG (1986) Inhibition of hydroxyapatite crystal growth by bone-specific and other calcium-binding proteins. *Biochemistry* 25:1176-1180
- (46) Roach HI (1994) Why does bone matrix contain non-collagenous proteins? The possible roles of osteocalcin, osteonectin, osteopontin and bone sialoprotein in bone mineralisation and resorption. *Cell Biol.Int.* 18:617-628
- (47) Weiner S, Wagner HD (1998) THE MATERIAL BONE: Structure-Mechanical Function Relations. *Annual Review of Materials Science* 28:271-298
- (48) Fratzl P, Fratzl-Zelman N, Klaushofer K, Vogl G, Koller K (1991) Nucleation and growth of mineral crystals in bone studied by small-angle X-ray scattering. *Calcif.Tissue Int.* 48:407-413
- (49) Currey JD (1988) The effect of porosity and mineral content on the Young's modulus of elasticity of compact bone. *J.Biomech.* 21:131-139
- (50) Boskey AL, Wright TM, Blank RD (1999) Collagen and bone strength. *J.Bone Miner.Res.* 14:330-335
- (51) Viguet-Carrin S, Garnero P, Delmas PD (2006) The role of collagen in bone strength. *Osteoporos.Int.* 17:319-336
- (52) Freeman JJ, Wopenka B, Silva MJ, Pasteris JD (2001) Raman spectroscopic detection of changes in bioapatite in mouse femora as a function of age and in vitro fluoride treatment. *Calcif.Tissue Int.* 68:156-162
- (53) Akkus O, Adar F, Schaffler MB (2004) Age-related changes in physicochemical properties of mineral crystals are related to impaired mechanical function of cortical bone. *Bone* 34:443-453
- (54) de Carmejane O, Morris MD, Davis MK, Stixrude L, Tecklenburg M, Rajachar RM, Kohan DH (2005) Bone chemical structure response to mechanical stress studied by high pressure Raman spectroscopy. *Calcif.Tissue Int.* 76:207-213
- (55) Morris MD, Finney WF, Rajachar RM, Kohn DH (2004) Bone tissue ultrastructural response to elastic deformation probed by Raman spectroscopy. *Faraday Discuss.* 126:159-68; discussion 169-83

CHAPTER 5

EXERCISE MODULATES THE PHENOTYPE OF BIGLYCAN-DEFICIENT MICE IN AN INBRED STRAIN-SPECIFIC MANNER BY ALTERING BONE TISSUE COMPOSITION AND MECHANICAL INTEGRITY

Introduction

Biglycan (bgn) is a small leucine-rich proteoglycan (SLRP) that is enriched in the extracellular matrix (ECM) of bone and other connective tissues [1-3]. Bgn is involved in the growth and differentiation of osteoblast precursor cells *in vitro* through its influence on signaling molecules from the TGF- β superfamily [4-7]. Biglycan also binds to collagen *in vitro*, influencing the fibrillogenesis of the collagen matrix [8], and can both promote and inhibit mineralization depending on the timing of expression [9].

Bgn-deficient mice exhibit a defect in the growth and differentiation of osteoblast precursor cells, possibly due to poor TGF- β and BMP signaling, and this results in alterations in the amount and quality of bone tissue production [6, 10, 11]. Bgn-deficient male mice bred on the C57BL6/129 (B6;129) inbred strain have decreased tissue-level yield strength along with structural-level deficiencies in yield deformation and yield work in the tibia [12]. However, this response to bgn-deficiency is inbred strain-specific, as there were no mechanical changes in C3H/He (C3H) mice in response to bgn-deficiency [13].

Altered tissue yield strength in bgn-deficient B6;129 mice, a property which is independent of the amount of tissue present, suggests that deficiencies in bone tissue quality are responsible. Matrix-level alterations in bgn-deficient B6;129 mice support the notion that changes in bone quality influence mechanical properties. For example, the diameter of collagen fibrils in bgn-deficient mice is larger and more variable and fibrils often exhibit notches, protuberances and irregular spacing [8, 14]. Bgn-deficient bones also have greater volumetric bone mineral density (vBMD) [12] and larger mineral

crystal size [15] compared with bones from wild type mice. Altered mineralization may be due to the altered collagen template upon which mineralization occurs or a change in the expression levels of other SLRPs as compensation [8, 16].

It is commonly stated that mechanical stimulation exerts its greatest influence on bone through structural adaptation and the accrual of bone mass [17]. However, mechanical loading also has effects on bone that influence the quality of the bone matrix [18, 19] in addition to any increase in bone mass or change in bone formation activity. For example, when male mice ran on a treadmill at a moderate intensity during growth (8-11 weeks of age), tissue-level strain to failure and structural post-yield deformation were increased [19]. Since post-yield properties of bone are primarily dictated by the organic compartment [20-23], exercise likely exerted its influence by changing the organic compartment in the developing bone. Since many diseases influence the mechanical integrity of bone through alterations in tissue quality, mechanical stimulation may be practical way to prevent and treat ECM deficiencies [24-26].

Inbred strain-specific responses to external stimuli including mechanical loading, unloading [27-30] and bone regeneration [31-33] exist and have demonstrated that the bones from C3H mice consistently fail to respond to changes in mechanical environment. Therefore, the current study was undertaken to test two hypotheses. First, the bones from B6;129 mice (both wild type and bgn-deficient) will be more responsive to exercise than the bones from C3H mice, where increased bone formation and altered matrix composition will increase the mechanical strength of the bone in the B6;129 inbred strain. Second, exercise-induced bone formation and altered matrix composition will compensate (return properties to WT control levels) for phenotypic deficiencies in tissue strength and bone size, and ultimately structural strength, in bgn-deficient B6;129 mice. However, because of the lack of phenotype in bgn-deficient C3H mice and the inability to respond to exercise, the C3H phenotype will not be affected by exercise.

These hypotheses were tested in wild type and bgn-deficient mice bred on B6;129 and C3H backgrounds. At 11 weeks of age, following 21 consecutive days of exercise, we investigated cross-sectional geometry and vBMD (via microCT), mechanical properties (tissue and structural-level via four-point bending) and tissue composition (via Raman Microspectroscopy) to uncover an inbred strain-specific response to exercise in

wild type and bgn-deficient mice, and to determine the ability of exercise to compensate for bgn-deficiency. Exercise-related changes in these properties relative to non-exercise controls were assessed in the cortical bone of male tibiae from both inbred strains and genotypes. Bgn-deficient exercise and control mice were compared with wild type control mice from the same inbred strain to assess the ability of exercise to compensate for phenotypic deficiencies in bone size and strength.

Materials and Methods

Animals

All animal procedures were performed at the University of Michigan with University Committee on Use and Care of Animals (UCUCA) approval (UCUCA animal approval protocol #8518). Biglycan-deficient (KO) and wild type (WT) breeder mice were the generous gift of Dr. Marian F. Young from the National Institute of Dental and Craniofacial Research (NIDCR). Mice from the B6;129 background strain were originally generated by homologous recombination in embryonic stem cells [34]. Mice from this background strain were then backcrossed to the C3H/HeNHsd (C3H) strain to a purity of greater than 95%. Upon arrival at the University of Michigan, the genotype of all breeder pairs was verified via polymerase chain reaction (PCR) using DNA extracted from a tail biopsy of each mouse, as previously described [35]. This process was repeated for the first F1 generation of mice from each breeder pair as verification.

To determine proper sample sizes for detecting effects of background strain, genotype and exercise, power calculations were performed based on previously published values for differences and standard deviations in mechanical and geometric properties between inbred mouse strains [36, 37], due to biglycan (bgn) deficiency [12] and in response to exercise [19] using a value of $\alpha=0.05$ and a power $(1-\beta)$ of 0.80. To statistically detect inbred strain-specificity in response to exercise (in both WT and KO groups), further power calculations were carried out based on expected ratios of values (exercise/control) between the two inbred strains [13]. To be able to statistically detect differences in primary outcome measures of interest based on expected differences (tibial

length, vBMD, cross-sectional size, strength at whole bone and tissue-levels, total deformation and failure strain), a sample size of n=15 was used for each group.

At 3 weeks of age, mice were weaned and maintained in standard cages with access to food, water and cage activity *ad libitum*. At 8 weeks of age (Day 0), mice from each background strain/genotype were randomly assigned to 1 of 2 weight-matched groups (exercise or control). In total, 2 inbred strains x 2 genotypes x 2 experimental groups x n=15 per group meant 120 mice were needed. Control mice remained confined to cages for the duration of the study. Exercise consisted of running on a treadmill (12 meters/minute at a 5° incline) for 30 minutes/day, 7 days/week for 21 consecutive days (Columbus Instruments, Model 1055M, Columbus, OH). Each lane of the treadmill was equipped with an adjustable-amperage (0-1.5 mA) shock grid at the rear of the belt to stimulate each mouse to run independently of all others. By the end of the second day of the experiment, all mice were running without the need of shock stimulation. Exercise and control mice were sacrificed on Day 20, following the last bout of running. Mice were sacrificed by CO₂ inhalation, at which time final body mass was measured and both tibiae were harvested, stripped of soft tissue, wrapped in gauze soaked in a calcium-buffered saline solution and stored at -20°C.

Micro Computed Tomography (μCT) Evaluation

Left tibiae were analyzed by micro computed tomography (μCT) to assess length, cross-sectional geometric properties and volumetric bone mineral density (vBMD). Bones were scanned at 18 μm/voxel resolution (GE/EVS MS-8 specimen scanner, GE Healthcare, London, Ontario, Canada) and three-dimensional images were reconstructed. Each three-dimensional data set was arranged as a series of 18 μm-thick slices oriented along the long axis of the tibia. Tibial length was measured directly on each reconstructed image from the most proximal portion of the chondyles to the most distal portion of the medial malleolus (MicroView version 2.1.2, GE Healthcare).

Cross-sectional geometry from the fracture site (to normalize whole bone mechanical properties, see methods section on mechanical testing) and both geometry and vBMD from a standard site in the diaphysis of each bone were determined. The

standard site was located at a position 792 μm proximal to the location where the tibia and fibula first become fused (TFJ), and was chosen to lie just distal to the mechanical loading region (which began 800 μm proximal to the TFJ). Averaged over all bones, this corresponded to a standard location that was $4.82 \pm 0.14\%$ of the total bone length proximal to the TFJ. Properties were determined from 6 μCT slices (108 μm) centered at each location.

After investigating histograms of voxel values from all standard sections, vBMD was determined at each section using a standard threshold level of 2000 (MicroView version 2.1.2, GE Healthcare). For the measurement of geometric properties, each section was thresholded into bone and non-bone voxels using a previously defined method [38]. Geometric properties for each region of interest were then determined using a custom analysis program. Properties of interest included cross-sectional area, cortical area, marrow area, average cortical thickness, anterior-posterior (AP) width, medial-lateral (ML) width and bending moment of inertia about the AP and ML axes (I_{AP} , I_{ML}).

Mechanical Testing

Left tibiae were brought to room temperature before testing and were kept hydrated in calcium-buffered saline until the test was complete. Each bone was tested in the ML direction (medial surface in tension) in a four-point bending configuration (Admet eXpert 450 Universal Testing Machine; Norwood, MA). The bone was positioned such that the TFJ was lined up with the outside edge of one loading roller. The bones were preloaded to 0.5 N, preconditioned for 15 seconds (2 Hz, mean load of $2 \text{ N} \pm 2 \text{ N}$) and then monotonically tested to failure in displacement control at a rate of 0.025 mm/sec. During each test, load and deflection were recorded, from which structural strength (yield force and ultimate force), energy or work (measured as the area under the force vs. displacement curve), stiffness (the slope of the linear portion of the force vs. displacement curve) and deformation (yield deformation, total deformation and post-yield deformation) were derived at the whole bone level [12, 19]. After testing, the distal end of each bone was placed in 70% ethanol.

During testing, the bone was visually monitored and the point of fracture initiation was noted and measured relative to the proximal end of the bone. In order to normalize structural-level mechanical properties, a subset of geometric properties at the fracture site was obtained from μ CT data (I_{AP} and the distance from the centroid to the tensile surface of the bone, c). Together with the load and deflection data, I_{AP} and c were used to map force and displacement (structural level properties dependent on bone structural organization) into stress and strain (predicted tissue level properties) from standard beam-bending equations for four-point bending:

$$Stress = \sigma = \frac{Fac}{2I_{AP}} \quad (MPa)$$

$$Strain = \varepsilon = \frac{6cd}{a(3L - 4a)} \times 10^6 \quad (\mu\varepsilon)$$

In these equations, F is the force, d is the displacement, a is the distance from the support to the inner loading point (3 mm) and L is the span between the outer supports (9 mm). The yield point was calculated using the 0.2% offset method based on the stress-strain curve [39]. The modulus of elasticity was calculated as the slope of the linear portion of the stress-strain curve.

Raman Microspectroscopy

Raman microspectroscopy was used to investigate differences in tissue composition as a function of age, genotype, exercise and background strain. Following mechanical testing, the distal half of all bones was dehydrated in graded ethanol (70%, 80%, 95%, 100%), defatted in Clear-Rite 3 (Richard-Allen Scientific; Kalamazoo, MI) and infiltrated in a liquid methylmethacrylate monomer (Koldmount™ Cold Mounting Liquid, Mager Scientific). The bones were then embedded in poly methylmethacrylate (Koldmount™ Cold Mounting Kit, Mager Scientific). Of the 15 specimens in each group, 6 bones were chosen at random for analysis. Using a low-speed sectioning saw (South Bay Technology, Model 650; San Clemente, CA) with a diamond wafering blade (Mager Scientific), thick sections (≥ 3 mm in thickness) were made and hand polished using wet silicon carbide abrasive discs. These sections were intended to be located at a

standard site distal to the TFJ. Because fracture did not occur in the same place in every bone, and these sections were hand cut and ground following mechanical testing, variation in this location occurred (the average distance of this section was $488 \pm 290 \mu\text{m}$ distal to the TFJ).

The Raman imaging system has been described [40-43]. Briefly, Raman scatter was excited using a 785 nm laser with a rectangular beam profile (Kaiser Optical Systems, Ann Arbor, MI). The beam was passed through a 20X objective onto the sample which focuses the line-shaped beam ($\sim 100 \mu\text{m}$ in length). Raman scattered light from every point on the line was simultaneously passed back through the objective and through a dichroic mirror to a charge coupled device (CCD) detector. Once Raman spectra were collected, band areas were determined for select Raman peaks representing specific components of the mineral and organic matrix. Three bands were investigated: a phosphate band (PO_4^{3-} ν_1 symmetric stretch at 957 cm^{-1}), a carbonate band (CO_3^{2-} ν_1 symmetric stretch at 1070 cm^{-1}) and the Amide I envelope (C=O stretch at $1595\text{-}1720 \text{ cm}^{-1}$). The Amide I band was decomposed into 2 smaller underlying bands at 1660 cm^{-1} and 1690 cm^{-1} . From these bands, 3 band area ratios were determined to characterize the chemical composition of the sample. The degree of mineralization in the tissue was determined from the mineral/matrix ratio by dividing the phosphate band by the Amide I band. The carbonate/phosphate ratio, which is indicative of the level of Type B carbonate substitution in the mineral (carbonate substituting in the crystal lattice for phosphate ions), was determined by dividing the carbonate band by the phosphate band. Finally, the collagen cross-linking ratio was determined by dividing the 1660 cm^{-1} band by the 1690 cm^{-1} band [44]. The area ratio between these two bands is indicative of changes in the amount of non-reducible/reducible cross-linking in Type I collagen. Therefore, this ratio increases with increasing number of stable cross-links. Mineral crystallinity information, which takes into account the size, shape and perfection of mineral crystals, was obtained from the inverse of the full bandwidth at half peak intensity of the phosphate band at 957 cm^{-1} .

A total of 12 spectral lines were collected from each sample. In each anatomic quadrant (anterior, posterior, lateral, medial), three total spectra were taken in regions

corresponding to periosteal, intracortical and endocortical locations. All 12 lines were averaged to obtain an overall measurement for each specimen.

Statistical Analysis

All statistical analyses were performed using Sigma Stat (Version 3.1, Systat Software Inc.) or SPSS (Version 11.0, SPSS Inc.). There were two statistical goals of this study. We first sought to determine if an inbred strain-specific response to exercise existed in WT mice and KO mice. For each property of interest, ratios of exercise/mean control values for each exercise sample within each inbred strain/genotype were calculated. We then examined statistical differences in ratios between inbred strains in WT mice followed by the difference in ratios in KO, an analog to 2-way ANOVA looking for the effects of background strain and exercise within each genotype. Second, we wanted to determine how the bgn-deficient phenotype was impacted by exercise. Within each inbred strain, Student t-tests were employed to investigate the effects of bgn-deficiency in control mice at 11 weeks of age (KO control versus WT control) and to see how the phenotype was altered with the addition of exercise (KO exercise versus WT control). Student t-tests were also employed to investigate the effects of exercise within each background strain/genotype (exercise versus control). In groups which failed to exhibit normal distributions or equal variance, Mann-Whitney rank sum tests were performed. For all investigations, a value of $p < 0.05$ was considered significant while a p-value between 0.05 and 0.10 was also noted.

Results

Effects of exercise in B6;129 WT mice (Left set of graphs in Figure 5.1-Figure 5.5)

In B6;129 WT mice, exercise increased collagen cross-linking and post-yield mechanical integrity without changes in bone geometry. Exercise did not impact body mass (Figure 5.1A) or tibial length (Figure 5.1C) in B6;129 WT mice compared with control levels. Exercise marginally increased the collagen cross-linking ratio in B6;129 WT mice ($p=0.098$, Figure 5.2A), but counter to hypothesis 1, no other measures of

tissue composition were significantly altered. Compared with control mice, exercise marginally increased failure strain ($p=0.064$, Figure 5.3A) and total toughness ($p=0.097$, Figure 5.3B) at the tissue-level of B6;129 WT mice. Counter to hypothesis 1, no cross-sectional geometric properties were impacted by exercise (Figure 5.4). In the absence of altered cross-sectional size, exercise still significantly increased post-yield deformation ($p=0.030$, Figure 5.5A) and failure deformation ($p=0.034$, Figure 5.5A) and marginally increased total work ($p=0.063$, Figure 5.5B) compared with control mice.

Effects of exercise in B6;129 KO mice (Right set of graphs in Figure 5.1-Figure 5.5)

In B6;129 KO mice, exercise changed tissue composition and increased tissue strength while decreasing bone ML width. In B6;129 KO mice, body mass was marginally decreased with exercise compared with control mice ($p=0.098$, Figure 5.1B), but tibial length was unaffected (Figure 5.1D). Exercise impacted tissue composition in the KO mice, where the carbonate/phosphate ratio was significantly increased ($p=0.036$, Figure 5.2B) and the collagen cross-linking ratio was marginally increased ($p=0.099$, Figure 5.2A). At the tissue-level, exercise marginally increased yield stress in B6;129 KO mice ($p=0.091$, Figure 5.3C). ML width significantly decreased with exercise ($p=0.012$, Figure 5.4A) resulting in a significant increase in the AP/ML ratio of the bone (data not shown, $p=0.005$) and a marginal decrease in I_{AP} ($p=0.055$, Figure 5.4B). Structural-level mechanical behavior was not impacted by exercise in B6;129 KO mice (Figure 5.5).

Bgn-deficient phenotype in B6;129 mice (KO control versus WT Control) and the ability of exercise to alter this phenotype (KO Exercise versus WT Control)

Bgn-deficiency in B6;129 mice caused decreased mechanical integrity through altered tissue composition and decreased cross-sectional size. In B6;129 mice, no bgn-deficient phenotypic difference was present in body mass at 11 weeks of age (Day 20 in Figure 5.1A and B). Tibial length was significantly lower in the KO control mice versus WT control mice ($p<0.001$, Figure 5.1C and D). The mineral/matrix ratio ($p=0.004$, Figure 5.2C), crystallinity ($p<0.001$, Figure 5.2D) and $vBMD$ ($p=0.011$, Figure 5.2E)

were significantly greater in KO control mice versus WT control mice, while the collagen cross-linking ratio was significantly decreased ($p < 0.001$, Figure 5.2A). No tissue-level mechanical properties were significantly different in KO control mice versus WT control mice, but yield strain ($p = 0.098$, Figure 5.3A), resilience ($p = 0.071$, Figure 5.3B) and ultimate stress ($p = 0.056$, Figure 5.3C) were marginally decreased, while failure strain ($p = 0.089$, Figure 5.3A) was marginally increased. KO control mice had smaller AP width ($p < 0.001$, Figure 5.4A), AP/ML ratio ($p < 0.001$, data not shown), I_{AP} ($p = 0.038$, Figure 5.4B), I_{ML} ($p = 0.005$, Figure 5.4B), cross-sectional area ($p = 0.004$, Figure 5.4C) and marrow area ($p < 0.001$, Figure 5.4C) versus WT control mice. At the structural-level, post-yield deformation ($p = 0.016$, Figure 5.5A) and failure deformation ($p = 0.014$, Figure 5.5A) were significantly increased in KO control mice versus WT control mice, while stiffness was significantly decreased ($p = 0.034$, Figure 5.5C), and yield force ($p = 0.062$, Figure 5.5D) and ultimate force ($p = 0.053$, Figure 5.5D) were marginally decreased.

Exercise in KO mice compensated for tissue-level mechanical deficiencies versus WT control mice, but maintained alterations in tissue composition, decreased cross-sectional size and decreased structural strength and stiffness. In B6;129 mice, exercise in KO mice resulted in lower body mass compared with WT control mice ($p = 0.003$, Figure 5.1A and B). Tibial length was also lower in KO exercise mice versus WT control mice ($p < 0.001$, Figure 5.1C and D). The carbonate/phosphate ratio ($p = 0.009$, Figure 5.2B), the mineral/matrix ratio ($p = 0.005$, Figure 5.2C), crystallinity ($p = 0.001$, Figure 5.2D) and vBMD ($p = 0.003$, Figure 5.2E) were all significantly greater in the KO exercise versus WT control mice, while the collagen cross-linking ratio was significantly decreased ($p = 0.022$, Figure 5.2A). Failure strain ($p = 0.001$, Figure 5.3A) and toughness ($p < 0.001$, Figure 5.3B) were significantly greater in KO exercise versus WT control mice, while yield strain was marginally decreased ($p = 0.090$, Figure 5.3A) and modulus was marginally greater ($p = 0.089$, Figure 5.3D). KO exercise mice had significantly smaller AP width ($p < 0.001$, Figure 5.4A), ML width ($p < 0.001$, Figure 5.4A), I_{AP} ($p = 0.004$, Figure 5.4B), I_{ML} ($p = 0.001$, Figure 5.4B), cross-sectional area ($p = 0.002$, Figure 5.4C), cortical area ($p = 0.028$, Figure 5.4C) and marrow area ($p < 0.001$, Figure 5.4C) versus WT control mice. At the structural level, KO exercise mice had significantly increased post-yield deformation ($p < 0.001$, Figure 5.5A), failure deformation ($p < 0.001$, Figure 5.5A)

and total work ($p=0.005$, Figure 5.5B) versus WT control mice. Stiffness ($p=0.005$, Figure 5.5C) and yield force ($p=0.001$, Figure 5.5D) were significantly decreased and ultimate force was marginally less ($p=0.068$, Figure 5.5D) in KO exercise versus WT control mice at the structural level.

Effects of exercise in C3H WT mice (Left set of graphs in Figure 5.6-Figure 5.10) and inbred strain specificity of the response to exercise

In C3H WT mice, exercise altered tissue composition but failed to influence tibial cross-sectional size or mechanical integrity. Exercise did not impact body mass (Figure 5.6A) or tibial length (Figure 5.6C) in C3H WT mice compared with control mice. Exercise significantly increased the collagen cross-linking ratio ($p=0.019$, Figure 5.7A), the carbonate/phosphate ratio ($p<0.001$, Figure 5.7B) and the mineral/matrix ratio ($p=0.041$, Figure 5.7C) in C3H WT mice compared with control mice. There were no effects of exercise on tissue-level mechanical properties (Figure 5.8), cross-sectional geometric properties (Figure 5.9) or structural-level mechanical properties (Figure 5.10) in C3H WT mice.

To investigate inbred strain specificity in response to exercise in WT mice for each property of interest, ratios of exercise/mean control values for each exercise sample within each inbred strain were calculated and statistically compared between inbred strains (C3H ratio versus B6;129 ratio). There were no inbred strain-specific effects of exercise on body mass or tibial length. Compositionally, an inbred strain-specific effect of exercise on the collagen cross-linking ratio was present (greater increase in C3H ratio, $p=0.032$). A marginal inbred strain-specific difference in response to exercise was present in resilience (decrease in B6;129 ratio, $p=0.055$). Both AP width ($p=0.038$) and the AP/ML ratio ($p=0.039$) were impacted by exercise in an inbred strain-specific way (decrease in C3H ratio in both cases). At the structural level, there was a marginal inbred strain-specific impact of exercise on pre-yield work (C3H ratio increased while B6;129 ratio decreased, $p=0.094$).

Effects of exercise in C3H KO mice (Right set of graphs in Figure 5.6-Figure 5.10) and inbred strain specificity of the response to exercise

In C3H KO mice, exercise altered tibial tissue composition but failed to influence cross-sectional size or mechanical integrity. In C3H KO mice, neither body mass (Figure 5.6B) nor tibial length (Figure 5.6D) were affected by exercise compared with control mice. Crystallinity was significantly increased in C3H KO mice with exercise ($p=0.003$, Figure 5.7D) and the collagen cross-linking ratio was marginally increased ($p=0.066$, Figure 5.7A) compared with control levels. No tissue-level mechanical properties were altered with exercise in C3H KO mice (Figure 5.8). AP width was marginally decreased ($p=0.059$, Figure 5.9A), but structural-level mechanical properties were unaffected by exercise in C3H KO mice (Figure 5.10).

To investigate inbred strain specificity in response to exercise in KO mice for each property of interest, ratios of exercise/mean control values for each exercise sample within each inbred strain were calculated and statistically compared between inbred strains (C3H ratio versus B6;129 ratio). In KO mice, body mass was altered with exercise in an inbred strain-specific way (ratio decreased in B6;129 mice, $p=0.034$), but tibial length was unaffected. There was a significant inbred strain-specific change in crystallinity in response to exercise (ratio increased in C3H mice, $p<0.001$) while the carbonate/phosphate ratio was marginally impacted (ratio increased in B6;129 mice, $p=0.087$). At the tissue-level, there were inbred strain-specific changes in resilience ($p=0.047$) and yield stress ($p=0.016$) in response to exercise while total toughness ($p=0.078$), ultimate stress ($p=0.059$) and modulus ($p=0.099$) were marginally impacted (ratio increased in B6;129 mice in all cases). AP width (ratio decreased in B6;129 mice, $p=0.019$), ML width (ratio decreased in B6;129 mice, $p=0.007$) and the AP/ML ratio (ratio decreased in C3H mice, $p<0.001$) had inbred strain-specific changes with exercise while the change in I_{AP} was marginal (ratio decreased in B6;129, $p=0.062$). No inbred strain-specific changes in structural-level mechanical properties were noted.

Bgn-deficient phenotype in C3H mice (KO control versus WT Control) and the ability of exercise to alter this phenotype (KO Exercise versus WT Control)

C3H KO mice had altered tissue composition and greater cortical thickness, but no mechanical properties differed versus WT mice. C3H KO control mice had elevated body mass at 11 weeks of age compared with WT control mice ($p=0.049$, Day 20 in Figure 5.6A and B) and tibial length was unchanged (Figure 5.6C and D). The collagen cross-linking ratio was significantly decreased in KO control mice compared with WT control levels ($p<0.001$, Figure 5.7A), while the carbonate/phosphate ratio ($p=0.028$, Figure 5.7B), the mineral/matrix ratio ($p=0.003$, Figure 5.7C) and vBMD ($p<0.001$, Figure 5.7E) were all significantly greater. Cortical thickness was significantly greater in KO control mice versus WT control mice ($p=0.001$, Figure 5.9D) and marrow area was marginally less ($p=0.093$, Figure 5.9A). There were no tissue-level (Figure 5.8) or structural-level (Figure 5.10) mechanical differences in KO control versus WT control mice.

Exercise in C3H KO mice maintained compositional differences and greater cortical thickness versus WT control mice, but failed to alter mechanical integrity. C3H KO exercise mice had increased body mass compared with WT control mice ($p=0.029$, Figure 5.6A and B) and tibial length was unchanged (Figure 5.6C and D). The carbonate/phosphate ratio ($p<0.001$, Figure 5.7B), the mineral/matrix ratio ($p=0.049$, Figure 5.7C), crystallinity ($p=0.028$, Figure 5.7D) and vBMD ($p=0.004$, Figure 5.7E) were all greater in KO exercise mice compared with WT control levels, while the collagen cross-linking ratio was marginally decreased ($p=0.065$, Figure 5.7A). Marrow area was significantly decreased in KO exercise mice versus WT control ($p=0.004$, Figure 5.9A), and cortical thickness was significantly greater ($p=0.009$, Figure 5.9D). No tissue-level (Figure 5.8) or structural-level (Figure 5.10) mechanical properties differed in KO exercise versus WT control mice.

Discussion

This study demonstrates that exercise (moderate running on a treadmill for 30 minutes per day for 21 consecutive days) can influence the mechanical integrity of bone

in the absence of new bone formation. Exercise failed to induce significant changes in bone formation in wild type or *bgn*-deficient mice of either B6;129 or C3H background strain (Figure 5.4 and Figure 5.7). Changes in tissue-level mechanical behavior [increased post-yield behavior in B6;129 WT mice Figure 5.3A and B) and increased yield stress in B6;129 KO mice (Figure 5.3C)] but the lack (or paucity) of new bone formation suggests that the effects of exercise were exerted primarily through alterations in the composition of pre-existing tissue.

A consistent result from this study was that exercise led to changes in mineral composition, but mechanical influences on the mineral phase were dependent on inbred strain and genotype. In the B6;129 mice, carbonate/phosphate ratio increased in the KO mice with exercise with no change in the WT mice (Figure 5.2A). In the C3H mice, changes in mineral occurred in both the WT mice (increased crystallinity, Figure 5.7) and the KO mice (increased mineral/matrix ratio and carbonate/phosphate ratio, Figure 5.7). While inbred strain-specific loading influences on bone mineral density have been demonstrated and hypothesized to be genetically regulated [45], this is the first indication of changes in the nature of mineral with exercise. This study also shows the first evidence of genotype-specific mineral changes in response to loading in a gene disruption model. *Bgn* has known roles in regulating mineral density and mineral composition *in vivo* [15]. In the absence of *bgn*, a lack of this regulation could result in differences in mineral composition in KO mice with exercise compared with the response in WT mice.

With exercise, either the degree of mineralization of the tissue (as reflected by vBMD and/or the mineral/matrix ratio) or the true nature of the mineral (as reflected by the carbonate/phosphate ratio or the crystallinity of the mineral) were increased, consistent with other studies which have demonstrated increased BMD with loading and exercise [19, 46, 47]. However, the mechanism behind increased mineral changes with exercise is unclear, especially in the absence of new bone formation. Direct physical stress may have induced a phase change in the mineral [48]. A more likely possibility involves the *in vivo* environment of the bone mineral. Because of the small size and tablet shape of hydroxyapatite crystals in bone [49-51], there is a large surface to volume ratio meaning a large area over which ions can be substituted or deposited on pre-existing crystals. Exercise increases the efficiency of intestinal absorption of calcium and

phosphorous, increasing the concentrations of these minerals in the blood [52, 53]. The same may be true for levels of carbonate. Exercise also increases fluid flow through the microporosity of the bone, due both to physical squeezing of extracellular fluid [54-56] as well as the effects of increased heart rate leading to increased circulation. Increased mineral ion concentrations coupled with increased fluid flow could expose the mineral present in the tissue to a newly-replenished solution that is potentially rich in ions, which could lead to the changes in mineral chemistry and crystal size noted in this study.

Another consistent observation across background strains and genotypes was that exercise resulted in an increase in the ratio of mature to immature collagen cross-links (Figure 5.2A and Figure 5.7A). The mechanism is unclear, but several possibilities exist. It is generally thought that the maturation from immature divalent cross-links to more mature trivalent cross-links is a spontaneous reaction [23]. Therefore, simply having more immature cross-links present may increase the rate of this reaction. Because of steric interactions, the lysine and/or hydroxylysine residues necessary for initial divalent cross-linking require that collagen molecules be in a proper orientation [57]. Therefore, a second possibility is that as the bone matrix is loaded, collagen fibrils are aligned. Alignment may also decrease the proximity of immature cross-links and therefore the likelihood of maturation into a trivalent form. Initial cross-linking requires the presence of lysyl oxidase (LOX), a copper-dependent enzyme which catalyzes the oxidative deamination of lysine and hydroxylysine residues in the telopeptide region of collagen molecules to prepare them for cross-linking [23, 58]. It is possible that mechanical loading may increase the local expression of LOX or may activate the enzyme [59-61]. *In vivo*, LOX is typically bound tightly to its substrate [58], so a final possibility is that increased fluid flow with loading could bring in a greater supply of LOX to induce new cross-link formation.

The bones of WT B6;129 mice were more responsive to mechanical stimulation than the bones from WT C3H mice. Exercise marginally increased failure strain and total toughness in B6;129 WT mice versus control mice (Figure 5.3A and B). The marginal increase in the collagen cross-linking ratio that occurred with exercise may be responsible for this change (Figure 5.2A), as collagen alterations are typically associated with post-yield behavior in bone [20-23]. In the C3H mice, exercise increased cross-linking,

carbonate/phosphate ratio and mineral/matrix ratio (Figure 5.7A-C), but these compositional changes failed to impact tissue mechanical integrity (Figure 5.8). Although mineral is typically correlated with strength/stiffness and collagen with post-yield and failure behavior [20], these relationships are not mutually exclusive. It is possible that changes occurring in mineral and cross-linking in C3H WT mice interacted in such a way as to leave the mechanical integrity of the tissue unchanged. Mechanical properties at the structural-level are derived from the combination of bone size and tissue-level mechanical integrity. Due to a lack of changes in bone size with exercise in both the B6;129 and C3H WT mice, mechanical changes that occurred at the tissue level directly impacted structural-level properties, as indicated by increased post-yield behavior in the B6;129 mice and no changes in the C3H mice.

As was the case in the WT mice, and as was hypothesized, the response to exercise in the B6;129 KO mice was more compelling than that of the C3H KO mice and had a greater impact on the bgn-deficient phenotype in B6;129 mice compared with C3H mice. Type B carbonate levels and levels of mature collagen cross-links were elevated in B6;129 exercise versus control mice (Figure 5.2). These compositional differences with exercise failed to significantly impact tissue-level mechanical behavior in exercise versus control mice (Figure 5.3). Exercise in B6;129 KO mice also failed to induce a bone formation response (Figure 5.4), again suggesting that exercise-induced compositional changes (Figure 5.2) reflect alterations in pre-existing tissue.

Depending on the level of hierarchy investigated, the modest changes with exercise in the B6;129 KO mice were still sufficient to significantly impact the bgn-deficient phenotype of this inbred strain. Phenotypic differences in tissue composition in B6;129 KO mice versus WT control mice (increased mineral/matrix ratio and crystallinity and vBMD; decreased levels of mature collagen cross-linking) were maintained in KO exercise mice versus WT control mice with the addition of increased carbonate/phosphate ratio (Figure 5.2). Exercise-induced changes in tissue composition in the KO mice had mostly positive influences on mechanical behavior at the tissue-level (Figure 5.3). With the exception of yield strain, phenotypic deficiencies (ultimate stress and resilience in KO control versus WT control mice) were compensated for and modulus was now greater in KO exercise mice compared with WT control levels. It is

probable that exercise-induced alterations in mineral were responsible for enhancements of tissue strength and modulus [20, 23, 62]. Failure strain was marginally greater in the KO control mice compared with WT control mice at 11 weeks of age, and exercise in the KO mice made this relationship significant while also increasing toughness. Though the collagen cross-linking ratio was still decreased in KO mice compared with WT levels (Figure 5.2A), there was a marginal increase with exercise which may be responsible for these post-yield benefits [20-23]. Increased post-yield behavior at the tissue-level directly impacted structural-level properties by maintaining phenotypically increased post-yield and failure deformation and increasing total work (Figure 5.5). However, since exercise failed to induce a bone formation response in the KO bones (Figure 5.4), geometric deficiencies due to bgn-deficiency were still present. Because of the dependence of structural level strength and stiffness on both bone size/shape and tissue-level behavior, decreased structural strength and stiffness persisted (Figure 5.5). Results in the B6;129 KO mice suggest that exercise was able to compensate for tissue-level deficiencies caused by bgn-deficiency through compositional alterations.

Exercise in the C3H KO mice had little effect at any level of the bone hierarchy investigated. Geometric properties were unaffected by exercise with the exception of a marginal decrease in AP width (Figure 5.9A). There was increased crystallinity with exercise in the KO mice and a marginal increase in the collagen cross-linking ratio (Figure 5.7). Changes in composition failed to impact tissue-level mechanical properties in C3H control versus exercise mice from either genotype (Figure 5.8). Therefore, similar to the response in C3H WT mice, there were no differences in structural-level mechanical properties in C3H KO exercise mice versus control levels (Figure 5.10). Because of the lack of response to exercise in the C3H KO bones, exercise had no impact on the mild phenotype of the C3H KO mice compared with C3H WT mice.

In summary, this study clearly demonstrates that exercise can elicit alterations in the bone ultrastructure which influence the composition and mechanical integrity of the bone tissue without changes in bone geometry, suggesting that mechanical stimulation may be a viable strategy to combat deficiencies in tissue quality that are associated with many diseases of bone. This study also demonstrates an inbred strain-specific response to exercise in wild type and bgn-deficient mice, and shows the first evidence of genotype-

specific changes in response to loading in a gene disruption model. Mice from the B6;129 inbred strain responded to exercise with changes in tissue composition which impacted the mechanical integrity of the bone tissue without the addition of new bone. In bgn-deficient B6;129 mice, alterations in tissue chemistry compensated for phenotypic mechanical deficiencies at the tissue-level. Compositional changes with exercise in C3H mice from both genotypes failed to alter mechanical properties.

Acknowledgements

I would like to acknowledge my coauthors on this manuscript:

Dr. Kurtulus Golcuk, Dr. Michael D. Morris and Dr. David H. Kohn.

I would also like to thank Dr. Marian F. Young from the National Institute of Dental and Craniofacial Research (NIDCR) for her generous gift of biglycan-deficient and wild type breeder mice from each inbred strain.

Funding sources for this study:

DoD/US Army DAMD17-03-1-0556; NIH T32-DE07057; NIH IPA Agreement;
Regenerative Sciences Training Grant R90-DK071506

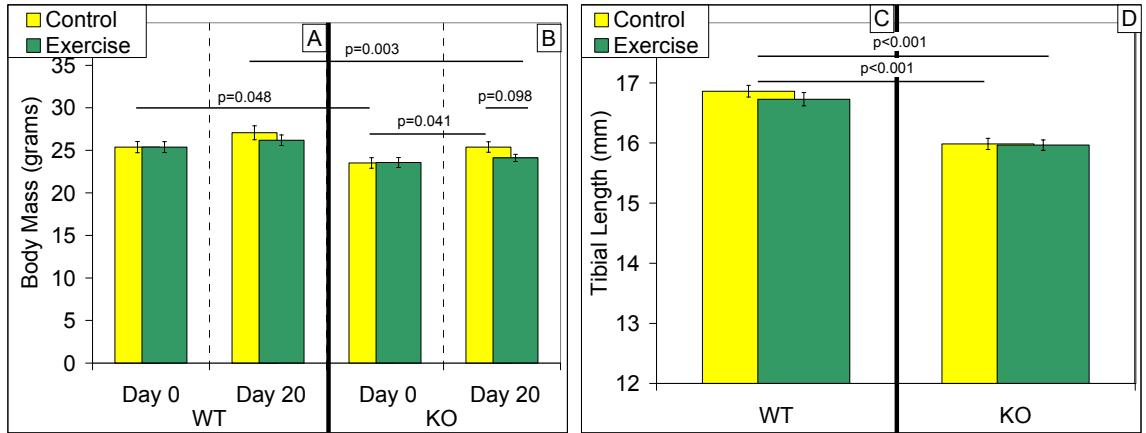


Figure 5.1: Body Mass (A,B) and tibial length (C,D) of wild type (WT) and bgn-deficient (KO) mice from the B6;129 inbred strain. Mice within each genotype were weight-matched at Day 0 (8 weeks of age). Only KO control mice gained weight during the study. Exercise did not impact body mass in WT mice. At Day 0, B6;129 KO mice weighed less than WT mice. By Day 20, there was no phenotypic difference in body mass in B6;129 mice, but because of marginally decreased body mass in KO exercise mice versus KO control mice at Day 20, KO exercise mice weighed less than WT control mice. Tibial length was not impacted by exercise in either genotype. Tibial length was less in the KO control mice versus WT control mice. Exercise in the KO mice maintained this deficiency in tibial length compared with WT control mice. Data are presented as mean \pm SEM.

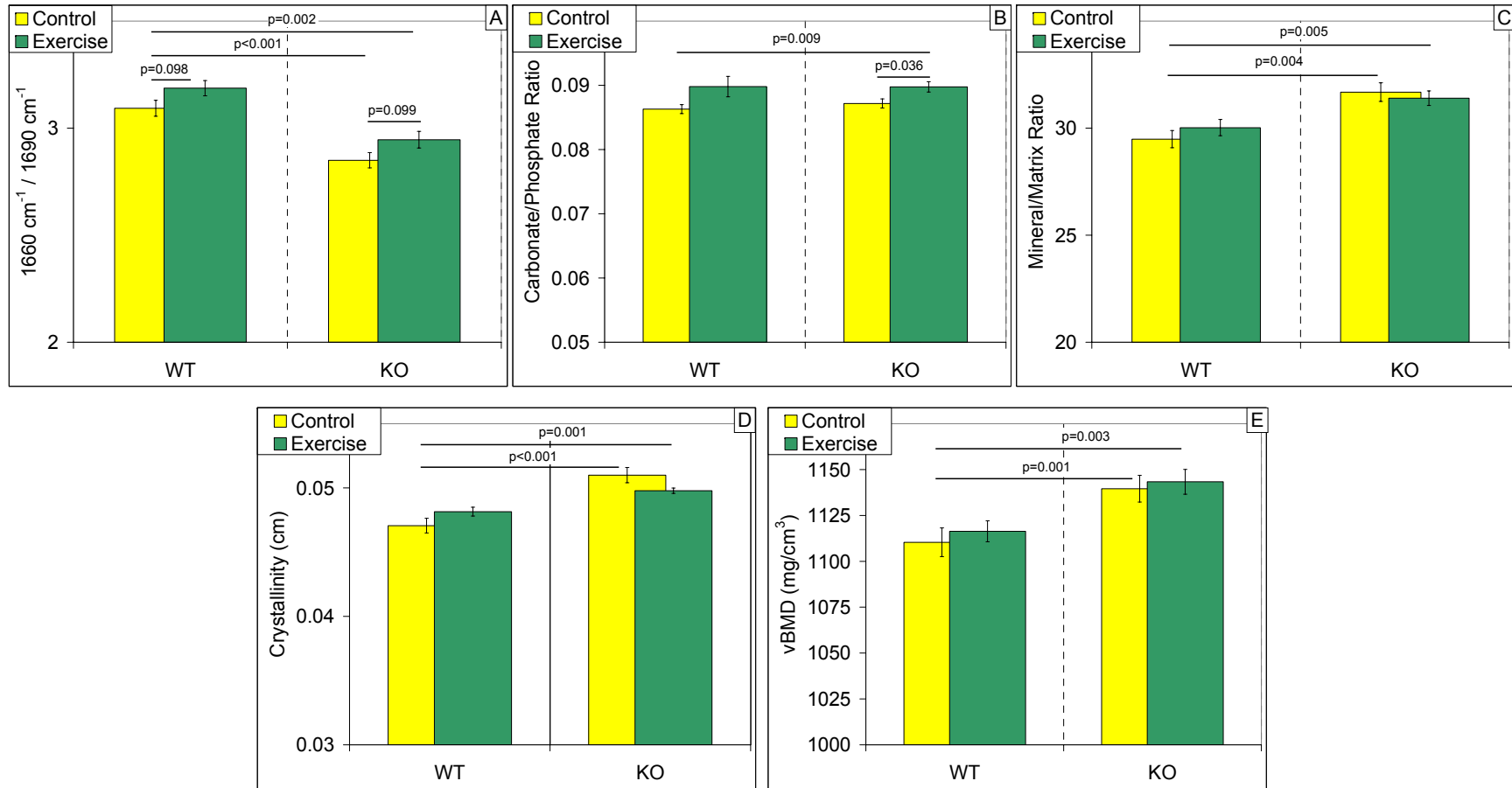


Figure 5.2: Tissue composition and volumetric bone mineral density (vBMD) in the tibial diaphysis of wild type (WT) and *bgn*-deficient (KO) B6;129 mice. In WT and KO mice, the collagen cross-linking ratio was marginally increased in exercise versus control mice. Exercise also increased the carbonate/phosphate ratio in KO mice versus KO control levels. The mineral/matrix ratio, crystallinity and vBMD were significantly greater in KO control mice versus WT control, while the collagen cross-linking ratio was significantly decreased. The carbonate/phosphate ratio, the mineral/matrix ratio, crystallinity and vBMD were all significantly greater in the KO exercise versus WT control mice, while the collagen cross-linking ratio was significantly decreased. Data are presented as mean \pm SEM.

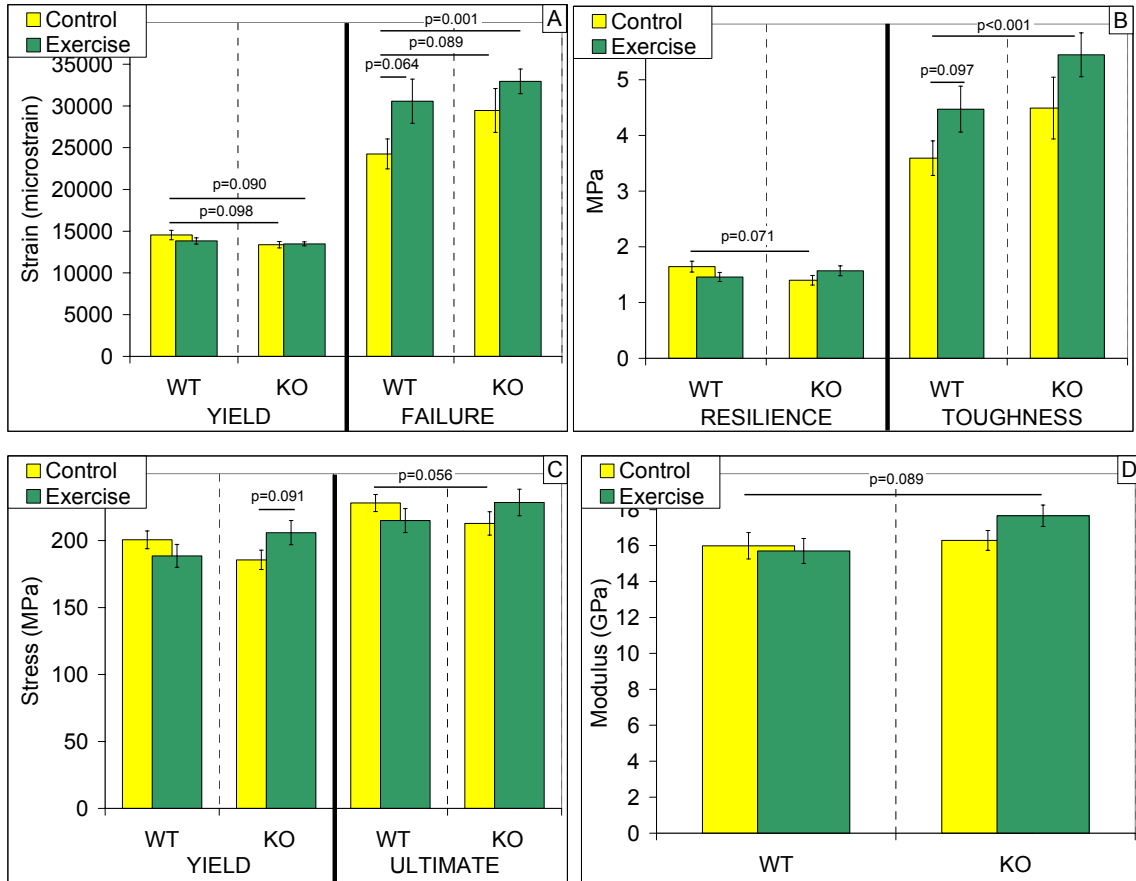


Figure 5.3: Estimated tissue-level mechanical properties from wild type (WT) and bgn-deficient (KO) B6;129 tibiae. In WT mice, failure strain and toughness were increased in exercise versus control mice. In KO mice, yield stress was marginally greater in exercise versus control mice. No tissue-level mechanical properties were significantly different in KO control mice versus WT control mice, but yield strain, resilience and ultimate stress were marginally decreased while failure strain was marginally increased. Failure strain and toughness were significantly greater in KO exercise versus WT control mice, while yield strain was marginally decreased and modulus was marginally greater. Data are presented as mean \pm SEM.

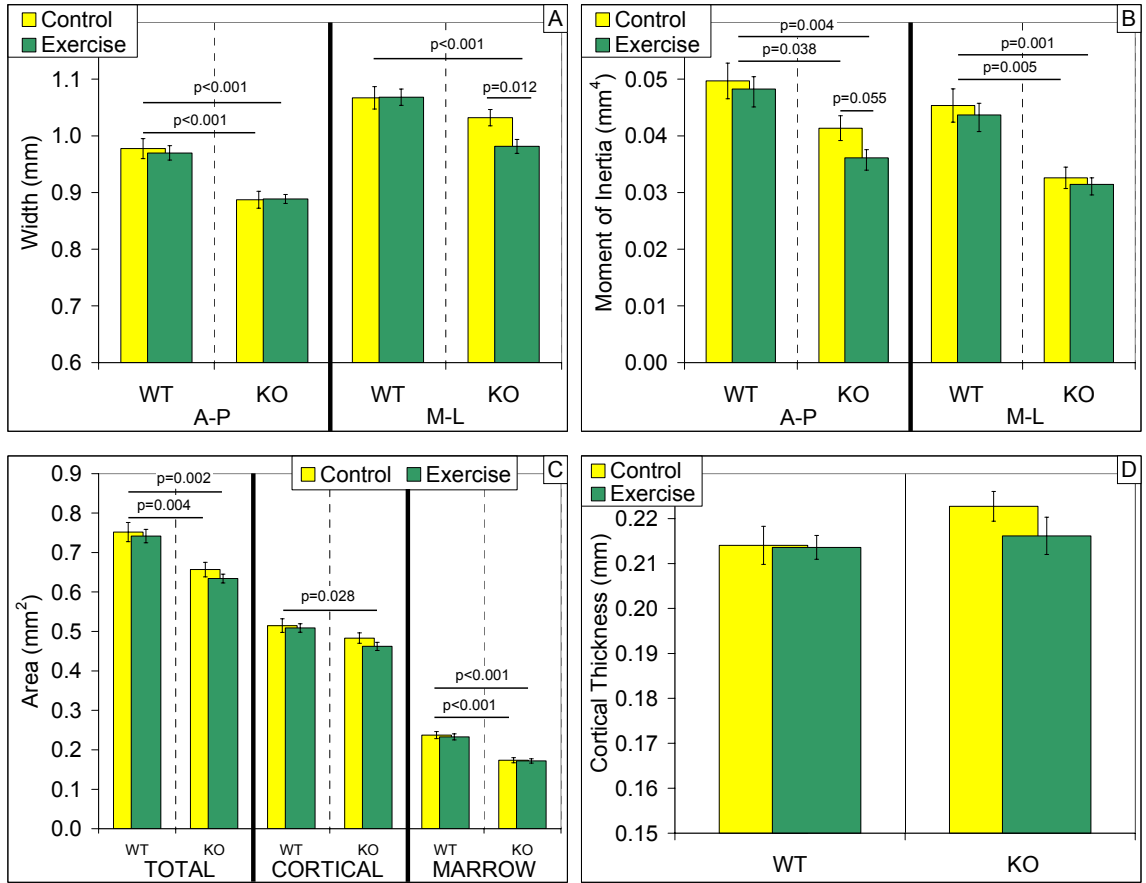


Figure 5.4: Standard site geometric properties of the tibial diaphysis in wild type (WT) and *bgn*-deficient (KO) B6;129 mice. No geometric properties were altered with exercise versus control mice in either genotype. KO control mice had smaller AP width, AP moment of inertia (MOI), ML MOI, total cross-sectional area and marrow area versus WT control mice. KO exercise mice had significantly smaller AP width, ML width, AP MOI, ML MOI, total cross-sectional area, cortical area and marrow area versus WT control mice. Data are presented as mean \pm SEM.

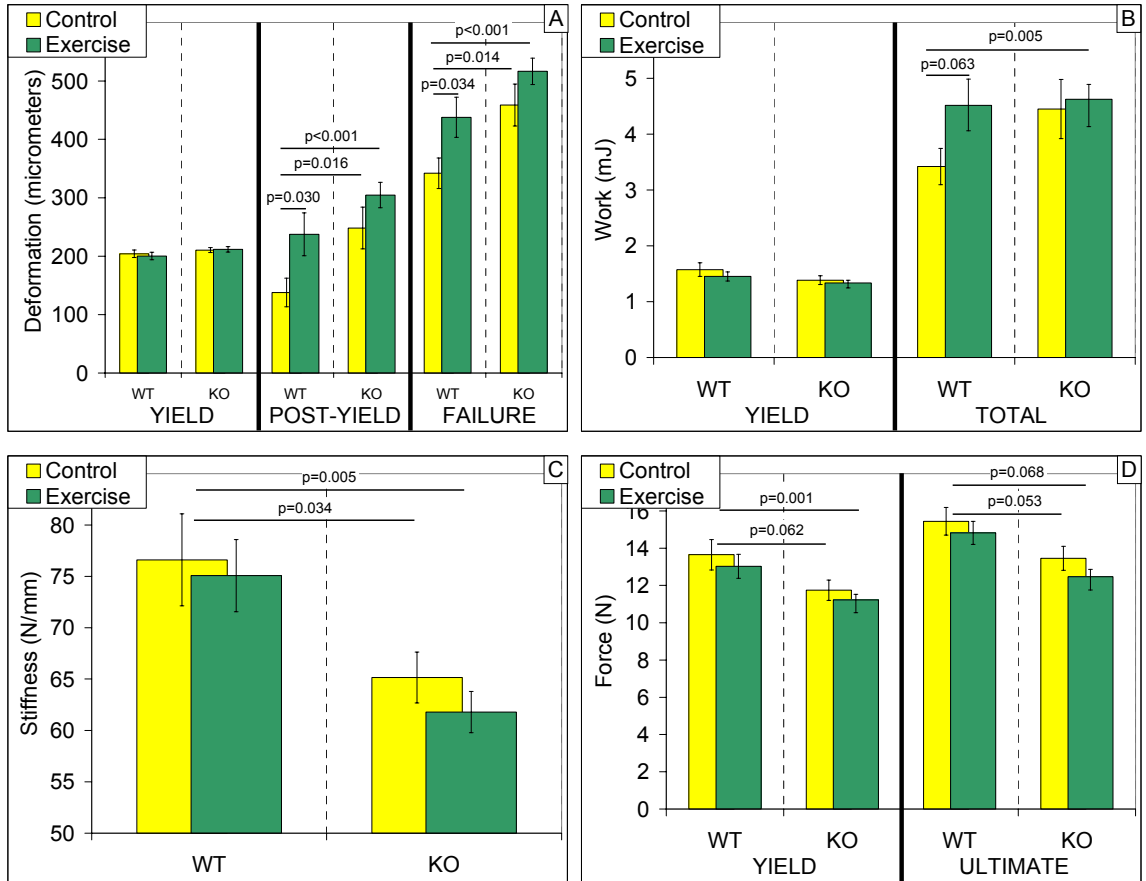


Figure 5.5: Structural-level mechanical properties from wild type (WT) and bgn-deficient (KO) B6;129 tibiae. In WT mice, post-yield deformation and failure deformation increased with exercise versus control mice and total work was marginally greater. No structural-level mechanical properties were altered with exercise in KO mice versus control mice. Post-yield deformation and failure deformation were significantly increased in KO control mice versus WT control mice, while stiffness was significantly decreased, and yield force and ultimate force were marginally decreased. KO exercise mice had significantly increased post-yield deformation, failure deformation and total work versus WT control mice. Stiffness and yield force were significantly decreased and ultimate force was marginally less in KO exercise versus WT control mice. Data are presented as mean \pm SEM.

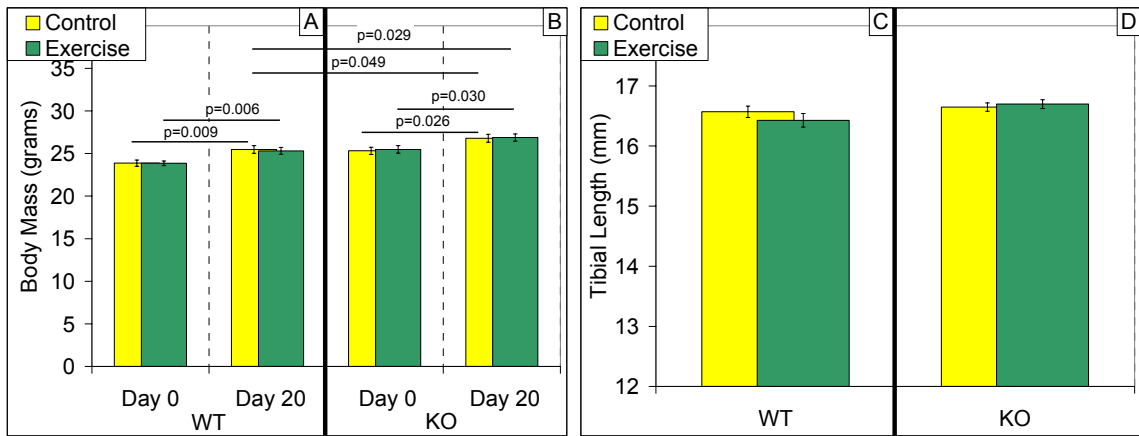


Figure 5.6: Body Mass (A,B) and tibial length (C,D) of wild type (WT) and bgn-deficient (KO) mice from the C3H inbred strain. Mice within each genotype were weight-matched at Day 0 (8 weeks of age). All groups gained weight during the study. Exercise failed to impact body mass in WT mice. At Day 0, C3H KO mice had elevated body mass compared with WT mice which was maintained at Day 20. In C3H KO mice, body mass was unaffected by exercise compared with control mice and therefore, body mass in C3H exercise KO mice remained elevated compared with WT control mice at Day 20. Tibial length was not impacted by exercise in either genotype. There was no difference in tibial length in KO Control or KO Exercise mice versus WT Control. Data are presented as mean \pm SEM.

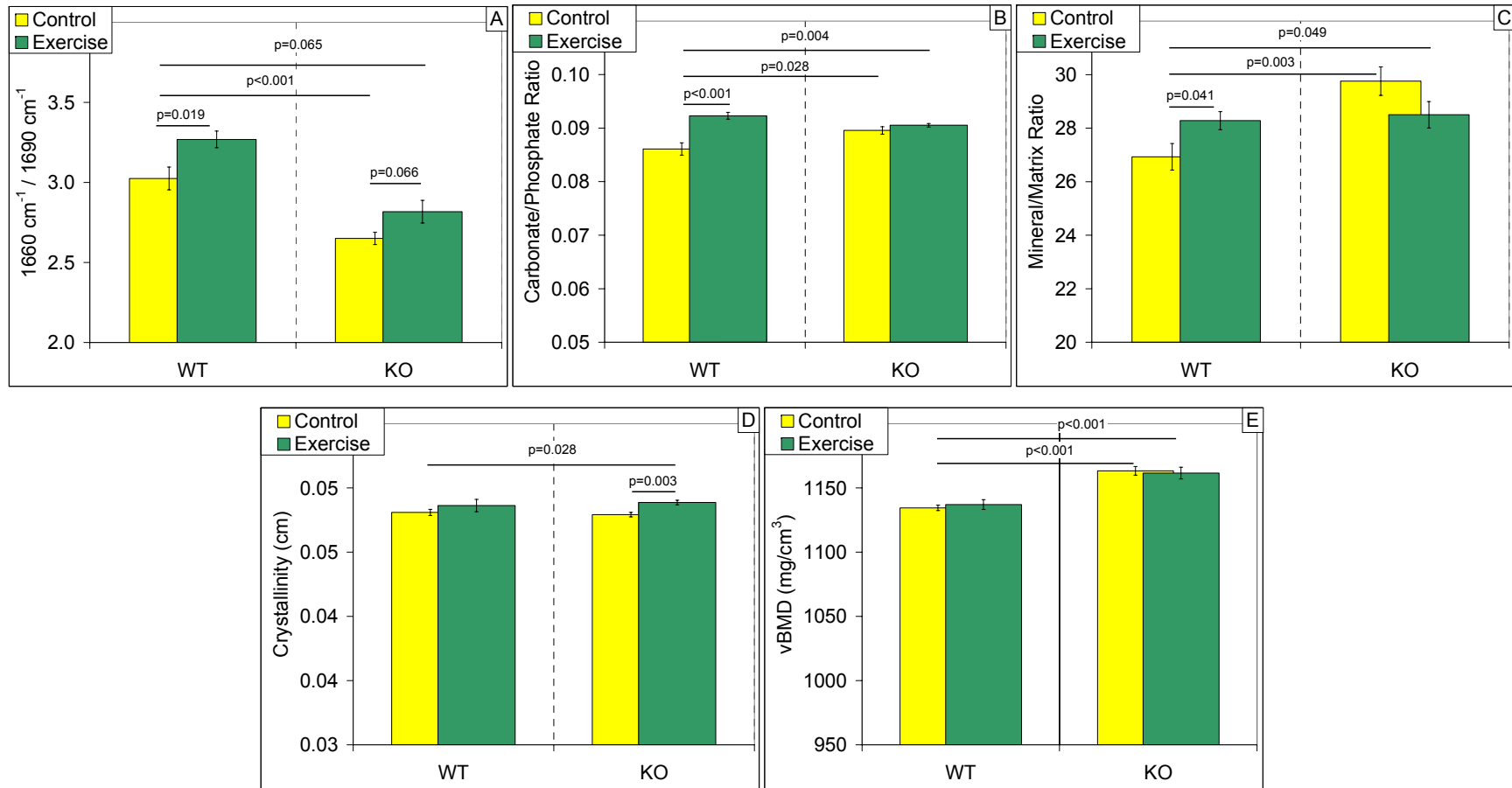


Figure 5.7: Tissue composition and volumetric bone mineral density (vBMD) in the tibial diaphysis of wild type (WT) and *bgn*-deficient (KO) C3H mice. In WT mice, the collagen cross-linking ratio, the carbonate/phosphate ratio and the mineral/matrix ratio were all increased in exercise versus control mice. In KO mice, exercise increased the collagen cross-linking ratio and crystallinity versus control mice. The collagen cross-linking ratio was significantly decreased in KO control mice compared with WT control levels, while the carbonate/phosphate ratio, the mineral/matrix ratio and vBMD were all significantly greater. The carbonate/phosphate ratio, the mineral/matrix ratio, crystallinity and vBMD were all greater in KO exercise mice compared with WT control levels, while the collagen cross-linking ratio was marginally decreased. Data are presented as mean \pm SEM.

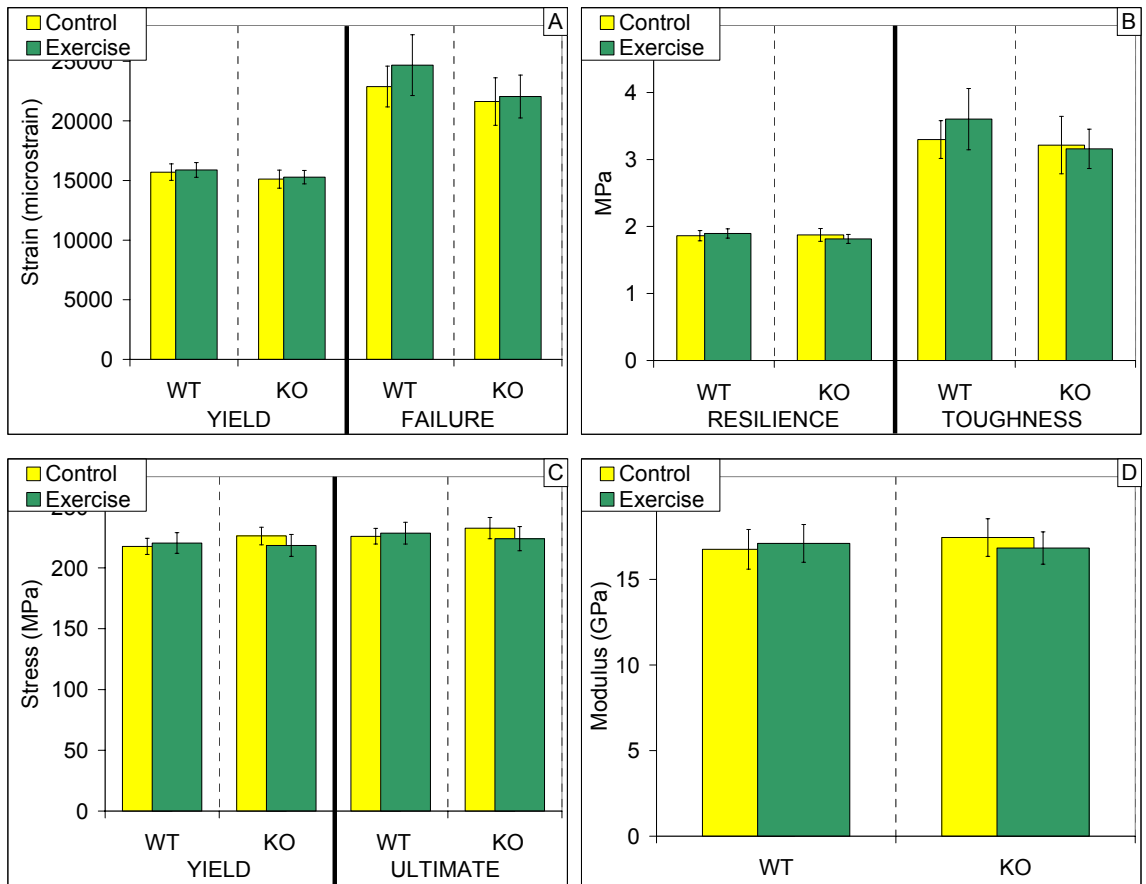


Figure 5.8: Estimated tissue-level mechanical properties from wild type (WT) and bgn-deficient (KO) C3H tibiae. No tissue-level mechanical properties were altered with exercise in either genotype. There were no phenotypic mechanical differences at the tissue level between KO control mice and WT control mice, and no properties were altered with exercise in KO exercise mice versus WT control mice. Data are presented as mean \pm SEM.

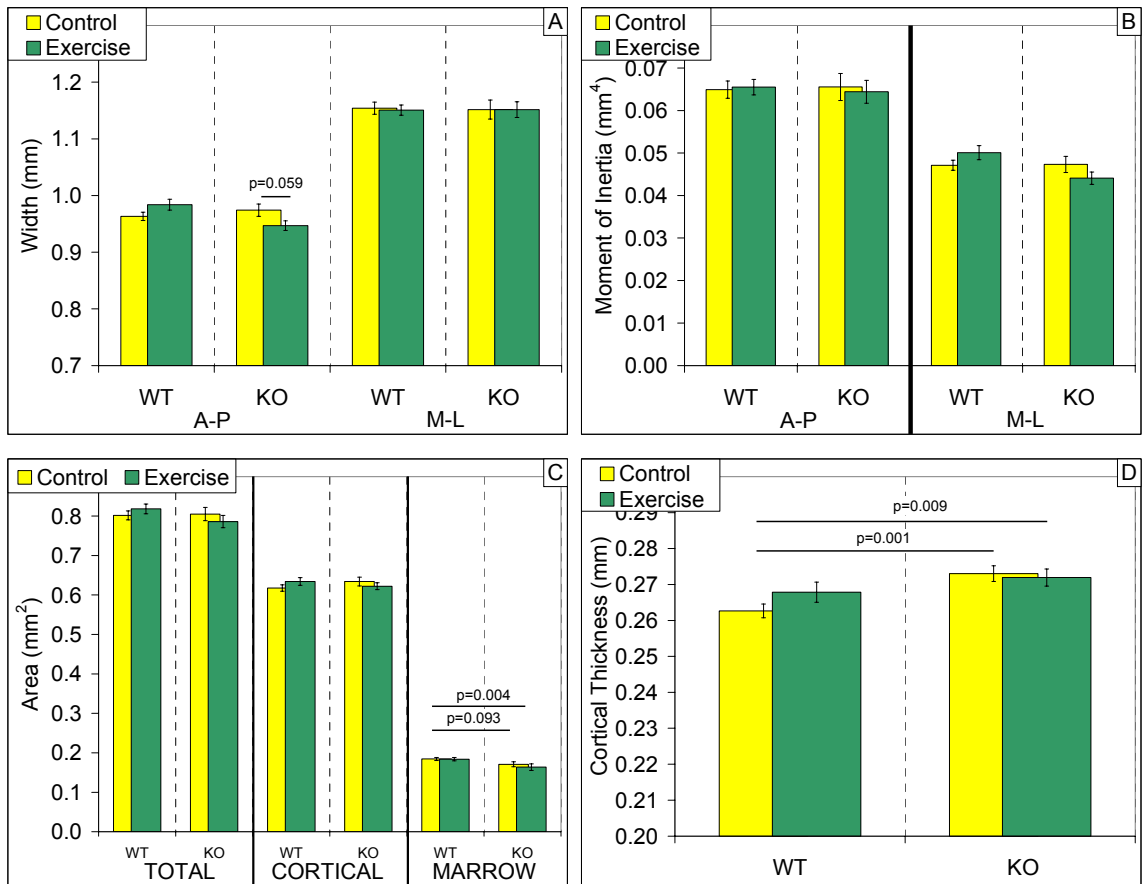


Figure 5.9: Standard site geometric properties of the tibial diaphysis in wild type (WT) and bgn-deficient (KO) C3H mice. In WT mice, no geometric properties were altered in exercise versus control groups. In KO mice, AP width was marginally decreased in exercise versus control mice. Marrow area was marginally less in KO control mice versus WT control mice and cortical thickness was significantly greater. Marrow area was significantly decreased in KO exercise mice versus WT control, and cortical thickness was significantly greater. Data are presented as mean \pm SEM.

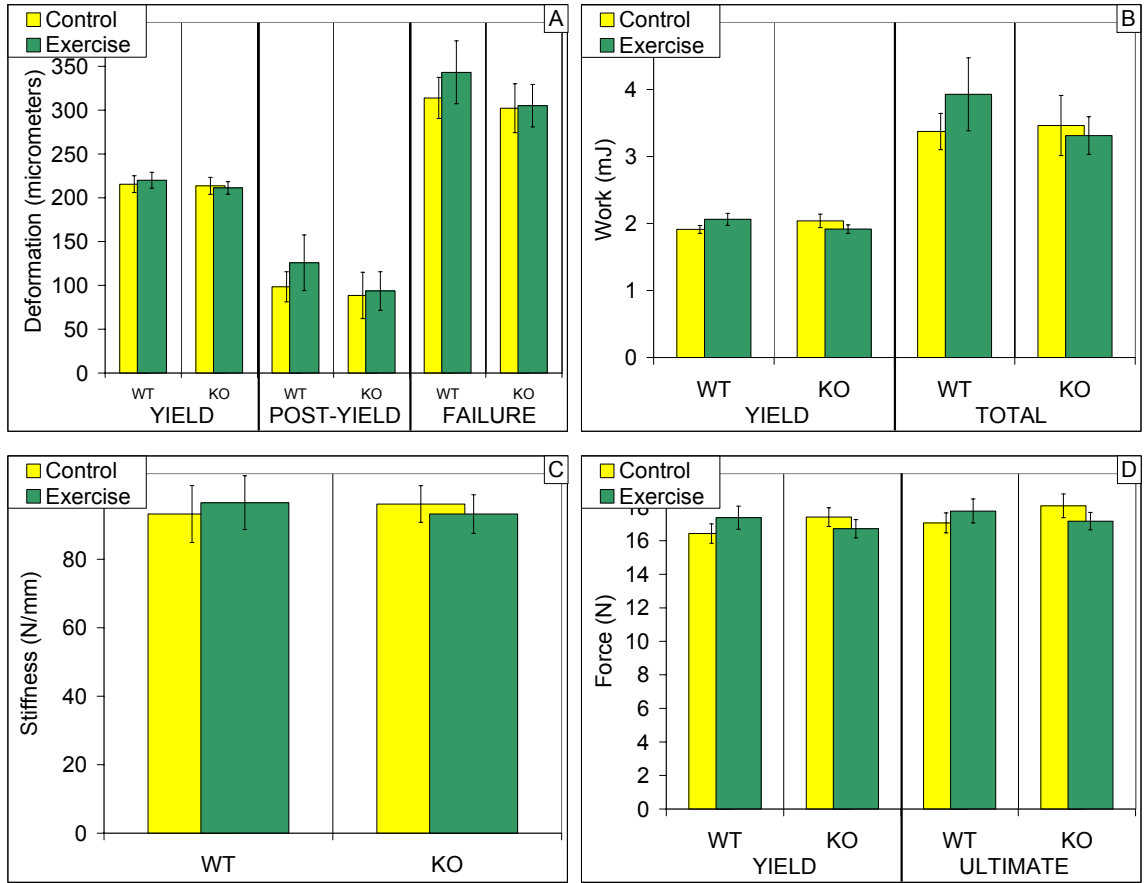


Figure 5.10: Structural-level mechanical properties from wild type (WT) and bgn-deficient (KO) C3H tibiae. No structural-level mechanical properties were altered with exercise in either genotype. There were no phenotypic mechanical differences at the structural level between KO control mice and WT control mice, and no properties were altered with exercise in KO exercise mice versus WT control mice. Data are presented as mean \pm SEM.

References

- (1) Fisher LW, Termine JD, Dejter SW, Jr, Whitson SW, Yanagishita M, Kimura JH, Hascall VC, Kleinman HK, Hassell JR, Nilsson B (1983) Proteoglycans of developing bone. *J.Biol.Chem.* 258:6588-6594
- (2) Bianco P, Fisher LW, Young MF, Termine JD, Robey PG (1990) Expression and localization of the two small proteoglycans biglycan and decorin in developing human skeletal and non-skeletal tissues. *J.Histochem.Cytochem.* 38:1549-1563
- (3) Matsuura T, Duarte WR, Cheng H, Uzawa K, Yamauchi M (2001) Differential expression of decorin and biglycan genes during mouse tooth development. *Matrix Biol.* 20:367-373
- (4) Takagi M, Yamada T, Kamiya N, Kumagai T, Yamaguchi A (1999) Effects of bone morphogenetic protein-2 and transforming growth factor-beta1 on gene expression of decorin and biglycan by cultured osteoblastic cells. *Histochem.J.* 31:403-409
- (5) Chen WB, Lenschow W, Tiede K, Fischer JW, Kalthoff H, Ungefroren H (2002) Smad4/DPC4-dependent regulation of biglycan gene expression by transforming growth factor-beta in pancreatic tumor cells. *J.Biol.Chem.* 277:36118-36128
- (6) Chen XD, Fisher LW, Robey PG, Young MF (2004) The small leucine-rich proteoglycan biglycan modulates BMP-4-induced osteoblast differentiation. *FASEB J.* 18:948-958
- (7) Bi Y, Stuelten CH, Kilts T, Wadhwa S, Iozzo RV, Robey PG, Chen XD, Young MF (2005) Extracellular matrix proteoglycans control the fate of bone marrow stromal cells. *J.Biol.Chem.* 280:30481-30489
- (8) Corsi A, Xu T, Chen XD, Boyde A, Liang J, Mankani M, Sommer B, Iozzo RV, Eichstetter I, Robey PG, Bianco P, Young MF (2002) Phenotypic effects of biglycan deficiency are linked to collagen fibril abnormalities, are synergized by decorin deficiency, and mimic Ehlers-Danlos-like changes in bone and other connective tissues. *J.Bone Miner.Res.* 17:1180-1189
- (9) Sugars RV, Milan AM, Brown JO, Waddington RJ, Hall RC, Embery G (2003) Molecular interaction of recombinant decorin and biglycan with type I collagen influences crystal growth. *Connect.Tissue Res.* 44 Suppl 1:189-195
- (10) Chen XD, Shi S, Xu T, Robey PG, Young MF (2002) Age-related osteoporosis in biglycan-deficient mice is related to defects in bone marrow stromal cells. *J.Bone Miner.Res.* 17:331-340

- (11) Chen XD, Allen MR, Bloomfield S, Xu T, Young M (2003) Biglycan-deficient mice have delayed osteogenesis after marrow ablation. *Calcif.Tissue Int.* 72:577-582
- (12) Wallace JM, Rajachar RM, Chen XD, Shi S, Allen MR, Bloomfield SA, Les CM, Robey PG, Young MF, Kohn DH (2006) The mechanical phenotype of biglycan-deficient mice is bone- and gender-specific. *Bone* 39:106-116
- (13) Wallace JM (2007) Investigating the Inbred Strain-Specific Response to Biglycan-Deficiency and Exercise: A Study in Genetically-Medicated Skeletal Adaptation. PhD Dissertation.
- (14) Ameye L, Aria D, Jepsen K, Oldberg A, Xu T, Young MF (2002) Abnormal collagen fibrils in tendons of biglycan/fibromodulin-deficient mice leads to gait impairment, ectopic ossification, and osteoarthritis. *The FASEB Journal* 16:673-680
- (15) Boskey AL, Young MF, Kilts T, Verdellis K (2005) Variation in mineral properties in normal and mutant bones and teeth. *Cells Tissues Organs* 181:144-153
- (16) Young MF, Bi Y, Ameye L, Chen XD (2002) Biglycan knockout mice: new models for musculoskeletal diseases. *Glycoconj.J.* 19:257-262
- (17) Carter DR, Van Der Meulen MC, Beaupre GS (1996) Mechanical factors in bone growth and development. *Bone* 18:5S-10S
- (18) Sahar ND, Kohn DH, Golcuk K, Morris MD Effects of Exercise on Bone Quality As Shown By Raman Microspectroscopy, paper No. 1619. 2006 Annual Meeting of the Orthopaedic Society
- (19) Wallace JM, Rajachar RM, Allen MR, Bloomfield SA, Robey PG, Young MF, Kohn DH (2007) Exercise-Induced Changes in the Cortical Bone of Growing Mice are Bone- and Gender-Specific. *Bone* 40:1120-1127
- (20) Boskey AL, Wright TM, Blank RD (1999) Collagen and bone strength. *J.Bone Miner.Res.* 14:330-335
- (21) Wang X, Shen X, Li X, Agrawal CM (2002) Age-related changes in the collagen network and toughness of bone. *Bone* 31:1-7
- (22) Garnero P, Borel O, Gineyts E, Duboeuf F, Solberg H, Bouxsein ML, Christiansen C, Delmas PD (2006) Extracellular post-translational modifications of collagen are major determinants of biomechanical properties of fetal bovine cortical bone. *Bone* 38:300-309

- (23) Viguet-Carrin S, Garnero P, Delmas PD (2006) The role of collagen in bone strength. *Osteoporos.Int.* 17:319-336
- (24) Rubin C, Turner AS, Bain S, Mallinckrodt C, McLeod K (2001) Anabolism. Low mechanical signals strengthen long bones. *Nature* 412:603-604
- (25) Rubin C, Recker R, Cullen D, Ryaby J, McCabe J, McLeod K (2004) Prevention of postmenopausal bone loss by a low-magnitude, high-frequency mechanical stimuli: a clinical trial assessing compliance, efficacy, and safety. *J.Bone Miner.Res.* 19:343-351
- (26) Ward K, Alsop C, Caulton J, Rubin C, Adams J, Mughal Z (2004) Low magnitude mechanical loading is osteogenic in children with disabling conditions. *J.Bone Miner.Res.* 19:360-369
- (27) Akhter MP, Cullen DM, Pedersen EA, Kimmel DB, Recker RR (1998) Bone response to in vivo mechanical loading in two breeds of mice. *Calcif.Tissue Int.* 63:442-449
- (28) Kodama Y, Dimai HP, Wergedal J, Sheng M, Malpe R, Kutilek S, Beamer W, Donahue LR, Rosen C, Baylink DJ, Farley J (1999) Cortical tibial bone volume in two strains of mice: effects of sciatic neurectomy and genetic regulation of bone response to mechanical loading. *Bone* 25:183-190
- (29) Kodama Y, Umemura Y, Nagasawa S, Beamer WG, Donahue LR, Rosen CR, Baylink DJ, Farley JR (2000) Exercise and mechanical loading increase periosteal bone formation and whole bone strength in C57BL/6J mice but not in C3H/HeJ mice. *Calcif.Tissue Int.* 66:298-306
- (30) Amblard D, Lafage-Proust MH, Laib A, Thomas T, Ruegsegger P, Alexandre C, Vico L (2003) Tail suspension induces bone loss in skeletally mature mice in the C57BL/6J strain but not in the C3H/HeJ strain. *J.Bone Miner.Res.* 18:561-569
- (31) Marusic A, Katavic V, Grcevic D, Lukic IK (1999) Genetic variability of new bone induction in mice. *Bone* 25:25-32
- (32) Li X, Gu W, Masinde G, Hamilton-Ulland M, Rundle CH, Mohan S, Baylink DJ (2001) Genetic variation in bone-regenerative capacity among inbred strains of mice. *Bone* 29:134-140
- (33) Hadi N, Price C, Nasser P, Morgan E, Einhorn TA, Gerstenfeld LC, Jepsen KJ Genetic Variation In The Regain of Bone Strength During Fracture Healing, Paper No. 0225. 2007 Annual Meeting of the Orthopaedic Society
- (34) Xu T, Bianco P, Fisher LW, Longenecker G, Smith E, Goldstein S, Bonadio J, Boskey A, Heegaard AM, Sommer B, Satomura K, Dominguez P, Zhao C,

- Kulkarni AB, Robey PG, Young MF (1998) Targeted disruption of the biglycan gene leads to an osteoporosis-like phenotype in mice. *Nat.Genet.* 20:78-82
- (35) Nielsen KL, Allen MR, Bloomfield SA, Andersen TL, Chen XD, Poulsen HS, Young MF, Heegaard AM (2003) Biglycan deficiency interferes with ovariectomy-induced bone loss. *J.Bone Miner.Res.* 18:2152-2158
- (36) Wergedal JE, Sheng MH, Ackert-Bicknell CL, Beamer WG, Baylink DJ (2005) Genetic variation in femur extrinsic strength in 29 different inbred strains of mice is dependent on variations in femur cross-sectional geometry and bone density. *Bone* 36:111-122
- (37) Akhter MP, Iwaniec UT, Covey MA, Cullen DM, Kimmel DB, Recker RR (2000) Genetic variations in bone density, histomorphometry, and strength in mice. *Calcif.Tissue Int.* 67:337-344
- (38) Kuhn JL, Goldstein SA, Feldkamp LA, Goulet RW, Jasion G (1990) Evaluation of a microcomputed tomography system to study trabecular bone structure. *J.Orthop.Res.* 8:833-842
- (39) Turner CH, Burr DB (1993) Basic Biomechanical Measurements of Bone: A Tutorial. *Bone* 14:595-607
- (40) Carden A, Rajachar RM, Morris MD, Kohn DH (2003) Ultrastructural changes accompanying the mechanical deformation of bone tissue: a Raman imaging study. *Calcif.Tissue Int.* 72:166-175
- (41) Pezzuti JA, Morris MD, Bonadio JF, Goldstein SA (2003) Hyperspectral Raman imaging of bone growth and regrowth chemistry. *Proceedings of SPIE* 3261:270
- (42) Timlin J, Carden A, Morris M (1999) Chemical Microstructure of Cortical Bone Probed by Raman Transects. *Appl.Spectrosc.* 53:1429-1435
- (43) Timlin JA, Carden A, Morris MD, Rajachar RM, Kohn DH (2000) Raman spectroscopic imaging markers for fatigue-related microdamage in bovine bone. *Anal.Chem.* 72:2229-2236
- (44) Paschalis EP, Verdelis K, Doty SB, Boskey AL, Mendelsohn R, Yamauchi M (2001) Spectroscopic characterization of collagen cross-links in bone. *J.Bone Miner.Res.* 16:1821-1828
- (45) Kesavan C, Mohan S, Oberholtzer S, Wergedal JE, Baylink DJ (2005) Mechanical loading-induced gene expression and BMD changes are different in two inbred mouse strains. *J.Appl.Physiol.* 99:1951-1957

- (46) Robling AG, Hinant FM, Burr DB, Turner CH (2002) Shorter, more frequent mechanical loading sessions enhance bone mass. *Med.Sci.Sports Exerc.* 34:196-202
- (47) Adami S, Gatti D, Braga V, Bianchini D, Rossini M (1999) Site-specific effects of strength training on bone structure and geometry of ultradistal radius in postmenopausal women. *J.Bone Miner.Res.* 14:120-124
- (48) Vaidya S, Karunakaran C, Pande B, Gupta N, Iyer R, Karweer S (1997) Pressure-induced crystalline to amorphous transition in hydroxylapatite. *J.Mater.Sci.* 32:3213-3217
- (49) Landis WJ (1995) The strength of a calcified tissue depends in part on the molecular structure and organization of its constituent mineral crystals in their organic matrix. *Bone* 16:533-544
- (50) Weiner S, Traub W (1992) Bone structure: from angstroms to microns. *FASEB J.* 6:879-885
- (51) Landis WJ (1996) Mineral characterization in calcifying tissues: atomic, molecular and macromolecular perspectives. *Connect.Tissue Res.* 34:239-246
- (52) Yeh JK, Aloia JF, Yasumura S (1989) Effect of physical activity on calcium and phosphorus metabolism in the rat. *Am.J.Physiol.* 256:E1-6
- (53) Yeh JK, Aloia JF (1990) Effect of physical activity on calciotropic hormones and calcium balance in rats. *Am.J.Physiol.* 258:E263-8
- (54) Duncan RL, Turner CH (1995) Mechanotransduction and the functional response of bone to mechanical strain. *Calcif.Tissue Int.* 57:344-358
- (55) Burger EH, Klein-Nulend J (1999) Mechanotransduction in bone--role of the lacuno-canalicular network. *FASEB J.* 13 Suppl:S101-12
- (56) Mullender M, El Haj AJ, Yang Y, van Duin MA, Burger EH, Klein-Nulend J (2004) Mechanotransduction of bone cells in vitro: mechanobiology of bone tissue. *Med.Biol.Eng.Comput.* 42:14-21
- (57) Amblard D, Lafage-Proust MH, Chamson A, Rattner A, Collet P, Alexandre C, Vico L (2003) Lower bone cellular activities in male and female mature C3H/HeJ mice are associated with higher bone mass and different pyridinium crosslink profiles compared to C57BL/6J mice. *J.Bone Miner.Metab.* 21:377-387
- (58) Rucker RB, Kosonen T, Clegg MS, Mitchell AE, Rucker BR, Uriu-Hare JY, Keen CL (1998) Copper, lysyl oxidase, and extracellular matrix protein cross-linking. *Am.J.Clin.Nutr.* 67:996S-1002S

- (59) Saito M, Soshi S, Fujii K (2003) Effect of hyper- and microgravity on collagen post-translational controls of MC3T3-E1 osteoblasts. *J.Bone Miner.Res.* 18:1695-1705
- (60) Hong HH, Pischon N, Santana RB, Palamakumbura AH, Chase HB, Gantz D, Guo Y, Uzel MI, Ma D, Trackman PC (2004) A role for lysyl oxidase regulation in the control of normal collagen deposition in differentiating osteoblast cultures. *J.Cell.Physiol.* 200:53-62
- (61) Wang Y, Botvinick EL, Zhao Y, Berns MW, Usami S, Tsien RY, Chien S (2005) Visualizing the mechanical activation of Src. *Nature* 434:1040-1045
- (62) Currey JD (1988) The effect of porosity and mineral content on the Young's modulus of elasticity of compact bone. *J.Biomech.* 21:131-139

CHAPTER 6

CONCLUSIONS

The studies in this dissertation were undertaken to investigate how biglycan-deficiency impacts the bones of two inbred mouse strains at multiple levels of the bone hierarchy. Inbred strain-specificity was also investigated in response to mechanical loading in the form of running. Finally, in an attempt to compensate for deficiencies caused by the absence of biglycan, exercise was superimposed on the simulated disease state. Taken as a whole, this dissertation establishes for the first time that an inbred strain-specific response to a genetic deletion exists, further develops the roles that biglycan plays in the chemical and physical makeup of bone and links these roles with bone mechanical integrity. The research presented in this dissertation also demonstrates that mechanical loading can modulate the quality of bone tissue through changes in pre-existing tissue without the addition of new bone and in doing so, can compensate for mechanical deficiencies caused by a gene deletion. These studies provide new insights into inbred strain research which has important implications to the interpretation of experimental investigations into the effects of genetic deficiencies and mechanical loading on skeletal structure and function. Exercise was shown to elicit alterations in the bone ultrastructure which influenced the quality and mechanical integrity of the bone tissue without changes in bone geometry, suggesting that mechanical stimulation may be a viable strategy to combat deficiencies in tissue quality that are associated with many diseases of bone.

To lend some direction to these studies, preliminary investigations were first performed in a single inbred strain (Chapters 2 and 3). These studies provided insight into how biglycan-deficiency and exercise impact the bones of growing mice bred on the C57BL6/129 (B6;129) background strain. Bgn-deficiency preferentially impacted cortical bone in the tibiae of 11 week old male mice (Chapter 2). Increased vBMD in the tibiae of bgn-deficient (KO) mice (Figure 2.4) demonstrated for the first time that bgn

plays a role in the regulation of mineralization *in vivo*. Increased vBMD was associated with decreased tissue-level yield strength (Figure 2.2). Exercise most-strongly influenced tibiae of 11 week old male mice as well (Chapter 3), where post-yield behavior at the structural (Figure 3.4) and tissue levels (Figure 3.5) was increased. Since exercise was superimposed upon growth, tissue-level mechanical changes were the result of the presence of new tissue and alterations in the quality of pre-existing tissue. Because the changes were predominantly in post-yield behavior, this suggests that exercise was influencing the organic component of the bone tissue. Since many diseases influence the mechanical integrity of bone through alterations in tissue quality (versus changes in tissue quantity), the results of Chapter 3 suggest that mechanical stimulation may be practical way to prevent and treat low bone mass and extracellular matrix (ECM) deficiencies [1-3].

***In Vivo* Influences of Biglycan on Collagen and Mineral (Chapter 4)**

Since bgn-deficiency and exercise both affected the same bone and gender in mice, the next round of studies was narrowed down to a single bone and a single gender. Experiments were designed to investigate the effects of bgn-deficiency in two inbred strains with known differences in bone mass, mineral density, mechanical properties, cellular activity and response to changes in their mechanical environment (Chapter 4). Bgn-deficiency impacts the bone matrix through negative regulation of osteoblast number and function, resulting in alteration in ECM structure and ultimately decreased mechanical integrity. Because C3H osteoblasts are highly active and robust versus osteoblasts from other inbred strains, and the bones of C3H mice are unresponsive to other insults, it was hypothesized that compared with the response in B6;129 mice, C3H mice would be relatively more resistant to changes in ECM production and mineralization associated with bgn-deficiency. Therefore, the negative mechanical effects of bgn-deficiency would be minimized in C3H mice relative to the effects in B6;129 mice.

Inbred strain specificity was investigated by statistically comparing the relative effects of the gene deletion in B6;129 mice (KO/mean WT values for each KO sample) with the effects in C3H mice (KO/mean WT value) at each age. As hypothesized, the

KO phenotype was more significant in B6;129 versus C3H mice at 8 weeks of age in terms of reduced cross-sectional geometry and structural mechanical integrity, resulting in an inbred strain-specific response to this genetic change. The relationship between inbred strain and bgn-deficient phenotype became more compelling by 11 weeks of age, impacting the B6;129 mice more than the C3H mice at all levels of the bone hierarchy that were investigated. Inbred strain-specific differences existed in body mass (increased ratio in C3H mice), tibial length (decreased ratio in B6;129 mice), mRNA expression (ratio increased in B6;129 for all genes), tissue composition (changes in KO mice from both inbred strains), tissue strength (decreased ratio in B6;129 mice for both yield and ultimate stress), cross-sectional geometric properties (deficiencies in multiple properties in B6;129 KO), structural strength (decreased ratio in B6;129 mice for yield and ultimate force), stiffness (decreased ratio in B6;129 mice) and ductility (increased ratio in B6;129 mice for post-yield and failure deformation).

KO mice from both inbred strains had a decrease in the collagen cross-linking ratio versus WT mice (Figure 4.2C), implying a change in the secondary structure of collagen most often associated with a decrease in the number of mature cross-links relative to immature cross-link levels [4]. KO mice from both inbred strains also had significantly greater vBMD (Figure 4.2A) and mineral/matrix ratio (Figure 4.2B) versus WT mice. However, B6;129 KO mice had significantly increased crystallinity (Figure 4.2D) while C3H KO mice had significantly increased carbonate/phosphate ratio (Figure 4.2E) versus WT mice, indicating that genetic differences between the two inbred strains are governing changes in the nature of the mineral in response to this gene deletion.

Altered collagen and mineral in KO bones suggest two scenarios to explain compositional differences in the bgn-deficient mice. In the first, bgn-deficiency causes direct changes in the collagen matrix, as supported by a decreased collagen cross-linking ratio in KO mice versus WT mice (Figure 4.2C), as well as changes in the expression of procollagen mRNAs (Figure 4.6). Since the collagen matrix is a template for mineralization, the mineral that forms on an altered matrix can be changed in both chemical composition and density [5], as supported by increased crystallinity in B6;129 KO mice versus WT mice (Figure 4.2D) and increased carbonate/phosphate ratio in C3H KO mice versus WT mice (Figure 4.2E). Mineral is thought to nucleate in the gap zones

of collagen, and SLRPs are known to localize within these zones [6]. It is therefore possible that mineral nucleation sites that are normally blocked by bgn are now exposed and more mineral can form, as supported by increased vBMD (Figure 4.2A) and mineral/matrix ratio (Figure 4.2B). A second scenario has the lack of bgn directly impacting mineralization. While bgn might facilitate the initial nucleation of mineral, crystal growth in preferential directions may be blocked by the presence of bgn near a specific crystal face [7-9], meaning that in the absence of bgn, crystals can grow to larger than normal dimensions. Unrestricted crystal growth along specific planes could explain the increase in vBMD (Figure 4.2A). As mineral beyond normal levels fills the spaces within collagen fibrils and the fibrils are distorted [10, 11], the dissociation/rupture of some cross-links may occur. The reason for inbred strain-specific differences in tissue composition may be due to a different combination of these two mechanisms due to genetic differences between the two inbred strains.

Structural-level mechanical phenotypes in the B6;129 and C3H KO mice were significantly different at both 8 and 11 weeks of age (Figure 4.5), due mostly to the inability of B6;129 KO mice to maintain WT cross-sectional size (Figure 4.4). At 8 weeks, C3H KO mice had significantly reduced cross-sectional size versus WT mice, but tissue level strength was elevated and brought structural-level strength up to WT levels. By 11 weeks, phenotypic geometric deficiencies in C3H KO mice were no longer present and, therefore, structural-level mechanical deficiencies were absent as well. This pattern of temporally-delayed bone formation in C3H KO mice has been shown in a study of marrow ablation [12]. In the B6;129 KO mice, deficiencies in cross-sectional size were present at 8 weeks of age and worsened by 11 weeks of age. Therefore, structural strength was decreased versus WT mice at both ages, indicating that the KO phenotype in B6;129 mice is driven by alterations in both tissue quality and tissue quantity.

Data from Chapter 4 demonstrate that the bgn-deficient phenotype was inbred strain-specific at 8 weeks of age, where decreased tibial length, smaller cross-sectional size and decreased structural-level stiffness and strength were present in the B6;129 KO mice. As hypothesized, properties in C3H KO mice (with the exception of measures of tissue composition) were indistinguishable from WT levels by 11 weeks. However, the relationship between inbred strain and bgn-deficient phenotype became more compelling

by 11 weeks of age due to differences in the B6;129 KO versus WT mice that spanned all levels of the bone hierarchy that were investigated. To the best of our knowledge, this study marks the first time an inbred strain-specific difference has been demonstrated in response to a genetic deletion in mice, and suggests that in the interpretation of data from genetic deletion models, these genetically-regulated responses need to be considered.

Mechanical Effects on the Bone Ultrastructure (Chapter 5)

The second major thrust of this dissertation was to develop an understanding of how mechanical loading induced by exercise changes the composition and mechanical integrity of bone and to investigate how the phenotype of *bgn*-deficient mice may be changed by mechanical stimulation. It was hypothesized that the bones from B6;129 mice (both wild type and *bgn*-deficient) would be more responsive to exercise than the bones from C3H mice, where increased formation and altered matrix composition would increase the mechanical strength of the bone in the B6;129 inbred strain. It was further hypothesized that exercise-induced bone formation and altered ECM composition would compensate for deficiencies in tissue strength and bone size, and ultimately structural strength, in *bgn*-deficient B6;129 mice. Because of the lack of a *bgn*-deficient phenotype in C3H mice and the hypothesized inability of C3H KO mice to respond to mechanical loading, it was further hypothesized that the *bgn*-deficient C3H phenotype would not be affected by running.

The form of exercise used in these studies was involuntary running, a physiologic activity which modulates the bone ECM in such a way as to increase post-yield behavior in the tibiae of B6;129 WT male mice (Chapter 3). Running failed to change the size or shape of the bones of WT or KO mice from either the B6;129 or C3H inbred strain (Figure 5.4 and Figure 5.9) and instead exerted its influence by altering the composition of pre-existing tissue (Figure 5.2 and Figure 5.7). Exercise consistently increased levels of mature collagen cross-links in all groups (both WT and KO mice from both inbred strains; Figure 5.2A and Figure 5.7A). Mechanical influences on the mineral phase of bone were dependent on inbred strain and genotype. However, either the carbonate/phosphate ratio (B6;129 KO mice, Figure 5.2B), the mineral/matrix ratio (C3H WT mice, Figure 5.7C), or the crystallinity of the mineral (C3H KO mice, Figure 5.7D)

were increased with exercise, consistent with other studies which have demonstrated increased BMD with loading and exercise [13, 14].

The bones of WT B6;129 mice were more responsive to mechanical stimulation than the bones from WT C3H mice. Exercise marginally increased failure strain and total toughness in B6;129 WT mice versus control mice (Figure 5.3), while no mechanical properties were influenced in C3H WT mice. Due to a lack of changes in bone size with exercise in both the B6;129 WT mice and C3H WT mice, mechanical changes that occurred at the tissue level directly impacted structural-level properties, as indicated by increased post-yield behavior in the B6;129 mice and no changes in the C3H mice.

As hypothesized, exercise in the B6;129 KO mice had a greater impact on the bgn-deficient phenotype in B6;129 mice compared with C3H mice. Exercise in B6;129 KO mice increased the mineral/matrix ratio and the collagen cross-linking ratio versus control mice (Figure 5.2). Tissue-level mechanical properties, cross-sectional size and structural-level mechanical properties were not affected by exercise in the B6;129 KO mice compared with control mice. However, depending on the level of hierarchy investigated, the modest changes with exercise in the B6;129 KO mice versus KO control mice were still sufficient to significantly impact the bgn-deficient phenotype of this inbred strain versus WT control mice. Exercise had mostly positive influences on mechanical behavior at the tissue-level (Figure 5.3). Phenotypic deficiencies (ultimate stress and resilience in KO control versus WT control mice) were compensated for and modulus was now greater in KO exercise mice compared with WT control levels. Failure strain was marginally greater in the KO control mice compared with WT control mice at 11 weeks of age, and exercise in the KO mice made this relationship significant while also increasing toughness. Increased post-yield behavior at the tissue-level directly impacted structural-level properties by maintaining phenotypically increased post-yield and failure deformation and increasing total work (Figure 5.5). However, since exercise failed to induce a bone formation response in the KO bones, geometric deficiencies due to bgn-deficiency were still present (Figure 5.4). Because of the dependence of structural level strength and stiffness on both bone size/shape and tissue-level behavior, decreased structural strength and stiffness persisted (Figure 5.5). Results in the B6;129 KO mice

suggest that exercise was able to compensate for tissue-level deficiencies caused by bgn-deficiency through compositional alterations.

In summary, data from the exercise studies clearly demonstrate that exercise can elicit alterations in the ECM of pre-existing bone which influence the quality and mechanical integrity of the tissue without changes in bone geometry. The ability to impact pre-existing tissue suggests that mechanical stimulation may be a potent therapy against deficiencies in tissue quality that are associated with many diseases of bone, particularly in adults. This study also demonstrates an inbred strain-specific response to exercise in both wild type and bgn-deficient mice, indicating that the response to exercise is genetically regulated.

Broader Implications of This Dissertation

The mouse gene disruption model remains one of the most important tools for uncovering the roles that different genes play *in vivo*. By deleting a mouse's ability to produce a particular gene (and ultimately the protein for which that gene codes), and investigating changes that occur in tissue structure and function across multiple levels of hierarchy, a greater understanding of how that protein functions can be ascertained. However, broad conclusions on protein function are often drawn from limited phenotypic characterizations. The studies contained in this dissertation have clearly illustrated that it is the responsibility of both the investigator and the reader to not over-interpret the data acquired from these studies. In order to be complete and accurate, gene disruption investigations need to take into account many variables that can limit the general applicability of these results including investigating both genders, looking at multiple bone locations both within and between bones and using multiple age groups. Perhaps most importantly, at least two different inbred strains should be used to ensure that the phenotype is not being driven or masked by genetic effects.

Recent studies have focused on the roles that bgn plays in regulating the differentiation and function of osteoblasts *in vitro* [15-20], while the studies contained in this dissertation clearly demonstrate roles of biglycan in regulating the organic and inorganic components of bone tissue *in vivo*. It is the combination of regulating osteoblastic differentiation and function as well as regulating the composition and

architecture of the bone ECM which defines the importance of biglycan in bone. Mice from different inbred strains have different inherent abilities to respond to or compensate for bgn's absence (e.g. the ability of C3H KO mice to maintain WT bone size by 11 weeks of age when the B6;129 KO bones are significantly smaller than WT), resulting in the inbred strain-specific bgn-deficient phenotype noted in this study.

Wolff's Law states that "every change in the form and function of a bone, or in its function alone, is followed by certain definite changes in its internal architecture and equally definite secondary alteration in its external confirmation, in accordance with mathematical laws [21]," implying that bone structure can and will adapt in response to changes in the mechanical environment. The form of mechanical stimulation used in the current study failed to elicit changes in the architecture of the cortical bone. However, exercise did impact the quality of the tissue by altering tissue composition. Although regressions had low correlation coefficients, mechanical behavior of the tissue was altered along with these changes in tissue composition.

This idea that compositional changes in pre-existing tissues can impact mechanical behavior is exciting. Many researchers and clinicians suggest that the best way to combat age-related bone diseases is to boost peak bone mass to its highest possible level early in life [22, 23], but this is not a practical way to treat a fifty-year-old patient. In the past several years, the idea that tissue quality is as important as tissue quantity has gained acceptance. Therefore, if mechanical stimulation can beneficially alter the quality of tissue that is already present, this may represent a valid and potentially powerful anabolic strategy to treat bone diseases in adults. Used in combination with anti-resorptive therapies, mechanical stimulation may represent a new frontier in the treatment of osteoporosis. Future studies need to be designed to investigate how mechanical loading directly influences tissue composition in adults, and what form of loading is most beneficial and most practical.

Future Studies

The studies contained in this dissertation answered many questions. However, many new questions were uncovered. In terms of biglycan deficiency and exercise, the most compelling questions are 1) what are the differences between B6;129 and C3H mice

that result in inbred strain-specific differences in response to bgn-deficiency, 2) why do compositional changes in response to bgn-deficiency and exercise differ between inbred strains, 3) what part of the response to exercise is cellular and what part is physicochemical and 4) what is the link between altered tissue composition and altered mechanical behavior. Both mineral composition and the ratio of mature to immature collagen cross links clearly change in response to both bgn-deficiency and exercise, and these changes are inbred strain-specific. However, it is unclear if compositional alterations are independent of one another or how these compositional changes directly impact mechanical behavior.

There are clear indications from mRNA expression and tissue compositional measures that the cellular response to bgn-deficiency is different between the 2 inbred strains studied. Extending studies of inbred strain-specificity in response to bgn-deficiency to the cellular level is an important next step in understanding what cellular mechanisms might be driving the differences that are seen at higher levels of the bone hierarchy. This could be performed *in vivo* and *in vitro*. *In vivo*, standard static histomorphometry could be performed on undecalcified sections to investigate osteoblasts and osteoclasts on the cortical surfaces. A lack of one type of cell, a change in cellular morphology or differences in cellular activity would help elucidate which cell type bgn-deficiency was primarily affecting, and how this effect of bgn-deficiency differed with background strain of the mice. qRT-PCR was used in the current studies to investigate genes associated with osteoblast differentiation and matrix production. By extending these molecular investigations to genes associated with resorption, the mechanisms governing the response to bgn-deficiency and inbred strain specificity in this response could be further defined. By looking into the numbers of osteocytes that are present in the cortical bone, it would be possible to extrapolate whether a deficiency in the ability of osteoblast to fully differentiate exists. To date, *in vitro* studies of bgn-deficiency have been inconsistent, using cells from each gender, multiple bone locations, different ages of mice and both inbred strains. Future studies could be standardized in an attempt to uncover genetic differences between the cells of the different inbred strains.

Other questions concerning biglycan deficiency include the choice of investigating cortical bone alone. Trabecular bone would be expected to have a higher

metabolic rate. Therefore, it is possible that because of cellular deficiencies associated with *bgn*-deficiency, a strong phenotype may also be present in trabecular locations. Further, because the C3H skeleton is predominantly cortical bone, an inbred strain-specific phenotype may be more compelling in trabecular locations. It was also demonstrated that while KO mice from both inbred strains initially lagged behind in terms cross-sectional geometric measures, C3H mice were able to compensate/adapt over time and reach WT cross-sectional size by 11 weeks of age. However, at the same time, tissue level modulus and strength in C3H KO mice dropped between 8 and 11 weeks of age. The question that is raised by these observations is what happens at an older age? Will the surge in cross-sectional geometry that occurred between 8 and 11 weeks of age be sustainable? Will tissue-level mechanical properties continue to drop until cross-sectional geometry can no longer compensate? These questions could be answered by investigating these *bgn*-deficient mice as they reach and pass skeletal maturity.

It is clear that the exercise regimen used in these studies was insufficient to induce a bone formation response, but this does not suggest that a cellular response was not involved in changing tissue composition. Understanding what cellular events occur following mechanical loading and uncoupling these cellular changes from the physicochemical effects of loading is an important future step. While the whole animal exercise experiments used in the current studies are important from a physiological standpoint, they do little to elucidate what cellular changes might be occurring in the bones themselves and how this response differs as a function of mouse inbred strain. Within the bone, the decision to respond to mechanical stimulation is likely made in very small niches, perhaps surrounding individual cells. However, the mechanism governing the response is unclear. To better define this mechanism, a more controlled mechanical loading scheme could be used such as axial loading of the tibia. Because of the shape of the tibia, axial loading causes AP bending to occur which places the anterior surface in tension and the posterior surface in compression. By coupling this type of controlled loading with techniques such as laser capture micro-dissection or *in situ* hybridization, individual cells and/or locations could be investigated following mechanical stimulation to determine what the initial cellular response is and how it changes over time. A possible way to investigate physicochemical effects of loading would be to sacrifice a

mouse and harvest the limb of interest. The limb could be kept hydrated in a saline solution at a pH of 7.4 to maintain tissue integrity, but would be left at room temperature long enough to ensure that any cells present in the limb were no longer viable. By then mechanically stimulating the bone in this condition and investigation compositional and mechanical changes that occur, one could directly conclude that the changes were due to physicochemical effects.

Modifying the exercise regime to produce a bone formation response is integral because a combination of increased bone quality and increased bone mass would represent a powerful way to treat disease related mechanical deficiencies in bone. It is also important to test the effects of exercise in older mice (both wild type and bgn-deficient) to determine if the aged skeleton responds to exercise in the same way as younger bones.

More detailed investigations of collagen and mineral might yield a better understanding of how the tissue ultrastructure changes in response to any number of variables such as disease or mechanical stimulation. Higher resolution imaging techniques could be used to investigate the collagen and perhaps its functional competence. Transmission electron microscopy of intact, non-decalcified tissue section would provide valuable information on the size, shape and organization of collagen fibrils and their association with mineral. Digestion assays can be used to quantify true number of mature and immature collagen cross-links. X-ray diffraction could be used to verify levels of Type B carbonate substitutions and crystallinity. Coupling these techniques with nanoindentation measures of true tissue-level mechanical properties would allow more powerful regressions of composition and mechanical integrity to be performed.

Summary

The studies contained in this dissertation demonstrate for the first time that the response to a gene deletion in mice is inbred strain-specific. Bgn-deficiency impacted both organic and inorganic compartments of bone *in vivo*. Due to growth-related deficiencies in cross-sectional size in B6;129 KO mice that were not present in C3H KO mice, the B6;129 bgn-deficient phenotype was more compelling at 11 weeks of age at

levels of organization ranging from the tissue ultrastructure to the whole bone. Because exercise failed to induce any changes in cross-sectional geometry in these studies, changes in mechanical integrity that occurred in response to exercise were the result of changes in tissue composition and quality. Changes in tissue-composition in the B6;129 KO mice compensated for tissue-level mechanical deficiencies in these mice and rescued the tissue-level mechanical phenotype. However, due to the lack of increased bone formation, structural-level mechanical deficiencies persisted. These data indicate that mechanical stimulation induced by exercise can alter compositional and mechanical properties in a model of diseased bone. Therefore, this type of mechanical loading may be effective as a therapeutic intervention for a variety of bone diseases associated with deficiencies in matrix-level bone quality.

References

- (1) Rubin C, Turner AS, Bain S, Mallinckrodt C, McLeod K (2001) Anabolism. Low mechanical signals strengthen long bones. *Nature* 412:603-604
- (2) Rubin C, Recker R, Cullen D, Ryaby J, McCabe J, McLeod K (2004) Prevention of postmenopausal bone loss by a low-magnitude, high-frequency mechanical stimuli: a clinical trial assessing compliance, efficacy, and safety. *J.Bone Miner.Res.* 19:343-351
- (3) Ward K, Alsop C, Caulton J, Rubin C, Adams J, Mughal Z (2004) Low magnitude mechanical loading is osteogenic in children with disabling conditions. *J.Bone Miner.Res.* 19:360-369
- (4) Paschalis EP, Verdelis K, Doty SB, Boskey AL, Mendelsohn R, Yamauchi M (2001) Spectroscopic characterization of collagen cross-links in bone. *J.Bone Miner.Res.* 16:1821-1828
- (5) Boskey AL (2003) Bone mineral crystal size. *Osteoporos.Int.* 14 Suppl 5:16-21
- (6) Matsuura T, Duarte WR, Cheng H, Uzawa K, Yamauchi M (2001) Differential expression of decorin and biglycan genes during mouse tooth development. *Matrix Biol.* 20:367-373
- (7) Hoang QQ, Sicheri F, Howard AJ, Yang DS (2003) Bone recognition mechanism of porcine osteocalcin from crystal structure. *Nature* 425:977-980
- (8) Romberg RW, Werness PG, Riggs BL, Mann KG (1986) Inhibition of hydroxyapatite crystal growth by bone-specific and other calcium-binding proteins. *Biochemistry* 25:1176-1180
- (9) Roach HI (1994) Why does bone matrix contain non-collagenous proteins? The possible roles of osteocalcin, osteonectin, osteopontin and bone sialoprotein in bone mineralisation and resorption. *Cell Biol.Int.* 18:617-628
- (10) Weiner S, Wagner HD (1998) THE MATERIAL BONE: Structure-Mechanical Function Relations. *Annual Review of Materials Science* 28:271-298
- (11) Fratzl P, Fratzl-Zelman N, Klaushofer K, Vogl G, Koller K (1991) Nucleation and growth of mineral crystals in bone studied by small-angle X-ray scattering. *Calcif.Tissue Int.* 48:407-413
- (12) Chen XD, Allen MR, Bloomfield S, Xu T, Young M (2003) Biglycan-deficient mice have delayed osteogenesis after marrow ablation. *Calcif.Tissue Int.* 72:577-582

- (13) Robling AG, Hinant FM, Burr DB, Turner CH (2002) Shorter, more frequent mechanical loading sessions enhance bone mass. *Med.Sci.Sports Exerc.* 34:196-202
- (14) Adami S, Gatti D, Braga V, Bianchini D, Rossini M (1999) Site-specific effects of strength training on bone structure and geometry of ultradistal radius in postmenopausal women. *J.Bone Miner.Res.* 14:120-124
- (15) Bi Y, Nielsen KL, Kilts TM, Yoon A, A Karsdal M, Wimer HF, Greenfield EM, Heegaard AM, Young MF (2006) Biglycan deficiency increases osteoclast differentiation and activity due to defective osteoblasts. *Bone* 38:778-786
- (16) Bi Y, Stuelten CH, Kilts T, Wadhwa S, Iozzo RV, Robey PG, Chen XD, Young MF (2005) Extracellular matrix proteoglycans control the fate of bone marrow stromal cells. *J.Biol.Chem.* 280:30481-30489
- (17) Chen XD, Fisher LW, Robey PG, Young MF (2004) The small leucine-rich proteoglycan biglycan modulates BMP-4-induced osteoblast differentiation. *FASEB J.* 18:948-958
- (18) Chen XD, Shi S, Xu T, Robey PG, Young MF (2002) Age-related osteoporosis in biglycan-deficient mice is related to defects in bone marrow stromal cells. *J.Bone Miner.Res.* 17:331-340
- (19) Parisuthiman D, Mochida Y, Duarte WR, Yamauchi M (2005) Biglycan modulates osteoblast differentiation and matrix mineralization. *J.Bone Miner.Res.* 20:1878-1886
- (20) Wadhwa S, Bi Y, Ortiz AT, Embree MC, Kilts T, Iozzo R, Opperman LA, Young MF (2007) Impaired posterior frontal sutural fusion in the biglycan/decorin double deficient mice. *Bone* 40:861-866
- (21) Wolff J (1892) *Das gesetz der transformation der knochen.* August Hirschwald, Berlin
- (22) U.S. Department of Health and Human Services, Office of the Surgeon General (2004) *Bone Health and Osteoporosis: A Report of the Surgeon General.*
- (23) Heaney RP, Abrams S, Dawson-Hughes B, Looker A, Marcus R, Matkovic V, Weaver C (2000) Peak bone mass. *Osteoporos.Int.* 11:985-1009

APPENDIX A

DEVELOPING THE STATISTICAL ANALYSIS TO DETECT INBRED STRAIN-SPECIFICITY

Overview of Statistical Design

Because this dissertation is attempting to show that a statistical difference exists between two major effects (percent change in bgn-deficient B6;129 mice relative to wild type B6;129 mice versus percent change in bgn-deficient C3HX mice relative to wild type C3HX mice), the power analysis was approached as the ratio of two ratios. An example of how this was addressed for the case of genotype x background strain (hypothesis 1, specific aim 1, Chapter 4) is detailed below.

	Wild Type	Knockout
B6;129	b	a
C3HX	d	c

 $\Rightarrow \frac{a/b}{c/d}$

Because this is a non-linear operation, a log transformation is performed on all data to linearize the problem.

$$\log\left(\frac{a/b}{c/d}\right) = \log\left(\frac{a}{b}\right) - \log\left(\frac{c}{d}\right) = \log(a) - \log(b) - \log(c) + \log(d)$$

Therefore, during the power analysis, the term used for the minimum detectable difference is $\log(a) - \log(b) - \log(c) + \log(d)$ where each term is actually the mean of the log transformed data for each parameter. For example:

length	log (length)
L_1	$\log(L_1)$
\vdots	\vdots
L_n	$\log(L_n)$
a = average ($L_1:L_n$)	log(a) = average [$\log(L_1):\log(L_n)$]

In each of the proposed experiments, 5 sets of data will be analyzed:

- 1) **Body Mass and Tibial Length**
- 2) **Tissue Composition:** collagen cross-linking ratio, carbonate/phosphate ratio, mineral/matrix ratio, crystallinity and volumetric bone mineral density.
- 3) **Tissue-Level Mechanical Properties:** yield stress, ultimate stress, elastic modulus, yield strain, failure strain, resilience, toughness
- 4) **Cross-Sectional Geometry:** anterior-posterior (AP) width, medial-lateral (ML) width, AP/ML ratio, AP bending moment of inertia, ML bending moment of inertia, total cross-sectional area, cortical area, marrow area, average cortical thickness
- 5) **Structural-Level Mechanical Properties:** yield force, ultimate force, stiffness, yield deformation, post-yield deformation, total deformation, yield work, post-yield work, total work

Using the measured mean and variability of each property from measured from B6;129 mice in Chapter 2 of this dissertation, a statistical power of 80% and a significance level of 0.05, sample size calculations were carried out for each property of interest assuming an analysis using Student's t-tests. Calculations were performed in a parametric manner for expected percent differences between bgn-deficient and wild type C3H mice for each parameter since data of this kind was not available in the literature.

An example of one of these calculations for the case of force to yield is detailed below. This is one of the most salient parameters measured, so it is important to be able to distinguish a difference in this response. The B6;129 wild type and bgn-deficient values are each converted to the log scale, and then the mean (μ) and standard deviation of each is calculated. Next the standard deviation of the C3H data is assumed to be equal

to the greatest standard deviation of the B6;129 data. Finally, the parametric study is carried out using commercially available software (SigmaStat 3.1, Systat).

	Wild Type B6;129 (WT)	log (WT)	Bgn-deficient B6;129 (KO)	log (KO)
	19.24	1.28	16.12	1.21
	32.11	1.51	15.95	1.20
	17.90	1.25	20.36	1.31
	17.22	1.24	14.61	1.16
	20.69	1.32	22.56	1.35
	31.65	1.50	20.88	1.32
			13.50	1.13
			31.88	1.50
			23.89	1.38
			17.06	1.23
mean	23.13	1.35	19.68	1.28
standard deviation	6.88	0.12	5.52	0.11

% Diff in C3H	Min Δ	n
+25%	0.166	10
+20%	0.148	12
+15%	0.131	15
+10%	0.111	21
+5%	0.090	31
+1%	0.074	45
-1%	0.065	58
-5%	0.047	109
-10%	0.023	450
-15%	0.001	237500
-20%	0.028	304
-25%	0.056	77
-30%	0.086	34
-35 %	0.118	19
-37 %	0.131	15
-40%	0.153	12
- 45%	0.190	8

The sample size necessary to detect a significant difference in change of yield force between the known response in B6;129 mice (-14.93% in bgn-deficient males) and the estimated response in C3H mice starting at $\pm 1\%$ is determined. Sample sizes become reasonable between -35% and -40% or +10% to +15%. $n=15$ was chosen which means a 37% decrease or 15% increase in this parameter in C3H mice is necessary in order to detect an inbred strain-specific difference versus the 15% decrease seen in B6;129 mice. Performing similar calculations for all other parameters revealed that in order to detect relative differences between background strains in response to genetic deletion with a sample size of $n=15$, changes of up to 45% in properties of interest in C3H mice would be necessary.

Similar parametric analyses for the major effects of background strain x exercise in wild type animals and for background strain x exercise in bgn-deficient mice demonstrated that a sample size of 15 was large enough to detect differences based on at most a 45% change in all properties for which primary differences between inbred strains were expected, with the exception of ultimate force in bgn-deficient exercised animals.

	KO Control vs WT Control			WT Exercise vs WT Control			KO Exercise vs KO Control		
	% Diff	< %	> %	% Diff	< %	> %	% Diff	< %	> %
Cortical Area	18.67	-3%	46%	-3.72	-17%	+10%	5.37	-12%	+27%
AP Width	13.56	-4%	+35%	3.53	-7.5%	+15.5%	-2.97	-20%	+18%
ML Width	21.59	+7%	+39%	0.86	-6%	+9%	-1.92	-15%	+13%
Cortical Thickness	0.06	-18%	+22%	-4.34	-14%	+8%	14.25	2%	+28%
Yield Force	-14.93	-41%	+20%	-3.02	-20%	+17%	26.21	-9%	+82%
Ultimate Force	-4.82	-32%	+32%	2.38	-15%	+24%	22.96	-5%	+61%
Total Deformation	5.85	-38%	+84%	11.06	-17%	+45%	0.7	-43%	+79%
Work to Yield	-0.58	-43%	+74%	-11.24	-32%	+15%	52.85	-0.05%	+165%
Failure Strain	9.44	-23%	+57%	27.84	-6%	+67%	4.92	-26%	+49%
vBMD	6	+5%	+7%	3.28	+1.4%	+5%	0.33	-1%	+2%

This table describes the necessary percent change in all primary outcome measures in C3H mice for each experimental condition to detect a statistical difference versus the response in B6;129 mice. The assumed sample size is n=15. The column labeled % Diff is the known % difference in the same property in B6;129 mice. <% means that the change in the value of the property must be below the shown percentage. >% means that change in the value of the property must be greater than the shown percentage.

APPENDIX B

INCREASED POST-YIELD PROPERTIES INDUCED WHEN EXERCISE IS SUPERIMPOSED ON GROWTH ARE MAINTAINED AFTER 2 WEEKS WITH ADDED STRENGTH

Introduction

Skeletal fragility leading to fracture is a significant medical and economic burden facing our society. Each year, an estimated 1.5 million Americans suffer a bone disease related fracture, resulting in direct care expenditures of 18 billion dollars a year, measured in 2002 dollars [1]. While many factors influence fracture risk (e.g. nutrition, hormones, pharmacological factors), one important factor is the amount of peak bone mass achieved during growth [2]. It has been suggested that the greater the peak skeletal mass attained during growth, the greater the reserve of bone tissue that can be drawn from later in life when age-related decreases in bone mass ensue [3-5]. Although genetic factors are responsible for as much as 70% of the variability in peak bone mass in humans [6-10], other controllable factors such as biomechanical forces imparted by physical activity also contribute to skeletal health for people of all ages.

Qualitative exercise-based mouse [11-14] and rat [15-17] models have almost universally shown a link between the loading of bone and increased bone formation, resulting in increased bone mass and maintenance or increase of mechanical properties. Since the mechanical competence of bone is a clinically important metric, information regarding the alteration of mechanical properties following an exercise regimen is essential to assess the efficacy of the exercise and its ability to be used as a measure against fracture. Using a murine treadmill exercise model, we demonstrated that 21 consecutive days of running during growth significantly increased structural post-yield deformation and tissue-level strain to failure in the tibial diaphyses of male C57BL6/129 mice, but these benefits came at the expense of structural pre-yield deformation as well as

structural and tissue-level strength [18]. Because these results were novel and unexpected, we were interested in further investigating the phenomenon.

Animals in our previous exercise study were sacrificed 3 days after the termination of running. Based on the results of this work, we speculated that while 3 weeks of exercise during growth was sufficient to elicit a formation response greater than that which was present with growth alone, this newly formed tissue which was exposed to mechanical stimulation was immature, lacking the mechanical integrity of fully organized and mineralized lamellar bone necessary to increase the bone's strength. We further speculated that changes were occurring within the pre-existing bone matrix as a toughening mechanism during exercise, possibly in the number and maturity of collagen cross links. Therefore, the purpose of this study was to test the hypothesis that given more time between the termination of exercise and sacrifice, newly formed bone will mature, and alterations that occurred in the pre-existing bone will further develop resulting in increased strength compared with animals sacrificed immediately following exercise. At 8 (beginning of exercise), 11 (end of exercise) and 13 (2 weeks after exercise) weeks of age, in the cortical bone of the tibial mid-diaphyses of C57BL6/129 male mice, changes due to growth, exercise and rest following exercise were assayed by four-point bending tests to determine mechanical properties at the whole bone (structural) and tissue levels, as well as histomorphometric analyses of bone formation and bone cross-sectional geometry were assessed.

Materials and Methods

Animals and Treatment

All animal procedures were performed at the University of Michigan with University Committee on Use and Care of Animals (UCUCA) approval (UCUCA animal approval protocol #8518). To determine proper sample sizes for detecting effects of exercise and age, power calculations were performed based on measured differences and standard deviations in geometric and mechanical properties in C57BL6/129 male mice due to running on a treadmill [18] using a value of $\alpha=0.05$ and a power ($1-\beta$) of 0.80 [19].

75 C57BL6/129 (B6;129) mice were purchased at 5 weeks of age (The Jackson Laboratories; Bar Harbor, ME). Animals were housed in standard cages and given access to food, water and cage activity *ad libitum*. On Day -11 before the start of the study, following an initial 1 week acclimation period, mice were randomly assigned to 1 of 5 weight-matched groups. These groups were again weighed on Day 0 to ensure weight-matching. One group (8 week control, 8wc) was sacrificed on Day 0 as a baseline control to assess the effects of growth during the study. Two groups (11 week exercise, 11we; 13 week exercise, 13we) began a running exercise regimen (12 meters/minute at a 5° incline for 30 minutes/day for 21 consecutive days; Columbus Instruments, Model 1055M; Columbus, OH) at Day 0, as previously described [18]. The remaining groups (11 week control, 11wc; 13 week control, 13wc) were confined to cages for the entirety of the study. One day following the end of the exercise regimen (Day 21), 11wc and 11we mice were sacrificed, at which time the left tibiae of each animal was harvested, stripped of soft tissue and stored at 4°C in a Ca²⁺-buffered saline solution for mechanical testing within 24 hours. 13wc and 13we mice were sacrificed on Day 35, and the left tibiae were treated in this same manner.

Intraperitoneal (IP) injections of calcein (20 mg/kg) were given throughout the study to assess bone formation. At day -10 and -3, 8wc mice were given IP injections to determine an initial growth rate in these mice. The remaining mice were given injections at Days 0, 9 and 19. The 13wc and 13we mice were given a final IP injection on Day 30, to determine if the anabolic effects of exercise continued after its cessation.

Mechanical Testing

Left tibiae were monotonically tested to failure in 4-point bending in displacement control (Admet eXpert 450; Norwood, MA) with a support span of 9 mm (L) and a loading span of 3 mm at a rate of 0.025 mm/sec. Before testing, the length of each tibia was measured from the most proximal portion of the tibial plateau to the most distal portion of the medial malleolus using digital calipers accurate to 0.01 mm (Mitutoyo, Aurora, IL). Tibiae were tested in the medial-lateral (ML) direction, with the medial surface in tension. The tibiae were positioned such that the most proximal point

of the junction of the tibia and fibula (TFJ) was aligned with the outside edge of the left-most support point. During each test, load and deflection were recorded, from which structural strength (yield and ultimate force), energy or work (measured as the area under the force vs. displacement curve to yield and to failure), stiffness (the slope of the linear portion of the force vs. displacement curve) and deformation (elastic deformation to yield, deformation to ultimate force, total deformation and post-yield deformation) were derived at the whole bone level.

During each test, the bone was closely monitored and the point of fracture initiation was noted. All fractures initiated on the surface of the bone that was in tension (the medial surface). Because fractures often propagated at an angle across the bone (i.e. oblique fractures), the half of the fractured bone containing both the fracture initiation site and a full planar section of bone at that site was processed for histology, embedded, and sectioned as described below (see histomorphometry section). The jagged edge of the bone was trimmed off, and a 150 μm thick planar section was obtained. Cross-sectional images at the fracture site were acquired (Nikon Eclipse TE 300) and analyzed using digital analysis software and a custom Matlab script (Image Pro-Plus v4.5, Matlab v6.0), from which geometric parameters (moment of inertia about the axis of bending (I) and c , distance from the centroid to the surface of the bone in tension) were determined. Together with the load and deflection data, c and I were used to derive estimated tissue-level mechanical properties from standard beam-bending equations for 4-point bending:

$$\text{Stress} = \sigma = \frac{Fac}{2I} \quad (\text{MPa})$$

$$\text{Strain} = \varepsilon = \frac{6cd}{a(3L - 4a)} \times 10^6 \quad (\mu\varepsilon)$$

In these equations, F is the force, d is the displacement, a is the distance from the support to the inner loading point (3 mm) and L is the span between the outer supports (9 mm). The modulus of elasticity was calculated as the slope of the linear portion of the stress vs. strain curve, and toughness was determined as the area under the stress vs. strain curve to a point of interest (e.g. yield point).

Histomorphometry

Following fracture testing, the fractured halves of all left tibiae were dehydrated in graded ethanol (70%, 80%, 95%, 100%), defatted in xylene and Clear-Rite 3 (Richard-Allen Scientific; Kalamazoo, MI) and infiltrated in a liquid methyl methacrylate monomer (Koldmount™ Cold Mounting Liquid, Mager Scientific). The bones were then embedded in methyl methacrylate (Koldmount™ Cold Mounting Kit, Mager Scientific). Using a low-speed sectioning saw (South Bay Technology, Model 650; San Clemente, CA) with a diamond wafering blade (Mager Scientific), sections approximately 150 µm thick were made at the fracture site (as described in the Mechanical Testing Section above) or just proximal to the TFJ for static and dynamic histomorphometry (the average distance of this section from the distal end of the bone was 6.85 ± 0.83 mm). These histomorphometric sections were hand ground and polished to a final thickness of between 50 and 75 µm using wet silicon carbide abrasive discs. Sections were imaged using the Nikon DAPI-FITC-TRITC triple band filter combination (DAPI excitation at 385-400 nm and emission at 450-465 nm; FITC excitation at 475-490 nm and emission at 505-535 nm; TRITC excitation at 545-565 nm and emission at 580-620 nm) at a magnification of 200X and analyzed using digital analysis software (Nikon Eclipse TE 300, Image Pro-Plus v4.5). All histomorphometric analyses were performed using standard ASBMR methods and nomenclature [20]. For static histomorphometry, cross-sectional geometric properties were determined (average cortical thickness, cortical area, marrow area, total cross-sectional area, AP and ML diameters, AP and ML moments of inertia). For dynamic measures, bone surface lengths (BS), labeled surfaces (single label - sLs; double label - dLs) and center-to-center interlabel distances (Ir.L.Th) were measured on both the endocortical and periosteal surfaces. The amount of time between each injection is indicated as Ir.L.t. Surface referent mineralizing surface (MS), mineral apposition rate (MAR) and bone formation rate (BFR) were then determined at each surface using the following calculation: $MS = [(0.5 \times sLs) + dLs]/BS$, $MAR = Ir.L.Th/Ir.L.t$, $BFR = MAR \times MS$.

Statistical Analysis

All data are presented as mean \pm standard error of the mean (SEM). Statistical analyses were performed on body mass, and all geometric, mechanical and histomorphometric properties using a two-way ANOVA checking for the main effects of exercise and age, followed by post-hoc Student-Newman-Keuls tests (Sigma Stat 3.0, Jandel Scientific). A value of $p < 0.05$ was considered significant while a p -value between 0.05 and 0.10 was also noted as a trend. For parameters displaying non-normal distributions, Mann-Whitney rank sum tests were performed.

Results

Growth-related effects between 8 and 13 weeks of age

Body weight was measured at multiple time points between 6.5 and 13 weeks of age (Figure B.1). At each individual time point, the 11wc and 13wc mice had similar body weights. When comparing between time points, body weight increased across all control groups for all time points (because of the number of interactions, p values are not shown in Figure B.1). The only exception is the 13wc body weight, which did not change between day 18 and day 35 ($p < 0.144$).

Supporting this increase in body weight between 8 and 13 weeks, the tibiae of male B6;129 mice were growing both longitudinally and radially, as evidenced by geometric properties which were greater at both 11 and 13 weeks of age compared with 8 weeks of age (Table B.1). These properties include cortical area and total cross sectional area, cortical thickness, AP and ML diameters (ML diameter was marginally greater at 11 weeks, $p < 0.055$), AP and ML moment of inertia and tibial length (data not shown, 8wc vs. 11wc: $p < 0.001$; 8wc vs. 13wc: $p < 0.001$). The majority of this growth occurred between 8 and 11 weeks of age, as there were only small percent differences in geometric properties between 11wc and 13wc mice, and no change was significant. These data are supported by histomorphometric measures in control mice which show that throughout the study, periosteal MS, MAR and BFR declined compared to baseline levels (Figure B.2). Of particular interest is that after 11 weeks of age (Day 19), the difference in periosteal MAR and BFR compared with the previous time point lost significance, suggesting that tibial expansion had reached a slow steady-state of growth.

While there was an increase in the amount of tissue over time, the mechanical properties of this tissue decreased with age (Table B.2). These properties include yield stress and ultimate stress, strain to ultimate stress and strain to failure, total toughness and modulus of elasticity, all of which were significantly less at 11 and 13 weeks of age compared with 8 weeks of age. As with the changes in geometric properties, these changes in tissue-level mechanical properties predominantly occurred between 8 and 11 weeks of age; with the exception of modulus of elasticity, which increased by 12% in 13wc mice over 11wc mice ($p < 0.163$), there were only small percent differences in all other tissue-level properties between 11 and 13 weeks of age, and none were significant. At the structural-level, post-yield deformation properties (deformation to ultimate force, deformation to failure and post-yield deformation) were significantly lower at 11 weeks of age compared with 8 weeks of age, but no differences in stiffness or strength were noted (Table B.3). These deformation properties were all still significantly lower at 13 weeks of age versus 8 weeks of age (post-yield deformation was now only marginally lower, $p < 0.085$), with the addition of decreased elastic deformation and increased stiffness. However, as with the geometric and tissue-level mechanical properties, there were no significant differences in any structural-level mechanical properties between 11 and 13 weeks of age. These data again imply that the majority of the growth related changes occurred between 8 and 11 weeks of age.

The effects of exercise superimposed upon growth between 8 and 11 weeks of age

There was a significant bone formation response due to exercise throughout the entirety of the exercise regimen, as demonstrated by elevated periosteal MAR at both the beginning (Days 0 to 9) and end (Days 9 to 19) of the exercise period (Figure B.2B) in exercise versus control mice. However, because of the lack of response in periosteal MS (Figure B.2A), there was no difference noted in periosteal BFR (Figure B.2C). Accompanying this lack of a change in BFR, no changes occurred in any geometric properties between 11we and 11wc animals (Table B.1), though there was a marginal increase in marrow area ($p < 0.078$) and a marginal decrease in tibial length (data not shown, $p < 0.066$). Because exercise was superimposed upon growth, all geometric

properties that were increased in 11wc mice versus 8wc mice were still greater in 11we versus 8wc mice, with the exception of total cross section area, which was marginally greater ($p < 0.070$).

At the tissue level, exercise significantly increased strain to ultimate stress and strain to failure and marginally increased total toughness ($p < 0.093$) in 11we versus 11wc mice (Table B.2). However, yield stress was marginally decreased compared with 11wc mice ($p < 0.085$). Similar to 11wc mice, yield stress, ultimate stress and modulus of elasticity were all decreased in 11we mice versus 8wc mice. However, whereas strain to ultimate stress, strain to failure and total toughness were decreased in 11wc mice versus 8wc mice, these properties were not different in 11we versus 8wc mice.

At the whole-bone level, exercise significantly decreased elastic deformation in 11we versus 11wc mice, while increasing post-yield deformation and marginally increasing work to failure (Table B.3; $p < 0.095$). Similar to 11wc mice, 11we mice had decreased deformation to ultimate force compared with 8wc mice. While 11wc mice had decreased post-yield and total deformation compared with 8wc mice, exercise in 11we mice maintained these properties at levels not different from 8wc animals. However, elastic deformation was significantly decreased, stiffness was significantly increased and ultimate force was marginally increased ($p < 0.066$) in 11we versus 8wc mice.

The effects of a 2 week tissue maturation period on exercised bones

In the 2 week period following the cessation of exercise, measures of bone formation show a reversal, with periosteal MS, MAR and BFR all dropping to level that were statistically similar, yet below control levels (Figure B.2). The result is that 13we tibiae had no differences in geometric properties when compared with 13wc mice or 11we mice sacrificed immediately following the termination of exercise, with the exception of a decrease in marrow area versus 11we (Table B.1).

No differences were noted in any structural-level mechanical properties between 13we and 11we mice (Table B.3). However, compared with 13wc mice, the 13we mice had a significant increase in deformation to ultimate force, while maintaining equivalent stiffness and strength. At the tissue-level, the 13we mice had significantly increased

yield stress, ultimate stress and modulus of elasticity compared with 11we mice, with no difference in strain to ultimate stress or strain to failure (the only 2 tissue-level properties that were greater in 11we mice versus 11wc mice). Again, when the 13we mice were compared with the 13wc mice, the 13we mice had greater strain to ultimate stress and strain to failure, while modulus, strength and toughness were not different.

Body weight changes due to exercise and tissue maturation

All groups were body weight matched at day -11, and body weights were again measured on day 0 to ensure that no changes had occurred (Figure B.1). Between days 0 and 18, the combined control animals were found to have gained weight (increased by 6.3%, $p < 0.009$) while the weight of the combined exercise animals remained unchanged ($p < 0.983$). The result was that body weight was decreased in the 11we versus 11wc mice (-5.9%, $p < 0.05$) as well as in the 13we versus 13wc animals (-7.6%, $p < 0.016$) at Day 18. However, there was no difference between the 11we and 13we mice ($p < 0.275$) or between the 11wc and 13wc mice ($p < 0.732$) at day 18. At the end of the study on day 35, the 13wc mice still had a marginally lower body weight (-5.5%, $p < 0.083$).

Discussion

This study demonstrates that male B6;129 mice are still growing at 8 weeks of age. When three weeks of exercise are superimposed upon this growth, post yield tissue-level and structural mechanical properties are increased in the tibial mid-diaphysis. This is in agreement with data from a previous experiment in which exercise increased post-yield properties, but at the expense of structural and tissue-level strength [18]. Following a 2 week tissue-maturation period, this newly acquired ductility is maintained with the addition of stiffness and strength, indicating that the beneficial effects of exercise can be maintained or even continue after exercise ends.

Our results show that the tibiae of B6;129 mice are still growing both longitudinally and radially at 8 weeks of age, as demonstrated by tibial length and multiple cross-sectional geometric properties at the tibial mid-diaphysis which were greater at 11 and 13 weeks of age versus 8 weeks of age (Table B.1). The majority of this growth is occurring between 8 and 11 weeks of age, as there were only small percent

changes in geometric properties between 11wc and 13wc mice, and no changes were significant. These data are echoed in histomorphometric measure of bone formation (Figure B.2). Though there was an increase in the amount of tissue over time, the mechanical properties of this tissue decreased with age (Table B.2). As with the geometric properties, these changes in tissue-level mechanical properties predominantly occurred between 8 and 11 weeks of age. With the exception of deformation characteristics (not including elastic deformation), structural level properties including stiffness and strength were unchanged with age. In fact, stiffness and strength increased, but these changes were not significant (yield force was marginally greater at 11 and 13 weeks versus 8 weeks, $p < 0.073$). These data suggest that during growth, the most important design goal is to carry loads without deforming the whole bone, which is best accomplished by a bone which is structurally stiffer and stronger without regard for tissue-level properties or structural post-yield deformation properties. Another interpretation is that growth increases tissue quantity (geometry) as opposed to tissue quality (toughness), leading to stiffer, stronger bones.

Perhaps the most significant results from this study relate to the tibial response to exercise during growth. Whereas growth increased structural stiffness and marginally increased structural strength, exercise superimposed upon growth increased structural- and tissue-level post-yield properties in 11we mice over 11wc animals, maintaining levels equivalent to 8wc mice by preventing the decline in these properties that was demonstrated with growth alone. However, no beneficial effects were seen in tissue-level strength or stiffness, which were still significantly decreased compared with 8wc mice. These data suggest that when exercise is superimposed upon growth, design goals change and adaptation to the new loading state now becomes an important design consideration. This design requirement may be best addressed by changes in ductility as opposed to changes in structural stiffness and strength alone. The result is that while 3 weeks of growth decreased tissue-level strain to failure and toughness, exercise superimposed on that growth increased strain to failure and marginally increased toughness over 11wc mice, maintaining levels indistinguishable from 8wc mice. Whereas strength represents the resistance to damage accumulation in a structure, toughness measures the damage tolerance of the structure. In the case of a rapidly growing bone which is subjected to an

increased loading condition, toughness may be the better design goal because it means the material does not have to be perfect, it only needs to be able to tolerate the damage that accrues without having a catastrophic failure. In this case, the increase in toughness suggests that the dominant effects of exercise during growth are to aid the bone's ability to tolerate damage, possibly by inducing changes in the pre-existing and newly forming bone matrix which allow for more energy absorption before fracturing primarily due to increased tissue ductility. Because post-yield properties were preferentially impacted, it is possible that the mechanism is an increase in the number and/or maturity of collagen crosslinks in the newly forming (due to growth) or in the pre-existing tissue due to the mechanical stimulation the bone is receiving [21, 22]

Upon the termination of exercise, metabolic changes that were noted throughout the entire exercise period (increased periosteal MAR) were lost, as measures of bone formation dropped below control levels. The net result is that with the exception of a decrease in marrow area, no other geometric properties were different in 13we versus 11we mice (and similarly no properties were different versus 13wc mice). In comparison to 11we mice, there were also no structural-level mechanical differences in the 13we tibiae meaning the structural post-yield benefits imparted with exercise were maintained. However, at the tissue level, the 13we mice had greater modulus and strength compared with 11we mice, while maintaining the newly acquired ductility induced by exercise. Compared with the 13wc mice, the 13we mice had greater structural- and tissue-level deformation characteristics with equivalent structural- and tissue-level stiffness and strength. Because no growth-related effects were noted between 11 and 13 weeks of age, these combined changes can be considered the enduring effects of exercise.

In comparison to results from a previous experiment [18], there are some inconsistencies in the current study. While the same increase in post-yield deformation and decrease in elastic deformation are seen here, no decrease in structural-level or tissue-level strength were observed, though yield stress was marginally decreased (Table B.2, $p < 0.085$). A possible explanation for this has to do with the mechanical testing apparatus and the test set-up. In the current study, a new testing machine was implemented with a different loading jig than was previously used. Further, the test location along the diaphysis was slightly different. These changes were made to try to

eliminate problems inherent when testing in 4-pt bending and using beam bending equations to derive estimated tissue-level properties. The net result is that the current tests produce more accurate force and displacement data, and when these data are used to derive tissue-level properties, the tissue properties are more accurate as well.

In summary, growth occurring between 8 and 13 weeks of age in B6;129 males increases tissue quantity and structural stiffness and strength in the tibial diaphysis while decreasing tissue-level properties and structural post-yield deformation characteristics. When exercise is superimposed on this growth, changes in bone geometry persist, but increased structural- and tissue-level post-yield characteristics compared with age-matched control animals prevent the decline in these post-yield properties caused by growth alone. This suggests mechanically-induced differences in the newly forming tissue (due to growth) as well as possible changes in the pre-existing matrix. Finally, when time was allowed after the termination of exercise for tissue changes to mature, tissue-level strength and stiffness were increased with maintenance of the exercise-induced structural- and tissue-level ductility. Because no growth related changes were present between 11 and 13 weeks of age, these differences suggest that the effects of exercise can continue after exercise ends.

Acknowledgements

I would like to acknowledge my coauthors on this manuscript:

Michael S. Ron and Dr. David H. Kohn.

Funding sources for this study:

DoD/US Army DAMD17-03-1-0556; NIH T32-DE07057; NIH IPA Agreement;
Regenerative Sciences Training Grant T90-DK071506

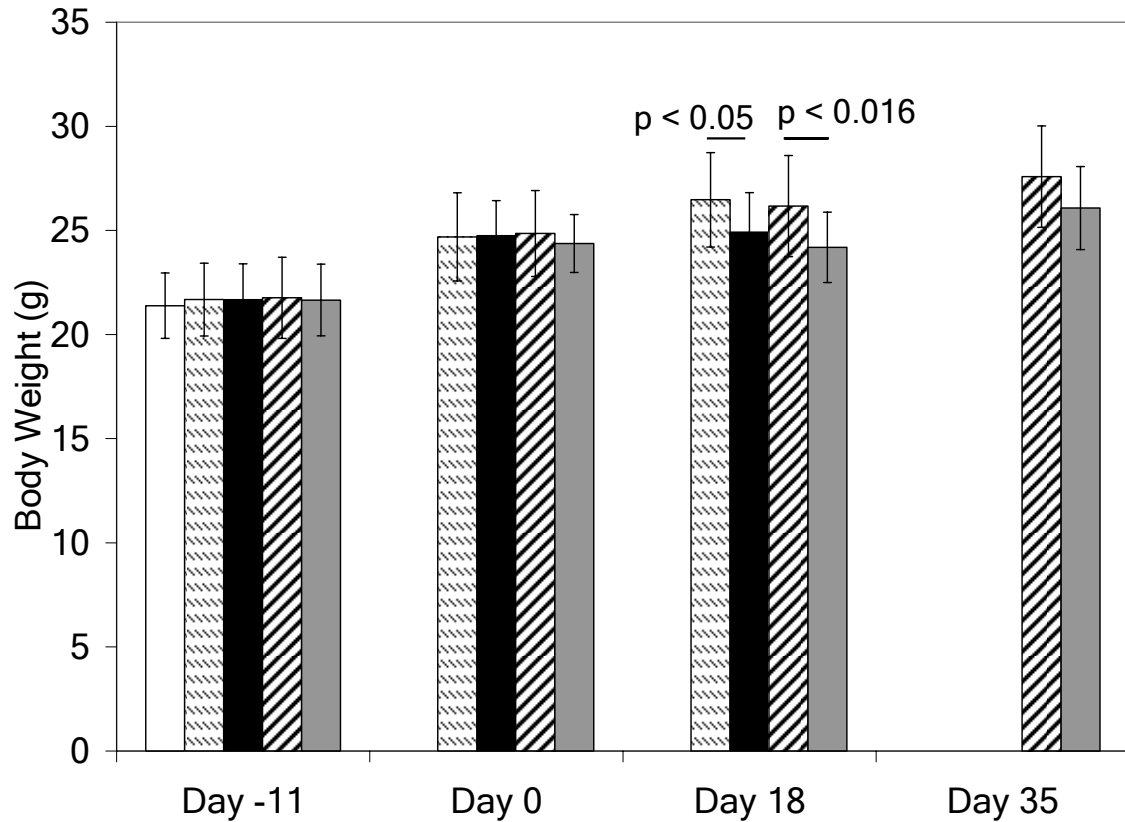


Figure B.1 : Body Weights Measurements at Days -11, 0, 18 and 35. All groups were body weight matched at day -11, and this remained true at day 0. At each time point, the 11wc and 13wc mice had similar body weights, but when comparing between time points, body weight increased across all control groups for all time points, with the exception of 13wc body weight, which did not change between day 18 and day 35. By day 18, body weight was decreased in the 11we versus 11wc mice as well as in the 13we versus 13wc animals. However, there was no difference between the exercise groups (11we, 13we) or the control groups (11wc, 13wc). At the end of the study on day 35, the 13we mice had a marginally lower body weight ($p < 0.083$). Data are presented as mean \pm SEM. \square = 8 week control, \square (with diagonal lines) = 11 week control, \blacksquare = 11 week exercise, \square (with diagonal lines) = 13 week control, \square (grey) = 11 week exercise.

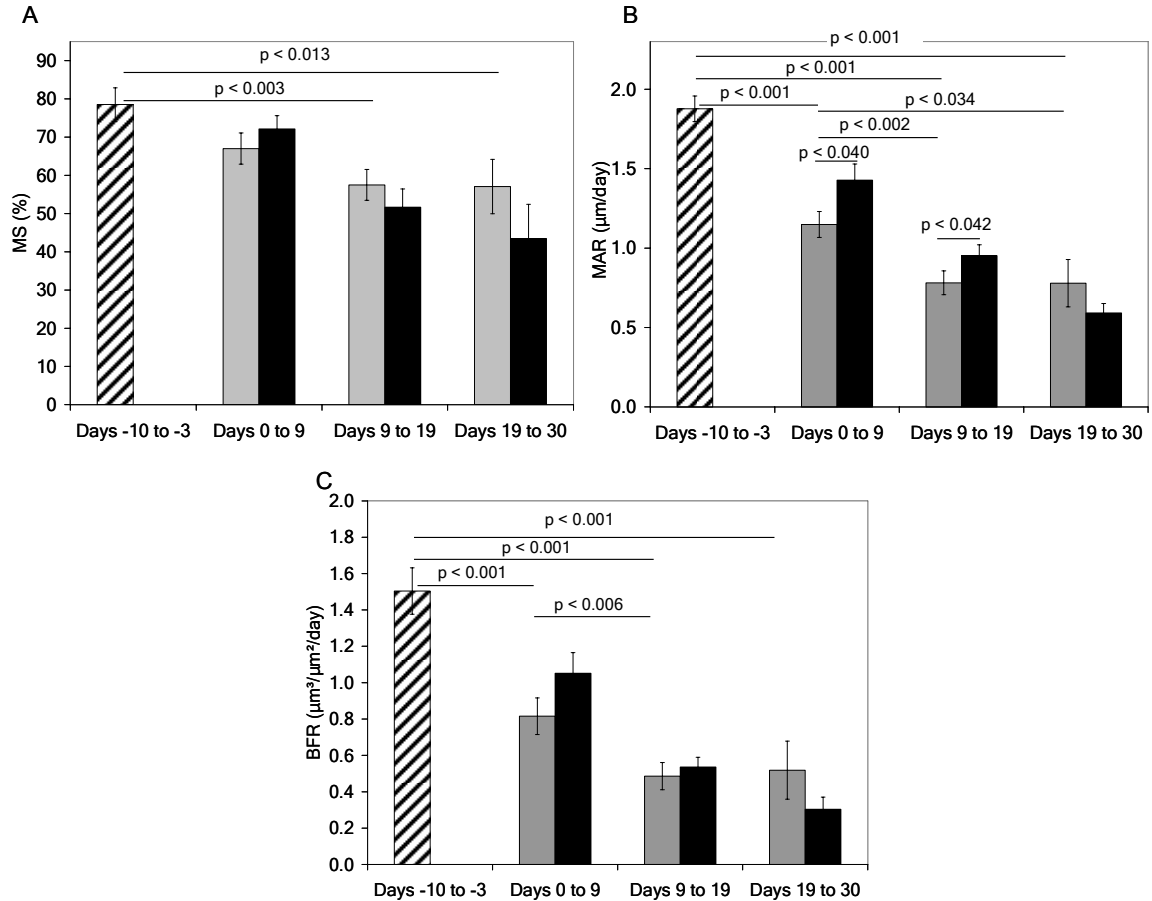


Figure B.2: Histomorphometry from days -10, -3, 0, 9, 19 and 30. Throughout the study, periosteal MS, MAR and BFR in control animals declined compared to baseline levels. In control mice after 11 weeks of age, the difference in MAR and BFR compared with the previous time point lost significance. There was a significantly elevated MAR at both the beginning (Days 0 to 9) and end (Days 9 to 19) of the exercise period in pooled exercise versus control mice. However, because of the lack of a response in MS, there was no difference noted in BFR. In the 2 week period following the cessation of exercise, measures of bone formation show a reversal, with MS, MAR and BFR all dropping to level that were statistically similar, yet below control levels. Data are presented as mean \pm SEM. ▨ = baseline, ▤ = all control mice, ▥ = all exercise mice.

Table B.1: Geometric Properties of the Tibial Diaphyses

Group	Cortical Area (mm)	Marrow Area (mm)	Total Cross Sectional Area (mm)	Cortical Thickness (μm)	AP Diameter (mm)	ML Diameter (mm)	AP Moment of Inertia (mm^4)	ML Moment of Inertia (mm^4)
8 week control	0.65 ± 0.01	0.26 ± 0.01	0.91 ± 0.02	228.22 ± 4.70	1.15 ± 0.03	1.07 ± 0.01	0.059 ± 0.002	0.066 ± 0.003
11 week control	0.75 ± 0.02^a	0.24 ± 0.01	0.99 ± 0.03^a	259.78 ± 6.86^a	1.23 ± 0.02^a	1.11 ± 0.02	0.072 ± 0.004^a	0.084 ± 0.004^a
11 week exercise	0.73 ± 0.02^a	0.27 ± 0.01	0.99 ± 0.03	248.50 ± 5.39^a	1.27 ± 0.03^a	1.12 ± 0.02	0.072 ± 0.004^a	0.088 ± 0.006^a
13 week control	0.75 ± 0.02^a	0.25 ± 0.01	1.00 ± 0.04^a	260.36 ± 7.52^a	1.26 ± 0.03^a	1.13 ± 0.02^a	0.075 ± 0.006^a	0.088 ± 0.008^a
13 week exercise	0.74 ± 0.02	0.24 ± 0.01^d	0.98 ± 0.02	258.95 ± 6.14	1.28 ± 0.04	1.08 ± 0.02	0.068 ± 0.003	0.090 ± 0.007

Data are presented as mean \pm SEM. A indicates $p < 0.05$ vs. 8 wc; b indicates $p < 0.05$ vs. 11wc; c indicates $p < 0.05$ vs. 13 wc; d indicates $p < 0.05$ vs. 11we.

Table B.2: Tissue-Level Mechanical Properties of the Tibial Diaphyses

Group	Yield Stress (MPa)	Ultimate Stress (MPa)	Yield Strain ($\mu\epsilon$)	Strain to Ultimate Stress ($\mu\epsilon$)	Strain to Failure ($\mu\epsilon$)	Toughness to Yield (MPa)	Total Toughness (MPa)	Modulus of Elasticity (GPa)
8 week control	189.64 \pm 7.13	220.54 \pm 5.29	20284 \pm 773	28275 \pm 1324	34841 \pm 2956	1.74 \pm 0.06	4.84 \pm 0.61	12.53 \pm 0.54
11 week control	163.91 \pm 5.29 ^a	177.89 \pm 4.24 ^a	19261 \pm 1596	24885 \pm 1007 ^a	26063 \pm 1400 ^a	1.60 \pm 0.14	2.86 \pm 0.23 ^a	9.66 \pm 0.50 ^a
11 week exercise	151.10 \pm 4.86 ^a	178.11 \pm 4.73 ^a	19654 \pm 840	28887 \pm 936 ^b	33318 \pm 2636 ^b	1.58 \pm 0.10	3.72 \pm 0.33	8.91 \pm 0.36 ^a
13 week control	164.19 \pm 4.70 ^a	182.9 \pm 5.25 ^a	19084 \pm 1049	23538 \pm 1187 ^a	24713 \pm 1587 ^a	1.63 \pm 0.14	3.06 \pm 0.35 ^a	10.82 \pm 0.64 ^a
13 week exercise	170.33 \pm 7.97 ^d	197.4 \pm 7.83 ^d	19787 \pm 778	28210 \pm 1369 ^c	33107 \pm 2681 ^c	1.69 \pm 0.09	3.72 \pm 0.29	10.84 \pm 0.59 ^d

Data are presented as mean \pm SEM. a indicates $p < 0.05$ vs. 8 wc; b indicates $p < 0.05$ vs. 11wc; c indicates $p < 0.05$ vs. 13 wc; d indicates $p < 0.05$ vs. 11we.

Table B.3: Structural-Level Mechanical Properties of the Tibial Diaphyses

Group	Yield Force (N)	Ultimate Force (N)	Elastic Deformation (mm)	Post-Yield Deformation (mm)	Deformation to Ultimate Force (mm)	Total Deformation (mm)	Work to Yield (mJ)	Work to Failure (mJ)	Stiffness (N/mm)
8 week control	13.99 ± 0.62	16.31 ± 0.56	0.279 ± 0.011	0.201 ± 0.040	0.389 ± 0.019	0.480 ± 0.042	1.89 ± 0.14	4.96 ± 0.64	66.66 ± 2.31
11 week control	15.78 ± 0.74	17.62 ± 0.82	0.264 ± 0.011	0.087 ± 0.022 ^a	0.330 ± 0.012 ^a	0.354 ± 0.022 ^a	2.00 ± 0.19	3.55 ± 0.32	71.09 ± 2.82
11 week exercise	15.31 ± 0.67	18.04 ± 0.70	0.232 ± 0.009 ^{a, b}	0.162 ± 0.027 ^b	0.342 ± 0.011 ^a	0.393 ± 0.030	1.90 ± 0.12	4.43 ± 0.39	76.03 ± 3.90 ^a
13 week control	16.60 ± 1.32	18.54 ± 1.37	0.241 ± 0.011 ^a	0.109 ± 0.028	0.300 ± 0.015 ^a	0.350 ± 0.029 ^a	2.10 ± 0.26	3.91 ± 0.47	83.83 ± 5.41 ^a
13 week exercise	15.55 ± 0.62	18.10 ± 0.70	0.251 ± 0.010	0.140 ± 0.020	0.358 ± 0.017 ^c	0.422 ± 0.037	1.97 ± 0.09	4.69 ± 0.45	77.75 ± 3.62

Data are presented as mean ± SEM. a indicates $p < 0.05$ vs. 8 wc; b indicates $p < 0.05$ vs. 11wc; c indicates $p < 0.05$ vs. 13 wc; d indicates $p < 0.05$ vs. 11we.

References

- (1) U.S. Department of Health and Human Services, Office of the Surgeon General (2004) Bone Health and Osteoporosis: A Report of the Surgeon General.
- (2) Heaney RP, Abrams S, Dawson-Hughes B, Looker A, Marcus R, Matkovic V, Weaver C (2000) Peak bone mass. *Osteoporos.Int.* 11:985-1009
- (3) Biewener AA (1993) Safety factors in bone strength. *Calcif.Tissue Int.* 53 Suppl 1:S68-74
- (4) Eisman JA, Kelly PJ, Morrison NA, Pocock NA, Yeoman R, Birmingham J, Sambrook PN (1993) Peak bone mass and osteoporosis prevention. *Osteoporos.Int.* 3 Suppl 1:56-60
- (5) Sambrook P, Kelly P, Eisman J (1993) Bone mass and ageing. *Baillieres Clin.Rheumatol.* 7:445-457
- (6) Christian JC, Yu PL, Slemenda CW, Johnston CC, Jr (1989) Heritability of bone mass: a longitudinal study in aging male twins. *Am.J.Hum.Genet.* 44:429-433
- (7) Hansen MA, Hassager C, Jensen SB, Christiansen C (1992) Is heritability a risk factor for postmenopausal osteoporosis? *J.Bone Miner.Res.* 7:1037-1043
- (8) Kelly PJ, Nguyen T, Hopper J, Pocock N, Sambrook P, Eisman J (1993) Changes in axial bone density with age: a twin study. *J.Bone Miner.Res.* 8:11-17
- (9) Pocock NA, Eisman JA, Hopper JL, Yeates MG, Sambrook PN, Eberl S (1987) Genetic determinants of bone mass in adults. A twin study. *J.Clin.Invest.* 80:706-710
- (10) Smith DM, Nance WE, Kang KW, Christian JC, Johnston CC, Jr (1973) Genetic factors in determining bone mass. *J.Clin.Invest.* 52:2800-2808
- (11) Umemura Y, Ishiko T, Yamauchi T, Kurono M, Mashiko S (1997) Five jumps per day increase bone mass and breaking force in rats. *J.Bone Miner.Res.* 12:1480-1485
- (12) Iwamoto J, Yeh JK, Aloia JF (2000) Effect of deconditioning on cortical and cancellous bone growth in the exercise trained young rats. *J.Bone Miner.Res.* 15:1842-1849
- (13) Notomi T, Okimoto N, Okazaki Y, Tanaka Y, Nakamura T, Suzuki M (2001) Effects of tower climbing exercise on bone mass, strength, and turnover in growing rats. *J.Bone Miner.Res.* 16:166-174

- (14) Huang TH, Lin SC, Chang FL, Hsieh SS, Liu SH, Yang RS (2003) Effects of different exercise modes on mineralization, structure, and biomechanical properties of growing bone. *J.Appl.Physiol.* 95:300-307
- (15) Warden SJ, Turner CH (2004) Mechanotransduction in the cortical bone is most efficient at loading frequencies of 5-10 Hz. *Bone* 34:261-270
- (16) Gross TS, Srinivasan S, Liu CC, Clemens TL, Bain SD (2002) Noninvasive loading of the murine tibia: an in vivo model for the study of mechanotransduction. *J.Bone Miner.Res.* 17:493-501
- (17) Robling AG, Burr DB, Turner CH (2000) Partitioning a daily mechanical stimulus into discrete loading bouts improves the osteogenic response to loading. *J.Bone Miner.Res.* 15:1596-1602
- (18) Wallace JM, Kohn DH (2007) Increased Post-Yield Mechanical Properties Induced When Exercise is Superimposed on Growth Are Maintained After 2 Weeks With The Addition of Strength. In Preparation
- (19) Moore DS, McCabe GP (2003) *Introduction to the Practice of Statistics.* 4W.H. Freeman & Company, New York, NY
- (20) Parfitt AM, Drezner MK, Glorieux FH, Kanis JA, Malluche H, Meunier PJ, Ott SM, Recker RR (1987) Bone histomorphometry: standardization of nomenclature, symbols, and units. Report of the ASBMR Histomorphometry Nomenclature Committee. *J.Bone Miner.Res.* 2:595-610
- (21) Banse X, Devogelaer JP, Lafosse A, Sims TJ, Grynpas M, Bailey AJ (2002) Cross-link profile of bone collagen correlates with structural organization of trabeculae. *Bone* 31:70-76
- (22) Knott L, Bailey AJ (1998) Collagen cross-links in mineralizing tissues: a review of their chemistry, function, and clinical relevance. *Bone* 22:181-187

APPENDIX C

**PROTOCOLS DEVELOPED FOR THE COMPLETION OF THIS
DISSERTATION**

Introduction

Because the various assays used in the experiments contained in this dissertation pulled techniques ranging from engineering to molecular biology, some new protocols were developed in the lab to properly and reproducibly carry out these experiments. This appendix covers those protocols which were developed de novo.

Protocol for processing mouse bones for undecalcified histology

Stage 1: Specimen Harvesting, Storage and Thawing

1. Materials

- 2 mL centrifuge tubes and rack (Fisher Catalog # 05-402-24B) – clearly labeled with sample number and bone (e.g. 151 RT)
- Gauze pads (Fisher Catalog Number 22-362-178)
- 70% EtOH – in squirt bottle
- Deionized Water – in squirt bottle
- Dissection Equipment (scissors, scalpel, forceps)
- Blue Bench Pads
- Gauze/Kimwipes
- Fine tip Sharpie
- Labeling tape
- Glass vials
- Ziplock bag

2. Harvesting Bones

- Spray down the laminar flow hood on the 6th floor with Clidox to disinfect. Lay out a blue bench pad and all dissection equipment in the hood.
- Mice should be sacrificed by CO₂ inhalation
- Cover cage with plastic lid attached to CO₂ tank
- Turn main valve of tank on (make sure that it reads at least 1000 psi).
- Turn the regulator on, slightly at first, to cause the mice to get slightly sleepy.
- After ~15-20 seconds, turn the regulator up, just high enough to see the bedding move slightly. Allow gas to flow for about 1 minute to ensure death.
- If further proof of death is required, cervical dislocation can be performed.

*** As soon as death is ensured, move quickly to ensure any cells/nucleic acids remain viable. Harvest one leg at a time to keep blood supply of 2nd leg intact.***

- Spray carcass with 70% EtOH to sterilize.
- Place mouse on its back. Holding the pelvis with the left hand and the femur (above the knee) with the right, gently tug on the femur until the femoral head pops out of the acetabulum (you will feel a slight pop).
- Using the middle finger of the left hand, push the internal organ away from the left leg while using the index finger of the same hand to stretch the leg open.
- Cut the skin/fur with a scalpel using a slicing motion, being careful to avoid the organs and the saphenous vein.
- Pull back the skin and hair as they are cut, and move around the newly exposed vein. Eventually, the femoral head will be visible.
- Cut between the femoral head and pelvis to remove leg.
- At this point, technique comes into play. All fur/soft tissue needs to be removed, but the fibrous periosteum needs to remain intact and in place. Peel the remaining skin/fur down the leg and over the ankle. Try to separate the femur from the tib/fib by bending the leg across the index finger of the left hand. Use the skin around the

ankle as a handle at one end (between the left middle finger and index finger) and the femoral head on the other end (under the left thumb).

- Induce tension at the joint to separate the two bones, and cut the ligaments connecting the two.
- Once separated, work with the tib/fib first. For most assays, the fibula is unnecessary, so if it is broken off, it is fine. However, try to keep it intact if possible. The best way to remove the muscles is to expose the ankle joint and cut all ligaments here.
- With the Achilles Tendon facing you, bend the ankle over the left index finger, again using the fur as a handle between the middle and index finger. Cut all ligaments, peeling them back under your finger as you go.
- Once all ligaments are cut, grip the muscle with Kimwipe to remove, but be careful to avoid the periosteum. Basically, you can just roll the muscle back, distal to proximal. It should pull right off at the proximal end.
- Finally, to remove the foot, bend over your finger in the same way and cut from the posterior side towards the anterior side between the distal tibia and the foot.
- Once cleaned, saturate a 2" x 2" gauze pad with dH₂O, place the bone at the lower left corner, and roll the pad into a tight roll. Place in a labeled 2 mL tube.
- Next, work with the femur. There isn't much technique here. Simply grab the soft tissue with a Kimwipe, possibly using your nail, and tear all of the muscle off the diaphysis. If necessary, use the scalpel or scissors to remove the remaining tissue at the ends of the bone. Store in same manner as the tibia.
- Perform same procedure on the left leg.
- Place all animal waste (tissue, carcasses) on the blue bench pad, wrap the bench pad up and place it in a Ziplock bag. Take this bag and place in the carcass freezer in the cold room on the 6th floor.
- Take empty cage and place in the cold room on the 6th floor.

3. Storage

- Make certain vials are clearly labeled with Sharpie.
- Store sections at -20°C until needed

4. Thawing

- Prior to beginning of mechanical testing or the dehydration process, thaw bones in vials at room temperature.
- Once bones are properly thawed, begin the dehydration protocol.

Stage 2: Fixation, Dehydration and Infiltration

1. Materials

- 100% Ethanol (store at room temperature)
- 95% Ethanol (store at room temperature)
- 80% Ethanol (store at room temperature)
- 70% Ethanol (store at room temperature)
- Xylene (Sigma # X 2377) – clears alcohol and lipid
- Clear-Rite 3 (Richard Allen Scientific Cat# 6901)
- Koldmount™ Methyl Methacrylate embedding kit (Mager Scientific, Part #CM-201)
- Liquid Monomer
- Powder Monomer (not needed for this protocol)
- Fine tip Sharpie
- Vacuum
- Waste Bottles
- Fume Hood

2. Schedule

Step	Reagent	Time (Hours)	Vacuum	Temperature
FIXATION	70% EtOH	Overnight	Yes	room
DEHYDRATION	80% EtOH	1-2	Yes	room
DEHYDRATION	95% EtOH	1-2	Yes	room
DEHYDRATION	95% EtOH	1-2	Yes	room
DEHYDRATION	100% EtOH	1-2	Yes	room
DEHYDRATION	100% EtOH	1-2	Yes	room
DEHYDRATION	Xylene	1-2	Yes	room
DEHYDRATION	Clear-Rite 3	1-2	Yes	room
INFILTRATION	Koldmount	Overnight	Yes	room

3. Repeat the following for each step

- Make certain the lids of the 2 ml tubes are clearly labeled. Try to avoid touching the lids, but to ensure you do not mix up the bones, leave them in numerical order.
- Dump current solution from vials into a waste bottle.
- Fill vials with next appropriate reagent.
- Keep tubes under vacuum (no lid on tube) for approximate dehydration time.
- Extend dehydration time, if needed, but by no more than several hours.
- Infiltration times listed are minimums.

Stage 3: Embedding Protocol

1. Materials

- 50 mL Falcon tubes with lids - whole for mixing
- Peel-Away plastic embedding molds
- Fine tip Sharpie
- Koldmount™ Methyl Methacrylate embedding kit (Mager Scientific, Part #CM-201)
 - Liquid Monomer
 - Powder Monomer
- Spatula for stirring
- Angled forceps
- Fume Hood

2. Embedding Process

- Perform all steps of the embedding process under a fume hood.
- Make a mixture of 2 parts powder monomer to 1 part liquid monomer by volume.
 - Measure out liquid and powder in separate 50 mL Falcon tubes, then add solid to liquid, about ¼ at a time, stirring constantly with wooden skewer.
 - Depending on the temperature of the liquid monomer, polymerization could take several minutes.

- While waiting for polymerization to begin, label molds with Sharpie.
- Once mixture is the consistency of honey, fill each mold.
 - If starting with 40 mL of powder and 20 mL of liquid, you can fill about 5-6 molds.
- DO NOT allow too much time to pass because mixture will solidify quickly once polymerization begins.
- As the MMA thickens and forms a skin, place each bone in its mold, trying to keep it straight.
- If necessary, remove the skin on top of the MMA with forceps.
- For fractured bones, put fracture side down.
- Allow molds to sit undisturbed for ~30-45 minutes until polymerization action is complete.
- If the molds are warm, the polymerization reaction is still occurring.

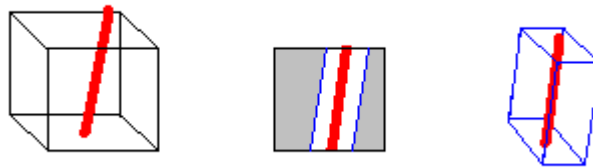
Stage 4: Specimen Sectioning, Mounting and Grinding/Polishing

1. Materials

- X-ray reading table (in B331)
- Band Saw
- Low speed sectioning saw (SouthBay Technologies, Model 650)
- Diamond wafering blade (320 grit, high concentration; Mager Scientific, Part #CM-152)
- Clear glass slides (3" x 1")
- White plastic slides (1" x 1")
- Cyanoacrylate super glue
- Paper towel
- Labeling Tape
- Fine tip Sharpie
- Grinding or polishing wheel with Silicon Carbide sand paper

2. Specimen Sectioning (for transverse cortical sections)

- Remove a section from its mold, making sure to mark the sample number on the block. Place section on X-ray table and mark a line parallel to the bone on each side far enough way from the bone itself as to ensure it will not be hit during trimming on the band saw. This will allow us to correct for mis-orientation in one direction.



- Trim down section using band saw in machine shop. If sample number is cut off, replace it.
- Once trimmed, polish away scuffing on the plastic using the polishing wheel and 600 grit paper. This should leave a relatively thin, fairly clear block.
- Glue the white plastic slide to the glass slide.
- Orient the block on a white plastic slide so that the ends are aligned perpendicular to the long sides of the slide. This allows us to correct for mis-orientation in a 2nd direction. Glue the block down to the plastic slide and label the slide with block number.
- Mount the slide in the saw's mounting assembly with the wafering blade parallel to the face to be sectioned.
- Prepare thin slices (~150-200 μm) at medium speed (5 speed setting).
- One full rotation of the positioning knob moves the section ~200 μm . To get ~150 μm , turn the knob one rotation, then turn it back about 5 marks.

3. Mounting Specimens

- Put a piece of labeling tape on one side of glass slide. Write the sample label on the tape.
- Flip this slide over
- Trim the slice down if necessary.

- Cover one side of the slice with cyanoacrylate super glue.
- With forceps, place slice glue side down on a glass slide and orient with long axis across (usually A-P direction in tibiae and M-L in femora):



- Hold down two opposing corners of the slice with forceps for about 10 seconds to force out any trapped air and glue. Repeat with other two corners.
- With paper towel, gently absorb any excess glue from around the slice and any glue that has come through the section.

4. Grinding/Polishing Specimens

- Grind sections down by hand using graded sandpaper:
 - For double labeled sections, grind with 600 grit paper for a few seconds until the section thickness is between 60 and 80 μm . If the section is thick hold the section down and turn the power on until the sections become somewhat transparent. The final section thickness should be between 50 and 75 μm .
- BE CAREFUL not to spend too much time grinding or you will grind away entire section.
- Move to 2400 (European) grit paper to remove scratch marks.
- Finish all section by polishing for about 30 seconds with 4000 (European) grit paper to polish surface.

Protocol For Harvesting and Preparing Whole Mouse Bones For qRT-PCR

Chemicals:

- 70 % Ethanol (in a squirt bottle)
- Water – in squirt bottle
- Liquid Nitrogen (LN2)

- RNA Stat-60 (in sterile reagent refrigerator, www.isotexdiagnostics.com)

Consumables

- Gloves
- Ice
- Heavy Duty Aluminum Foil (sterile)
- 1000 µl pipette tips (sterile)
- 1.5 ml Centrifuge tubes - one for each bone, labeled (sterile)
- A second one is needed if flushing bones
- Scalpel Blades (size 21 for a Number 4 blade - sterile)
- Blue Bench Pads
- Kimwipes
- Thin Sharpie
- Insulin Syringes (one for each flushed bone, 500 cc, 28 g, sterile)
- Ziplock bags for animal disposal

Equipment

- Insulated ice bucket
- Insulated LN2 bucket
- Gloves for handling LN2
- Scalpel (sterile)
- Large Forceps (for use with LN2 bucket)
- Hammer
- 2 chucks of aluminum
- 1000 µl pipetter

Do Under Strict RNase-Free Conditions – Treat All Equipment/Consumables that will contact bone/marrow so that they is RNase free

Autoclaving at 250° for 35 minutes and dry for 25 minutes per instructions on autoclave*

Harvesting Bones

- Fill insulated LN2 bucket with 1-1.5 L of LN2 (and place aluminum pieces inside) and clamp lid.
 - BE CAREFUL when unlatching lid – it may splash/steam.
- Fill syringes (1 for each bone to be flushed) with RNA-STAT and recap.
 - When recapping, do not hold in hand. Bring syringe in from side and slide cap over making sure that it goes in straight and does not come out the side of the cap.
- Fill ice bucket with ice (4th Floor) and place syringes in the ice bucket.
 - Cover ice bucket with lid when not in use.
- Spray down the laminar flow hood on the 6th floor with Clidox to disinfect. Further spray with 70% EtOH and wipe dry. Lay out a blue bench pad and all dissection equipment in the hood
- Place all dissecting instruments in a beaker filled with 70% EtOH.
- Mice should be sacrificed by CO₂ inhalation, one at a time to ensure that nucleic acid degradation does not occur.
 - Cover cage with plastic lid attached to CO₂ tank
 - Turn main valve of tank on (make sure that it reads at least 1000 psi).
 - Turn the regulator on, slightly at first, to cause the mice to get slightly sleepy.
 - After ~15-20 seconds, turn the regulator up, just high enough to see the bedding move slightly. Allow gas to flow for about 1 minute to ensure death.
 - If further proof of death is required, cervical dislocation can be performed.

*** As soon as death is ensured, move quickly to ensure any cells/nucleic acids remain viable. Harvest one leg at a time to keep blood supply of 2nd leg intact.***

- Spray carcass with 70% EtOH to sterilize.
- Place mouse on its back. Holding the pelvis with the left hand and the femur (above the knee) with the right, gently tug on the femur until the femoral head pops out of the acetabulum (you will feel a slight pop).

- Using the middle finger of the left hand, push the internal organ away from the left leg while using the index finger of the same hand to stretch the leg open.
- Cut the skin/fur with a scalpel using a slicing motion, being careful to avoid the organs and the saphenous vein.
 - Pull back the skin and hair as they are cut, and move around the newly exposed vein. Eventually, the femoral head will be visible.
- Cut between the femoral head and pelvis to remove leg.
- At this point, technique comes into play. All fur/soft tissue needs to be removed, but the fibrous periosteum needs to remain intact and in place. Peel the remaining skin/fur down the leg and over the ankle. Try to separate the femur from the tib/fib by bending the leg across the index finger of the left hand. Use the skin around the ankle as a handle at one end (between the left middle finger and index finger) and the femoral head on the other end (under the left thumb).
- Induce tension at the joint to separate the two bones, and cut the ligaments connecting the two.
- Once separated, work with the tib/fib first. For most assays, the fibula is unnecessary, so if it is broken off, it is fine. However, try to keep it intact if possible. The best way to remove the muscles is to expose the ankle joint and cut all ligaments here.
 - With the Achilles Tendon facing you, bend the ankle over the left index finger, again using the fur as a handle between the middle and index finger. Cut all ligaments, peeling them back under your finger as you go.
- Once all ligaments are cut, grip the muscle with Kimwipe to remove, but be careful to avoid the periosteum. Basically, you can just roll the muscle back, distal to proximal. It should pull right off at the proximal end.
- Finally, to remove the foot, bend over your finger in the same way and cut from the posterior side towards the anterior side between the distal tibia and the foot.

IF USING FLUSHED BONE

- Using the scalpel, cut both epiphyses off of the bone leaving just a metaphyseal/diaphyseal section.
- Carefully place the needle of the syringe into the marrow cavity and depress the plunger to remove the marrow into a 1.5 ml Falcon tube. Repeat if necessary.
 - If any marrow is hanging off the bone, scrape it into the tube with the syringe

FOR WHOLE BONE OR FLUSHED BONE

- Place the bone in its labeled 1.5 mL tube, and submerge in the bucket of LN2 until later.
- Next, work with the femur. There isn't much technique here. Simply grab the soft tissue with a Kimwipe, possible using your nail, and tear all of the muscle off the diaphysis. If necessary, use the scalpel or scissors to remove the remaining tissue at the ends of the bone.
- Flush and store as above.
- Perform same procedure on the left leg.
- Place all animal waste (tissue, carcasses) on the blue bench pad, wrap the bench pad up and place it in a Ziplock bag. Take this bag and place in the carcass freezer in the cold room on the 6th floor.
- Take empty cage and place in the cold room on the 6th floor.

TO BE PERFORMED IN ROOM 2208 (under chemical hood)

- Tear off a piece of foil (6-8 inches). Fold this piece over on itself 4-5 times.
- Remove aluminum pieces from the LN2 using the large forceps.
- Place the aluminum foil on the cold metal, and place a bone in the middle of the foil piece. Immediately pound the bone with the hammer until flat. Flip and repeat.
- Using the small edge of the second cold aluminum piece (with a paper towel to insulate), smash along the length of the bone (through the foil).
- Repeat the other direction.
- Fill the labeled 1.5 mL tube with 1 mL of RNA-STAT

- Open the foil and remove the pulverized bone into a 1.5 ml centrifuge tube using the pipette tip.
- Close lid and vortex this sample for about 15 seconds to make sure all bone chips are exposed to RNA-STAT and are suspended, then immediately drop in the LN2 to snap-freeze.
- Samples can be stored for several months at -80 °C.

Protocol For Total RNA Isolation From Whole Bones

Chemicals:

- Chloroform (ACS grade)
- 100% Isopropanol (ACS grade)
- 75% Ethanol (ACS grade)
- RNase/DNase-free Water (DEPC-treated best)

Consumables

- Gloves
- 30 µl, 100 µl, 200 µl and 1000 µl Pipette tips (sterile)
- 1.5 ml Centrifuge tubes (sterile)
- 200 µl Eppendorf thin-walled PCR tubes w/domed lids (sterile)
- Ice

Equipment

- Insulated Ice Bucket
- 20 µl pipette
- 100 µl pipette
- 200 µl pipette
- 1000 µl pipette
- 1.5 ml test tube racks
- 200 µl PCR tube rack

- Vortexer (Fisher MiniVortexer, Rm. 2208)
- Centrifuge (Eppendorf 5415R, Rm. 2208)
- Biorad SmartSpec 3000 UV Spectrophotometer (Rm. 2208)
- Microcuvette (black sample holder; UV quartz; path length 10 mm; 100 μ L volume)
- GeneAmp PCR System 2700 Thermal cycler (Rm. 2208)

Do Under Strict RNase-Free Conditions – Treat All Equipment/Consumables that will contact bone/marrow so that they is RNase free

Autoclaving at 250° for 35 minutes and dry for 25 minutes per instructions on autoclave*

5 General Procedures:

1. Homogenization – done in previous step when bone was harvested
 - RNA Stat-60 has organics (guanidine thiocyanate, phenol)
 - Mix with cells/tissue \Rightarrow denature everything in dish
 - Pipette \Rightarrow lyse cells/shear DNA
 - RNA = single strand; shearing \rightarrow opening/closing, but we're not analyzing structure, just volume, so denaturing/damage acceptable
2. Extraction
 - Add chloroform – extracts RNA
3. Precipitation
 - Precipitate total RNA in alcohol with low salt solution
 - NB: RNA Stat contains salt
 - Spin
4. Washing/Elution
 - Wash with ethanol
 - Re-suspend – in H₂O
5. Measure OD

FOR PURPOSES OF EXAMPLE, THE FOLLOWING STPES WILL BE EXPLAINED ASSUMING THAT 15 BONES ARE BEING PROCESSED, JUST TO GIVE AN IDEA OF THE AMOUNS OF REAGENTS AND THE TIMING NECESSARY.

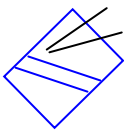
RNA Extraction

- If samples were frozen after previous step, thaw on ice.
- Set the centrifuge to fast cool to 4°C.
- Turn on the UV Spec to allow it to warm up.
- Clean all counters with 70% EtOH and RNase-ZAP to ensure that all contaminating RNase is removed.
 - RNA is extremely sensitive to RNase. Make sure that all dust and dirt are removed from area, as these tend to have a lot of RNase present.
- Vortex samples vigorously to make sure everything is mixed well.
- Spin down the samples (4°C, 10 minutes, 12,000 g)
 - Label 2 new 1.5 ml tubes for each sample
 - Aliquot all reagents that will be needed. This ensures that the full bottles are not contaminated and makes things easier to work with.
 - For 15 samples, need:
 - 4 ml of chloroform – DO NOT PUT IN POLYPROPYLENE, AS THE CHOLORFORM WILL EAT THE TUBE. USE POLYSTYRENE TUBES.
 - 10 ml 100% isopropanol (IPA)
 - 25 ml of 75% EtOH
 - 50 ml of DNase-free, RNase-free H2O
- Separate the sample into the 2 new tubes.
 - There should be about 800-900 µl of each sample. Separate 150 µl into one tube, and place the remainder in the other
 - This remaining RNA will be re-frozen at -80°C, either to be used for µ-array studies or if RT needs to be repeated.
- Put both tubes on ice and repeat with remaining samples.
- At this point, pool bones.

- I pool 5 bones together into one sample meaning that for 15 bones, I have n=3.
- I have about 400 μ l of each RNA sample reserved for PCR. I will add 150 μ l of each to the pool, making a total of 750 μ l per pooled sample.
- Add 200 μ l chloroform per 1 ml RNA STAT60 used to each tube, using a new pipette tip for each tube.
 - We need about 150 μ l of chloroform per sample.
- Vortex well for about 20 sec.
- Leave at room temperature for 2-3 minutes.
- Centrifuge at 12,000 g max for 15 minutes at 4°C (rcf on centrifuge = relative centrifugal field).
 - Need to balance centrifuge – equal # tubes placed 180° apart (add dummy tubes if necessary)
 - While centrifuging, prepare a new, labeled 1.5 ml tube for each sample, and add 400 μ l of IPA to each tube.
 - Also, refreeze the left over samples at -80°C.

RNA Purification/Precipitation

- Using new pipette tip for each tube, pipette the upper (clear) layer into the new 1.5 ml centrifuge tube that contains the IPA



- Sample will separate into 3 layers: aqueous (RNA) + red (DNA + protein) + white interface between the two that contains protein and cell matter. Take care to avoid red layer & thick white interface, therefore try to pipette most but not all of clear layer
- Use a small tip and be very careful.
- Hold tube at angle to see layers/interface better. Pipette from top (aqueous layer less dense) – if see beads/bubbles, the protein phase was disturbed.
- If you accidentally get some of the phases mixed, just spin it down again
- Vortex each tube for 3-5 seconds.
- Leave at room temperature for 15 minutes
- Centrifuge for 10 minutes at 12,000 g max at 4°C

- If this remains at room temperature or is centrifuged for a longer time, samples which contain less RNA may have a chance to precipitate.
- Should find white pellet (RNA precipitate) at bottom of tube
- Remove supernatant (liquid) with pipette – BE CAREFUL TO LEAVE PELLETT!
- Add 1 ml of 75% ethanol.
- Vortex briefly and centrifuge for 5 minutes at 7,500 g max at 4°C.
 - All centrifugation steps in the DNase digestion are performed at room temperature, so after this final centrifugation, open the centrifuge and allow it to remain open to warm up.
- Pipette out ethanol and leave tubes uncovered for 10 minutes to allow the pellet to dry.
 - Don't let RNA pellet dry completely (this ↓ solubility)
 - While waiting, label new 200µl PCR tubes for each sample.

RNA Washing/Elution

- Re-suspend dried pellet in 60 µl DEPC-treated water, mixing up and down to make sure it is completely dissolved.
- Transfer to 0.2 mL PCR tube
- Vortex, and place in thermal cycler at 55°C for 10 minutes.
 - Label the DNase column for DNase digestion and place in the 2 ml collection tube.
 - Label a new 1.5 mL tube for each sample.
 - Depending on if you will do the RNA quantification before DNase treatment:
 - 1) If yes: Add 60 µl of H₂O to the new 1.5 ml tube
 - 2) If no: Add 40 µl of H₂O to the new 1.5 ml tube
 - Go get DNases and RDD buffer and place on ice (need 3 x 55 µl aliquots and the other aliquot that is in the fridge).

Read Optical Density

- Microcuvettes take up to 100 μl samples, but this amount may saturate the system (the absorbance may be high, and the system is only accurate for absorbance values between 0.5 and 1.5). Therefore, use 20 μl of solution and 80 μl of DEPC- H_2O (i.e. dilute 1:5)
- Briefly pipette $\uparrow\downarrow$ to mix
- Wash the microcuvette with 70% EtOH and allow to dry before using.
- Make sure the outside of the cuvette is wiped clean with a Kimwipe before making any readings.
- Power up the system and allow it to warm up
- Once powered up, go through settings to make sure the proper user is set.
- Push “DNA/RNA” button
- Cycle through arrays using “select” until you reach RNA, then push “enter”
- For RNA, set the conversion factor to 40 $\mu\text{g}/\text{mL}$ and press “enter”
- When asked if there are any sample replicates, push “select” until no is highlighted, then push “enter”
- Push the dilution factor button and set to proper dilution level (you have a 1:5 dilution, so enter 5)
- Fill microcuvette with 100 μL of water, place in holder, close lid and push “read blank”.
- Empty microcuvette and fill with 100 μL of diluted sample, place in holder, close lid and push “read sample.”
- Once sample is read, empty microcuvette, rinse with water and fill with next sample. Repeat until all samples are read.
- When finished, choose to print full report.
- Clean microcuvette with 70% EtOH, allow it to dry and place back in holder.
- Turn machine off
- UV spec automatically calculates [DNA], but if you want to check by hand:
 - Concentration = $(\text{OD}_{260}) \times (\text{dilution factor}) \times (\text{NA factor})$
 - [Note: OD_{260} is the optical density reading at a wavelength of 260 nm]

- We want a ratio of A260/A280 between 1.8 and 2, which represents pure nucleic acid.
- A ratio considerably lower than 1.8 (around 1.5) is contaminated with protein and/or phenol from the extraction process.

Transfer the remaining 40 μ l of each sample from 0.2ml tube to the new 1.5ml tubes and proceed directly to DNase digest!!

Only store these samples temporarily. If not performing PCR within days, do not isolate RNA until ready!

Protocol For Cleaning RNA Samples With DNase

Chemicals:

- Qiagen RNeasy Mini Kit (cat. no. 74104) – Store at room temperature
- Qiagen RNase-Free DNase Set (cat. no. 79254) – Store at 4°C
- β -Mercaptoethanol
- 96-100% EtOH

Consumables

- Gloves
- 30 μ l, 100 μ l, 200 μ l and 1000 μ l Pipette tips (sterile)
- Ice

Equipment

- Insulated ice bucket
- 100 μ l pipetter
- 200 μ l pipetter
- 1000 μ l pipetter
- 1.5 ml test tube rack
- Vortexer (Fisher MiniVortexer, Rm. 2208)
- Centrifuge (Eppendorf 5415R, Rm. 2208)

- Biorad SmartSpec 3000 UV Spectrophotometer (Rm. 2208)
- Microcuvette (black sample holder; UV quartz; path length 10 mm; 100 μ L volume)
- Fume Hood
- Microcuvette (black sample holder; UV quartz; path length 10 mm; 100 μ L volume)
- GeneAmp PCR System 2700 Thermal cycler (Rm. 2208)

General Notes:

- Procedure should be used after RNA isolation and before RT-PCR to get rid of any contaminating DNA within RNA sample.
- The procedure will decrease the overall yield of RNA, so use cautiously.
- Buffer RLT and Buffer RW1 contain a guanidine salt and are therefore not compatible with bleach.
- All steps should be performed at room temperature working quickly. This includes all centrifugation steps. Therefore, after the last centrifugation during RNA extractions, allow the centrifuge to stay open to heat up to room temperature.
- Before 1st use:
 - β -Mercaptoethanol (β -ME) must be added to buffer RLT before use. β -ME is extremely toxic and should only be dispensed under a fume hood. Add 10 μ l β -ME per 1 ml Buffer RLT in a 15 mL falcon tube. This solution is stable for up to 1 month after mixing.
 - Buffer RPE is supplied as a concentrate. Before using for the first time, add 4 volumes of EtOH (96-100%) as indicated on the bottle to obtain a working solution.
 - A DNase stock solution should be made by dissolving all solid DNase in 550 μ l of the RNase-free water provided. Be sure not to lose any of the DNase I when opening the vial.
 - Do not vortex the reconstituted DNase I because it is especially sensitive to physical denaturation. Mix only by gently inverting tube.

- For long term storage, divide the stock into 10 aliquots of 55 μl each and store for up to 9 months at -20°C . Thawed aliquots should not be refrozen – store at 4°C for up to six weeks.

Buffer the RNA:

This step will assume that you are immediately following RNA isolation and that treatment columns are already labeled and the volume of each sample has already been adjusted to 100 μl .

- Under the fume hood, add 350 μl Buffer RLT and mix thoroughly by pipetting – not on column yet!.
- Under the fume hood, add 250 μl of EtOH (96-100%) and mix thoroughly by pipetting. DO NOT CENTRIFUGE
- Apply the sample (700 μl) to the labeled column. Gently close the lid and centrifuge for 15 seconds at ≥ 8000 rcf at $20-25^{\circ}\text{C}$. Discard flowthrough.
- Add 350 μl Buffer RW1 to the RNeasy column and centrifuge for 15 seconds at ≥ 8000 rcf at $20-25^{\circ}\text{C}$ to wash. Discard flowthrough.

DNase Treatment

- Create a DNase/Buffer RDD master mix:
 - Add 10 μl DNase I stock solution to 70 μl Buffer RDD for each sample.
 - Make enough for n samples + 15%
 - For 12 samples – add 140 μl DNase, 980 μl RDD buffer
 - For 15 samples – add 170 μl DNase, 1190 μl RDD buffer
 - For 24 samples – add 290 μl DNase, 2030 μl RDD buffer
 - Gently invert to mix.
- Pipette 80 μl of the DNase/buffer directly onto the RNeasy silica-gel membrane, close lid and leave on benchtop for 15 minutes.
 - Label 200 μl PCR tubes for left-over cleaned RNA (1 for each sample, up to 24 total samples). Label as corresponding to the numeric order of the samples.

- Add 350 μ l Buffer RW1 to the RNeasy column and centrifuge for 15 seconds at \geq 8000 rcf at 20-25°C. Discard flowthrough.
- Transfer the RNeasy column into a new 2 ml collection tube.
- Add 500 μ l Buffer RPE to the column. Gently close the lid and centrifuge for 15 seconds at \geq 8000 rcf at 20-25°C to wash the column. Discard flowthrough.
- Add another 500 μ l Buffer RPE to the column. Gently close the lid and centrifuge for 2 minutes at \geq 8000 rcf at 20-25°C to dry the silica gel membrane. Discard flowthrough.
- Transfer the RNeasy column to a new 1.5 ml collection tube.

Elute RNA

- Add 30-50 μ l DEPC-water directly onto the RNeasy silica-gel membrane, gently close the lid and centrifuge for 2 minutes at \geq 8000 rcf at 20-25°C to elute.
 - If expected RNA yield is >30 μ g, repeat the previous step with a second volume of DEPC-water.
 - I can elute in 30 μ L of DEPC, use 20 μ L to determine the concentration, and still be left with enough RNA for the next step.

AT THIS POINT, IF CONTINUING DIRECTLY TO RT, THE RT REAGENTS NEED TO BE PLACED ON ICE TO THAW!!!

Read Optical Density

- Microcuvettes take up to 100 μ l samples, but this amount may saturate the system (the absorbance may be high, and the system is only accurate for absorbance values between 0.5 and 1.5). Therefore, use 20 μ l of solution and 80 μ l of DEPC-H₂O (i.e. dilute 1:5)
- Briefly pipette $\uparrow\downarrow$ to mix
- Wash the microcuvette with 70% EtOH and allow to dry before using.
 - Make sure the outside of the cuvette is wiped clean with a Kimwipe before making any readings.
- Power up the system and allow it to warm up

- Once powered up, go through settings to make sure the proper user is set.
- Push “DNA/RNA” button
- Cycle through arrays using “select” until you reach RNA, then push “enter”
- For RNA, set the conversion factor to 40 µg/mL and press “enter”
- When asked if there are any sample replicates, push “select” until no is highlighted, then push “enter”
- Push the dilution factor button and set to proper dilution level (you have a 1:5 dilution, so enter 5)
- Fill microcuvette with 100 µL of water, place in holder, close lid and push “read blank”.
- Empty microcuvette and fill with 100 µL of diluted sample, place in holder, close lid and push “read sample.”
- Once sample is read, empty microcuvette, rinse with water and fill with next sample. Repeat until all samples are read.
- When finished, choose to print full report.
- Clean microcuvette with 70% EtOH, allow it to dry and place back in holder.
- Turn machine off
- UV spec automatically calculates [DNA], but if you want to check by hand:
- Concentration = (OD₂₆₀) X (dilution factor) X (NA factor)
 - [Note: OD₂₆₀ is the optical density reading at a wavelength of 260 nm]
- We want a ratio of A₂₆₀/A₂₈₀ between 1.8 and 2, which represents pure nucleic acid.
 - A ratio considerably lower than 1.8 (around 1.5) is contaminated with protein and/or phenol from the extraction process.

At this point, if performing qRT-PCR, all samples must be run through RT at the same time. This means that the now cleaned RNA needs to be frozen at -80°C until ready. The RNA is only stable for a short time in the freezer, so these experiments need to be planned accordingly.

All RT reactions need to start with the same amount of RNA in each sample, so wait until all of the RNA has been isolated from all groups (only pertains if running through RNA isolation more than once), determine which group will have the lowest yield and use this amount to proceed with RT. The hope would be that we can use about 1 µg of RNA from each pooled sample.

Protocol For Cleaning RNA Samples With DNase

Chemicals:

- Invitrogen SuperScript™ First-Strand Synthesis System for RT-PCR (cat# 11904-018)
- DEPC-treated H₂O

Consumables

- Gloves
- 0.2-10 µl Pipette tips (sterile)
- 30 µl Pipette tips (sterile)
- 100 µl Pipette tips (sterile)
- 200 µl Pipette tips (sterile)
- 200 µl Eppendorf thin-walled PCR tubes w/domed lids (sterile)
- 500 µl PCR tubes
- Ice

Equipment

- Insulated ice bucket
- 10 µl pipette
- 20 µl pipette
- 100 µl pipette
- 200 µl pipette
- Vortexer (Fisher MiniVortexer, Rm. 2208)
- Centrifuge (Eppendorf 5415R, Rm. 2208)

- GeneAmp PCR System 2700 Thermal cycler (Rm. 2208)
 - I also use Chris Fenno's larger thermal cycler in Rm 3204)
- Centrifuge tube adapters for PCR tubes
 - For 500 µl tubes, place inside of 1.5 mL

General Notes:

- Use equal amounts of RNA in all samples. To this point, samples should have been stored at -80°C for as little time as necessary to get through all of the samples.
- Keep and transport enzymes on ice (i.e. bring iced enzymes to tubes for reactions)
- Keep tubes closed and on ice when pipetting (ice prevents reaction from starting early)
- When working with enzymes avoid bubbles during pipetting/mixing – may negatively influence enzyme activity
- Gently vortex/spin the enzymes to mix.
- IMPORTANT: when using the thermal cycler in room 2208, remember to place tubes into small off-white holding rack before placing onto the plate, and cover with silicone mat to keep tubes from melting.
- All steps to be performed in the thermal cycler are already programmed.
- The assumption is that all groups have 15 bones that were pooled into 3 samples. To proceed with RT, the maximum amount of pooled sample that can be used is 7.5 µl (from 1 ng to 5 µg of total RNA). Therefore, working with the group that had the lowest yield, determine how much RNA will be used and use this amount (in µg) for all other samples.

1st Strand Synthesis – Step I: Denature RNA

- Place samples on ice and briefly vortex all samples before use
- Place tubes from PCR kit on ice, and briefly vortex before use
- Label blank tubes on side and on the tongue of the lid and place on ice

3 Primer Options:

1. Oligo(dT) - primes from 3' end of cDNA / string of TTTT - binds to all poly(A)

2. Random Hexamers - prime internal to poly(A) tail, all RNAs are template, used for large message- also is used to prime things like rRNA 18s which do not have a polyA tail.

3. GSP (gene specific primer) - specific to RNA want to amplify – not used in this protocol

- Prepare 0.5 mL tubes for each sample as follows, to a total volume (V_T) = 10 μ l
 - $V_T = n \mu$ l of sample + 1 μ l dNTP + 1 μ l Oligo(dT) + 0.5 μ l Random Hexamers + Balance DEPC-treated H₂O to 10 μ l
- Gently mix , then incubate at 65°C for 5 minutes to denature the RNA.
 - While incubating at 65°C, prepare the following reaction mixture (A):
 - Prepare enough for n + 15%
 - Add reagents in the order listed
 - Mg is a required cofactor for many enzymes
 - DTT is a stabilizing anti-oxidant

For 1 reaction
2 μ l 10X RT buffer
4 μ l 25 mM MgCl ₂
2 μ l 0.1 M DTT
1 μ l RNaseOUT

1st Strand Synthesis – Steps II, III: Anneal Oligos & Begin RT (cDNA Synthesis)

- Place on ice for at least 1 minute.
 - This rest on ice keeps the oligos bound.
 - This is an easy step to miss so be careful
- Add 9 μ l of reaction mixture A into each tube of RNA/primer mixture.
- Vortex and briefly spin down
- Place tubes in the thermal cycler (ready at 25°C), and add 1 μ l of SuperScript RT enzyme
 - Mix around with the tip of the pipette to make sure it gets dispersed

- Incubate at 25°C for 10 min, then at 42°C for 50 min, then at 70°C for 15 min to terminate reaction

*** These two steps are programmed as one program in the thermal cycler***

- Place tubes on ice

1st Strand Synthesis – Steps IV: Remove RNA

- Briefly centrifuge to collect reactions
- Add 1 µl RNase H to each tube and incubate at 37°C for 20 min
 - RNase H degrades RNA in the RNA-DNA hybrids, leaving only single stranded cDNA
- Place tubes in freezer at -20°C if doing PCR later. This should be stable for up to 4-5 months.

*** Volume is now about 20 µl (after evaporation effects). This will be diluted 10X to a final volume of 200µl, then aliquoted .***

Protocol For qRT-PCR

Chemicals:

- TaqMan Universal Master Mix supplied (2X, ABI P/N 4304437, 333 rxns, Green)
- TaqMan One-Step RT-PCR Master Mix Reagents Kit (2X, ABI P/N 4309169, Purple)
- Universal Mouse Reference RNA (Stratagene Cat No. 740100, 400 µg) or
- XpressRef Universal Reference Total RNA (www.superarray.com, Cat No. GA-005,
 - 2 tubes with 100 µl each at a concentration of 1.0 µg/µl).
- TaqMan Gene Expression Assays – primers which have already been designed
 - Inventoried Assays – P/N 4331182
 - Non-Inventoried Assays – P/N 4351372
- Custom TaqMan® Gene Expression Assays – primer which need to be designed

- DEPC-treated H₂O
- 70% Ethanol
- RNase-Zap

Consumables

- Gloves
- 0.2-10 µl Pipette tips (use new/autoclaved package to keep RNase-free !)
- 30 µl Pipette tips (use new/autoclaved package to keep RNase-free !)
- 50 µl Pipette tips (use new/autoclaved package to keep RNase-free !)
- 100 µl Pipette tips (use new/autoclaved package to keep RNase-free !)
- 200 µl Pipette tips (use new/autoclaved package to keep RNase-free !)
- 1.5 ml Centrifuge tubes (sterile or autoclaved)
- 200 µl ABI PRISM™ Optical Tubes (Prod. No 4316567)
- ABI PRISM™ Optical Caps (Prod. No. 4323032)
- Ice

Equipment

- Insulated ice bucket
- 0.2 ml tube rack (96 slots)
- 10 µl pipette
- 20 µl pipette
- 100 µl pipette
- 200 µl pipette
- Vortexer (Fisher MiniVortexer, Rm. 2208)
- Centrifuge (Eppendorf 5415R, Rm. 2208)
- Dual-Opposing Micro Centrifuge
- Centrifuge tube adapters for PCR tubes

General Notes:

- This entire process (filling an entire 96 well reaction plate) needs to be done in as little time as possible.

- If possible, use new packages of pipette tips and tubes when working with RNA
- Enzyme mixtures need to be GENTLY mixed before each use. This should be done by gently rotating and inverting tubes
- Keep and transport enzymes on ice (i.e. bring iced enzymes to tubes for reactions). The shorter the time at room temperature, the better.
- Keep tubes closed and on ice when pipetting (ice prevents reaction from starting early)
- When working with enzymes avoid bubbles during pipetting/mixing – may negatively influence enzyme activity

The first step when running qRT-PCR involves verifying that each primer mixture works and that the RT step for each sample actually worked.

Step 1a (1st variation) - Prepare Stratagene universal reference mouse RNA (UMRR) for use.

The UMRR comes as two tubes with 200 µg of RNA each dissolved in ethanol. This RNA must be prepared for use. Work with only one tube, keeping the other stored at -80°C.

- Centrifuge the tube at 12,000g for 15 minutes at 4°C.
- Carefully remove the supernatant.
- Wash the pellet in 70% EtOH.
- Centrifuge the tube at 12,000g for 15 minutes at 4°C.
- Carefully remove the supernatant and air-dry the pellet at room temperature for 30 minutes to remove retained EtOH.
- Resuspend the pellet in DEPC-treated H₂O to a concentration of 1X (i.e. add 200 µL of H₂O to 200 µg of RNA).
- To reduce the number of Freeze/Thaw cycles, this 200 µl sample should be aliquoted into 4, 50µl tubes and frozen at -80°C.

Step 1a (2nd variation) - Prepare XpressRef universal reference mouse RNA for use.

The UMRR comes as two tubes with 100 µg of RNA each dissolved in 100 µl of water. This RNA must be prepared for use. Work with only one tube, keeping the other stored at -80°C.

- Centrifuge the tube according to the instruction in the box.
- To reduce the number of Freeze/Thaw cycles, this 100 µl sample should be aliquoted into 2, 50µl tubes and frozen at -80°C.

Step 2 – Preparations of Standard Dilutions for Standard Curve

Starting with one of the 50 µl aliquots of reference RNA (1X):

- Pipette 10 µl of the 1X reference RNA into a new tube. To this, add 90 µl of DEPC-H₂O. This is now the 0.1X sample.
- Pipette 10 µl of the 0.1X reference RNA into a new tube. To this, add 90 µl of DEPC-H₂O. This is now the 0.01X sample.
- Pipette 10 µl of the 0.01X reference RNA into a new tube. To this, add 90 µl of DEPC-H₂O. This is now the 0.001X sample.
- These reference dilutions can be frozen and used each time a standard curve is needed, rather than thawing a full 50 µl aliquot each time.

Step 3 - Standard curves for each transcript

Before running PCR for the first time (and each time a sample is run), a standard curve needs to be made for each primer. Usually this needs to be done in triplicate for each transcript, but when testing the transcripts for the first time, do this once for each transcript.

The reaction mixture needed for standard curves is the TaqMan One-Step RT-PCR Master Mix. Because we are starting with RNA, RT and PCR need to be done at the same time. This master mix comes with 2 enzymes that need to be pre mixed (Call this Mixture A). 15.5 µl of this will be needed for each subsequent 30 µl standard curve reaction so plan accordingly:

- Add 1 part of the 40X MultiScribe RT and RNase Inhibitor Mix to 20 parts of the 2X Master Mix.
 - E.g. Mix 100 μ l of the Master Mix with 5 μ l of the 40X MultiScribe
 - Make enough for n + 10% reactions
- Primer/probe mixtures need to be thawed on ice before beginning. These should be mixed very gently by inverting the tube or flipping the bottom of the tube, until the purple color is evenly distributed.
 - These primers can be thawed/frozen about 10 times before degradation occurs. They are very expensive, so use sparingly.
- For each reaction in each standard curve, create the following mixture:

Reagent	Volume (μl)
Mixture A	15.5
Primer/Probe Mixture	1.5
RNA sample	1
DEPC H ₂ O	12
Total	30

Before running the samples, place in the bilateral mini-centrifuge to ensure that the samples are mixed and all bubbles are removed. Before doing this, clip the connectors between the tubes to be able to determine which tube is which after spinning

****For standard curves (even if actual samples are included on the plate), the first step of PCR must be at 48°C for 30 minutes.****

Step 4 - Verification of each primer and each cDNA template

Before running PCR for the first time, a verification needs to be run to ensure that all of the cDNAs that were synthesized during the RT step are viable. Further, the viability of each primer/probe combination needs to be confirmed.

- Determine the number of 8-tube strips that will be needed, put them in the tube rack and cover the entire rack with parafilm. Put this on ice and perform all steps on ice for the remainder of the set-up.
- If using the SSII method to make cDNA (following the protocol I have already made), this has already been diluted down appropriately.
- Because the primers have already been verified, each primer and sample combination will be setup as follows:

	Tube 1
Reagent	Volume (µl)
2 Step Taqman Universal PCR Master Mix	15
Primer/Probe mixture	1.5
cDNA sample	1
DEPC Water	12.5
Total Volume	30

- To be most efficient, a master mix needs to be made that contains the water, the PCR master mix and the Primer/probe mixture.
- I am going to describe a situation where 24 samples will be run at one time (2 background strains X 2 genotypes X 2 exercise groups X 3 samples per group).
 - For 24 samples (make enough for 30) and 4 primers, this is how this would break down:
 - Label 4 1.5 ml tubes, one for each primer
 - Add 375 µl of H₂O to each tube
 - Add 450 µl of 2 Step Universal Master Mix (Green tube) to each tube and place the tubes on ice.
 - Add 45 µl of primer/probe mixture to each tube and place on ice
 - Now fill out the tubes:
 - Starting with Row A and B, uncover and add 29 µl of the first primer master mix to each.
 - Continue with the remaining rows until all 4 primer/probe mixtures have been used, then cover the entire plate with parafilm again.

- Uncover column 1. Place 1 μ l of sample 1 into A, C, E, and G. Place 1 μ l of sample 13 into B, D, F, and H.
- Cover column one with a strip of caps.
- Continue filling tubes until the entire plate is filled out.
- For each odd column, clip the first connector on the cap strip and for each even column, clip the second connector.
- Spin 2 strips at a time and replace back into plate in proper orientation and column number.
- MAKE SURE THAT FOR THESE RUNS, THE FIRST STEP OF PCR IS AT 50°C FOR 2 MINUTES (SINCE NO STD CURVE) AND THAT THE REACTION VOLUME IS 30 μ l.

Step 5 - Running qRT-PCR

Once verification has been made of all primers and sample, the reaction plate can be filled for qRT-PCR. Each transcript needs to be run with all samples and a standard curve. Each run must contain a standard curve (in triplicate) and each sample (in quadruplicate at least). If you can fit 2 primers on one plate, do it.

- Quadruplicate samples here are technical replicates. Doing replicate samples reduces noise in the final measure.
- For each group, there are 3 samples. One of these samples needs to be chosen and run (in quadruplicate) as the main sample. Later, a second run can be performed (in duplicate at least) of a second sample to serve as a biological replicate. If trends are the same for the biological replicate, nothing more need to be done. If not, the 3rd sample must be run.
- First, set up the tray with the necessary number of tube strips. Cover the first 3 columns with parafilm, and then cover the remaining tubes with a second piece of parafilm. Keep this on ice during the entire process.
- When running PCR, the 8-tube strips must be placed in the machine vertically.
- I will describe this process for 8 samples and 2 primer/probe mixtures – this is one of my biological replicates.

- Create the necessary master mix for each standard curve as follows (for 2 primers in triplicate):
 - There are 12 samples in each standard curve, so we make enough for 15 samples
 - Mix 460 μl of Master Mix with 23 μl of 40X Multiscribe RT in tube A and place on ice.
 - Create a standard curve (S) master mix for each primer/probe (make enough for 15 tubes):
 - Add 180 μl of H₂O to each tube.
 - Add 232.5 μl of Mixture A to each tube and place on ice.
 - Add 22.5 μl of each primer to its tube, close and place on ice.
 - Wait to set up the tubes until the sample mixtures have been made
- Create the necessary master mix for each sample as follows (for 2 primers and 8 samples in quadruplicate):
 - Create a PCR master mix for each primer/probe (have 32 tubes, make enough for 38 tubes):
 - Add 475 μl of H₂O to each tube.
 - Add 570 μl of Mixture 2 Step Universal Master Mix (Green tube) to each tube and place the tubes on ice.
 - Add 57 μl of each primer to its tube, close and place on ice.
- Now fill out the plate, starting with the standard curves first.
 - Uncover Row A-D and fill all tubes with 29 μl of the first primer/probe mixture.
 - Add 1 μl of 1X to each tube in Row A.
 - Add 1 μl of 0.1X to each tube in Row B.
 - Add 1 μl of 0.01X to each tube in Row C.
 - Add 1 μl of 0.001X to each tube in Row D.
 - Recover Row A-D, and uncover the remaining tubes and repeat with the second primer/probe mixture.
 - Cover the 3 columns with a strip of caps.
- Fill out the remainder of the plate.

- Uncover Row A and add 29 μl of the first primer/probe mixture to each tube.
- Uncover Row B, C, D and repeat.
- Recover the tubes with parafilm.
- Uncover Row H and add 29 μl of the second primer/probe mixture to each tube.
- Uncover Row G, F, E and repeat.
- Recover the tubes with parafilm.
- Starting with column 5, uncover and add 1 μl of sample 1 to each tube.
- Cover this column with a strip of caps.
- Repeat for the remaining columns with each respective sample.
- For each odd column, clip the first connector on the cap strip and for each even column, clip the second connector.
- Spin 2 strips at a time and replace back into plate in proper orientation and column number.
- MAKE SURE THAT FOR THESE RUNS, THE FIRST STEP OF PCR IS AT 48°C FOR 30 MINUTES AND THAT THE REACTION VOLUME IS 30 μl .